Catalina H. Musinoi Hagen

The effect of surface roughness and topography on the organic coating/steel interface stability

Doctoral thesis

Catalina H. Musinoi Hagen

Doctoral theses at NTNU, 2020:304

NTNU
Norwegian University of Science and Technology
Thesis for the Degree of
Philosophiae Doctor
Faculty of Engineering
Department of Mechanical and Industrial
Engineering

◻ NTNU
Norwegian University of
Science and Technology

◻ NTNU
Norwegian University of
Science and Technology

◻ NTNU

Catalina H. Musinoi Hagen

The effect of surface roughness and topography on the organic coating/steel interface stability

Thesis for the Degree of Philosophiae Doctor

Trondheim, October 2020

Norwegian University of Science and Technology
Faculty of Engineering
Department of Mechanical and Industrial Engineering

NTNU
Norwegian University of
Science and Technology

To Sara, Ingri and Audun

And the rest of my family.

And to the strong Sofonea/Hanes/Musinoi branches of the family tree, that stretched their arms high enough to give me this bright view of the future.

Preface

The thesis is submitted to the Norwegian University of Science and Technology (NTNU), as a part of the requirement for the Philosophiae Doctor degree (PhD). The work was conducted between 2015-2016 and 2017-2019 at the Department of Mechanical and Industrial Engineering, NTNU, under the supervision of Professor II, Ole Øystein Knudsen. Professor Roy Johnsen was co-supervisor. Funding was provided by the Research council of Norway under the contract number 235239/O70.

The thesis was initiated after reports of premature disbonding of organic coatings applied on steel in the maritime and offshore industry in Norway. Blast cleaning is recommended as a steel pre-treatment for most protective coatings in aggressive environments. In practice, blast cleaning is sometimes omitted though, due to functional requirements, logistical or economic reasons, and coatings have to be applied on smooth surfaces. Organic coatings have been found to disbond earlier than expected on such surfaces.

The aim of this PhD thesis is to provide a deeper insight into the understanding of the effect of surface roughness and topography on the coating/steel interface stability in humid air and corrosive conditions.

The corrosion resistance of organic coatings on surfaces patterned with periodic peaks of varying peak-to-valley heights, Rz, was studied in accelerated tests to identify the substrate roughness parameter that contributes most to the stability of the coating/steel interface. Next, the mechanism by which roughness and topography contributes to the stability in humid air and corrosive conditions was investigated in-situ, by employing the scanning Kelvin probe technique (SKP). Grit blasted or grinded surfaces were used for reference.

To micro-pattern the steel surfaces with the topography of interest, conventional machining techniques like turning and milling were initially employed. Later, a partner was identified in the Nano Micro Facility at the Karlsruhe Institute of Technology (Germany). Here, ultrafast femtosecond lasers were employed to cut various patterns into the steel sample surfaces (August 2018-April 2019). At the same time, the newly acquired custom-made height-regulated SKP (Wicinski–Wicinski GbR) required many hours of preparation, installation and

training before useful testing could be performed. Industrial coatings were employed in the corrosion resistance test, while for the SKP technique a model coating was used.

During the work on this thesis, I have had the chance to attend three conferences. The Nordic Corrosion Congress in 2015 (Norway), NACE Corrosion 2016 (Canada) and AETOC 2017 (Germany). I presented parts of my work, as oral presentations of peer reviewed conference articles, at the first two of these.

Trondheim, May 2020

Catalina H. Musinoi Hagen

Abstract

The study in this thesis, focused on the effect of surface roughness and topography on the organic coating/steel interface stability in humid air and corrosive conditions.

A strong correlation between roughness, Rz, and corrosion resistance of coated surfaces was seen in corrosion tests, ISO 12944-9 (Paper I). Steel surfaces were patterned by machining to have periodic peaks of varying peak-to-valley heights, Rz. Grit blasted surfaces were used for reference. The coating was a two-component commercial polyamine cured epoxy mastic. Increasing the roughness on machined surfaces to 30 µm, decreased significantly the disbonding in corrosion resistance tests. By introducing tilted asperities while keeping the effective contact area in general unchanged, disbonding decreased even further. The results suggest that mechanical anchoring has a substantial influence on the protective coating/steel interface stability in corrosive conditions.

For the next steps (Paper II and Paper III), steel surfaces were patterned by ultrafast laser structuring to have controlled periodic peaks of varying Rz and geometry. Grinded surfaces were used for reference. A model poly(vinyl butyral-co-vinyl alcohol-co-vinyl acetate) (PVB) coating was used. By the combination of the in-situ SKP technique and X-ray photoelectron spectroscopy (XPS), it was demonstrated that the steel surface oxidises underneath adhering coating, depending on oxide condition from the start. The changes in surface oxide under the coating were found to be independent of the topography or roughness of the steel substrate. On smooth surfaces however, the oxidation resulted in loss of adhesion. The in-situ SKP technique was also employed to investigate the cathodic disbonding (CD) in humid air and wet adhesion loss in inert atmosphere (3 ppm O_2). CD and wet adhesion loss depended on surface roughness. A significant effect was found even when compensating for the increased effective contact area. Surfaces with features that enabled mechanical interlocking forces, had the best CD resistance and wet adhesion properties. Hence, the effect of surface roughness on CD rate and wet adhesion must partly be explained by mechanical adhesion forces.

Acknowledgements

Contents

List of Symbols and Abbreviations

Parameter	Description	Typical units
A	Actual surface profile area. The effective contact area	mm²
A_0	Geometrical area	mm²
C	Capacitance	F
E_{corr}	Corrosion potential	V vs ref.
E_{OC}	Open circuit potential	V vs ref.
L	Actual surface profile length. The effective contact length	mm
L_0	Geometrical length	mm
Pc	Peak density	Peaks/cm
r	Wenzel's roughness factor	
Ra	Arithmetic roughness average distance for five sampling lengths within the measurement length l	µm
Rz	Average maximum peak to valley distance for five sampling lengths within the measurement length l	µm
RH	Relative humidity	%
t	Time	s
T	Temperature	°C
V_{cpd}	Contact potential difference	V

W_A	Work of adhesion	J/m^2
γ	Specific surface tension of material	J/m^2 or N/m
θ	Contact angle	°
$\theta_{apparent}$	Apparent contact angle	°
$\theta_{apparent,W}$	Apparent contact angle, Wenzel state	°
$\theta_{intrinsic}$	Intrinsic contact angle	°
μ_e^{SKP}	Chemical potential of Kelvin probe's electron	J/mol
μ_e^{sample}	Chemical potential of sample's electron	J/mol
$\bar{\mu}_e^{sample}$	Electrochemical potential of metal sample's electron	J/mol
τ	Tortuosity, see L	
Φ^{SKP}	Work function, Kelvin probe	eV
Φ^{sample}	Work function, metal sample	eV
φ	Galvani potential	V
χ^{SKP}	Surface potential, Kelvin probe	V
χ^{sample}	Surface potential, metal sample	V
ψ^{SKP}	Volta potential, Kelvin probe	V
ψ^{sample}	Volta potential, metal sample	V
AFM	Atomic force microscopy	

CD   Cathodic disbonding

PVB   Poly(vinyl butyral-co-vinyl alcohol-co-vinyl acetate)

SKP   Scanning Kelvin probe

Parameter	Description	Typical units
A	Actual surface profile area. The effective contact area	mm²
A_0	Geometrical area	mm²
C	Capacitance	F

1 Introduction

The most commonly used method for protecting steel against corrosion, is the application of organic coating [1]. Organic coatings consist of a continuous vehicle, the binder, in which pigments and additives are added [2]. Both oxygen and water are penetrating organic coatings at a rate depending on the coating formula and thickness, but in general present at high enough levels to sustain considerable corrosion rates [3, 4]. In spite of this, coatings protect against corrosion [5].

The traditional explanation for the protective action of organic coatings has been that coatings provide a high resistance between anodes and cathodes on the substrate [6], either ionic or electronic [6, 7]. The slower the current flow, the slower the electrochemical processes. This view has been challenged during the past couple of decades. Essentially, the protective action by organic coatings is to prevent electrochemical reactions underneath the coating [8]. Another vital property of the organic coating is now more believed to be its ability to protect the passivating surface oxide on the substrate, i.e. that the oxide actually provides the corrosion protection [2, 9].

When defects in the coating result in the exposure of the substrate, corrosion on the bare steel will spread underneath the coating and cause electrochemical disbonding depending on several factors, including the oxide composition [9-11], the coating formulation [12-14], oxygen partial pressure [15], electrochemical potential [16-18] and surface roughness [19].

This thesis raises the question of how the steel surface roughness and topography affect the coating/steel interface stability in humid air and corrosive conditions. *The modification of*

surface roughness and topography – on the micro-scale – to increase the coating/steel interface stability, is hence the general theme of this thesis.

Although the importance of surface roughness to the adhesion of organic coatings on a metallic substrate has long been recognised [20-22], the mechanism through which a micro-rough surface contributes to stabilise the coating/steel interface is still under debate. While the scientific community has focused mostly on chemical bonds and intermolecular forces [23], conventional wisdom in the heavy-duty protective coating industry emphasises mechanical forces and recommends blast cleaning by grit blasting as pre-treatment for most protective coatings in aggressive environments. Coating standards and technical data sheets specify blast cleaning as pre-treatment for surfaces to be coated [24-26], for optimal coating performance by enabling mechanical interlocking between coating and substrate, i.e. mechanical adhesion forces. In practice, however, grit blasting is sometimes not feasible for roughening of a surface, due to functional requirements, logistical or economic reasons, for example on machined parts and equipment.

Machining is a manufacturing technology heavily implemented in the industry, which produces smooth surfaces that often are not grit blasted before being coated. Coatings applied on machined surfaces are generally found to degrade early with subsequent corrosion of the steel substrate [27], confirmed in several studies [28-30]. Early in this study, it became evident that the machining process itself did not explain the premature coating failure, but rather the roughness and topography of the steel surface.

Various studies have addressed the role of surface roughness on the stability of the coating/steel interface in humid and corrosive conditions. However, all of them have been performed on samples with non-uniform, heterogeneous topographies having a stochastic distribution of roughness heights [28, 29, 31-35]. The previous studies have in addition argued that an increased corrosion resistance is due to an increased effective contact area, as this will either offer more available area for bonds at the interface [36], or by increasing the interfacial path [19], which has been shown to decrease the kinetics of failure [31, 35, 37, 38].

It is acknowledged that increasing the roughness of the substrate and hence the effective interfacial contact area, all phenomena involving surface energies per unit area such as wetting and work of adhesion will be affected. Both physical and chemical interactions that

are related to the unit area of the interface will increase [36, 39-41], and so will the contribution of mechanical forces to adhesion [42].

The work presented in this thesis shows the significant effect of mechanical interlocking on the coating/steel stability in humid and corrosive conditions, i.e coated steel surfaces in humid air atmospheres with defects covered with electrolytes (e.g. seawater or humid air in marine atmospheres). Mechanical adhesion is promoted by surface irregularities that the coating can anchor to, and increases with increased interfacial area [43-45]. Experience has shown that coating/steel interfaces without mechanical interlocking, fail early when exposed to corrosive conditions [46-48].

A first requirement for optimal adhesion is that the coating completely wets the surface, but surface roughness influences strongly the wetting and wettability of metals [22]. Hence, the profile must balance the need for good anchoring with the coating with the need for good wetting [49]. However, the physical adhesion strength of organic coatings to steel has little correlation with their protective performance. Even though the required initial adhesion is achieved, electrochemical processes at the coating/steel interface have been documented to destabilise the bonds and cause disbonding [8, 50]. Hence, the contribution from mechanical interactions at the coating/steel interface to the stability of this area, must be studied under exposure to corrosive conditions.

The steel surface roughness and topography are believed to affect the coating/steel interface stability in humid air and corrosive conditions by the following relationships:
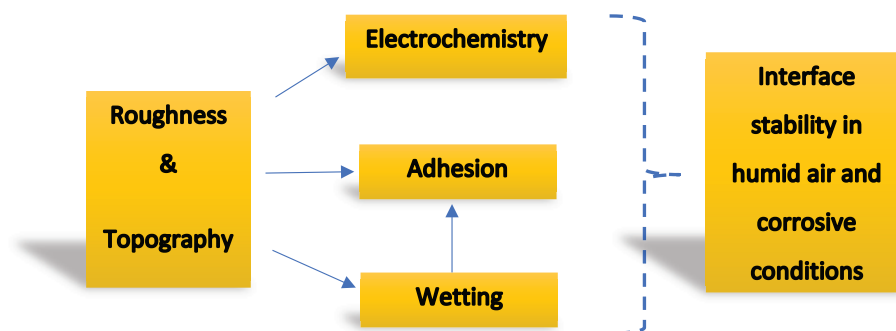
Figure 1. The suggested effects of steel surface roughness and topography on the stability of the organic coating/steel interface in humid air and corrosive conditions.

- 3 -

1.1   Objectives

The overall objective of the thesis is to provide a deeper insight to the understanding of the effect of surface roughness and topography on the coating/steel interface stability in humid air and corrosive conditions.

The research questions were formulated like this:

1) Why do industrially machined and coated steel surfaces disbond prematurely? (Paper IV, Conference paper)

2) Will a laboratory control of the coating process eliminate the disbonding? Which is the most important surface topography parameter? (Paper V, Conference paper)

3) If we increase the roughness of machined surfaces, will these have the same corrosion resistance as grit-blasted surfaces when coated? (Paper I)

4) What is the mechanism by which roughness contributes to the stability when an electrolyte covered defect is present in the coating? (Paper II)

5) What is the mechanism by which roughness contributes to the stability in humid air conditions? (Paper III)

To answer the questions above and accomplish the overall goal for the study, the approach was to implement the following specific tasks:

1. Gain an overview of the problems related to the failure of industrial organic coatings on industrially machined surfaces.

2. Accumulate fundamental knowledge about the stability of organic coatings on steel.

3. Involve the manufacturing group at NTNU to pattern steel surfaces with various topographies at different roughness, Rz, by machining. Evaluate the corrosion resistance of epoxy coatings on such surfaces in accelerated corrosion tests.

4. Install and put in service at SINTEF/NTNU a newly acquired custom-made height-regulated SKP instrument.

5. Become familiar with the theoretical background for the instrument as well as the experimental methodology.

6. Apply for access at the Nano Micro Facility at the Karlsruhe Institute of Technology (Germany), and involve the scientific group there in the surface structuring of samples needed in this project.

7. Evaluate the cathodic disbonding and wet-adhesion resistance of a PVB model coating on surface structured steel by the in-situ SKP technique. Determine the oxide composition at the surface with XPS.

8. Investigate the effect of humid air on the coating/steel interface, and the resistance to cathodic disbonding as a function of the surface oxide condition and oxidation, by the in-situ SKP technique in combination with XPS. The stabilising effects of surface roughness are also investigated.

1.2   Thesis outline

This thesis consists of six chapters, a reference section and five appended papers. Chapter 2-5 present relevant theory and previous work for the understanding of the published research results. Chapter 6 provides the key contributions of this thesis, sorted by academic publications, discussing the concluding remarks and the strengths and limitations of the thesis. A detailed overview is given below.

Chapter 1 presents a general overview of the motivation for this work, the objectives, and the thesis outline.

Chapter 2 briefly introduces adhesion theories, before presenting and discussing the recognised mechanisms for protection of steel against corrosion by organic coatings.

Chapter 3 discusses the electrochemical disbonding of organic coatings seen as a break-down of the protection mechanisms. The cathodic disbonding mechanism is next presented as the dominant electrochemical disbonding mechanism on steel surfaces in humid air atmospheres.

Chapter 4 presents and discusses the effect of substrate topography on the ability of the organic coating to protect steel in corrosive conditions.

Chapter 5 presents the materials and test methods relevant for this study. The SKP technique is presented together with the theory necessary to understand and use the technique.

Chapter 6 presents the academic publications, discusses the concluding remarks and the strengths and limitations for this work.

2 Corrosion protection of steel by organic coatings

This chapter briefly introduces the adhesion theories, before presenting and discussing the recognised mechanisms for protection of steel against corrosion by organic coating:

- Barrier mechanism
- Protection of passivating surface oxides
- Corrosion inhibiting mechanisms

2.1   Adhesion theories

Adhesion is a complex phenomenon covering several scientific fields. Coating adhesion mechanisms have been reviewed by Venables [48], Fourche [51] and recently by Baldan [39]. It is recognised that adhesion on the macroscopic scale originates from contributions at different length scales: On the molecular scale adhesion results from chemical bonds and physical interactions, while mechanical interactions originating from asperities at the micro-level, act on the micro- to macro-scale [41, 52]. The chemical interactions (primary bonds), and physical interactions (secondary bonds) are listed in Table 1 with information about type of force, bond strength and interatomic distance.

Although secondary bonds are weaker than primary bonds, these types of bonds are formed at most interfaces, while primary bonds require certain chemical conditions to be met [52]. The exact importance of chemical bonds versus physical bonds is still under debate. Mechanical interactions are possible where the geometry of the substrate allows for penetration [48, 49], mechanical hooking or interlocking [53].

Table 1: The bond strength of different bond types and their strength [54], and the distance these are acting over together with the type of forces involved in the bond creation[55].

	Bond type	Type of force	Distance [Å]	Bond strength [kJ/mol]
Primary bonds	Ionic	Electrostatic forces (Coulomb interactions)	1-2 (2.8 Å in NaCl)	600-1100
	Covalent	Wave function overlap	1-3 Å	60-700
	Metallic	Free valence sea interaction	2.9 Å for Fe	110-350
Secondary bonds	Hydrogen (Acid-base interactions)	Directional dipole-dipole interaction	1-3 Å	< 40
	Van der Waals	1)Dipole-dipole (Keesom)	Few to several hundred Å	4-20
		2)Dipole- induced dipole (Debye)		< 2
		3)Dispersion forces (London)		0.08-40

Several adhesion mechanisms have been proposed based on the different bonds and interactions. However, the adsorption theory and the mechanical interlocking theory are the two most widely accepted theories for coating-metal adhesion [20, 43, 48, 56, 57]. The adsorption theory involves secondary bonds and may be purely physical (physisorption) or it may involve the formation of primary bonds across the interface (chemisorption). The theory

- 8 -

states that if sufficient intimate contact is achieved between two materials, they will adhere as a result of intermolecular or interatomic forces. The mechanical interlocking relies on the mechanical keying of binder into the asperities and irregularities in the substrate surface. The mechanical interlocking mechanism has however not been investigated as thoroughly as the other adhesion mechanisms [20, 56, 57]. See Chapter 4 about the importance of mechanical interlocking to the stability of the coating/steel interface.

2.1.1 Fundamental versus practical adhesion

A first prerequisite for coating adhesion and stability is the contact between coating and substrate, known as wetting [22]. The wetting at equilibrium is given by the tension balance in the horizontal direction for a drop of liquid placed on a perfectly smooth solid surface, as described by Young's equation [58], see Eq. (1).

$$\gamma_{LV} \cos \theta = \gamma_{SV} - \gamma_{SL} \tag{1}$$

The equation gives the relationship between the surface tension γ_{SV} of the solid S (in vapour V) and γ_{LV} of the liquid L (in vapour V), in equilibrium with the interfacial tension γ_{SL} between the solid and the liquid. According to the equation, three different wetting states will be reflected by the contact angle, θ, formed between the drop and the solid underneath: High wetting ($\theta < 90^{\circ}$), partial wetting ($\theta = 90^{\circ}$) and low wetting ($\theta < 90^{\circ}$), see Figure 2. The contact angle can be measured by different techniques.
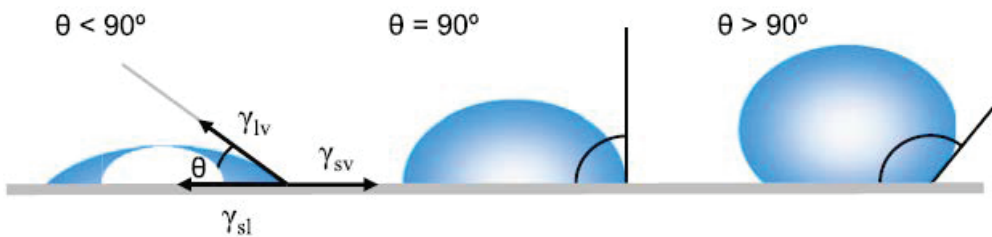
Figure 2. Illustration of contact angles formed by a drop of liquid on a perfectly smooth surface. Figure from [59].

However, the contact angle in Young's equation is an ideal angle measured only on smooth surfaces, while actual surfaces tend to be rough. Wenzel's roughness factor, r, was derived for

this purpose [60], see Eq. (2). A is the geometrical area, and A_0 is the effective contact area or the actual surface profile area.

$$r = \frac{A}{A_0} \tag{2}$$

Hence, Wenzel's roughness factor is a 3D measure of roughness. Increasing Wenzel's roughness factor means a larger effective contact area between the liquid and the surface. The roughness affects the measured contact angle and therefore Young's equation. The measured contact angle is therefore called an apparent contact angle, and a function of the roughness and the intrinsic contact angle, see Eq. (3).

$$cos\,\theta_{apparent,W} = r \times cos\,\theta_{int\,rinsic} \tag{3}$$

The practical implication of Wenzel's equation is that roughness affects the wetting properties of solid surfaces, by making hydrophilic surfaces $(\theta_{\text{intrinsic}} < 90^\circ)$ more hydrophilic and hydrophobic surfaces $(\theta_{\text{intrinsic}} > 90^\circ)$ more hydrophobic. Hence adding roughness to hydrophilic surfaces, i.e. metals, makes them more easily wetted by polar coatings such as epoxies, but also water.

Another implication follows directly from this relationship: When measuring contact angles on solid surfaces with the intention to calculate their surface tensions, γ_{SV}, the measured contact angles must be modified with the roughness factor to yield the intrinsic contact angle. However, even after correction for roughness, the validity of the Young's equation is questioned when the deviation from ideal smooth surfaces increases [21, 22, 61].

The approach in the Young's equation assumes that there are no differences between the chemical nature of surface molecules on the rough surface versus on the smooth surface [21, 22]. However, rough surfaces are e.g. electrochemically more active. Anodic reactions are accelerated with roughness, explained by a reduction in the electron work function with surface roughness [62, 63]. Electrons become thus more available on a rough surface, and the chance for oxidation increases.

Upon wetting of a substrate by the coating, the thermodynamic work of adhesion, W_A, between the solid and the solidified coating (but here denoted as liquid) may be expressed according to Dupré [64], see Eq. (4).

$$W_A = \gamma_{SV} + \gamma_{LV} - \gamma_{SL} \tag{4}$$

The definition assumes that only secondary bonds are acting across the interface. W_A represents the attraction at the interface (Jm^{-2}) but measured as the work required to separate the interface between the two and create new surfaces. By combining Eq. (1) and Eq. (4), the result is known as the Young-Dupré equation [64], see Eq. (5)

$$W_A = \gamma_{LV}(1 + \cos\theta) \tag{5}$$

The equation implies that the thermodynamic work of adhesion may be quantified by measuring the surface tension of the liquid and the contact angle between the liquid coating and the solid surface of interest. By the relationship, a low contact angle gives the highest work of adhesion. A positive W_A implies that energy is needed for the separation, resulting in a thermodynamically stable interface, while a negative W_A indicates an unstable interface and loss of adhesion.

Many researchers have tried to correlate the measured adhesion strength with the theoretical work of adhesion of coatings. However, it was pointed out early that the adhesive forces caused by molecular attraction would be higher than the adhesion found experimentally. Different theories have been suggested to explain the observed difference. Reinhart suggested that the inherent strength of the bonds is affected by stresses in the coating induced during bond formation, or during the in-service application [65], see Figure 3.

Several other authors pointed out that the test methods commonly employed to measure adhesion, introduce geometrical factors that affect the measurement and includes the energy dissipated in the material due to viscoelastic and plastic deformation during testing [21, 54, 66]. The measured adhesion strength is therefore believed to also contain contributions from substrate properties [67], and Mittal therefore made the distinction between the fundamental and the practical adhesion.

```
A- MAXIMUM ADHESION - CAUSED BY FORCES OF MOLECULAR ATTRACTION
              MAXIMUM BOND STRENGTH POSSIBLE

              B - INHERENT STRENGTH OF BOND                    L-LOSS
   DETERMINED BY ABILITY OF MOLECULES OF ADHESIVE AND ADHEREND   CAUSED BY
   TO ATTAIN MOLECULAR NEARNESS. DEPENDS ON WETTING OF          INCOMPLETE
   ADHEREND BY ADHESIVE                                          WETTING

   C-RESIDUAL STRENGTH OF          S- INTERNAL STRESS ON
        BOND                            BOND


                          E      F      DEFECTS IN TEST MAY PRODUCE UNMEASURED
                                        STRESS ON BOND E, OR REDUCE EFFECT OF
                                        INTERNAL STRESS ON BOND, F.

   D-MEASURED STRENGTH
      OF BOND
   BREAKING OF BOND BY
   EXTERNALLY APPLIED STRESS

      THIS CHART IS QUALITATIVE, NOT QUANTITATIVE, NO SIGNIFIGANCE IS ATTACHED TO THE
      RELATIVE LENGTHS OF THE LINES. A IS ALWAYS GREATER THAN B, AND B GREATER THAN C
```

Figure 3. Reinhart's chart of the adhesion strength measured from tests and how it relates to the theoretical adhesion. Figure from [65].

In addition, *the weak boundary layer* theory was proposed to explain the differences in the measured adhesion as opposed to the expected theoretical adhesion [68]. The theory stated that adhesion is always affected by impurities at the interface, weakening the adhesion. Such impurities at the interface may be related to chlorides [69, 70] or rust [71-73], but may be any substance at the interface preventing contact between the coating and the substrate.

In conclusion: Stresses in the film, introduced either during bond formation or during the film formation, will weaken the adhesion. In adhesion measurements, energy dissipated by plastic and elastic deformation of the coating may result in a higher measured adhesion strength compared to the theoretically expected value. Properties of the substrate will contribute to the measured adhesion strength, both by affecting the intrinsic adhesion directly when the effective contact area increases, and by allowing the coating to dissipate energy during the initiation and propagation of disbonding. Asperities may result in mechanisms that dissipate forces that otherwise would destruct coating/metal bonds [74], see Chapter 4.2. Finally, impurities at the interface prior/during film formation will decrease the measured adhesion strength.

2.1.2   Wet adhesion

Wet adhesion was introduced as a term by Leidheiser and Funke during the early 80's to describe coating adhesion when the coating is exposed in a humid environment. They emphasised the role of wet adhesion to coating lifetime [75]. It has since been debated. The major difficulty in studying wet adhesion is the lack of satisfactory test methods to quantitatively measure adhesion in wet conditions [76], though this is also difficult for dry conditions [4]. The second unsolved problem is the mechanism by which water affects the adhesion. It is recognised that i) adhesion in wet conditions is lower than in dry but due to residual adhesive forces not all adhesion is lost [75] and that ii) after drying, adhesion may be regained [77].

See Chapter 3.1 for more information about the accumulation and effect of water on the interfacial stability.

2.1.3   Adhesion tests

A considerable amount of work has been devoted to design methods to assess adhesion properties, and a review of the literature in 1995 indicated that 350 different techniques were available [78]. The choice of method is dependent on many factors, such as 1) the mechanical properties of the coating and the substrate, 2) the interface properties, 3) the microstructure of the coating/substrate system 4) coating thickness, and 5) the intended application [79].

The test methods can be subdivided into pull-off tests, double cantilever beam (DCB), bending tests (three-point, four-point, mixed mode), blister tests, scratch and cross-cut, end-notch flexure (ENF), and indentation tests (cross-sectional) [74]. There is no universal approach to determine the interfacial adhesion strength. Even a unidirectional test will develop locally different stresses (multi-scale effect) resulting possibly in a variety of different dissipative mechanisms, which again can contribute differently to the macroscopic adhesion energy, making the comparison of adhesion results obtained by different techniques difficult [45, 74, 79]. In practice, adhesion can only be quantified with reference to a specific type of test or usage. Different methods for measuring adhesion will give different results [80]. For a given coating, the best adhesion test method is the one that simulates as close as possible the probable service conditions. For coated samples intended for corrosion protection, adhesion should be measured on water saturated coatings, as wet adhesion is lower than dry adhesion,

see Chapter 2.1.2. However, there is no industrial standard specifically for wet adhesion testing. Performing wet adhesion tests according to the procedures specified for dry adhesion, just modified by the exposure of samples to water, is difficult and sensitive to measurement errors [80].

As measurements of adhesion strength are problematic, an interesting solution to the problem is the fracture mechanics approach, where crack propagation an the interface is assessed [41, 52, 74, 81].

It is important to note that although adhesion testing is commonly used for qualification of organic coatings as well as quality control and quality assurance, initial adhesion strength values do not necessarily correlate with their corrosion protection performance or service life. Electrochemical processes at the coating/steel interface will destabilise the bonds and cause disbonding, even for strongly adhering coatings [8, 50].

2.2 The mechanisms for corrosion protection

The most widespread method for corrosion protection of steel, is the application of organic coatings [1, 2, 8]. Several mechanisms on how organic coatings protect steel against corrosion have been suggested: 1) By acting as a barrier to water, oxygen and aggressive species, 2) by protecting the passivating surface oxide on the substrate surface, and 3) by serving as a reservoir for corrosion inhibiting pigments. Historically, the barrier mechanism has been considered the most important of them, although the definition of "barrier" has been reformulated. It is now generally agreed that organic coatings provide a barrier to ionic species, opposed to water and oxygen.

The three mechanisms will be presented and discussed in the following sections.

2.2.1 Barrier properties

The physical barrier properties of coatings have received much attention, and historically, organic coatings were assumed to protect mainly by retarding the diffusion of water and oxygen to the metal substrate. However, several critical arguments have been made with respect to this mechanism: 1) The amount of water and oxygen at the interface does not necessarily depend on the uptake into the coating, as this will mostly be determined by the

coating-steel interface properties [82], and 2) the amount of oxygen and water present in organic coatings are normally sufficient to sustain considerable corrosion rates [83, 84]. The opposite has also been demonstrated: Although strong barrier properties were documented, at localised spots underneath the coating, corrosion happened [76].

Mayne and co-workers proposed in the 1950's that organic coatings protect the metal substrate by resisting ionic currents [5]. Hence the barrier property was now explained as an ionic barrier. When electrochemical reactions happen at steel surfaces, electrons are transported through the metal, and to complete the electrical circuit ions must be transported by the electrolyte. The ionic resistance has been highlighted as a critical factor [1-3, 6, 84] , but it is understood and explained in various ways.

While some understand the ionic resistance to be a coating property, where ions have to pass the coating at both anodic and cathodic sites [6, 85], others understand it as a property of the coating-metal interface. Ionic resistance is in this latter context dependent on adhesion or maintenance of an intimate molecular contact between the organic coating and active sites of the metal substrate [37]. The wet adhesion properties of the coating/steel interface are hence important for the ionic resistance of the coating [3]. The formation of an aqueous phase at the interface lowers the electrical resistance between cathodic and anodic sites along the interface [86] and increases the transport rate of hydrated cations along the interface during electrochemical processes [87]. Direct ionic pathways between anodic and cathodic sited are indeed found for various electrochemical disbonding processes, as cathodic disbonding [87-89]. For these processes, the cell current does not need to pass through the coating but along the interface.

When ionic resistance is understood as a suppression to ions permeating into the coating both at anodic and cathodic sites, coating heterogeneity plays an important role [50]. Several studies have been carried out to investigate this theory, and Mayne suggested that ions enter the coating through the matrix of the coating which is non-uniform and will consist of regions of low specific resistance, "D"-areas with 10^6–10^8 Ω cm, and areas with higher resistance, "I" type [6]. An alternate theory proposes the ionic transport to happen at discrete channels, as small imperfections or pores in the matrix [90, 91].

Whatever the mechanism for ionic permeation and transport, the ionic resistance has been found to vary with coating thickness and exposure time. A linear current-potential relationship for coated steel under cathodic polarisation has been found in several studies, showing that the ohmic resistance of the coating controls the current. The magnitude of the ionic resistivity of protective barrier coatings has been found to vary from $10^9 \, \Omega$ cm to $10^{13} \, \Omega$ cm [85, 92]. Other studies have shown that for an epoxy coating, typical values for electrical resistivity are > $10^{14} \, \Omega$ cm when dry and falling to $10^{10} \, \Omega$ cm when saturated with water, between 1% and 2% by mass [93]. A protective barrier coating should have a resistivity of more than $10^9 \, \Omega$ cm [94].

It is recognised that by impeding ions from entering and reaching the steel surface, a more extended double layer will be the result at the steel surface [2, 4]. With the addition of the coating, the dissolution of the metal is thus inhibited [82, 95]. Metal dissolution is high on bare metal due to the large electric field, $10^7 \, \text{V cm}^{-1}$, associated with the double layer formed when a metal is covered by electrolyte (assuming the double layer is 1 nm thick and the potential drop across the double layer formed with an electrolyte is around 0.5-1 V). See Figure 4 about the effect of organic coatings on the electric fields on metals.
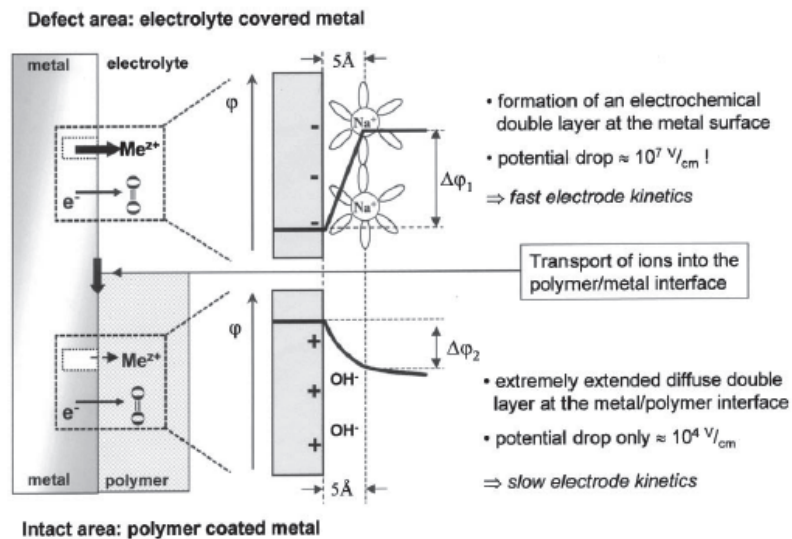

Figure 4. Schematic of the double layer formed at the interface for an electrolyte covered metal and a coated metal. Figure from [2].

2.2.2   *Protecting the passivating surface oxide*

Passive metals are covered by tight, adhering oxides, separating the metallic surface from the environment. When a protective organic coating covers a metal, the oxide is also protected, and an oxide that would not be protective when exposed to the environment, is now protective [3,4].

The passivation of the iron surface proceeds in several steps. In air atmosphere, following formation of new iron surface e.g. by grinding, polishing, blast cleaning or cold rolling, an oxide layer containing a high concentration of Fe^{2+} species or states, is formed. The Fermi level is determined by this concentration [15], and to begin with, it is close to the conduction band [96]. The Fe^{2+} states result in a p-type of oxide with a narrow bandgap, which allows charge carriers to be easily available for electrochemical reduction reactions [97]. Fe^{2+} species can thus be regarded as defects in the oxide. With further exposure to air, these Fe^{2+} species are oxidised to Fe^{3+}, and the Fermi level slowly decreases, while the electrode potential increases. When the oxide surface is wetted by humid air, iron is oxidised at the iron/oxide interface to iron cations, while oxygen dissolved in the thin water layer is ionised at the oxide/electrolyte interface to oxygen anions. The growth proceeds with the inward migration of oxygen ions from the electrolyte-oxide interface, to react with metal ions to form the inner part of the oxide, and iron ions that migrate outwards from the iron-oxide interface towards the oxide/electrolyte interface to react with the oxygen ions and to form the outer part [98]. The oxide is considered to have a bipolar character, that consists of an Fe^{2+} rich anion-selective inner layer and an Fe^{3+} rich cation-selective outer layer [97]. The electrons from the anodic reaction at the iron/oxide interface are transported through the oxide to the cathodic reaction at the electrolyte/oxide interface. As the oxide thickens, the resistance against transport of ions in the oxide increases and the steel passivates [98]. There are several theories discussing the limitations to oxide growth. In general these either explain the limitation with decreased permeation of the oxide film by cations, transport kinetics inside the oxide or metal cation dissolution at the oxide/electrolyte interface [99]. The effect of oxide semiconducting properties on cathodic disbonding has been investigated [100] and an increased Fe^{3+}/Fe^{2+} ratio was found beneficial [101].

In corrosive environments, this layer is attacked by aggressive ions. Thus, the destabilisation of the oxide by the environment activates the metal underneath.

Although the mechanism is not experimentally proven yet, authors have suggested that protecting the oxide layer and aiding passivity is an important function of the organic coating [3], or even stating that the oxide film is part of the protection system together with the coating, from the standpoint of limiting corrosion currents [102]. It has, however, been suggested that the protection provided by the oxide layer starts to decline once the oxide is hydrated at the coating/steel interface [48].

2.2.3 *Reservoir for corrosion inhibiting pigments*

The inhibitive action of pigments added to organic coatings, is differentiated by the way they protect against corrosion. There are three basic mechanisms by which the pigments can contribute to protection: Barrier protection, passivation protection and sacrificial protection [103].

The barrier protection is achieved by slowing the transport of water, oxygen and ions to the steel substrate. These pigments are *inactive* pigments, e.g. glass and aluminium flakes.

Coatings providing protection by passivating pigments contain *active* substances that are slightly water soluble. These pigments are mainly used in coatings for atmospheric conditions. The barrier properties and the active effect of the pigments should be balanced. Just enough moisture should be allowed to permeate the coating, allowing to dissolve the pigments and carry them to the surface. Here they react with the surface and produce a passive layer by converting the steel substrate into a passive oxide containing the pigment compound. Phosphates and chromates have been the most used compounds for inhibitive action [103].

Coatings relying on sacrificial protection, contain active pigments that corrode instead of the underlying metal; hence a galvanic protection effect is achieved. Following, only the pigments in galvanic contact with the steel substrate will contribute to this effect [104]. Usually this is achieved with zinc rich primers [105]. A typical coating system used on marine and offshore installations in the atmospheric zone, consists of a zinc-rich primer, an intermediate epoxy barrier coat and a topcoat resistant to ultraviolet light (UV) [106, 107].

Last, it is to be noted that much research is currently carried out worldwide to design self-healing coatings in which active corrosion inhibitors are delivered to the site of coating

degradation only when active corrosion starts [108]. The passivating pigments mentioned above are effective all the time, regardless of whether there is a defect in the coating or not.

3 Electrochemical disbonding of organic coatings on steel

This chapter discusses the electrochemical disbonding of organic coatings seen as a break-down of the protecting mechanisms. The CD mechanism is next presented as the dominant electrochemical disbonding mechanism on coated steel surfaces in humid air atmospheres, starting from coating defects covered with electrolytes [82, 84, 87], e.g. seawater or humid air in marine atmospheres.

The resistance of the coating to the incorporation of water at the coating/steel interface and the transport of ions either through already disbonded coating or along the interface, are recognised to be rate determining for the loss of adhesion strength at the steel-coating interface [87, 109].

The mechanisms involved in the degradation of organic coatings depend on: i) The nature of the metal substrate, ii) the nature of the interfacial region between the coating and the metal, iii) the nature of the coating and iv) the properties of the environment to which the coated metal is exposed [92]. There are several environmental factors that can accelerate the coating degradation by inducing chemical and mechanical damage of the coating film, facilitating the access of water, oxygen and ions to the interface [4]:

- Pollutants present at the steel surface to be coated
- Ultraviolet (UV) radiation
- Elevated temperature
- Leaching of components from the coating

- Ozone and other aggressive species
- Abrasion or other mechanical stresses

During exposure to a corrosive environment, several conditions may act synergistically in the degradation of the coating-steel interface: i) The incorporation of water at the interface lowers coating adhesion [47, 48, 75] and allows for electrical contact between local anodes and cathodes at the coating-steel interface [86] , ii) cyclic wet/dry exposure that increases the internal stresses in the coating and lead to microcracking at the coating surface [19], iii) the cathodic oxygen reduction reaction will increase the local pH and produce intermediates, affecting the coating-substrate bonds [4, 50], and iv) the anodic dissolution of steel will produce corrosion products that exert stresses on the coating-substrate interface or undermine the coating.

Corrosion reactions advancing underneath the coating are the ultimate failure mode of protective coatings [4]. These are found to initiate at damages or weaknesses in the coating [2, 110, 111] and depending on the coating system, the exposure environment and the substrate. They propagate by anodic undermining [2, 87], CD [15, 83, 111-113] or mechanical lifting the coating from the substrate, i.e. oxide wedging [114]. Corrosion creep is the dominant electrochemical degradation mechanism for protective organic coatings on steel in atmospheric conditions [87]. The process of CD is dominant when defects in the coating are covered with an electrolyte. This is the case mainly for submerged and buried steel [4], but also in atmospheric conditions when the surface is wet [84]. Cathodic disbonding can also contribute to the corrosion creep mechanism [89, 115, 116].

3.1 The incorporation of water and oxygen at the interface

Diffusion of water in organic coatings is suggested to happen by different processes. It can diffuse via the free volume between binder polymer chains, voids in the coating, directly through the coating matrix [117], heterogeneities[118] or through regions with defects, especially if film layers are too thin [119]. Diffusion coefficients for transport through the bulk have been obtained based on different diffusion models, and are found to depend on several coating parameters as e.g. coating chemistry, thickness, curing and void distribution [15, 120]. In addition, water can be carried with the cations that move along the interface from electrolyte filled defects into the intact interface under corrosive conditions [84, 121].

The nature of the water in the coating and at the interface is still questioned. Depending on the system, at the interface, water may be present on oxide surfaces in the form of molecular water or dissociated as hydroxides and protons [122]. Water can be adsorbed both by chemisorption and physisorption. Chemisorption results in hydroxide ions bonded to the surface, while physisorption results in bonded molecular water. Hydrogen bonds are in both cases involved [123].

Hydroxide ions are believed to be more easily adsorbed on hydrophilic surfaces. It has, however, been claimed in several studies that the surface hydroxide density alters the number of oxide/coating interactions, such that the number of hydroxide groups on the surface correlates positively with the adhesion of polymers [9, 10, 124]. Hence water in dissociated form may play a mediating role at the interface. A higher number of surface hydroxides has recently been shown to increase wet adhesion through increased ionic bond formation [125].

The role of molecular water at the interface is to the opposite suggested to explain wet de-adhesion, defined as the reduction of adhesion strength by ingress of water. It has been suggested that there will always be present a sufficient amount of voids and non-bonded areas at the interface, which can accommodate several water molecules [75]. From these local points, water can start spreading laterally by two possible mechanisms: One relying on a chemical destruction of bonds (thermodynamically driven hydrolysis where water substitutes the coating in the coating-oxide bond) and one relying on a mechanical process [75].

The thermodynamics of adhesion indicate that if only secondary interactions are acting across the interface, water will almost always desorb an organic adhesive from a metal oxide surfaces [54]. Non-specific van-der Waals interactions are the most common coating/steel interactions that result in bonds at the interface [52], but water is known to replace an organic coating from a steel surfaces if only these interactions are acting across the interface [48, 54, 87]. In dry state, coating-steel bonds resulting from Van der Waal interactions, typically range in the order of 25 kJ/mol, while water-steel interactions exhibit binding energies of up to 60 kJ/mol, and therefore can replace the coating [95]. Secondary bonds are never enough to counteract bond weakening and de-adhesion by water, argue Venables and Brockman, and suggest that mechanical adhesion is needed to oppress the incorporation of water at the interface [48], and to persist complete de-adhesion when bonds are hydrolysed [47].

Leidheiser and his group advocated that all coating/steel de-adhesion by water is determined by the strength of the interface to mechanically resist water from forming multilayers at the interface [75]. They proposed the de-adhesion mechanism by water to have several stages, starting with water moving through the coating, either through pores or bulk coating. Next, water reaches the interface. Here it starts to accumulate in regions of weak adhesion between the coating and the metal substrate, while stresses in the coating will permit a lateral spreading, see Figure 5.
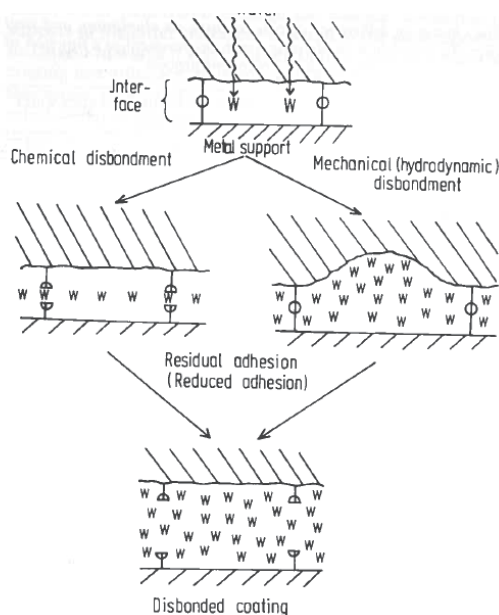
Figure 5: The two mechanisms proposed as responsible for the loss of adhesion due to water present in the coating and at the interface. Leidheiser proposed the mechanical disbondment mechanism to the right [75].

The mechanical driven de-adhesion by water can be counteracted by either treating the steel surfaces to create oxides with tailored surface energy properties that enhance adhesion [10, 100, 123, 124] or to manufacture coatings with adhesion promoting chemistry [87, 108].

Another strategy is to add roughness to the surface such that mechanical interactions are aided [47, 48]. They are believed to suppress water accumulation at the interface [48] and total rupture of bonds when accumulation has happened [47], thus increasing the hydrolytic stability of the coating at the interface.

In a recent study it was shown that for epoxy coating thicknesses below 250 μm, the time needed for water to reach the interface coincided with the time needed to loose adhesion, when mechanical interactions were excluded at the interface by polishing the substrates [120].

Oxygen is believed to be incorporated at the interface by diffusion through the coating at high enough rates to sustain e.g. the CD reaction [16]. However, it is believed that the incorporation also happens by diffusion along the interface from defects. The diffusion rate of oxygen studied on 80 μm thick coated steel samples with a NaCl covered defect, was found to 4.4×10^{-8} cm^2 s^{-1} for transport through the coating, while it was calculated to 10^{-5} cm^2 s^{-1} along the coating interface [15, 83, 112]. The results were suggested to indicate that oxygen diffusion to the disbonding front may happen along the interface close to coating defects, and through the coating further away from defects. See Chapter 3.3 for information about the effect of oxygen on the coating/steel oxide/steel interface stability.

3.2   Transport of hydrated ions along the interface

The transport of hydrated ions is regarded as an important piece in the puzzle of the electrochemical disbonding of coatings. Corrosion processes underneath coatings have been found to mostly propagate by the formation of a galvanic cell with the separation of the anode and cathode. In this cell, electrons are transported through the steel or via a metallic connection, and ions are carried by the electrolyte to complete the electrical circuit of the cell. While water and oxygen may be transported through organic coatings by diffusion, the transport of hydrated ions is recognised to be mainly along the coating-steel interface, starting from locations of defects in the coating [82, 84, 87], and for most coating/steel systems, to be the rate determining step. In later years it has been shown that ion migration in an electrostatic field along the coating/steel interface is dominant even in extremely oxygen deficient humid atmosphere [121, 126].

The ionic mobility may be dependent on the initial structure of the steel-coating interface and the structural changes to it caused by water ingression i.e. swelling of coating [10], and the resulting wet de-adhesion.

3.3 Cathodic disbonding

CD is a mechanism leading to the separation of a coating from the substrate, caused by the oxygen reduction reaction at the interface. This failure mechanism is of great relevance to coated steel under cathodic protection. CD happens however also without cathodic polarisation, and is also found on other metals like zinc [121, 126-128].

Several groups of scientists have studied the CD mechanism. Much of the work has been carried out with model coatings on polished steel at open circuit potential (OCP) with the SKP technique [2, 15, 109, 129]. As open circuit conditions are of most relevance for the work presented in this study, the emphasis will – if nothing else is mentioned - be on the OCP studies. It should be mentioned though that CD at OCP conditions is not principally different in nature from CD under cathodic polarisation. The main difference is the potential at the coating defect, and therefore the disbonding kinetics, while the adhesion loss mechanism and transport of reactants are the same.

From defects in the coating, CD will proceed depending on the degree to which the coating/substrate interface can serve as a cathode [10, 87, 109]. In such conditions, corrosion products at the defect may in the later stages reverse the pattern of electrochemical activity [89, 116], with rust serving as the cathodic reactant and new anodes being initiated underneath the coating.

The electrochemical reactions of interest involves the anodic oxidation of steel, see Eq. (6).

$$Fe \rightarrow Fe^{2+} + 2e^- \tag{6}$$

In humid air, the Fe^{2+} containing film initially formed, contains a small but increasing contribution of Fe^{3+} [130]. The initial inner layer of Fe^{2+} can be further oxidised by available oxygen to an outer Fe^{3+} layer of (hydr)oxide [12, 131, 132] of $FeOOH/Fe_2O_3$. The oxide oxidation, result in a steady decrease of Fe^{2+} states in the oxide, and the enrichment of the film by Fe^{3+} states, thus resulting in a more anodic potential [82, 87]. See Chapter 2.2.2 for information on the growth of the oxide. When an electrolyte containing NaCl ions is present at the defect, the anodic dissolution will proceed as described in Eq. (6) along with various reactions governing the dissolution and precipitation of corrosion products on steel in aqueous solution [133-135]. The reactions at the defect are beyond the scope of this study.

The primary oxidation agent in the system is oxygen, through the oxygen reduction reaction, see Eq. (7).

$$O_2 + 2H_2O + 4e^- \rightarrow 4OH^- \tag{7}$$

The reactions when combined, is the driving force in the CD process. The CD circuit consists of an anodic zone of defect coating surrounded by a cathodic coated area. Bare steel activates anodically according to Eq. (6). Intact steel-coating interface and the defect are set in electrolytic contact by a lateral ingress of hydrated ions from the defect, and the intact interface at the disbonding front serves as a cathode galvanically coupled with the anode at the defect. Cathodic oxygen reduction according to Eq. (7) will then accelerate. In parallel, also coupled to the anodic defect, Fe^{3+} oxide states are partially reduced (underneath the coating) to Fe^{2+} states [117, 133]. This increases the density of Fe^{2+} states [82]. The pH in the thin surface electrolyte layer increases as a consequence of the OH$^-$ produced by the oxygen reduction reaction in Eq. (7). As a consequence of the oxide phase transformations, the structure and morphology of the oxide is changed, and may contribute to the loss of adhesion [87, 133].

The adhesion loss is nonetheless recognised to be driven by the local alkalisation caused by the oxygen reduction reaction [4, 131, 136]. However, as will be shown in Chapter 3.3.2.2, the oxygen reduction reaction also results in the formation of aggressive intermediates as free radicals and peroxides. Several studies have shown that these intermediates may also be implicated in the CD mechanism [15, 112, 128, 137, 138]. It has been suggested that the free radicals will degrade the coating concurrently with the alkaline destruction of the coating/steel bonds at the interface, and that the resistance of the coating towards alkaline destruction and free radicals will determine the exact mode of disbonding [137].

Per definition, the CD front is found at the transition between delaminated and intact coating [15, 83, 112]. The disbonding front advances into the intact coating leaving behind disbonded coating. A schematic of the disbonding area has been suggested [139], see the disbonding front highlighted in red in Figure 6. The disbonding front is hence at the transition between disbonded coating and intact coating.
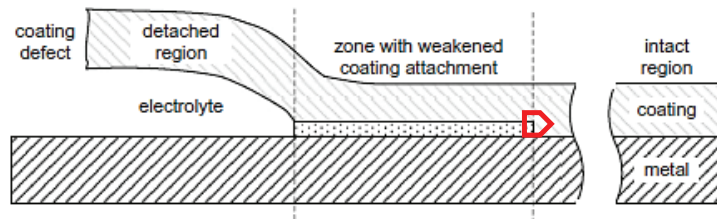
Figure 6. Schematic diagram of the cathodic disbonding mechanism. Figure from [139].

The potential difference between the disbonding front and the intact interface, is believed to be the electrochemical driving force for the ingress of ions and hence the propagation of the disbonding front [15, 83, 84, 112, 140-142].

3.3.1   Failure mechanism

Three different mechanisms have been suggested to explain the adhesion loss during CD, differing in the locus of failure. The importance of their contribution depends on the substrate, the coating and the environmental conditions [50].

- In the oxide: Structural and morphological changes of the oxide.
- In the coating: Chemical degradation of the coating.
- The interface: Breaking of adhesive bonds.

3.3.1.1   Structural and morphological changes of the oxide

Changes in oxidation state of the iron oxide will cause structural and morphological changes of the oxide. The oxygen reduction reaction occurring underneath the coating at the steel surface, oxidises Fe^0 and Fe^{2+} states at the surface [12, 82, 87, 131], and consequently the chemistry and structure of the oxide is changed, which may contribute to the loss of adhesion [87, 133].

During CD, the trivalent iron may slowly be reduced to divalent iron again [117, 133]. In aerated environments, the oxygen reduction reaction, Eq. (7), will be the prevailing reaction.

3.3.1.2   Chemical degradation of the coating

This type of failure occurs within the coating in the immediate vicinity of the interface [82], noted to leave coating residue on the steel surface [143]. The mechanism is suggested to involve a degradation of the binder by various processes: Alkaline bond-breaking caused by OH⁻ [144] has been seen in the case of polybutadienes, polyethylenes and epoxy esters [103, 145], or bond breaking due to oxidative attacks of the binder by aggressive intermediate products formed during the oxygen reduction reaction, as hydrogen peroxide and radicals [15, 82, 137]. Adding different radical scavengers to an epoxy model coating, was shown to reduce CD [137]. It has been suggested that the oxidative attack on the binder by radicals involves an attack on the most reactive functional group. For epoxies it may be the hydrogen atom on the secondary carbon atom situated in the alpha position to the oxygen in the ether bond, or nitrogen atoms in the tertiary amine bond [137]. The results from experiments with radical scavengers can however not be taken as conclusive evidence, as their addition is also expected to reduce the formation of OH⁻.

3.3.1.3   Interfacial failure with bond breaking

This type of failure occurs with no traces of coating remaining on the steel surface [35]. It is by several authors believed to be the most important mechanism for CD [82, 111, 143, 146].

Knudsen has provided experimental evidence for bond breaking caused by hydroxide ions solely, without the involvement of radicals [4]. Aluminium pigments were found to reduce CD significantly only when present in the first coating layer, in contrast to being applied in subsequent coat layers [136]. The pigments were found to corrode, and it was suggested that the reaction would buffer the interfacial electrolyte by removing hydroxide according to Eq. (8).

$$Al_2O_3 + 2OH^- \rightarrow 2AlO_2^- + H_2O \qquad (8)$$
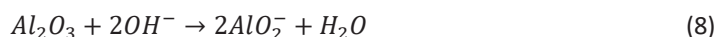
The oxide on the surface of the pigments reacts with hydroxide at pH higher than 9 [147] and this removes OH⁻ locally. However, the aluminium pigments will remove hydroxide even more effectively by alkaline corrosion under hydrogen evolution according to Eq. (9).

$$2Al + 2H_2O + 2OH^- \rightarrow 2AlO_2^- + 3H_2 \qquad (9)$$
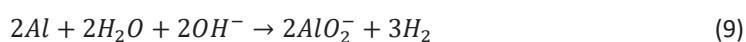
Another possible effect is that aluminium pigments act as an oxygen scavenger, hence they remove oxygen before it reaches the interface, by consuming it in the corrosion reaction in Eq. (10).

$$4Al + 3O_2 + 4OH^- \rightarrow 4AlO_2^- + 2H_2O \tag{10}$$
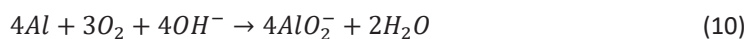
Knudsen's study strongly indicates that radicals are less involved in the breaking of interfacial bonds. Others have however argued that intermediates are sufficiently stable to be present at the interface together with hydroxides, and to cause more damage than hydroxide ions [110].

3.3.2   Key parameters

The cations and their mobility, the oxygen concentration and the potential, play an important role in the CD mechanism.

3.3.2.1   The cations and their mobility

A high ratio of the electrolyte's cation to anion has been found in disbonded regions, both on the disbonded coating and on the substrate [35, 121, 148]. The type of anion appears to have little influence on the rate of CD [87]. The mobility and transport of cations to the disbonding front controls the CD rate as long as the cathodic reduction reactions is not inhibited by electron transfer kinetics, as is the case with insulating conversion coatings on steel [11, 112, 149]. An inhibition of the oxygen reduction reaction will lower the potential at the intact coating/steel interface, hence decreasing the potential difference between this region and the disbonded region that makes the driving force for the ingress of ions and hence the CD mechanism [15, 87].

The mobility of cations along the coating-substrate interface has been found to be 2-5 orders of magnitude higher compared to the bulk coating, and it is therefore believed that cations are transported along the interface from defects [84, 117, 150]. Leidheiser suggested that although CD under open circuit is fed by cations transported only laterally in the aqueous film under the coating [148], they could also partially be transported through the coating when a cathodic potential was applied [151]. Later work has shown that the transport of ions through the bulk of various types of coatings is unlikely, unless there are pores or other defects in the

coating [85, 152-154]. In a long term study of epoxy coated steel under cathodic protection, it was found that transport of cations through the bulk of the coating resulted in blistering of the coating due to osmotic pressure caused by the NaOH formed under the coating [155].

A series of experiments on epoxy coated steel polarised to -0.81 V_{SHE} , confirmed that sealing *the defect* with epoxy glue stopped the CD [156, 157]. When sealing *the coating* with aluminium foil, the disbonding was slowed down but not stopped. It was concluded that cations are hence transported along the interface from the defect, and with this transport route closed, CD stops. When closing the transport route through the coating, CD is strongly inhibited but not stopped. Hence cations are still fed from the defect, while water and oxygen now also must be carried and incorporated along the interface. The observation of the disbonding progress to follow a parabolic kinetics, i.e. disbonded distance is proportional to the square root of time, also excludes transport of cations through the coating. This path does not depend on the distance to the defect [112].

The cations migrate to the disbonding front to ensure electroneutrality, i.e. to balance the hydroxide ions formed in the oxygen reduction reaction [18, 87, 102, 121, 126]. An increased potential difference accelerates the ion transport, while no incorporation of ions and hence no disbonding is seen if potential of defect and intact interface are inverted [15]. Therefore, decreasing the oxygen concentration will lower the potential in the region with the intact coating/steel interface, weakening the electric field and slowing down the ionic transport rate. The dependence of the disbonding rate on the type of cation has been documented in the sequence $Cs^+> K^+>Na^+> Li^+$ [15, 83, 112, 142, 158]. This is consistent with the sequence of the diffusion coefficients of the alkali cations in bulk electrolyte, and it was therefore earlier believed that ionic transport would also happen by diffusion. The bigger the hydrated cation, the slower the diffusion [112]. Diffusion coefficients for ion transport processes have therefore been calculated from CD studies both in air [112] and in inert atmospheres, based on the presumption that ionic transport happens due to diffusive processes [117]. In recent years Posner has nonetheless shown experimentally that cations are only transported by migration, even in inert atmospheres in the absence of a galvanic cell, and suggested it was due to excess of negative charge at the oxide surface [87, 121, 126]. Cations were found to migrate along the surface even on *bare* steel surfaces.

Cathodic disbonding produces an electrolyte filled gap between the disbonded coating and the substrate, where cations migrate with relatively low resistance, determined by the dimensions of the gap and the electrolyte concentration. Ahead of this region, the cations enter a high resistance intact coating/steel interface where the disbonding process is occurring [111, 158]. Here, the coating is at least partly still adhering. In any case, the interactions at the coating/steel interface affects the resistance against ionic migration along the interface and thus the CD rate. To reduce cation mobility, it has been suggested to either modify the coating for increased crosslinking at the interface [101], or to change the steel substrate by: 1) Adapting the polarity of the oxide to the polarity of the coating [98], 2) increasing roughness [31, 35, 37, 38], or 3) changing the surface texture such that the CD process has to propagate across peaks and texture lines [19].

The lateral ingress of ions in the CD mechanism is in addition to the importance for the CD mechanism, believed to enhance wet de-adhesion as well, as hydrated ions carry water to cathodic sites where the coating/steel bond is weakened by the cathodic oxygen reduction reaction [50, 102]. The smaller the cation, the more water molecules it will carry.

3.3.2.2   The oxygen reduction reaction

The prominent cathodic reaction on steel in aerated neutral or alkaline media down to a potential of -0.6 V_{SHE}, is the oxygen reduction reaction. At lower potentials, the hydrogen evolution reaction in Eq. (11) is expected to dominate.

$$2H_2O + 2e^- \rightarrow H_2 + 2OH^- \tag{11}$$

However, the ohmic potential drop under the disbonded coating and in the disbonding front measured by SKP is so high, that the oxygen reduction will be the only cathodic reaction under the coating, both at OCP and under normal cathodic protection potentials (-0.6 to -0.92 V_{SHE}) [148].

The oxygen reduction reaction may proceed in several steps either sequentially or concurrently [138], resulting finally in the formation of hydroxide ions, via specific types of

peroxides and free radical intermediates. The oxygen reduction reaction in Eq. (7), consists of several steps, producing aggressive short-lived intermediates as peroxides and radicals (denoted by $\bullet$) see below [123, 138]:

$$O_2 + e^- \rightarrow O_2^- \bullet$$
$$O_2^- \bullet + H_2O \rightarrow O_2H \bullet + OH^-$$
$$O_2H \bullet + e^- \rightarrow O_2H^-$$
$$O_2H^- + H_2O \rightarrow H_2O_2 + OH^-$$
$$H_2O_2 + e^- \rightarrow OH \bullet + OH^-$$
$$\underline{OH \bullet + e^- \rightarrow OH^-}$$
$$2H_2O + O_2 + 4e^- \rightarrow 4OH^-$$
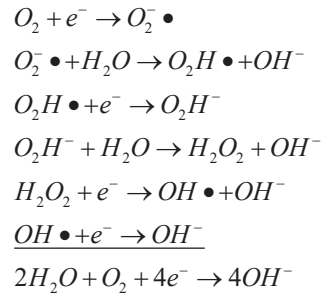
It has been shown that on bare steel without surface oxide, hydroxide is the only product from the oxygen reduction reaction, while on oxide covered steel surfaces, stable peroxide ions are always present [138].

Oxygen reduction is strongly inhibited on coated steel because the metal dissolution and transport of cations are strongly suppressed. A small amount of oxygen that diffuses through the coating, may however be reduced with local iron oxide oxidation as the anodic counter reaction [82, 87]. The oxygen reduction reaction pulls the potential of the intact interface to more anodic potentials, by oxidizing Fe^0 and Fe^{2+} states at the steel surface, as discussed above. This goes on until the process is slowed down and inhibited against further electron transfer by the passivating oxide layer [96]. Hence at intact coating-steel interfaces, an anodic potential will be measured, reflecting an inhibited metal dissolution with thicker oxide films of higher Fe^{3+}/Fe^{2+} ratio [111], see Figure 7.

However, if there is electrolytic contact between regions with intact coating/steel interface and regions with coatings defects, the inhibition of the oxygen reduction reaction is released with the formation of a galvanic element. At the defect, the anodic dissolution of steel is balanced by cathodic reactions happening at the coating steel interface as far underneath the coating as the hydrated ions have been incorporated and managed to make an electrolytic connection to the defect. The cathodic reactions will be the oxygen reduction reaction and partial reduction of oxide [82].
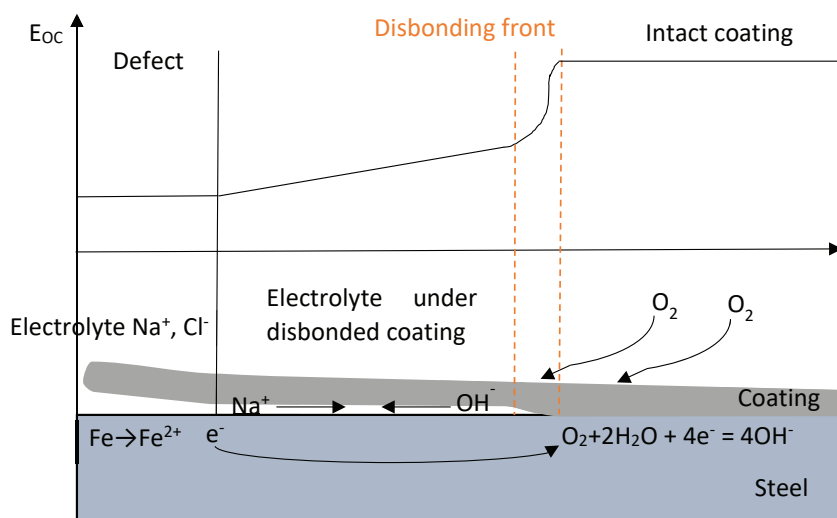
Figure 7: Schematic representation of the CD mechanism, where the different potentials reflect the kinetics for anodic dissolution at the defect and the oxygen reduction reaction at the disbonding front and under the intact coating. Figure adapted from [159].

The susceptibility to CD is markedly influenced by the oxide film [10, 123]. Disbonding rates are seen to depend on the oxygen reduction rate on the specific substrate [148]. To slow down the oxygen reduction reaction, it has therefore been suggested to apply insulating conversion layers e.g. a phosphate layer, or to reduce the density of Fe^{2+} donor states in the iron oxide layer by oxidizing Fe^{2+} to Fe^{3+} states [101]. It has been shown that the resistance of iron oxides, i.e. their semiconductor behaviour, is determined by the amount of Fe^{2+} cations in the oxide structure [123]. The increased presence of trivalent iron in the oxide film is not favourable to the oxygen reduction reaction due to reduced electronic conductivity of this film. A Fe^{3+}/Fe^{2+} ratio of 10 or more was shown to significantly decrease the oxygen reduction rate [101, 160].

Different surface treatments, e.g. non-conductive SiO_2 layers that inhibit the electron transfer and hence the oxygen reaction [11] , and active pigmentation of the coating [111] will also kinetically inhibit the oxygen reduction reaction

CD rates have also been found to decrease with decreased oxygen concentration [161] and oxygen partial pressure [15], correlating very well with theory addressing the importance of the potential difference between the disbonding front and the intact coating/steel interface on the CD rate. As explained above, the more the oxygen reduction reaction is inhibited, the

less positive the potential of the intact interface will be [111] and the less the potential gradient and the electrical field needed for ionic migration along the interface [87, 162].

3.3.2.3   Time dependence

The disbonding rates of model coatings on polished steel and electro galvanised steel, have been shown to depend on the square root of time [4]. This has been reported both for PVB [12] and epoxy coatings [18, 157, 163]. The square root dependency, also referred to as parabolic disbonding kinetics, has previously been misinterpreted to demonstrate that disbonding rates can be predicted by Fick's second laws of diffusion [61] and hence related to the interfacial cation mobility and transport rate, see Eq. (12).

$$\frac{\partial c_i}{\partial t} = -D_i \frac{\partial}{\partial} \left(\frac{\partial c_i}{\partial x} \right) = -D \frac{\partial^2 c_i}{\partial x^2} \tag{12}$$

c_i is the concentration of the component i, t is the diffusion time, x is the distance from a reference point and D_i the diffusion coefficient of the specific diffusing species.

However, in later years it has been showed that ion migration in an electrostatic field is dominant even in extremely oxygen deficient humid atmosphere [121, 126]. The progress follows parabolic kinetics, reflecting interfacial transport of ions as the rate determining step.

The disbonded distance X_{del} is then related to the time of electrolytic contact (t_{del}) and an initiation time, (t_i), by Eq.(13) [12]. Here, *k* is the disbonding rate constant.

$$X_{del} = k_{del}\sqrt{(t_{del} - t_i)} \tag{13}$$

By plotting disbonded distance against the square root of time and extrapolating to zero disbonding, it has been found that CD only happens after an initiation time, t_i [38, 164]. The initiation time for CD is understood as the time needed for diffusion of water and oxygen into the coating and establishment of the galvanic cell [16, 165]. The initiation time is seen to increase with increased coating thickness [148].

A transition from parabolic to linear disbonding kinetics has been proposed to be consistent with an interfacial cathodic process, most probably the oxygen reduction reaction, becoming the rate-determining step [131]. This is understood as decreased activation-controlled rates

of O_2 reduction at the substrate-coating, such that the oxygen reduction reaction is becoming rate determining.

A general power law of disbonding kinetics not assuming any specific disbonding mechanism, can be expressed as in Eq. (14) [113], where a is an exponent. See Eq. (14).

$$x_{del} = kt_{del}^{a} \qquad (14)$$

. The initiation time is disregarded. The equation can be written as in Eq. (15) giving a linear relationship between the logarithm of disbonded distance and the logarithm of time.

$$log(x) = log(k) + a * log(t) \qquad (15)$$

The exponent a may vary between 0.5 for a transport-controlled mechanism and 1.0 for a kinetically controlled mechanism. If the disbonding is proportional to the square root of time, the exponent is 0.5, indicating that the transport of hydrated ions at the coating/substrate interface determines the CD rate [8]. This has been reported both for PVB on steel [12] and PVB on electrogalvanised steel [111, 113, 166] but also for epoxy coatings on steel [18, 157, 163]. However, for an epoxy coating on blast cleaned steel the exponent was found to be 0.79 [4].

It is recognised that cathodic polarisation speeds up the disbonding process [4, 15, 17, 112] [157].

4 Effect of surface roughness and topography on interfacial stability

It was shown in the previous chapter, that the incorporation of water and oxygen at the interface as well as the transport of ions along this interface, leads to the breakdown of organic coatings with subsequent corrosion of the substrate. This chapter presents and discusses the effect of substrate roughness and topography on the ability of the organic coating to protect steel in humid air and corrosive conditions.

In this work, the term "*roughness*" will be used when addressing the height and length of the substrate profile, i.e. the effective contact area between coating and substrate, while the term "*topography*" will be used when referring to the geometry and arrangement of the interfacial peaks, usually understood as surface texture [167].

Surface roughness appears across many scales, encompassing 13 orders of magnitude from the kilometre-scale mountain peaks to the atomic-scaled bumps [168]. Roughness controls various mechanisms related to friction [169, 170] and adhesion [171-173]. In electrochemical studies it is observed that rough surfaces are more active [62, 63]. Anodic reactions are accelerated with roughness, and it is suggested that electrons become more available on a rough surface. It has therefore been pointed out that rough surfaces cannot be regarded as smooth surfaces that happen to be rough [21, 22]. The reason is not only the difficulties of measuring the true area of such surfaces – as roughness is present across so many scales - but also because of the modified energy of the surface molecules due to the topological configuration they take up. Therefore, it may be difficult to discriminate between chemistry and roughness [171]. However, results from studies having a fracture mechanical approach

on the coating/metal interface stability, suggest that the contribution from the roughness-induced adhesion dominates the total adhesion strength on the macro-level, over the interfacial contributions resulting from physical and chemical interactions [41, 81, 174].

In the heavy-duty coating industry, the roughness of the steel surfaces to be coated is increased by the addition of asperities measured on the micro-scale, e.g. by blast cleaning. The roughness of the surface is commonly described by traditional surface roughness parameters as Ra, the arithmetic roughness average distance for five sampling lengths within the measurement length l, Rz, the average maximum peak to valley distance for five sampling lengths within the measurement length l, and the peak density Pc as the number of peaks within a centimetre. See ISO 4287 and ISO 4288 for a detailed description of the roughness parameters [175, 176]. The first two parameters, Ra and Rz, represent the height of the surface profile.

According to the literature, the roughness and topography of the steel surface affects the interfacial stability by:

- Influencing wetting kinetics.
- Increasing the effective contact area at the coating/steel interface, thus i) offering more sites for bonds and ii) increasing the lateral path length that hydrated ions must overcome at the interface.
- The interfacial topography modifies the ability of the steel surface for mechanical interactions with the coating, thus affecting the interface's ability to withstand the initiation and propagation of electrochemical reactions.

The relationships were shown on a general level in Figure 1. In Figure 8 the various aspects and their relations are illustrated in detail, as they are understood by the author.

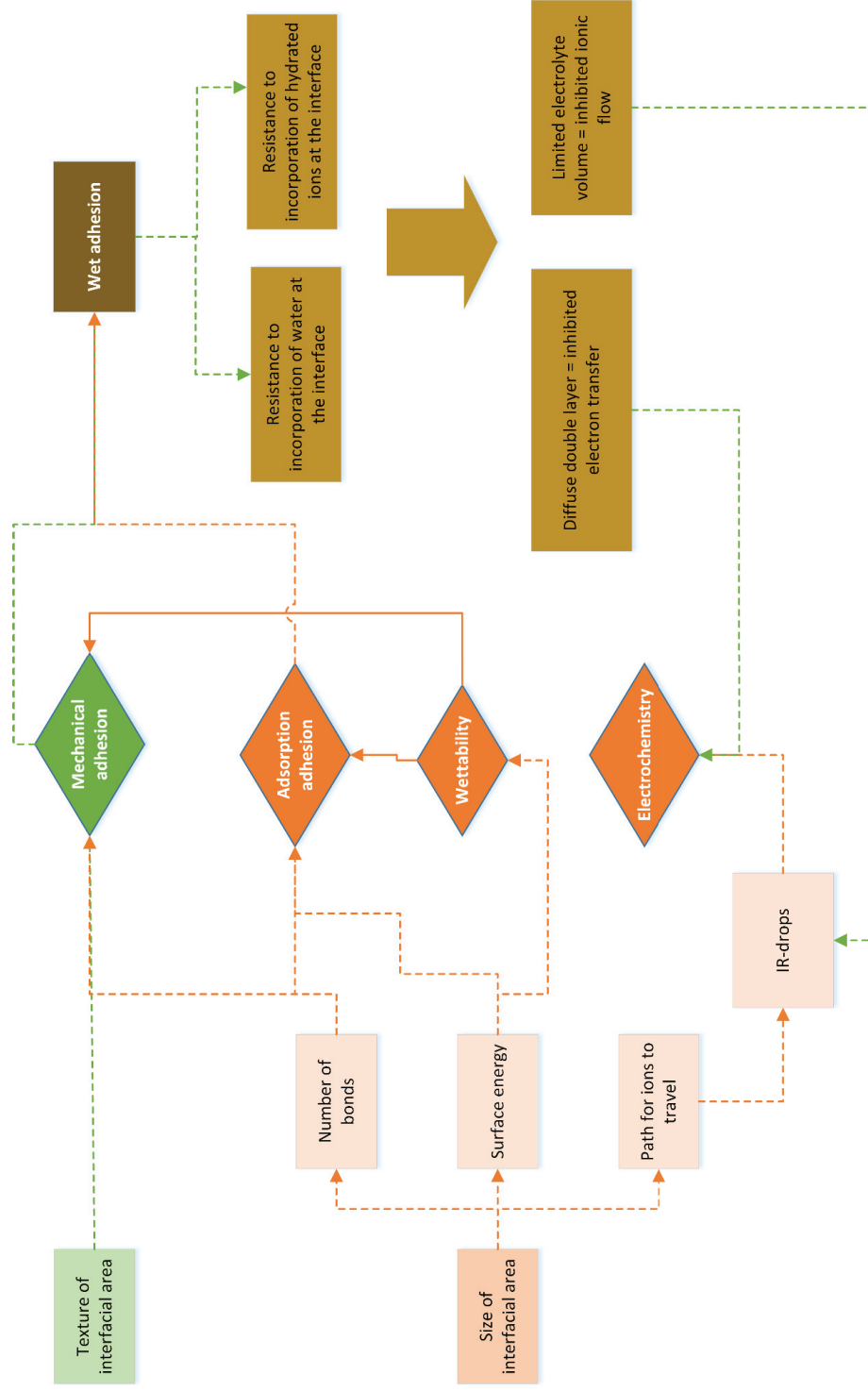Effect of surface roughness and topography on interfacial stability

Figure 8: The relationship between the texture and dimension of the interfacial substrate area and wettability, adhesion, and electrochemistry at the interface.

4.1 The interfacial area

First, increasing roughness, increases the interfacial area of the substrate. This affects all phenomena involving surface energies per unit area, such as the wettability of the steel surface and the work of adhesion. The work of adhesion, Eq. (4), and the surface energy terms discussed in Chapter 2.1.1, are energies per unit area. If the substrate is completely flat, there will be no problem to define the contact area. However, increasing the interfacial area by increasing roughness will increase the number of bonds and affect both physical and chemical interactions that are related to the unit area of the interface [36, 39-41]. In addition, as the number of irregularities for mechanical interaction increases, the increase will also lead to an increased contribution of mechanical adhesion [42, 43]. The relationship between topography and adhesion measured in adhesion tests, is still debated, as are adhesion tests in general. In one study, an increase in roughness was found not to affect dry adhesion while it increased the wet adhesion [177]. In another study, roughness was found to be less important for adhesion than texture [40].

Another acknowledged effect of the interfacial area size is on the electrochemistry at the interface. The effect of the actual length of the surface profile at the interface, defined by a tortuosity parameter, was analysed in CD studies [31, 35, 178, 179]. As the CD was found to decrease with increased interfacial profile length, it has been suggested that the effective ionic mobility along the interface is reduced by the more tortuous path [31, 35, 37, 38]. Therefore changes in the surface profile will alter the interfacial path and hence the kinetics of failure, if interfacial transport of ions is the rate controlling step [143].

4.2 The interfacial topography

Already in 1925 McBain and Hopkins suggested that mechanical adhesion makes an important contribution to the adhesion strength of joints [180], and it has in several studies been argued that the surface texture of the substrate is of more significance than the roughness values per se.

When roughness is added at a surface – and the effective contact area increases – it happens by the addition of specific asperities. The asperities develop friction forces at the coating/substrate interface, which will be determined by the specific structure and height of the asperities, see Figure 9. In the final example in the figure, also the mechanical strength of

the coating will contribute to the adhesion, since the coating cannot be separated from the substrate without breaking.
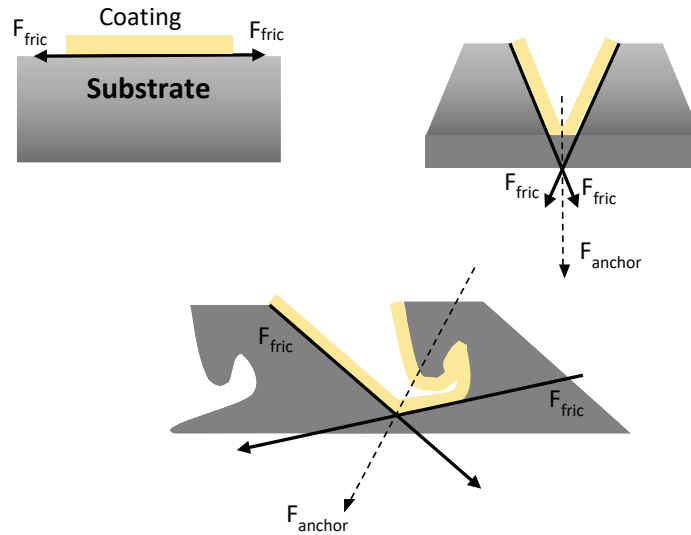
Figure 9. Sketch of the anchoring force F_anchor of a coating as function of the topography of the substrate. Adapted from [45].

The balance of friction forces acting at the coating/steel interface will determine the mechanical interlocking force, also called the anchoring force, or simply the mechanical adhesion force [45]. The effective contact area is in either case a key property, as it scales the contribution of friction forces to the total mechanical adhesion force according to the relationship in Eq. (16).

$$F_{mechanical} = F_{anchor} = \overline{\mu}\,\overline{P}R \tag{16}$$

where $\overline{\mu}$ is the mean friction coefficient related to the friction forces between the coating and the substrate and depending on the specific topography, R is Wenzel's roughness factor and $\overline{P}$ is the mean theoretical pressure needed to keep the coating from sliding off the substrate at a given inclination [44]. The relationship in Eq. (16) indicates that the mechanical interlocking force will increase with increased effective contact area.

Adhesion studies have shown that the topography of the substrate may divert the path of a crack away from the weaker interface and into the stronger coating [41, 43, 181]. Asperities may result in mechanisms that dissipate forces that otherwise would destruct coating/metal bonds [74]. It was suggested that sharp asperities at the interface may yield greater adhesion enhancement [181]. Abrupt changes in surface height are responsible for regions of high local *toughness*, due to better stress distribution [182].

The mechanical adhesion may thus contribute to the total amount of adhesion, according to Eq. (17).

$$W_{total} = W_0 + W_{Mechanical} \qquad (17)$$

Where W_0 is the thermodynamic work of adhesion, and $W_{Mechanical}$ contains the terms reflecting contributions induced by roughness and topography. These are dissipative contributions, such as plasticity and friction around asperities, and crack path diversion by these asperities [41]. In addition, the increased area also contributes to the mechanical work of adhesion. Contributions from mechanical interactions have been claimed to make up most of the total adhesion forces at the interface for an organic coating $W_{Mechanical} >> W_0$ [41, 81, 174].

As was explained above, mechanical interactions between the substrate and the coating will depend on the texture, and it has been suggested to distinguish between interlocking and hooking. It is suggested that only the irregularity of type a in Figure 10 will lead to mechanical interlocking, while for b the result is mechanical hooking and for c the adhesive strength will depend on the direction of the applied force [53].
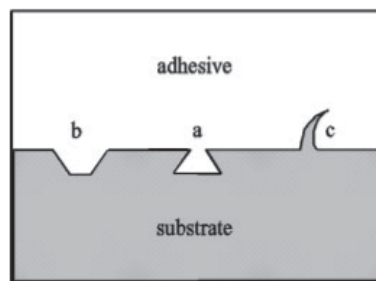

Figure 10: The three types of surface irregularities that can contribute in characterizing a surface as rough. Figure from [53].

In any case, it is important to consider the effect of water at the coating/steel interface on adhesion, as discussed in Chapter 3.1.

During exposure to a humid environment, molecular water can be accommodated at the surface either by a thermodynamic de-adhesion process (hydrolysis) or by a mechanical process [75]. In addition, under humid conditions the coating may swell with the ingress of water, which will add another factor in the weakening of the interfacial coating/steel bonds. It is argued that mechanical interactions at the interface will impede accumulation of water at the interface [48], but also to withstand total rupture of bonds and de-adhesion when water has accumulated at the interface and bonds are assumed weakened by the water [47]. The result is increased wet adhesion properties at the interface [48].

This will further promote a narrow electrolyte path along the interface, increasing the electrolytic resistance and the ohmic potential drop along the interface [183]. Increased resistance to accumulation of water at the interface is believed to retard the ingress of ions [121] and their mobility [86]. A high electrical resistance between cathodic and anodic sites along the interface slows down electrochemical disbonding mechanisms like CD [10]. The interfacial ingress of ions does, however, not require the incorporation of water at the interface or wet de-adhesion [121], although the opposite has been observed. In an inert atmosphere it was found that interfacial ion ingress resulted in the weakening of bonds, suggested to be caused by the water molecules carried by the hydrated ions [117]. It is generally acknowledged that hydrated ions will help in the de-adhesion of coating at the interface by an (electro)osmotic process [38, 50, 102, 159].

The lateral ingress of hydrated ions from defects is seen to be determining the longevity of the coating system on steel, although the initial required adhesion strength - measured in conventional adhesion tests - is achieved, as discussed in Chapter 3.3. The meaning is that although adhesion is important, it has to be evaluated in a larger context.

Experimental evidence has been provided for the role of mechanical interlocking to the CD mechanism: According to various studies a lack of mechanical interlocking results in low wet adhesion [28, 29, 47, 48]. Low wet-adhesion properties have been documented to affect CD negatively [109, 184]. On surfaces abraded with SiC paper in one direction, producing parallel abrasion lines, CD was found to progress faster parallel to the lines than perpendicular to the

lines [19]. Mechanical interlocking may play a key role for coating/steel stability, also during the early stages of CD the mechanism. The cathodic oxygen reduction reaction proceeds underneath intact coating, although slowly, in air atmosphere. During the oxidation, both structural and morphological changes in the oxide [87, 133], can lead to a weakening of the bonds long before the actual CD. Swelling of the coating due to absorption of water may have the same effect.

Also during other electrochemical disbonding mechanisms e.g. corrosion creep, mechanical interlocking may aid stability [185]. Higher level of corrosion creep was found on surfaces with rounded features in contrast to the ones with sharp irregularities at the surface [33]. On surfaces with ability for mechanical interlocking, disbonding decreased with 55% in comparison to surfaces with similar effective contact area at the interface without ability for mechanical interactions [29].

4.3 Summary on the role of surface roughness and topography on the coating/steel interface stability

Contributions on the molecular scale

The simplest theory of promotion of stability at the coating/steel interface due to roughening of the surface, is the increase in the surface area available for the formation of bonds, provided that the coating can completely wet the steel surface. The number of physical and chemical interactions will increase.

Contributions on the micro-scale

The increase of roughness will happen with the addition of specific asperities to the substrate surface. Asperities may result in mechanisms that dissipate forces that otherwise would destruct coating/metal bonds. As the density of high toughness regions is increased, the effective toughness of the coating/steel joint also increases.

The asperities will develop friction forces to the coating and will result in mechanical interactions and a mechanical adhesion force that scales up with the effective contact area at the interface.

Contributions on the macro-scale

Based on the discussed contributions on the lower scale, the effects on the macro-scale are:

- Mechanical interactions may impede molecular water from reaching the interface, and resist the destabilisation of the interface when hydrolysis has taken place. Mechanical interactions may help dissipate stresses when coating swells with water uptake.

- During the CD process, mechanical interactions add resistance against the lateral ingress of hydrated ions. It also adds stability when hydrated sodium ions transport water to the interface, thus causing destabilisation by an (electro)osmotic effect. Mechanical interactions help stabilise the interface supressing hence complete bond rupture.

- Mechanical interactions add resistance against bond rupture caused by voluminous corrosion products spreading from the defect in atmospheric conditions at open circuit in electrochemical disbonding mechanisms as corrosion creep.

- Mechanical adhesion is scaled up by the effective contact area.

5 Methods and materials

This chapter presents the methods and materials used in this study. Detailed description of preparation of the samples and the test methods are documented in the appended conference papers and journal articles and will not be repeated here. However, certain decisions were made on the coating types and the test methods employed that will be addressed in closer detail here.

In addition to field testing, there are in general two main laboratory approaches when studying the long-term stability of coatings. Either one can use standardised accelerated test methods where coating systems are exposed under specified aggressive conditions, or to use sensitive in-situ techniques for investigating the samples during exposure. The latter approach often requires the use of simplified model systems in order to have more rapid degradation, while the former approach is specifically developed for investigating state-of-the-art industrial coating systems. The two approaches may also be combined, e.g. by analysing samples from accelerated tests with the sensitive SKP technique [186, 187].

In this work the effect of topography on the stability of the coating/steel interface has been studied with different methods, see Table 2.

5.1 Overview

In the work reported in Paper I, an epoxy paint system of several layers - applied on either laboratory grit blasted or machined steel surfaces - was subject to the accelerated corrosion test described by ISO 12944-9 [188]. See Chapter 5.2.1 for information about the blast cleaning method, and Chapter 5.2.2 about the machining methods. The epoxy coating system

and the application are presented in Chapter 5.3.1, while the accelerated test method is presented in Chapter 5.4.1.

In the work reported in Paper II and III, a model coating was applied on steel surfaces either grinded or laser structured, and the coating degradation was studied by the in-situ SKP technique. The composition of the bare steel surfaces was analysed by XPS. See Chapter 5.2.3 for information about the laser structuring method. The model coating is described in Chapter 5.3.2, while the SKP technique is briefly reviewed in Chapter 5.4.2.

In Paper IV, degradation of commercial epoxy coatings on industrially machined or grit blasted steel surfaces is reported. The coatings were applied by industry partners.

For Paper V, surfaces were machined by industry partners or grit blasted either in the lab or by industry partners. Paint application with two-component epoxy mastics was performed in the lab.

Paper IV and V (conference papers) present initial testing for benchmarking coating performance on machined steel relative to state-of-the-art blast cleaning. The accelerated cyclic ageing test method described by ISO 12944-9 [Ref] and the CD test described by ISO 15711 were used [189]. In addition, adhesion tests were performed, pull-off according to ISO 4624 [190] and cross-cut according to ISO 2409 [191]. In Paper IV, the coated samples were subject to impact toughness tests as well, according to ISO 6272-1 [192].

Table 2. Summary of pre-treatments, coating types and tests employed for each published, or submitted, research paper.

Paper	Pre-treatment	Coating	Test methods and characterisation
Paper I	Laboratory machined Laboratory blast-cleaned	Epoxy mastic Laboratory paint-application	ISO 12944-9 Contact angle
Paper II	Laser structured Grinded	Model coating Laboratory paint-application	In-situ SKP CD XPS
Paper III	Laser structured Grinded Electrochemical reduction of oxide	Model coating Laboratory paint-application	In-situ SKP study of oxidation and CD XPS
Paper IV	Industrially machined	Industrial paint-application	ISO 12944-9 ISO 4624

(Conference paper presented at Nordic Corrosion Congress 2015)	Industrially blast-cleaned		ISO 2409 ISO 6272-1
Paper V (Conference paper presented at CORROSION 2016)	Industrially machined Industrially and laboratory blast-cleaned	Laboratory paint-application	ISO 12944-9 ISO 15711 ISO 4624 ISO 2409

5.2   Steel surface preparation

5.2.1   Blast cleaning

Blast cleaning is a widely used method for cleaning and producing roughness on a steel surface before coating application. As this method is the standard industrial method for adding surface roughness to steel, much of the literature on blast cleaning relevant for the CD mechanism has already been reviewed elsewhere in this document. Nonetheless, it is to be noted that the method has been under discussion in the coating industry with regards to the combination of parameters necessary to achieve the preferred surface roughness, e.g. blasting media type, particle size and velocity [49, 193]. A thorough review of industrial blast cleaning is presented by Momber [194]. In this context it has been suggested that the optimal blasted steel surface profile has a profile height, Rz of 50-75 µm, with a peak density of 40-60 peaks/cm. The roughness needs however to comply with the specific coating system chosen.

The laboratory blast-cleaned surfaces were grit blasted with aluminium oxide (Al_2O_3) of various sizes between 0.2 – 1.0 mm, in an in-house cabinet. Based on a collective experience, the nozzle was held at 45 ° angle and 5-10 cm above the surface of the sample, producing highest uniformity of surface roughness. The grit blasting process generated surfaces with a random distribution of irregular cavities and coarse morphologies with undercuts. Surfaces with Rz between 27 to 48 µm were obtained, see Figure 11.

The industry partners performed grit blasting to Sa 2.5 and medium roughness Rz of 50 – 75 µm, according to their in-house specifications, generally following requirements in ISO 8501-1. Blasting media and procedures were not specified or reported.
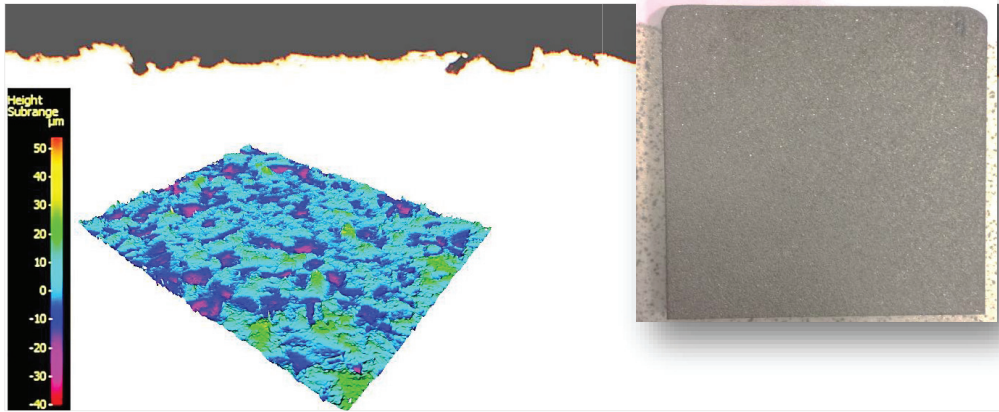
Figure 11. Optical microscope image of cross section of a grit blasted example sample, with a 3D images (left) of the surface area scanned by focus-variation with an Infinite focus microscope (IFM). The colours indicate the level of roughness, see the scale bar. In the upper right corner, a top view image of the surface.

5.2.2   Machining

Machining is a manufacturing technology heavily implemented in the industry for controlled removal of material in what is now called subtractive manufacturing. Some of the reasons that make machining commercially and technologically important are that machining: i) Is applicable to most materials, ii) can produce a variety of geometries to a part, iii) can achieve closer tolerances than most other processes, and iii) can create good surface finishes [195]. Steel components utilised in structural as well as non-structural applications therefore often undergo machining.

The laboratory machined surfaces for this study, were produced by face turning and face milling, which are both commonly used machining processes by the industry.

Face turning is a turning process where a single-point tool removes material from a rotating work piece, by moving perpendicular to the axis of the workpiece as seen in Figure 12 [195]. It is not restricted to cylindrical profiles.
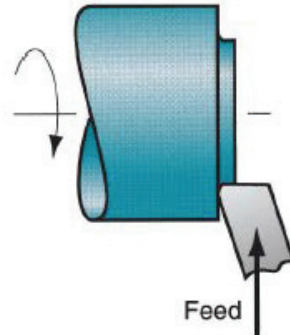
Figure 12: The face turning process achieved by a single-point tool that moves perpendicular to the axis of a rotating work piece. Figure from [195].

Face milling is a process where a rotating multiple-edged cutting tool is moved over a fixed surface, along a particular direction and angle of the axis of the work surface as seen in Figure 13 [195].
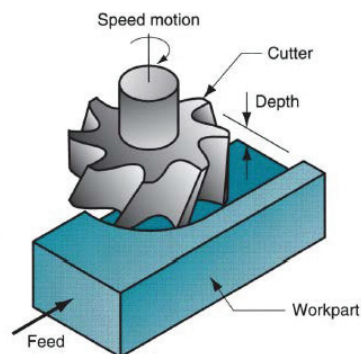
Figure 13: The face milling process where a rotating multiple-edged cutting tool is moved over a fixed surface. Figure from [195].

The parameters were chosen carefully with the intention of creating surfaces with a variation of Rz values, and comparable to the ones found on surfaces after grit blasting. The diameter of the milling cutter was 80 mm. The feed in the milling operation was in the range 0.35-0.73 mm/tooth, and in the range 0.15-0.75 mm/rev in the turning operation. The nose radius of the cutting edges used to produce the samples were 0.2 mm with the exception for one of the

surfaces, where the nose radius of the cutting edge was 0.4 mm. Two types of periodic surface profiles were produced by this combination of machining parameters: 1) Surfaces with a periodic distribution of peaks triangular in profile and 2) surfaces with a periodic distribution of rectangular, tilted peaks. See Figure 14. The roughness Rz on surfaces patterned with periodic triangular peaks was measured to be in the range 7–252 µm. Surfaces patterned with periodic rectangular, tilted peaks were in the range 224–683 µm.
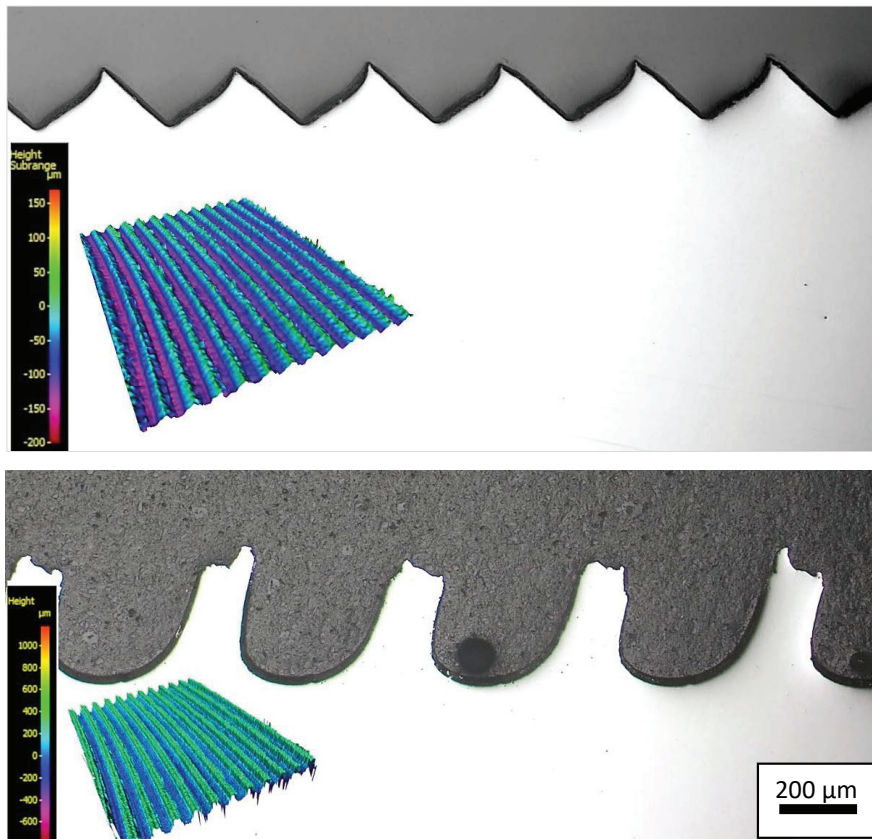
Figure 14. Optical microscope images of cross section of laboratory (experimentally) machined example samples, with 3D images (left) of the surface area scanned by focus-variation with an optical Infinite-Focus Microscope (IFM). The colours indicate the level of roughness, see the scale bar.

5.2.3   Laser structuring

Laser machining is a method widely employed for modification of surface topography, either for hydrophobic surface fabrication [196], for increase in active surface area of electrodes

[197] or for adhesion enhancement before coating [45]. Ultrafast laser structuring enables cold ablation and offers the possibility of contactless rapid manufacturing of functional designs with high flexibility and process reliability [197, 198]. It also allows for production of a uniform and homogenous surface texture.

A laser equipped working station can be seen in Figure 15.
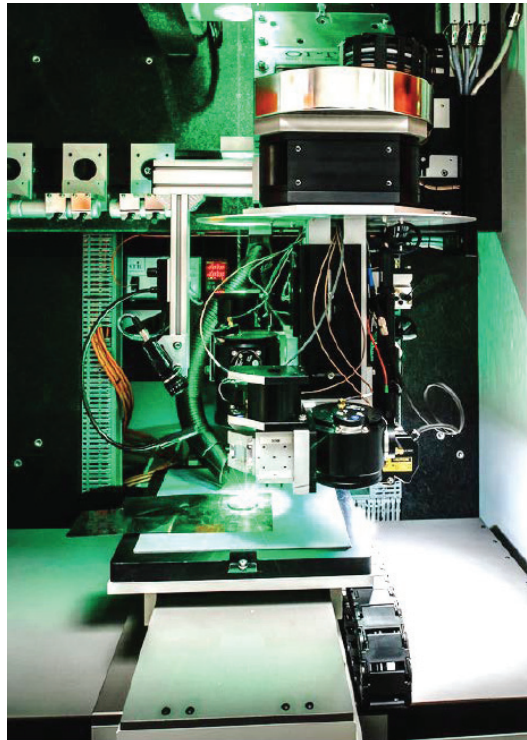
Figure 15: Micromachining workstation equipped with a tuneable short pulse fibre laser [199].

A typical drawback of the laser cutting method is the production of a heat-affected zone (HAZ). During the laser processing, laser parameters such as the laser pulse duration τ affects the thermal diffusion into the surrounding material, as described by Eq. (18).

$$\delta_w = \sqrt{4\kappa \cdot \tau} \tag{18}$$

where δ_w is the thermal diffusion length and κ denotes the thermal diffusivity of the material [197]. This issue has been addressed by developing ultrafast lasers, such as femtosecond (fs)

lasers with pulse length τ in femtosecond (10^{-15} s) range. Other ultrashort laser pulses are in range of the picosecond (10^{-12}). In the case of femtoseconds lasers, the thermal diffusion into the material can be almost ignored [200]. Pulses of 350 fs have been used for cutting sheet lithium electrodes, which gave a thermal diffusion length smaller than 0.5 nm [197]. However, the heat accumulation can be very high locally, scaled up by the laser repetition rate (V_{rep}) [201]. In the work presented here, femtosecond lasers with 350 fs and 380 fs pulse durations were used for structuring the steel surface. Within a surface layer of a few nm, a temperature rise in the order of 1000 K might be expected [202]. Together with the presence of oxygen, the process resulted in thermal oxidation in the 3 nm of the outer steel surface.

The structuring was performed at the Nano Micro Facility at Karlsruhe Institute of Technology in Germany (KNMF). The cooperation was initiated after applying for access at the facilities through an open call for proposals. Our objective was to produce structures that would enable us to evaluate the importance of structure height Rz and shape, and hence the effect of increase effective contact area at the interface, as well as the contributions from mechanical interlocking, on the stability of the coating/steel interface. A cross section of the specified structures are shown in Figure 16.
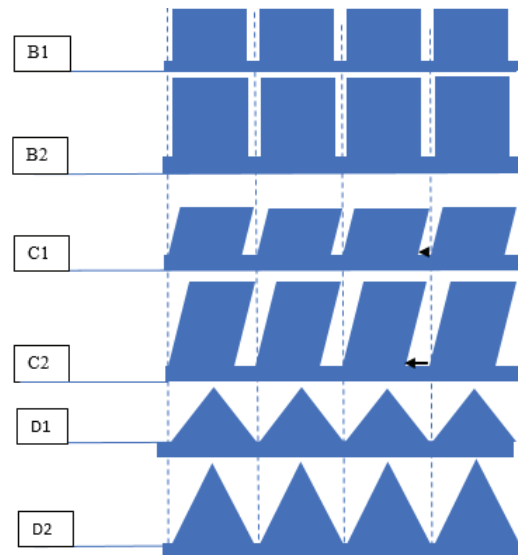
Figure 16. The structures we applied for to produce at KNMF with ultrafast laser structuring.

The peaks were proposed to have the height Rz=25 µm and Rz=50 µm. The C type peaks were especially interesting in this respect, as the tilted peaks may offer additional interlocking according to Figure 9 and Eq. (16).

During the production of the samples, it became apparent that the specified sample structures were difficult to produce by the lasering process. Finally, the surfaces shown in Figure 17 were produced. The C1 samples were not possible to prepare within reasonable budget limits and therefore cancelled.

The laser patterning consisted of a series of equidistant and uniform lines of peaks and grooves with the specified shapes, see Figure 18.

100 µm
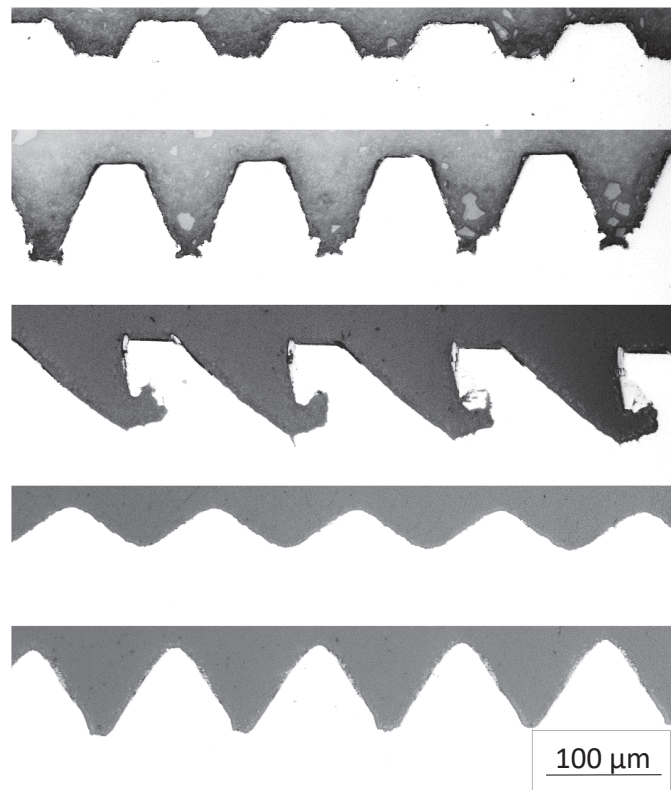
Figure 17. Optical microscope images of cross-sections of the surfaces B1 and B2, C2 and D1 and D2 in that order. Surface C2 was simply called surface C in the papers submitted for publishing.
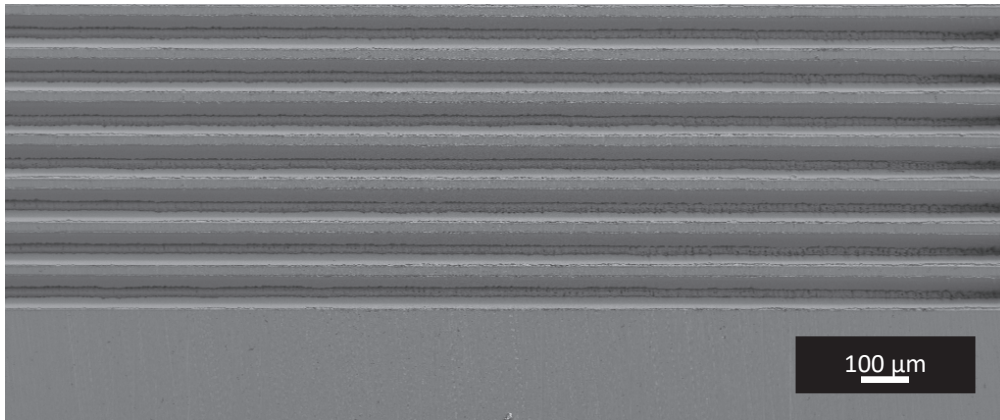
Figure 18. SEM micrograph showing plan-view of the laser structured B2 surface. The equidistant lines produced by laser structuring gives a periodic pattern of peaks at specified shape and height Rz.

5.3 Coating types

5.3.1 Epoxy coating

Epoxy based coatings are commonly used for corrosion protection of steel, as they provide very good adhesion as well as high resistance against chemicals, water and aggressive ions [4, 103]. Commercial epoxy coatings are typically chemically cured products, by mixing the resin with a curing agent immediately before application. The base of solvent-borne epoxy resins is most often a bisphenol A or bisphenol F [103], while the most common curing agents are amides, amines or phenols.

The active functional group in the resin is the epoxide ring, which is opened by the curing agent in the cross-linking reaction. The molecular weight of the epoxy resin affects its characteristics, see Table 3 [203]. Smaller molecules have the possibility for a higher crosslink density, resulting in lower flexibility but improved chemical resistance. The bonds between the epoxy binder and steel is suggested by Nakazawa to occur mainly by chemical bond-formation between surface oxide and the oxygen atom in the phenoxy group. The bonding happens via a dissociation between the phenoxy oxygen and carbon in the epoxy, to give the oxygen-iron bond [204, 205], see Figure 19. In this model, the phenoxy group is directly involved in the interfacial bonding mechanism and the energy varies with the type of surface oxide present.
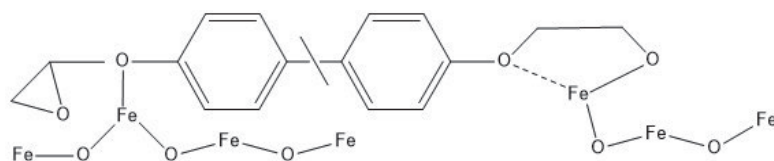
Figure 19: Mechanism of epoxy adhesion to iron oxide, by the involvement of phenoxy oxygen.

This theory goes against another acknowledged binding mechanism that involves the creation of hydrogen bonds (secondary bonds) to hydroxy groups in the surface oxide, see Figure 20 [76, 124].
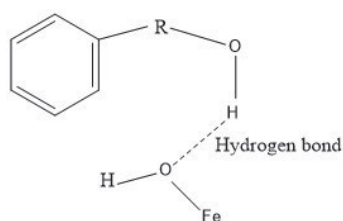
Figure 20: Mechanism of epoxy adhesion to iron oxide surfaces, by hydrogen bonding.

Table 3: The effect of molecular weight of epoxy resins on its characteristics. Adapted from [203].

	Effect of increasing epoxy resin molecular weight
Wetting	Increases
Adhesion	Increases
Crosslink density	Decreases
Solvent resistance	Decreases
Chemical resistance	Decreases
Impact resistance	Increases
Flexibility	Increases

The epoxy coating used in the work presented here, was a commercial two-component polyamine cured epoxy mastic coating specially designed for surfaces with poor surface preparation, a so-called surface tolerant coating. It can be used as primer, mid coat, finish coat or as a single coat system in atmospheric and immersed environments.

5.3.2   PVB coating

Poly(vinyl butyral-co-vinyl alcohol-co-vinyl acetate) (PVB), is a non-toxic transparent coating that is mainly composed of vinyl butyral with hydroxyl and acetate groups. The resin is mainly used on laminated glass where it exhibits good adhesion, preventing glass splinters from flying if the glass laminate is broken in accidents [206]. The chemical structure is shown in Figure 21 [206].
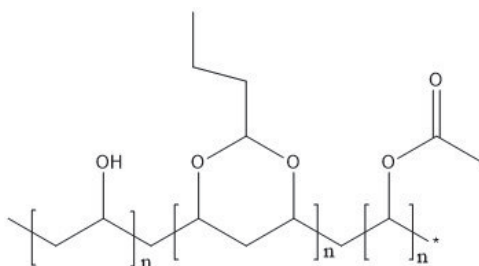
Figure 21: The chemical formula of poly(vinyl butyral-co-vinyl alcohol-co-vinyl acetate) (PVB) [206]. The alcohol is seen to the left, the butyral in the middle and the acetate to the right.

PVB is, however, also a widely used as a model coating matrix for fundamental corrosion investigation [108]. The use of this model system is well recognised for in-situ studies, including CD mechanism studies with the SKP [12, 13, 38, 131, 159, 207-209], and studies of the effect of water on adhesion [210]. In most of these studies the coating has been applied with a draw-down bar in a thickness between 30-40 µm. Studies of disbonding kinetics have, however, also been performed on 1-5 µm thin spin coated PVB layers [127, 128, 211, 212].

PVB has also been used to study interfacial degradation, and to correlate accelerated test results to field performance [146, 213]. The PVB coating is useful for coating degradation studies due to its relatively weak wet adhesion that allows for rapid assessment, combined with relatively good barrier properties. Compared to epoxies, PVB is a poor barrier against water and oxygen.

The CD of PVB has been shown to be controlled by cation migration along the interface [159], and failure of the coating-metal bond is proposed to result from the increase alkalinity at the interface in combination with the increased electro-osmotic pressure [38, 159]. The migration of sodium ions to the location of OH- production exerts an (electro)osmotic pressure that

tends to force off partially disbonded PVB. The electro-osmotic factor on the CD mechanism, has been proposed to be effective for all kinds of coatings [50]. Hence, the disbonding mechanism of the model coating is comparable to that of macroscopic thick polymers [214].

While there may be some controversy about whether results on model coatings are relevant for commercial coatings, it is acknowledged that in-situ investigation of interfacial coating degradation provides unique results on a mechanistic level, and that reducing the number of parameters enables the study of individual parameters [82, 83]. The findings in ex-situ failure analysis can then be understood. That implies that everything from metal composition, oxide film, interface topography and coating composition must be controlled and kept as simple as possible [215].

According to Figure 21, the PVB molecule has both hydrophilic groups (hydroxyl, butyral and acetate) and a hydrophobic vinyl chain. The hydrophilic groups can interact with the oxide/hydroxide on the steel surface. A relationship between surface oxide chemistry and adhesion strength has been demonstrated [10]. The coating employed in this study contains 88 % w/w vinyl butyral, 11% w/w hydroxyl and 1% w/w acetate and was delivered by Sigma Aldrich.

5.4   Test methods

5.4.1   Accelerated tests

The most reliable method for testing the protective properties of organic coatings is to perform field exposures in environments that are representative to operating conditions [216-218]. This is time consuming, as the coatings are designed to withstand the corrosive environment and the degradation may take years. In addition, results from field tests may have poor reproducibility, since rain, sun irradiation and sea water spray differ from place to place and even from year to year in same locations [146, 219]. Still, field testing is a vital part of coating development, coating selection and studies of degradation mechanisms, and field test sites are found all over the world.

Accelerated tests offer the opportunity of rapid results and have therefore been developed by coatings manufacturers and scientists to simulate long-term coating degradation. There is a wide range of different types of accelerated tests available, and usually several variants of

each type. For the evaluation of atmospheric corrosion protection, there are several salt spray tests such as ISO 9227 [220] and ASTM B-117 [221], and cyclic corrosion tests such as ISO 12944-9 and ASTM D5894 [222]. For CD testing there are more than 20 international test standards [223]. To identify the proper method for a specific application, knowledge beyond the information given by a specific test standard is required [224].

Selection of protective coating systems for offshore oil and gas installations on the Norwegian Continental shelf is mainly done according to the NORSOK M-501 standard [225]. There is a requirement for pre-qualification testing which is done according to ISO 12944-9 [188]. This is a cyclic wet/dry corrosion test, widely used for testing the performance of marine and offshore coatings, and found to have a certain correlation to field performance [217, 218], see Table 4 for description of the test cycle.

Table 4: Description of ISO 12944-9 test cycle [188].

Day 1	Day 2	Day 3	Day 4	Day 5	Day 6	Day 7
UV/condensation — ISO 16474-3			Neutral salt spray — ISO 9227			Low-temp. exposure at (-20 ± 2) °C

A 50 mm long and 2 mm wide scribe is machined down to the steel substrate on the test panels with dimensions 150 x 75 x 5 mm to initiate corrosion. The test primarily evaluates the resistance against corrosion creep and chalking, although cathodic disbonding sometimes is also observed. Blistering, cracking or penetration of rust will also be considered as a fail result.

A risk with accelerating is that they may change the corrosion mechanisms compared to real environments [186, 218]. The accelerated tests are inducing an ageing of the coating with different acceleration factors and introduce hence possible changes in corrosion mechanisms. Another drawback is the repeatability and reproducibility issues observed with such tests [226]. Last but not less important, is that results from accelerated tests only offer information about the averaged global response of the coating and provide therefore only data about the overall performance of the coatings. As multiple degradation processes occur simultaneously during such tests, they provide no information about degradation mechanisms. Detailed

information on the failure mechanism are better studied by in-situ methods that allow to analyse the individual degradation mechanisms separately [125, 215].

In addition to the accelerated test methods mentioned, there are several electrochemical techniques for the study of the corrosion resistance and stability of coated metals. There have been several reviews of these techniques, and a detailed description is outside the scope of this work. It may however be mentioned that among the direct current (DC) techniques, one can measure the OCP, E_{OC}, by potentiodynamic polarisation according to ISO 15711 [189]. A widely used alternating current (AC) technique is electrochemical impedance spectroscopy (EIS). In general, these techniques measure the global response of the coated metal. From the results you may deduce that defects are present, but you cannot localise them or study the effect they have on the surrounding coating. One of the main drawbacks of EIS, is that the separate impedances of the coating and the coating/metal interface are not determined. There may be a strong impedance against ionic transport through the coating, while the impedance of the interface is still unknown [88]. In the CD mechanism, ions are transported along the interface, which is impossible to detect by EIS. Only local techniques, such as the SKP, give information about the performance at localised defects, and the local potential distribution at the interface.

5.4.2 *The scanning Kelvin probe technique*

An overview is given here on the background and theory for this technique. For a detailed review, the articles referred to below will be helpful.

The SKP is a sensitive tool to determine the electrochemical conditions at the coating-steel interface [9, 109, 121, 126, 141, 210, 227-233], and to evaluate in-situ the electrochemical disbonding mechanisms on coated steel [2, 11, 15, 82-84, 111-113, 117, 142, 234]. It is however also employed in ex-situ studies, for quantification of the disbonding behaviour acquired in other types of tests [19, 146, 187, 213, 219]. The instrument has been used as a reference electrode and the technique has been applied also for electrochemical studies of atmospheric corrosion of bare and coated metals [140, 141, 235-237] and as a tool to characterise the redox state of surface oxides [101]. The reason it has become such a valued technique in corrosion studies, is that it allows to measure highly localised the electrochemical activity of a metal, through insulating dielectric layers of organic coatings up to several

hundred of microns thick [186, 187] or through ultra-thin layers of electrolyte. This is done non-destructively and without touching the surface.

The SKP technique belongs to the group of scanning probe microscopy (SPM) techniques [238]. Both the SKP and the Scanning Kelvin Probe Microscope (SKPFM) allow for surface potential or work function measurements. The lateral resolution of the SKPFM is on the nm scale, while it is on the µm scale for the SKP and usually in the range of 50-250 µm. However, the SKPFM potential mapping on coated metals is a difficult method to apply in-situ and therefore mostly performed ex-situ. The measurements are often significantly influenced by sample topography and the analysis therefore requires careful interpretation. In SKPFM, the signal is expected to depend strongly on the tip to sample distance [239]. In addition, the resolution is in many cases too high for studying corrosion processes, but it is well suited for studies of the effect of submicron particles on corrosion, as encountered on aluminium. The differences between the SKP and the SKPFM have been thoroughly discussed elsewhere [239-241].

The drawback of the SKP technique is that it requires considerable efforts in sample preparation and conditioning for reliable measurements. It is also to be noted that although no commercial SKP today based on the Kelvin technique gives nanometric resolution, there have been attempts to develop high resolution SKPs [242].

5.4.3   The study of electrode potentials by the SKP technique

The technique has its background in the discovery of the "contact electrification" of metals made by W. Thomson, the later Lord Kelvin, in the 19th century [230]. Even if many of the terms explaining this phenomenon can be related to electrochemistry, much of the theory refers to the electronic properties of metals. The correlation between electrochemical and electronic properties is not always straight forward, but approximations exist [243-245].

The SKP technique in general, is based on the fact that a potential difference exists *and is measurable* on the outer surface of two metals that have been electrically connected but are *separated* by a small gap, see Figure 22.
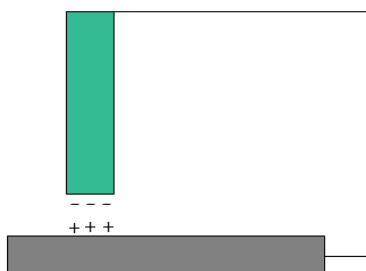
Figure 22: The contact potential difference between metals electrically coupled but separated by a small gap.

This potential difference is present because conductive metals, when unconnected, will have electrons at different Fermi levels (the energy level of electrons in conductive metals) [242]. At the moment of connection, the electrons will distribute themselves in such way that thermodynamic equilibrium is established, and the Fermi levels equalise.

The direction of the electron flow during this equilibration, is determined by the work function, Φ. The work function is defined as the energy required to remove one electron from the Fermi level within the bulk material, to a place "right outside" where the electrons are not affected by chemical interactions, usually considered to be at ≈ 10 nm and referred to as an energy level E_{vac} [245, 246]. A lower work function can be regarded as an increased tendency for electron transfer. The work function is a fundamental property of materials, and is found to be determined by the top few layers of atoms, hence it depends to a large extend on the surface conditions [247]. However, any changes in structure, composition and contamination or any subtle alteration of surface properties, will be mirrored by a change in the work function of the metal under study, and detected by the SKP as a change in the contact potential difference [9, 62, 124, 231, 233, 247-249].

When the materials have reached the same Fermi level, the difference in work functions within the materials will still be effective, so the electric potential outside each metal does not change. This induces the appearance of an electrostatic field that builds up in the gap between the metals that are electrically connected. The potential of this field is the contact potential difference, V_{cpd}, which reflects the difference in the work function between the metals [242]. This concept is utilised when the tip of the SKP scans over a metal surface, see Figure 23 [250].
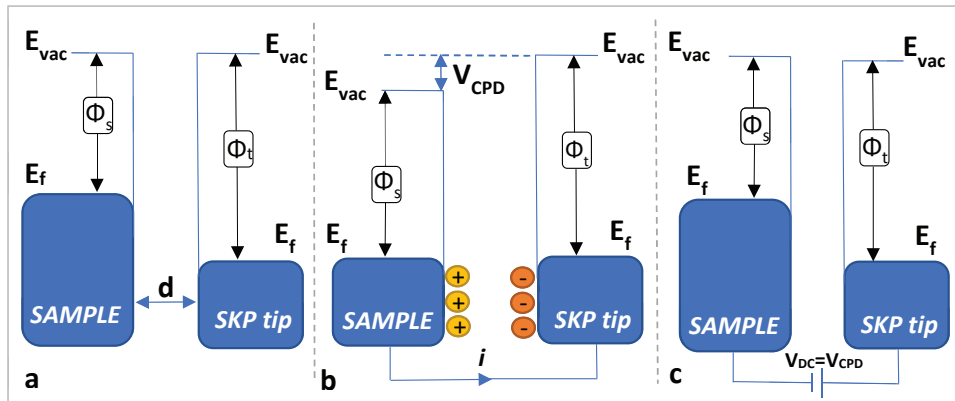
Figure 23: Schematics showing how the different energy levels of the electron, influence the interaction between metals. a) Two materials having different work functions and Fermi levels, are placed next to each other. b) When electrically coupled with a wire but separated by a small gap, the difference in work functions will induce a contact potential difference at the surface between them. The Fermi levels align. c) In the SKP technique, a voltage is applied such that the charges do not build up at the gap.

When the metal sample is placed under a vibrating needle to which it is electrically connected, and the needle is positioned close to the metal surface, a measurable current is induced. A capacitor is formed between the needle and the sample surface, which is charged by the V_{cpd} between the needle and the sample. To convert the V_{cpd} to some quantitative information about the sample, it is convenient to calibrate the SKP to a standard reference electrode, like $Cu/CuSO_4$ [96].

To convert the measurement to qualitative knowledge about corrosion processes taking place on the metal sample, one must understand the electrochemical system and the equations behind the measurements with the SKP [109]. The electrochemical potential of the metal has to be defined in relationship to the metal's work function, Φ, that is in reference to a vacuum level.

The definition of electrochemical potential, of a metal, $\tilde{\mu}$, is according to Eq. (19)

$$\tilde{\mu_i} = \mu_i + z_i F \varphi \tag{19}$$

Where μ_i is the *chemical work* necessary to transfer an electron from infinity and into the bulk metal. The other term reflects the *electric work* needed for this transfer, where z_i is the charge of the species, F is the Faraday constant and φ is the Galvani potential [251]. The

electrochemical potential has the units of J/mol and is hence a quantity with units of energy. The Galvani potential is given by the sum of the Surface potential χ and the Volta potential ψ, according to Eq. (20).

$$\varphi = \chi + \psi \qquad (20)$$

The Volta potential, ψ, represents the work necessary to transfer the electron from infinity and to the position "right outside" at ≈10 nm. For a sample that is not connected to other metals, the Volta potential is regarded as zero, hence $\psi=0$ [123, 230]. The term χ is the electrostatic work necessary to transfer an electron from "right outside" and through the surface [230, 245, 247]. This work corresponds to the potential drop between the potential just inside the material and the potential just outside the material [252]. It is usually positive, as the metal subsurface is positively charged, while an "electron cloud" forms above [246]. This contradicts the concept of the electrical double layer, where the metal is usually negatively charged, while the first layer in contact with this surface consists of negative charges.

See Figure 24 for the schematic illustration of the relationship between the work function and the Volta potential energy as well as the Galvani and Surface potential energies [246].
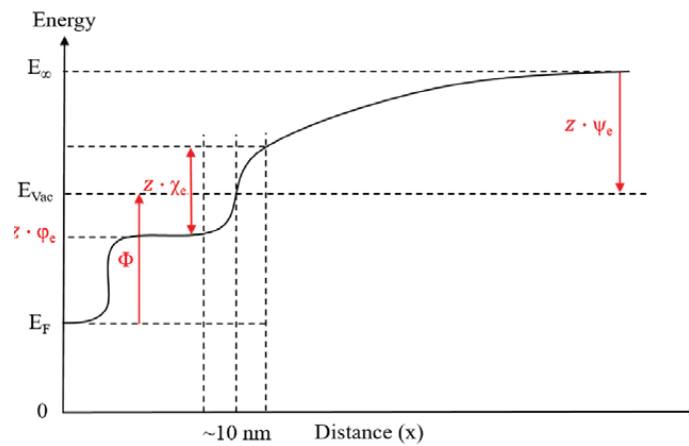
Figure 24. The relationship between the work function Φ, the surface potential χ and the Volta potential ψ [246].

For a dry electrode, the definition of the work function is the negative of the electrochemical potential, $\tilde{\mu}$.

$$\Phi = -\widetilde{\mu_i} \tag{21}$$

To make the relationship in Eq. (21) applicable also for metal samples covered by electrolyte layers or a coating, it is necessary to define and include additional terms in the total energy balance for the electron. The definition must comprise the necessary energy to move the electron through different layers, e.g. various electrochemical double layers. When measuring the V_{cpd} in corrosion/coating studies, we have three main scenarios, see below:

➢ Scenario 1, Electrolyte covered metal (Defect in the coating): 1a) Metal-electrolyte-gas (humid) and 1b) metal-oxide-electrolyte-gas.
➢ Scenario 2, Intact coating/metal interface: 2a) Metal-coating-humid air and 2b) metal-oxide-coating-humid air
➢ Scenario 3, Delaminated coating: 3a) Metal-electrolyte-coating-humid air and 3b) metal-oxide-electrolyte-coating-humid air

There are two additional scenarios, both in the presence of ultra-thin electrolyte layers: 4a) Metal-humid air and 4b) metal-oxide-humid air.

In Chapter 5.4.3.1, the equations for the electrolyte covered metal will be derived according to available theory, for a general understanding [83, 101, 123, 230].

5.4.3.1   Scenario 1: Electrolyte covered metal

To calculate the energy needed to transfer an electron from an electrolyte covered metal through the electrolyte and to a place "right outside", an additional energy term must be introduced, see Eq. (22). Here, the EDL is the electrical double layer at the metal surface.

$$\Delta\phi_{sample}^{electrolyte} = \text{Galvani potential drop across metal-electrolyte interface (EDL)} \tag{22}$$

Next, the energy E_{sample}, needed to transport one electron (z is replaced with -1 in the previous equations) from within the metal to a place outside, is expressed by using the work function concept and the potential drop across the metal-electrolyte according to Eq. (23).

$$E_{sample} = -\tilde{\mu}_e^{sample} = -\left(\mu_e^{sample} - F\Delta\phi_{sample}^{electrolyte} - F\varphi_{electrolyte}^{gas}\right)$$

$$= -\mu_e^{sample} + F\Delta\phi_{sample}^{electrolyte} + F\varphi_{electrolyte}^{gas} \tag{23}$$

Since the sample is not connected to the SKP, it is uncharged, and the Volta potential is zero, the term $F\varphi_{electrolyte}^{gas}=F\chi_{electrolyte}^{gas}$. See Eq. (24).

$$E_{sample} = -\left(\mu_e^{sample} - F\Delta\phi_{sample}^{electrolyte} - F\chi_{electrolyte}^{gas}\right)$$

$$= -\mu_e^{sample} + F\Delta\phi_{sample}^{electrolyte} + F\chi_{electrolyte}^{gas} \tag{24}$$

When the sample is connected to the SKP, $\psi \neq 0$, and Eq. (24) will then have an additional term, see Eq. (25).

$$E_{sample} = -\mu_e^{sample} + F\Delta\phi_{sample}^{electrolyte} + F\chi_{electrolyte}^{gas} + F\psi^{electrolyte} \tag{25}$$

For SKP probe, the energy E_{SKP} representing the energy needed for electron transport when the probe is not connected to the sample, is given by Eq. (26).

$$E_{SKP} = -(\mu_e^{SKP} - F\chi_{SKP}^{gas}) \tag{26}$$

When connected to the sample, the equation will have additional terms, see Eq. (27).

$$E_{SKP} = -\left(\mu_e^{SKP} - F\chi_{SKP}^{gas} - F\psi^{SKP}\right) = -\mu_e^{SKP} + F\chi_{SKP}^{gas} + F\psi^{SKP}$$

$$= \Phi^{SKP} + F\psi^{SKP} \tag{27}$$

When the sample and the SKP are connected, their Fermi levels will align. Hence the energies have to balance each other, $E_{sample} = E_{SKP}$. This leads to Eq. (28).

$$-\mu_e^{sample} + F\Delta\phi_{sample}^{electrolyte} + F\chi_{electrolyte}^{gas} + F\psi^{electrolyte} = \Phi^{SKP} + F\psi^{SKP}$$

$$-\mu_e^{sample} + F\Delta\phi_{sample}^{electrolyte} = \Phi^{SKP} + F\psi^{SKP} - F\chi_{electrolyte}^{gas} - F\psi^{electrolyte} \tag{28}$$

Converting the energy to potentials, we obtain Eq. (29) .

$$\frac{-\mu_e^{sample}}{F} + \Delta\phi_{sample}^{electrolyte} = \frac{\Phi^{SKP}}{F} + \Delta\psi_{electrolyte}^{SKP} - \chi_{electrolyte}^{gas} \tag{29}$$

The left-hand side defines the half-cell reaction for a solution-covered metal, while the right-hand side can be simplified. The term Φ^{SKP} is more or less constant when the gas composition

and surface contamination of the needle is constant but found to drift 50 mV in 6 hours for the SKP employed in this study. The term $\chi_{electrolyte}^{gas}$ is assumed to be very small and constant for an electrolyte [159]. See Eq. (30).

$$V_{Half\ cell}^{sample} = \Delta\psi_{SKP}^{electrolyte} + \text{constant} + \text{negl.} = V_{CPD} + \text{constant} \tag{30}$$

From this relationship, by calibrating the needle to a known reference potential like $E_{SHE}=0$ V, the result is Eq. (31).

$$V_{sample} = V_{Half\ cell}^{sample} + V_{Half\ cell}^{reference} \tag{31}$$

Such that Eq. (30) shows the relationship between the measured contact potential difference and the electrode potential, V_{sample}. See Eq. (32).

$$V_{Sample} = V_{CPD} + E_{1/2}^{reference} + \text{constant} = V_{CPD} + \text{constant} \tag{32}$$

Practically, the V_{sample} is the *corrosion potential* of the metal sample studied [2].

When metal oxides are present on the surface of the metal sample, then the term for the potential drop over the metal sample-electrolyte interface in Eq. (22), will incorporate contributions from: The Galvani potential drop over the metal-oxide interface, the Galvani potential drop $\Delta\phi o_x$ over the oxide layer due to a varying composition of the oxide or ion transport from the inner to the outer interface [253], and the Galvani potential drop over the oxide-electrolyte interface [9].

$$\Delta\phi_{sample}^{electrolyte} = \Delta\phi_{sample}^{oxide} + \Delta\phi o_x + \Delta\phi_{oxide}^{electrolyte} \tag{33}$$

Following the derivation steps outlined above, the other important cases that can be distinguished, will be indicated.

5.4.3.2 Scenario 2: Intact metal/coating interface

The organic coating is labelled as polymer in the following equations. For a coated metal sample connected to the SKP probe, we have the energy balance given by Eq. (34).

$$\frac{-\mu_e^{sample}}{F} + \Delta\phi_{sample}^{polymer} = \frac{\Phi^{SKP}}{F} + \Delta\psi_{polymer}^{SKP} - \chi_{polymer}^{gas} \tag{34}$$

If an oxide was present on the metal surface underneath the coating, we would have to take in consideration the contributions from the redox properties of the oxide. The redox properties will mirror the equilibrium between the Fe^{2+} and Fe^{3+} species in the oxide:

$$Fe^{3+} + e^- = Fe^{2+} \tag{35}$$
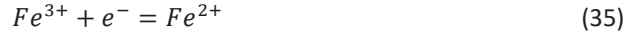
The resulting Eq. (36) shows that the V_{cpd} measured, reflects the possible degree of oxidation of the *outer* oxide surface, even when a coating is present [9, 101].

$$\Delta\psi_{polymer}^{SKP} = \frac{-\Phi^{SKP}}{F} + \chi_{polymer}^{gas} + \Delta\varphi_{polymer}^{ox-out} - \frac{\Delta\mu_{Fe^{2+}\_out/Fe^{3+}\_out}^{0}}{F} + \frac{RT}{F} ln\frac{[Fe^{3+}\_out]}{[Fe^{2+}\_out]} \tag{36}$$

In this expression, the only factors that are not constant, are the potential drop across the oxide/coating interface and the ratio of Fe^{3+} to Fe^{2+}, hence the result is Eq. (37).

$$\Delta\psi_{polymer}^{SKP} = const. + \Delta\varphi_{polymer}^{ox-out} + \frac{RT}{F} ln\frac{[Fe^{3+}\_out]}{[Fe^{2+}\_out]} = V_{CPD} \tag{37}$$

While there have been many conflicting results concerning the structure of passive film on iron [254], it is believed that the electronic behaviour is affected by the Fe^{2+} content in the oxide structure. The lower the content, the lower is the rate of electron transfer reactions of the oxide, and the more positive the V_{cpd} will be [101]. In order to determine the effect of the applied coating to the measured V_{cpd}, the potential of the bare and coated surface can be measured and compared.

5.4.3.3   Scenario 3: Delaminated coating

This case considers a situation where an electrolyte film is present between the coating (called polymer here) and the metal substrate [2].

$$-\frac{\mu_e^{sample}}{F} + \Delta\phi_{sample}^{electrolyte} = \frac{\Phi^{SKP}}{F} + \Delta\psi_{polymer}^{SKP} - \chi_{polymer}^{gas} - \Delta\phi_{Donnan} \tag{38}$$

The term $\Delta\phi_{Donnan}$ represents the potential drop caused by the electrolyte/coating interface, but is negligible for concentrated electrolyte or uncharged coatings [83, 255]. The term $\chi_{polymer}^{gas}$ is the surface potential of the polymer in the respective gas, and is assumed to be constant for a given coating and stable in time [84].

When an oxide is present at the interface, the situation resembles the case seen for electrolyte covered oxide, see Eq. (33). The V_{cpd} does not distinguish between the metal-oxide surface and the pure metal surface when an electrolytic double layer is present under the delaminated coating.

5.4.3.4   Scenario 4: Metal or oxide substrate in humid air

For a metal in humid air, the V_{cpd} indicates solely the difference between the SKP's and the metal's work functions.

$$\Delta\psi_{sample}^{SKP} = \Phi^{SKP} - \Phi^{sample} \tag{39}$$

When there is an oxide present at the interface, and there is no electrolyte that can contribute to an electrical double layer, the redox properties of the oxide must be considered, and Eq. (40) shows

$$\Delta\psi_{ox-out}^{SKP} = \frac{\Phi^{SKP}}{e} - \chi_{ox-out}^{gas} + \Delta\mu_{Fe^{2+}\_out/Fe^{3+}\_out}^{0} - RT\,ln\frac{[Fe^{3+}\_out]}{[Fe^{2+}\_out]} \tag{40}$$

In this expression, the only factor that is not constant, is the ratio of Fe^{3+} to Fe^{2+}, see Eq. (41)

$$\Delta\psi_{ox-out}^{SKP} = const. + RT\,ln\frac{[Fe^{3+}\_out]}{[Fe^{2+}\_out]} \tag{41}$$

5.4.3.5   System description

The SKP used in this study measures both the potential and topography of the sample. It hence belongs to the second generation of SKPs following the first generation designed by Baikie, which only allowed for potential measurements [256, 257]. The SKP measurements are performed in a steel chamber, which in addition to function as a Faraday cage, allows for climatic control. Both humidity and oxygen concentration can be measured and altered. See Figure 25 for information about the inside of the steel chamber and the sample holder employed in this study.
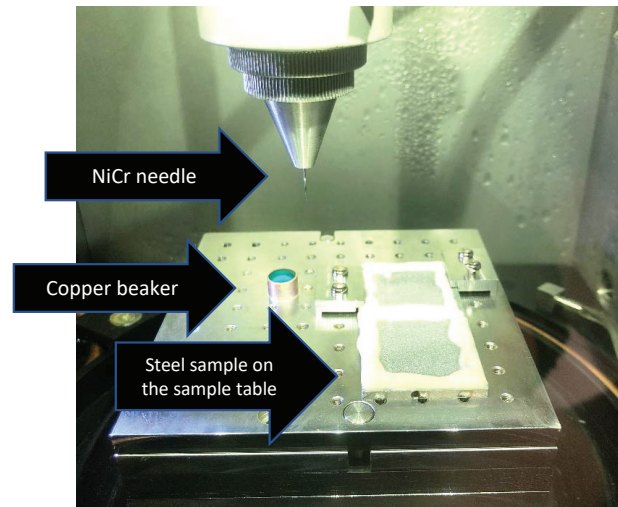
Figure 25: The SKP stage with a sample, the SKP probe which here is NiCr needle, and a copper beaker filled with copper sulphate solution, i.e. a Cu/CuSO₄ reference electrode.

The SKP is comprised of a needle with a flat end, that vibrates above the sample surface at a certain frequency and amplitude. The SKP used in this work vibrates at 957 Hz with a 5 μm amplitude. The work distance, d_0, is 60 μm. The vibration and the movement of the needle above the surface, is accurately controlled by a double coil and permanent magnet displacement device [258], see Figure 26.
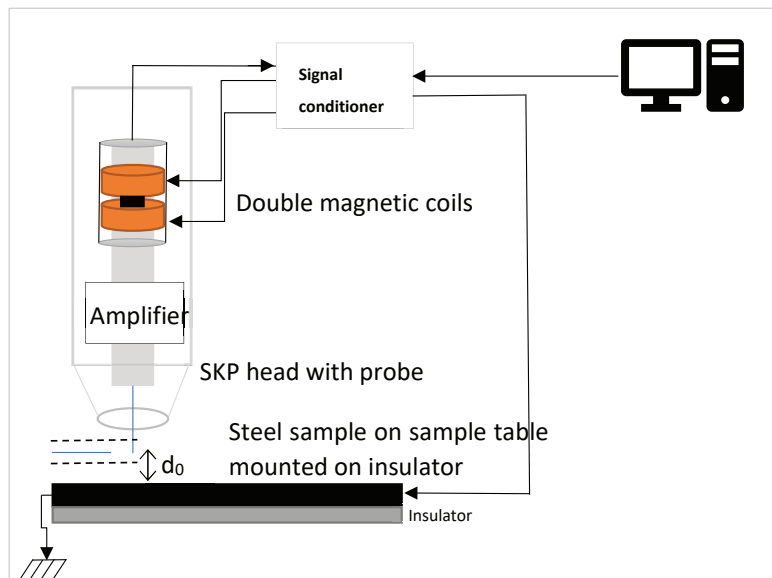
Figure 26. Schematic circuit of the SKP employed in this study.

The voltage (AC) input on the coil driver, which controls the vibration of the magnet and hence the vibration of the needle, is 2.2 V but is amplified up to an output of 12 V. A DC signal of $\pm$ 500 mV (OFF(P)) is also applied to the double coil, see in order to fine tune the needle position above the surface. If the DC voltage on the coils exceeds a set limit, the distance is compensated by stepping the positioner motor, hence measurements where topography variates much, will take longer time to perform. The height control of the SKP head is thus achieved by a combination of the double magnetic coils and the motorised stepping positioner on which the KP head assembly is mounted. Currents of 10^{-13} A are measured, then processed and amplified to a corresponding voltage which is the value of interest with this technique (V_{cpd}).

5.4.3.6   Potential shifts

In conclusion, the potential measured by the SKP is determined by the electrode potential in the interfacial region, and is known to be affected by several conditions: The oxide composition [101], interactions between the organic phase and the steel oxide surface [9, 231, 232], oxide/coating interactions [10, 124] and the penetration of humid gasses to the interface [231-233]. When the SKP technique is employed in the study of electrochemical disbonding of organic coatings, the incorporation of ions at the interface is believed to be the earliest stage of the electrochemical disbonding processes [158] and detectable as a potential shift [83, 112, 140, 142]. However, there have been contradictive interpretations of the observed potential shift and it may be difficult to differentiate between incorporation of ions and incorporation of water [109]. But it has been pointed out that the potential shifts will be substantial in the presence of ions [11, 117] and observable as a sigmoid potential profile in time moving away from the defect. Water ingress and wet de-adhesion processes will lead to a uniformly decrease in the potential for the entire interface area and have linear potential profiles [109]. It has been pointed out that the hydrolytic destabilisation of bond is the actual first stage of electrochemical disbonding processes, as the replacement of coating/metal bonds with water/metal bonds, will lower the resistance to lateral transport of ions at the interface [123].

6 Contributions, concluding remarks, strengths and limitations

6.1   Contributions

The aim of this work was to provide a deeper insight into the understanding of the effect of surface roughness and topography on the organic coating/steel interface stability in humid air and corrosive conditions.

With respect to the key action tasks described in Chapter 1, the list below gives an overview of how the tasks were executed and achieved during the PhD project:

1. Gain an overview of the problems related to the failure of industrial organic coatings on industrially machined surfaces. **See Paper IV and Paper V.**

2. Accumulate fundamental knowledge about the stability of organic coatings on steel. **See Chapter 2-4.**

3. Involve the manufacturing group at NTNU to pattern steel surfaces with various topographies at different roughness, Rz, by machining. Evaluate the corrosion resistance of epoxy coatings on such surfaces in accelerated corrosion tests. **See Chapter 5.1.2 and Paper I.**

4. Install and put in service at SINTEF/NTNU a newly acquired custom-made height-regulated SKP instrument. **See Chapter 5.3.2, and Paper II and III.**

5. Become familiar with the theoretical background for the instrument as well as the experimental methodology. **See Chapter 5.3.3.**

6. Apply for access at the Nano Micro Facility at the Karlsruhe Institute of Technology (Germany), and involve the scientific group there in the surface structuring needed in this project. **See Chapter 5.1.3.**

7. Evaluate the cathodic disbonding and wet-adhesion resistance of a PVB model coating on surface structured steel by the in-situ SKP technique. Determine the oxide composition at the surface with X-ray photoelectron spectroscopy (XPS). **See Paper II.**

8. Investigate the effect of humid air on the coating/steel interface, and the resistance to cathodic disbonding as a function of the surface oxide condition and oxidation, by the in-situ SKP technique in combination with XPS. The stabilising effects of surface roughness are also investigated. **See Paper III.**

Five publications have been submitted in the course of this PhD study: Two conference papers and three journal articles. The conference papers were presented orally at conferences and published in conference proceedings after a peer review process. Two of the journal articles have already been published, and the third is in review. Two master theses have in addition been executed in connection with this work.

In the following, the five publications are listed with their respective abstracts, while the full texts are attached in the appendix.

➢ **Paper I (Journal paper):** This paper describes how roughness and topography may contribute to the corrosion resistance of an organic coating and discusses whether machining can be comparable to blast cleaning with respect to coating durability. The hypothesis investigated was: "If we increase the roughness of machined surfaces by altering the machining parameters, these will give the same coating durability as grit-blasted surfaces".

C. M. H. Hagen, A. Hognestad, O. Ø. Knudsen, and K. Sørby. *The effect of surface roughness on corrosion resistance of machined and epoxy coated steel*, Progress in Organic Coatings, vol. 130, pp. 17-23, (2019) [30]

ABSTRACT By incorporating periodic micro-patterns on steel substrates, the effect of surface roughness on corrosion resistance of a two-component polyamine cured epoxy mastic coating has been studied. Machining was employed to pattern the surfaces with periodic peaks of varying peak-to-valley heights, Rz. The focus of the study was to find the surface parameter that contributes most to the stability of an organic coating in corrosive environment, and to evaluate if machining can be comparable to blast cleaning with respect to coating durability. A strong correlation between roughness (Rz) and corrosive delamination of coated surfaces was seen. Increasing Rz from 57 µm to 252 µm on surfaces with triangular peaks, increased the effective contact area by 40% and decreased delamination by 30%. By introducing tilted asperities at Rz=224 µm while keeping the effective contact area in general unchanged, delamination decreased another 55%. Hence, an increased Rz is found to be only partially beneficial, and the profile shape is more significant than the roughness value per se. The results suggest that mechanical interlocking has a substantial influence on the interfacial stability of protective coatings in corrosive environments. By optimal selection of cutting parameters, machining can give surfaces where protective coatings have long lifetime.

Author contributions:

C.H.M.Hagen, Phd candidate: Planned and performed lab-work; analysed results, performed literature review and wrote the article.

A.Hognestad, MSc: Planned and performed lab-work; paper review and input.

O. Ø.Knudsen, Senior scientist/Professor: Input to experimental part; paper review and input.

K. Sørby, Professor: Planned the machining parameters to be used for the face turned samples in the paper; paper review and input.

> **Paper II (Journal Paper):** This paper describes the effect of mechanical interlocking on the CD mechanism. Cathodic disbonding of a PVB coating on surfaces laser patterned with peaks of specific height and geometry was investigated in-situ by SKP. The wet adhesion loss in oxygen deficient atmosphere (3 ppm. O_2) was also evaluated. The hypothesis investigated was: "Roughness, but especially the substrate's topography

contributes to coating stability in humid and corrosive conditions by mechanical interlocking".

C.M.H. Hagen, O.Ø. Knudsen, A.H. Zavieh, and W. Pfleging. *Effect of laser structured micro patterns on the polyvinyl butyral/oxide/steel interface stability.* Progress in Organic Coatings, 2020. **147**: p. 105766.[259]

ABSTRACT This work investigated the effect of steel substrate roughness and topography on cathodic disbonding resistance and wet adhesion of the polyvinyl butyral/oxide/steel interface. Laser structuring was employed to pattern steel surfaces with controlled, periodic peaks of different peak-to-valley height, Rz, and geometry. Grinded smooth samples were used for reference. The in-situ scanning Kelvin probe technique was used to follow the cathodic disbonding in humid air and wet adhesion loss in inert atmosphere (3 ppm O_2). Both cathodic disbonding and wet adhesion loss depended on the ability of the surface for mechanical adhesion, even when compensating for the increased effective contact area. X-ray photoelectron spectroscopy excluded the possibility for oxide chemistry effects on the delamination rate. Surfaces with features that enabled mechanical interlocking forces, had the best cathodic disbonding resistance and wet adhesion properties.

Author contributions:

C.H.M.Hagen, Phd candidate: Applied for collaboration with KNMF (Germany); planned and performed lab-work with exception of XPS analysis; analysed results, performed literature review and wrote the article

O. Ø.Knudsen, Senior scientist/Professor: Input to experimental part; paper review and input.

A.H.Zavieh, Dr.: Performed XPS analysis; input on how to understand results; paper review.

W.Pfleging, Professor: Planned the machining parameters to be used for the laser structured samples in the paper; guided the team at KNMF (Germany) for the production of the samples; paper review.

> ➢ **Paper III (Journal paper):** This paper describes the oxidation of the steel surface underneath the coating with exposure to humid air and the effect of the surface oxide and oxidation on the cathodic disbonding resistance, including the stabilizing effects of the steel topography and roughness. The hypothesis investigated was: "The steel surface underneath an organic coating oxidises, which affects the cathodic disbonding resistance. Mechanical interlocking stabilises the interface during the oxidation process."

C.M.H. Hagen, O.Ø. Knudsen, R. Johnsen, A.H. Zavieh, and W. Pfleging. *Oxidation of coated steel during exposure to humid air and effects on cathodic disbonding - a qualitative study,* submitted 2020 to Electrochimica Acta, [260].

ABSTRACT This work investigated the oxidation of steel under a poly-vinyl butyral coating during exposure to humid air, and the effects on cathodic disbonding. Laser structuring and grinding was employed to pattern steel surfaces with periodic peaks of different peak-to-valley height, Rz, and geometry. Using a combination of the in-situ scanning Kelvin probe technique and X-ray photoelectron spectroscopy, it has been demonstrated that the steel surface oxidises underneath adhering coating, depending on oxide condition from the start. The amount of oxidised iron species increased significantly with exposure, and the relative amount of the various oxidation states shifted towards trivalent iron. The changes in surface oxide under the coating were found to be independent of the topography or roughness of the steel substrate. On smooth surfaces however, the oxidation resulted in loss of adhesion. The cathodic disbonding rate depended on iron oxide condition and oxidation level. Mechanical interlocking and increased surface roughness increased the stability of the interface and the cathodic disbonding resistance.

Author contributions:

C.H.M.Hagen, Phd candidate: Applied for collaboration with KNMF (Germany); planned and performed lab-work with exception of XPS analysis; analysed results, performed literature review and wrote the article.

O. Ø.Knudsen, Senior scientist/Professor: Input to experimental part; paper review and input.

R.Johnsen, Professor: Input to experimental part; paper review and input.

A.H.Zavieh, Dr.: Performed XPS analysis; input on how to understand results; paper review.

W.Pfleging, Professor: Planned the machining parameters to be used for the laser structured samples in the paper; guided the team at KNMF (Germany) for the production of the samples; paper review.

The following papers have been published and presented at conferences:

> **Paper IV (Conference paper presented at The Nordic Corrosion Congress in 2015 (Norway)):** This paper describes the rapid degradation of coatings applied on machined surface, by employing several tests. The hypothesis investigated was: "Coatings applied directly on industrially machined surfaces degrade rapidly by cathodic disbonding and corrosion creep due to weak adhesion".

C.M.H. Hagen, A. Kristoffersen, O.Ø. Knudsen, *Corrosion protection of smooth surfaces – coating adhesion [28]*

ABSTRACT Coatings on machined surfaces are generally found to degrade early, and this has been attributed to poor adhesion. Good adhesion normally requires blasting, but not all surfaces can be blast cleaned due to other functional requirements, such as seal (flange surface) or assembly (tightness of nuts). Our findings show that machined surfaces had poor resistance to cathodic disbonding and corrosion creep. Impact toughness was found on the average to be four times lower on machined surfaces than on blasted surfaces. Dry adhesion tests gave no discernible difference between machined and blasted surfaces. Wet adhesion testing, however, indicated that adhesion was strongly weakened on machined surfaces by permeation of water into the coating.

Author contributions:

C.H.M.Hagen, Phd candidate: Analysed results, performed literature review and wrote the article.

A.Kristoffersen, MSc: Planned and performed the lab-work.

O. Ø.Knudsen, Senior scientist/Professor: Input to experimental part; paper review and input.

> ➤ **Paper V (Conference paper presented at NACE Corrosion 2016 (Canada)):** This paper describes the effect of increasing peak density and roughness, either by machining or grit blasting, on corrosion creep and cathodic disbonding. The hypothesis investigated was: **"**Increasing peak density and roughness will decrease corrosion creep and cathodic disbonding by increasing adhesion strength.**"**

C.M.H. Hagen, A. Kristoffersen, O.Ø. Knudsen, *The effect of surface profile on coating adhesion and corrosion resistance [29]*

ABSTRACT Coatings on machined surfaces are generally found to degrade early and this has been attributed to poor adhesion. Good adhesion normally requires blasting, but surfaces machined for functional requirements, such as seal (flange surface) or assembly (tightness of nuts) are not blasted before being coated. The effect of surface roughness, peak density and contact area on coating adhesion and protective performance has been studied. Machined and grit blasted samples have been tested for corrosion creep, cathodic disbonding and adhesion. The results showed that machined surfaces have lower contact area than blasted samples. The contact area increased with decreasing peak density for both blasted and machined samples. Adhesion loss was however positively related to the contact area on machined surfaces and inversely related on blasted surfaces. High peak density seems to be key factor for increasing coating adhesion on machined surfaces, while a high peak density seemed to decrease adhesion on profiles with sharp features and high surface roughness.

Author contributions:

C.H.M.Hagen, Phd candidate: Planned and performed the lab-work; analysed results, performed literature review and wrote the article.

A.Kristoffersen, MSc: Planned and performed lab-work.

O. Ø.Knudsen, Senior scientist/Professor: Input to experimental part; paper review and input.

6.2   Concluding remarks

The aim of this work was to obtain a better understanding of the effect of roughness and topography on the stability of the coating/steel interface in humid air and corrosive conditions.

The corrosion resistance of organic coatings on surfaces patterned with periodic peaks of varying height and shape was studied in accelerated coating degradation tests to identify the substrate roughness parameters that contribute most to the stability of the coating/steel interface. Next, the mechanism by which roughness and topography contributes to the stability in humid air and corrosive conditions was investigated in-situ, by employing the SKP technique. Grit blasted or grinded surfaces were used for reference.

The work presented in the conference papers (Paper IV and Paper V) clarified the importance of machining – both as one of the most used manufacturing technologies, but also as a process for micro structuring steel surfaces to get specific roughness and texture – for the premature coating failure experienced on smooth machined surfaces. Mainly Paper I, II and III will be considered in the further discussion. It is primarily the work presented in these papers that contributes to the understanding of the effect of surface roughness and topography on the stability of the coating/steel interface, on a mechanistic level.

The main findings from Paper IV and Paper V, suggested the following:

i)   As long as lubricants etc. that may prevent contact between the coating and the substrate are removed before painting, the machining process represents no additional risk for premature coating failure compared to any smooth surface produced by other methods. Hence premature disbonding on smooth surfaces is an effect of the roughness and topography of the substrate, and not the machining process.

ii)   Coatings on smooth surfaces were found to have low impact toughness compared to grit blasted surfaces, on the average four times lower. Hence, coating defects may more easily be caused by impacts on smooth surfaces. The explanation for this is most likely that the surface roughness and topography do not allow for interfacial dissipation of forces. This is in accordance with previous studies on this matter [41, 52, 74, 81, 174, 181].

- 80 -

iii) Adhesion tests showed no differences in dry adhesion for coatings applied on machined versus grit blasted surfaces. However, adhesion tests performed after immersing samples in water indicated that wet adhesion was strongly reduced on machined surfaces. The low wet adhesion on smooth surfaces correlated with low corrosion resistance, thus confirming results from previous studies on this matter [40-42]. Hence, wet adhesion properties – if measured correctly – can give an indication of the interfacial coating/steel stability in corrosive conditions. We documented and concluded however, that adhesion tests, especially when performed in dry conditions, may give misleading results. Different methods for measuring adhesion will give different results [80]. The wet adhesion tests were found to be very sensitive to measurement errors. In the pull-off tests, dollies must be glued with the same glue used for dry conditions, but the glue may be affected by the water in the film. Water may also evaporate during curing of the glue. The cross-cut test is a qualitative test but may be more suitable for evaluating wet adhesion than the pull-off test.

iv) In the industry, a maximum roughness is often specified for machined surfaces due to functional requirements such as seal or assembly in mind. Also, there are cases with no functional requirements, but where grit blasting is omitted due to other reasons. In these cases, modifying the machining parameters to give a rougher surface will improve coating durability.

In Paper I, machining parameters to create surfaces that could result in coating performance comparable to grit blasted surfaces were specified. In paper II and III, specific surface topographies were produced by laser structuring to investigate their effect on coating/interface stability and coating disbonding more accurately in-situ by SKP. In addition, the surface oxide was reduced before coating application to investigate qualitatively the effect of oxidation under the coating during exposure on disbonding behaviour. The main findings in Paper I [30], Paper II [259] and Paper III [260] can be summarised as follows:

v) In accelerated cyclic corrosion tests simulating offshore atmospheric conditions, the coatings disbonded on smooth surfaces by corrosion creep, following a CD front. Coatings applied on smooth surfaces had very low resistance to the corrosion assisted disbonding.

vi) Increasing surface roughness, by machining asperities triangular in profile with increasing roughness, increased the effective interfacial contact area and decreased the disbonding rate. Increasing the roughness on machined surfaces to Rz=30 μm, decreased significantly the disbonding in corrosion resistance tests.

vii) However, grit blasted surfaces with 6 times lower roughness (Rz) still showed even lower disbonding rate.

viii) When the geometry of the machined asperities favoured mechanical interlocking to the coating, the disbonding rate decreased significantly and below the rate measured on blast cleaned surfaces.

ix) No relationship was found between the Wenzel corrected contact angles and the disbonding behaviour. However, the validity of the Young's equation on rough surfaces is questionable, even after correction for roughness [21, 22, 61]. See the relationship given in Eq. (17).

x) The CD and wet adhesion behaviour were studied on surfaces patterned by laser structuring or grinding. Surfaces with periodic peaks of different size and geometry were prepared. The wet adhesion loss - studied in inert atmosphere (3 ppm O_2) - was found to improve on surfaces with features that enabled mechanical interlocking forces. Surfaces with ability for mechanical interlocking had also the best CD resistance. The increased roughness resulted in increased effective contact area between coating and substrate, and partly explained the improved CD resistance, but not all. Hence, CD resistance was improved by both increasing the effective contact area and the surface's ability for mechanical interlocking. The results show that CD and wet adhesion depend on the ability of the surface for mechanical adhesion.

xi) By the combination of the in-situ SKP technique and XPS, it was demonstrated that the steel surface oxidises underneath adhering coating, depending on oxide condition from the start. The potential of electrochemically reduced and coated surfaces exposed to 95% RH for 4 hours increased by 0.25 V, from about -0.09 V_{SHE} to about 0.16 V_{SHE}. By analysing the surface before and after exposure by XPS, it was demonstrated that the amount of trivalent iron had increased significantly with exposure, on the expense of divalent and metallic iron. Although industrial coatings are formulated with barrier properties exceeding the PVB's,

with incorporated phases that decrease the porosity and increase the transport path for deleterious species [4, 103], the disbonding mechanism of the model coating is comparable to that of other organic coatings [214]. Oxidation processes under intact coating as observed in this study are believed to happen but at slow rates [8, 93].

xii) On smooth surfaces, the oxidation under the coating resulted in loss of adhesion. However, samples that were allowed to develop a thicker surface oxide by exposure to ambient laboratory conditions prior to coating application, showed a stable potential of about 0.36 V_{SHE} during exposure to humid air and experienced no adhesion loss.

xiii) Smooth surfaces are hence in general believed to have low hydrolytic stability and therefore poor wet adhesion properties. On smooth surfaces, or on surfaces with poor ability for mechanical interlocking, water accumulation at the interface may happen more readily, due to the low strength of the interface to mechanically resist water from spreading [75]. Smooth surfaces have less available sites for bonding and lack asperities that can dissipate forces when coating swells with water uptake.

xiv) Any structural changes happening at the steel oxide/coating interface with exposure to humid air - both with the accumulation of water at the interface and due to the oxidation of the substrate surface - will thus affect the resistance to CD. After the addition of a NaCl electrolyte to the defect, the migration of Na^+ (sodium) ions to the location of oxygen reduction exert an (electro)osmotic pressure, that tends to force off coating partially disbonded as a result of previous oxidation and wet de-adhesion. This was seen from in-situ SKP measurements in Paper III where the CD resistance was strongly affected by any previous exposure to humid air.

xv) Mechanical interactions are believed to be a key factor for the interfacial stability at the macro level both during exposure to humid air, but also when electrolytes are present at defects in the coating. Hence mechanical interactions are a key factor for the resistance of the interface to the initiation and progress of electrochemical reactions.

6.3   Strengths and limitations

Roughness increases the effective contact area at the coating/steel interface, resulting in an increase in physical and chemical interactions and hence number of bonds at the interface. It also increases the interfacial path that hydrated ions have to travel laterally. Roughness is most efficient for interfacial stability when it provides mechanical interactions at the coating/steel interface. The oxidation of the steel surface results in structural and morphological changes at the oxide surface, and partially mechanically weakened bonds by humidity may ultimately fail. Mechanical interactions – scaled up with the increase in effective contact area – add stability in humid and wet conditions. Wet conditions can be understood both as the conditions when the interface is exposed to humidity entering vertically, or laterally with the ingress of hydrated ions from an electrolyte covered defect. During electrochemical disbonding mechanisms such as corrosion creep and cathodic disbonding, the roughness improves interfacial stability significantly, but the effect cannot be explained by increased effective contact area alone. Mechanical interactions are therefore believed to be a key factor for the interfacial stability at the macro level both during exposure to humid air, but also when electrolytes are present at coating defects. Hence mechanical interactions are a key factor for the resistance of the interface to the initiation and progress of electrochemical reactions.

The main **strength** of this thesis is that it addresses for the first time on a mechanistic level the effect of roughness and topography on the stability of the coating/steel interface in humid and corrosive conditions, and doing so by employing for the first time:

- Controlled 3D roughness profiles hence excluding the stochastic nature of roughness, therefore allowing for a quantitative validation of the experimentally determined disbonding rates.
- Measurements over a large range of roughness values.
- Peaks of various geometries.

Grinding and blast cleaning have earlier been the chosen methods when studying the effect of roughness on e.g. adhesion and CD heterogeneous topographies having a stochastic distribution of roughness heights [28, 29, 31-35]. The random nature of roughness geometry

produced by those methods prohibits quantitative experimental comparison of results on surfaces with heterogenous roughness.

This is the second time, at least according to published literature, the SKP technique is employed *in-situ* on coated microscopic rough steel substrates, evaluating the interface stability on the macro-scale [34]. Dam et al. had however a small variation of roughness, with Ra $0 – 1$ µm, in their study. The in-situ investigations in this work, were performed on surfaces with 0.4 - 64 µm Rz and effective contact area values of $1.01 – 2.3$.

The previous in-situ studies that have evaluated the stability of the coating/steel interface, have investigated effects on the molecular scale, e.g. related to surface energies for oxide surfaces, or to the adsorption of different organic compounds at the interface. All such studies were performed on polished surfaces.

The study in general ranges over a wide set of test methods: Accelerated cyclic tests, accelerated CD tests, SKP technique to measure the coating/steel interface behaviour in humid conditions (both air and inert atmosphere), and in corrosive conditions with electrolyte covered defect. In addition, both industrial and model coatings were employed. Hence discussion and conclusions are well rooted both on mechanistic grounds and testing of industrial coatings and surface pre-treatments employed by the industry.

The study documented in addition that machining may be used to create surfaces with equivalent coating durability to those that have been grit blasted. Increasing the roughness on machined surfaces to 30 µm, decreased significantly the disbonding in corrosion resistance tests.

The work presented in this thesis has its **limitations**. Steel surfaces were structured with a significant roughness. When introducing roughness, the chemistry of the surface may be changed. As both electrochemical properties of the substrate surface and the adhesion strength of the interfacial bonds may be affected with change in chemistry, it may be difficult to discriminate between effects from chemistry and roughness when studying the stability of the coating/steel interface. Therefore, the chemistry of the surface must either be well-controlled or well-characterized. However: roughness introduces difficulties when analysing the surface composition and energies. Measuring contact angles on surfaces with high

roughness is difficult, and it is also questionable what information such contact angle measurements give. Even after correcting measured contact angles with Wenzel's roughness factor, the validity of the Young's equation with increased departure from ideal smooth surfaces, is questionable.

Likewise, surface oxide compositions are usually analysed on flat surfaces. The XPS method employed, relies on an energetic response from the surface, which can be used to determine the iron oxide content. On surfaces with asperities with different geometries, the ion beam is hitting the surface at different angles and results may not be comparable, even though repeatable. The XPS results were obtained from analysed areas of 0.7 x 0.3 mm, to ensure that the results represent the surface and not local inclusions or defects.

The in-situ experiments in paper II and III were performed with a thin model PVB coating. It was seen that the application of this coating to the patterned steel substrates did not affect the measured potential on the coated surfaces – neither on the ones with reduced oxides nor on the ones with native, as-prepared oxides. Similar results have been measured for coatings without the ability for chemical interactions with the substrate, hence relying on van der Waals or mechanical interactions [9]. Contributions from mechanical interactions have been claimed to make up most of the total adhesion forces at the interface for an organic coating, as mechanical adhesion is expected to be much larger than the adhesion relying on secondary bonding forces [41, 81, 174]. Therefore, the chemistry of the surfaces has not affected the in-situ investigations, and the contribution from the macro level topographical features to the bond strength is significantly more important than the effect of surface oxide composition on the molecular level. Hence, a detailed knowledge of the chemistry of the film is not of utmost importance for the qualitative interpretation of the data.

The importance of the surface composition has previously been proved for the CD mechanism [10]. Oxide layers rich in Fe^{3+} will inhibit the electron transfer processes, and hence the oxygen reduction rate and CD [101]. Therefore, the change in surface chemistry when changing roughness, may affect the electrochemical stability of the interfacial bond. However, in the mechanistic in-situ studies on the effect of roughness on CD, the highest Fe^{3+}/Fe^{2+} ratio measured on the patterned surfaces was 1.26 and the lowest was 0.80. Hence, both the ratio and the variation between the surfaces were too small to affect the oxygen reduction reaction

and the cathodic disbonding behaviour. In addition, a potential difference of 60 mV was measured between the surface with the highest and lowest potential, which confirms that the electrochemical properties of the surfaces were quite similar. Hence, the variations in surface oxide chemistry are insignificant and assumed not to be responsible for the CD resistance and wet adhesion properties measured. The XPS analysis and surface potentials measured by SKP on bare substrates contribute to this recognition.

Few conventional adhesion tests have been performed, and only in the studies presented in Paper IV and Paper V. After experimenting with pull-off and cross-cut tests on samples that first had been immersed in water, we concluded that conventional adhesion tests, especially in wet conditions, are too sensitive to experimental errors and give little information about the actual adhesion forces between the coating and the substrate, nor about the stability of the interfacial bonds in humid and corrosive conditions. The adhesion strength measured in such macroscopic tests, is therefore not necessarily predictive for the resistance of the coating/steel interface to electrochemical degradation, to the extent that adhesion strength actually has an effect on electrochemical degradation. In paper II we therefore employed the SKP technique to evaluate wet adhesion properties by a novel method. Wapner et al. found that the ingress of electrolyte along the interface from a defect measured in inert gas, may result in wet de-adhesion [117]. If the potential in the vicinity of the defect does not return to values corresponding to the pristine coating/steel interface when changing from inert air to oxygen atmosphere, the coating disbonded with the incorporation of hydrated ions along the interface in inert atmosphere.

6.4   Future work

There are topics still not covered which should be addressed in further investigations:

- Employing surfaces with periodic patterns, on which various oxides are produced under controlled conditions, would allow for even more insight into the effect of surface roughness and topography versus surface chemistry.
- Employing surfaces with tilted asperities in profile, as surface C (see Figure 17), but at lower heights. Evaluate how the interfacial stability is affected when the effective

contact area thus is reduced, while the ability for mechanical interlocking is unchanged. The tests would give even more insight into the importance of mechanical interlocking over the increase in the effective contact area.

- Initiate a scientific collaboration with the Material's Mechanics group at the Eindhoven University of Technology in The Netherlands. The group under the leadership of O. van der Sluis deals with the stability of the coating/metal interface by continuum modeling and also at the atomistic level by molecular dynamics, but without including electrochemical concepts and concerns in their models.

REFERENCES

1. Stratmann, M., R. Feser, and A. Leng, *Corrosion protection by organic films.* Electrochimica Acta, 1994. **39**(8–9): p. 1207-1214.
2. Grundmeier, G., W. Schmidt, and M. Stratmann, *Corrosion protection by organic coatings: electrochemical mechanism and novel methods of investigation.* Electrochimica Acta, 2000. **45**(15–16): p. 2515-2533.
3. Mills, D.J. and S.S. Jamali, *The best tests for anti-corrosive paints. And why: A personal viewpoint.* Progress in Organic Coatings, 2017. **102**: p. 8-17.
4. Knudsen, O.Ø. and A. Forsgren, *Corrosion control through organic coatings*. Second Edition ed. Corrosion Technology. 2017: Productivity Ptress. 255.
5. Mayne, J.E.O., *The Mechanism of the Inhibition of the Corrosion of Iron and Steel by Means of Paint.* Official Digest, 1952. **24**: p. 127.
6. Mayne, J.E.O., *The Mechanism of Protection By Organic Coatings.* Metal Finishing, 1966. **12**(143): p. 437-441.
7. Mayne, J.E.O., *The Mechanism of the Protective Action of Paints*, in *Corrosion*, L.L. Shreir, Editor. 1976, Newnes-Butterwoths: London. p. 24.
8. Lyon, S.B., R. Bingham, and D.J. Mills, *Advances in corrosion protection by organic coatings: What we know and what we would like to know.* Progress in Organic Coatings, 2017. **102**: p. 2-7.
9. Wielant, J., et al., *SKP as a tool to study the physicochemical interaction at buried metal–coating interfaces.* Surface and Interface Analysis, 2010. **42**(6-7): p. 1005-1009.
10. Wielant, J., et al., *Cathodic delamination of polyurethane films on oxide covered steel – Combined adhesion and interface electrochemical studies.* Corrosion Science, 2009. **51**(8): p. 1664-1670.
11. Wapner, K., M. Stratmann, and G. Grundmeier, *Application of the Scanning Kelvin Probe for the study of the corrosion resistance of interfacial thin organosilane films at adhesive/metal interfaces.* Silicon Chemistry, 2005. **2**(5): p. 235-245.
12. Williams, G., et al., *Dopant Effects in Polyaniline Inhibition of Corrosion-Driven Organic Coating Cathodic Delamination on Iron.* Journal of The Electrochemical Society, 2006. **153**(10): p. B425-B433.
13. Williams, G. and H.N. McMurray, *Inhibition of corrosion driven delamination on iron by smart-release bentonite cation-exchange pigments studied using a scanning Kelvin probe technique.* Progress in Organic Coatings, 2017. **102**: p. 18-28.
14. Posner, R., et al., *Electrochemical investigation of the coating/substrate interface stability for styrene/acrylate copolymer films applied on iron.* Corrosion Science, 2010. **52**(1): p. 37-44.
15. Leng, A., et al., *The delamination of polymeric coatings from steel. Part 3: Effect of the oxygen partial pressure on the delamination reaction and current distribution at the metal-polymer interface.* Corrosion Science, 1999. **41**(3): p. 599-620.
16. Bi, H. and J. Sykes, *An investigation of cathodic oxygen reduction beneath an intact organic coating on mild steel and its relevance to cathodic disbonding.* Progress in Organic Coatings, 2015. **87**: p. 83-87.
17. Bi, H. and J. Sykes, *Cathodic delamination of unpigmented and pigmented epoxy coatings from mild steel.* Progress in Organic Coatings, 2016. **90**: p. 114-125.
18. Skar, J.I. and U. Steinsmo, *Cathodic disbonding of paint films: transport of charge.* Corros. Sci., 1993. **5**(8): p. 1385-9.

19.   Khun, N.W. and G.S. Frankel, *Effects of surface roughness, texture and polymer degradation on cathodic delamination of epoxy coated steel samples.* Corrosion Science, 2013. **67**: p. 152-160.

20.   Packham, D.E., *The mechanical theory of adhesion - a seventy year perspective and its current status*, in *First international congrenss on adhesion science and technology*, W.J.v. Ooij and H.R. Andersen, Editors. 1998, VSP: Utrecht, Netherlands. p. 28 p.

21.   Packham, D.E., *Surface roughness and adhesion*, in *Adhesion Science and Engineering*, M. Chaudhury and A.V.Pocius, Editors. 2002, Elsevier Science B.V.: Amsterdam. p. 317-349.

22.   Packham, D.E., *Surface energy, surface topography and adhesion.* International Journal of Adhesion and Adhesives, 2003. **23**(6): p. 437-448.

23.   Lee, L.H., *The Chemistry and Physics of Solid Adhesion*, in *Fundamentals of Adhesion*, L.H. Lee, Editor. 1991, Plenum Press: London. p. 1-86.

24.   ISO 8501-1, *Preparation of steel substrates before application of paints and related products - Visual assessment of surface cleanliness - Part 1: Rust grades and preparation grades of uncoated steel substrates and of steel substrates after overall removal of previous coatings*. 2007, International Organization for Standardization: Geneve.

25.   ISO 8503-4, *Surface roughness characteristics of blast-cleaned steel substrates - Part 4: Method for the calibration of ISO surface profile comparators and for the determination of surface profile - Stylus instrument procedure.* 2012, International Organization for Standardization: Geneve.

26.   ISO 8503-2, *Preparation of steel substrates before application of paints and related products - Surface roughness characteristics of blast-cleaned steel substrates - Part 2: Method for the grading of surface profile of abrasive blast-cleaned steel - Comparator method.* 2012, International Organization for Standardization: Geneve.

27.   Knudsen, O., *Review of Coating Failure Incidents on the Norwegian Continental Shelf since the Introduction of NORSOK M-501*, in *CORROSION 2013*, NACE, Editor. 2013, NACE

28.   Hagen, H.M.C. and O.Ø. Knudsen, *Corrosion protection of smooth surfaces - coating adhesion*, in *Nordic Corrosion Congress*, T. Hemmingsen, Editor. 2015: Stavanger. p. p.12.

29.   Hagen, C.H.M., A. Kristoffersen, and O.Ø. Knudsen, *The Effect of Surface Profile on Coating Adhesion and Corrosion Resistance*, in *CORROSION 2016*, NACE, Editor. 2016, NACE Vancouver. p. p. 15.

30.   Hagen, C.M.H., et al., *The effect of surface roughness on corrosion resistance of machined and epoxy coated steel.* Progress in Organic Coatings, 2019. **130**: p. 17-23.

31.   Sørensen, P.A., et al., *Influence of substrate topography on cathodic delamination of anticorrosive coatings.* Progress in Organic Coatings, 2009. **64**(2–3): p. 142-149.

32.   Rincon Troconis, B.C. and G.S. Frankel, *Effect of Roughness and Surface Topography on Adhesion of PVB to AA2024-T3 using the Blister Test.* Surface and Coatings Technology, 2013. **236**(0): p. 531-539.

33.   Ward, D., *An Investigation Into The Effect Of Surface Profile On The Performance Of Coatings In Accelerated Corrosion Tests*, in *CORROSION 2007*. 2007, NACE: Houston, TX. p. p. 16.

34. van Dam, J.P.B., et al., *Effect of surface roughness and chemistry on the adhesion and durability of a steel-epoxy adhesive interface.* International Journal of Adhesion and Adhesives, 2020. **96**: p. 102450.

35. Watts, J.F. and J.E. Castle, *The application of X-ray photoelectron spectroscopy to the study of polymer-to-metal adhesion. Part 2 The cathodic disbondment of epoxy coated mild steel.* Journal of Materials Science, 1984. **19**: p. 2259-72.

36. Jamali, S.S. and D.J. Mills, *Steel surface preparation prior to painting and its impact on protective performance of organic coating.* Progress in Organic Coatings, 2014. **77**(12, Part B): p. 2091-2099.

37. Kendig, M., et al., *Environmental Integrity of Coating/Metal Interface*. 1990. 60.

38. Williams, G., H.N. McMurray, and D.A. Worsley *Cerium(III) Inhibition of Corrosion-Driven Organic Coating Delamination Studied Using a Scanning Kelvin Probe Technique.* Journal of The Electrochemical Society, 2002. **149**(4): p. B154-B162.

39. Baldan, A., *Adhesion phenomena in bonded joints.* International Journal of Adhesion and Adhesives, 2012. **38**: p. 95-116.

40. Islam, M.S., L. Tong, and P.J. Falzon, *Influence of metal surface preparation on its surface profile, contact angle, surface energy and adhesion with glass fibre prepreg.* International Journal of Adhesion and Adhesives, 2014. **51**(0): p. 32-41.

41. Sluis, O.v.d., S.P.M. Noijen, and P.H.M. Timmermans, *On the effect of microscopic roughness on macroscopic polymer-metal adhesion*, in *Solid state lighting reliability: components to systems*, W.D.v. Driel and X.J.Fan, Editors. 2013, Springer.

42. Hölck, O., et al., *Comparative characterization of chip to epoxy interfaces by molecular modeling and contact angle determination.* Microelectronics Reliability, 2012. **52**(7): p. 1285-1290.

43. Kim, W.-S., et al., *Evaluation of mechanical interlock effect on adhesion strength of polymer–metal interfaces using micro-patterned surface topography.* International Journal of Adhesion and Adhesives, 2010. **30**(6): p. 408-417.

44. Kromer, R., et al., *Laser surface patterning to enhance adhesion of plasma sprayed coatings.* Surface and Coatings Technology, 2015. **278**: p. 171-182.

45. Kromer, R., et al., *Laser Patterning Pretreatment before Thermal Spraying: A Technique to Adapt and Control the Surface Topography to Thermomechanical Loading and Materials.* Journal of Thermal Spray Technology, 2016. **25**(3): p. 401-410.

46. Nazarov, A., et al., *An SKP and EIS investigation of amine adsorption on zinc oxide surfaces.* Surface and Interface Analysis, 2011. **43**(10): p. 1286-1298.

47. Brockmann, W., *Durability of Adhesion Between Metals and Polymers.* The Journal of Adhesion, 1989. **29**(1-4): p. 53-61.

48. Venables, J.D., *Adhesion and durability of metal-polymer bonds.* Journal of Materials Science, 1984. **19**(8): p. 2431-2453.

49. Roper, H., E.E.F. Weaver, and J. Brandon, *The effect of peak count of sourghess roughness on coating performance.* The Journal of Protective Coatings and Linings 2005(June): p. 52-65.

50. Kendig, M. and D.J. Mills, *An historical perspective on the corrosion protection by paints.* Progress in Organic Coatings, 2017. **102**: p. 53-59.

51. Fourche, G., *An overview of the basic aspects of polymer adhesion. Part I: Fundamentals.* Polymer Engineering & Science, 1995. **35**(12): p. 957-967.

52. Noijen, S.P.M., et al., *Numerical prediction of failure paths at a roughened metal/polymer interface.* Microelectronics Reliability, 2009. **49**(9): p. 1315-1318.

53. van der Leeden, M.C. and G. Frens, *Surface Properties of Plastic Materials in Relation to Their Adhering Performance.* Advanced Engineering Materials, 2002. **4**(5): p. 280-289.

54. Kinloch, A.J., *The science of adhesion, part 2: Mechanics and mechanisms of failure*, in *Adhesion and Adhesives: Science and Technology*, A.J. Kinloch, Editor. 1982, Chapman Hall: London. p. 56-97.

55. Meyer, E., et al., *Normal forces at the atomic scale*, in *Nanoscience:Friction and rheology of the nanometer scale*. 1998, World Scientific Publishing Co.Pte.Ltd.

56. Packham, D.E., *The Mechanical Theory of Adhesion—Changing Perceptions 1925-1991.* The Journal of Adhesion, 1992. **39**(2-3): p. 137-144.

57. Packham, D.E. and C. Johnston, *Mechanical adhesion: were McBain and Hopkins right? An empirical study.* International Journal of Adhesion and Adhesives, 1994. **14**(2): p. 131-135.

58. Young, T., *III. An essay on the cohesion of fluids.* Philosophical Transactions of the Royal Society of London, 1805. **95**: p. 65-87.

59. Yuan, Y. and T.R. Lee, *Contact Angle and Wetting Properties*, in *Surface Science Techniques*, G. Bracco and B. Holst, Editors. 2013, Springer Berlin Heidelberg: Berlin, Heidelberg. p. 3-34.

60. Wenzel, R.N., *Resistance of solid surfaces to wetting by water.* Industrial & Engineering Chemistry, 1936. **28**(8): p. 988-994.

61. Hiemenz, P.C. and R. Rajagopalan, *Principles of colloid and surface chemistry*. 3rd ed. 1997, New York - Basel: CRC Press. 672.

62. Li, W. and D.Y. Li, *On the correlation between surface roughness and work function in copper.* The Journal of Chemical Physics, 2005. **122**(6): p. 064708.

63. Y. X, Q., et al., *Electrochemical behaviour of high nitrogen bearing stainless steel in acidic chloride solution: Effects of oxygen, acid concentration and surface roughness.* Electrochimica Acta - ELECTROCHIM ACTA, 2009. **54**: p. 2298-2304.

64. Dupré, *Theorie Mechanique de la Chaleur.* Phil.Mag., 1869. **5**(30).

65. Reinhart, F.W., *Nature of adhesion.* Journal of Chemical Education, 1954. **31**(3): p. p. 128.

66. Kinloch, A.J., *The science of adhesion, part 1: Surface and interfacial aspects.* Journal of Materials Science, 1980. **15**(9): p. 2141-2166.

67. Mittal, K.L., *Adhesion measurement: Recent progress, unsolved problems, and prospects*, in *Adhesion measurement of thin films, thick films, and bulk coatings*, K.L. Mittal, Editor. 1978, ASTM: Philadelphia, PA.

68. Bikerman, J.J., *Problems in adhesion measurement*, in *Adhesion measurement of thin films, thick films, and bulk coatings*, K.L. Mittal, Editor. 1978, American Society for Testing and Materials: Philadelphia, Pa. p. 30-38.

69. Axelsen, S.B. and O. Knudsen, *The effect of water-soluble salt contamination on coating performance*, in *CORROSION 2011*. 2011, NACE.

70. Morcillo, M., *Soluble salts: their effect on premature degradation of anticorrosive paints.* Progress in Organic Coatings, 1999. **36**(3): p. 137-147.

71. de la Fuente, D., J. Simancas, and M. Morcillo, *Effect of variable amounts of rust at the steel/paint interface on the behaviour of anticorrosive paint systems.* Progress in Organic Coatings, 2003. **46**(4): p. 241-249.

72. Bjrgum, A., et al. *Repair coating systems for bare steel: Effect of pre-treatment and conditions during application and curing*. 2007. Nashville, TN, United states: National Assoc. of Corrosion Engineers International.

73. Knudsen, O., A.K. Kvernbraten, and A. Bjrgum. *Performance of maintenance coatings applied on rusty steei surfaces*. 2009. Atlanta, GA, United states: National Assoc. of Corrosion Engineers International.

74. van der Sluis, O., et al., *Advances in Delamination Modeling of Metal/Polymer Systems: Continuum Aspects*, in *Nanopackaging: Nanotechnologies and Electronics Packaging*, J.E. Morris, Editor. 2018, Springer International Publishing: Cham. p. 83-128.

75. Leidheiser, H. and W. Funke, *Water Disbondment and Wet Adhesion of Organic Coatings on Metals: a Review and Interpretation.* J. Oil Colour Chem. Assoc., 1987. **70**(5): p. 121-132.

76. Rouw, A.C., *Model epoxy powder coatings and their adhesion to steel.* Progress in Organic Coatings, 1998. **34**(1): p. 181-192.

77. Leidheiser Jr, H., *Corrosion of Painted Metals--a Review.* Corrosion, 1982. **38**(7): p. 374-383.

78. Bull, S.J. and L.J. Balk, *Adhesion and delamination of interfaces.* Journal of Physics D: Applied Physics, 2010. **44**(3): p. 030301.

79. Chen, J. and S.J. Bull, *Approaches to investigate delamination and interfacial toughness in coated systems: an overview.* Journal of Physics D: Applied Physics, 2010. **44**(3): p. 034001.

80. Knudsen, O.Ø., *Methods for quantitative measurement of adhesion*. 1999, SINTEF: Trondheim. p. p. 26.

81. Noijen, S.P.M., et al., *A semi-analytic method for crack kinking analysis at isotropic bi-material interfaces.* Engineering Fracture Mechanics, 2012. **83**: p. 8-25.

82. Grundmeier, G. and M.Stratmann, *Adhesion and de-adhesion mechanisms at polymer/metal interfaces: Mechanistic understanding based on in situ studies of buried interfaces.* Annual Review of Materials Research, 2005. **35**: p. 571-615.

83. Leng, A., H. Streckel, and M. Stratmann, *The delamination of polymeric coatings from steel. Part 1: Calibration of the Kelvinprobe and basic delamination mechanism.* Corrosion Science, 1998. **41**(3): p. 547-578.

84. Stratmann, M., *2005 W.R. Whitney Award Lecture: Corrosion stability of Polymer-Coated Metals - New Consepts Based on Fundamental Understanding.* Corrosion, 2005. **61**(12): p. 1115-1126.

85. Steinsmo, U. and E. Bardal, *Factors Limiting the Cathodic Current on Painted Steel.* Journal of Electrochemical Society, 1989. **136**(12): p. 3588-3594.

86. Funke, W., *Toward a unified view of the mechanism responsible for paint defects by metallic corrosion.* Industrial & Engineering Chemistry Product Research and Development, 1985. **24**(3): p. 343-347.

87. Posner, R., O. Ozcan, and G. Grundmeier, *Water and Ions at Polymer/Metal Interfaces*, in *Design of Adhesive Joints Under Humid Conditions*, M.L.F. Silva and C. Sato, Editors. 2013, Springer Berlin Heidelberg: Berlin, Heidelberg. p. 21-52.

88. Sykes, J.M., et al., *Does "coating resistance" control corrosion?* Progress in Organic Coatings, 2017. **102**: p. 82-87.

89. Doherty, M. and J.M. Sykes, *Micro-cells beneath organic lacquers: a study using scanning Kelvin probe and scanning acoustic microscopy.* Corrosion Science, 2004. **46**(5): p. 1265-1289.

90. Taylor, S.R., *Chapter 22 - The role of intrinsic defects in the protective behavior of organic coatings*, in *Handbook of Environmental Degradation of Materials*, M. Kutz, Editor. 2005, William Andrew Publishing: Norwich, NY. p. 449-461.

91. Moongkhamklang, P. and S.R. Taylor, *The delineation of ionic pathways in organic coatings using a molecular probe technique.* Progress in Organic Coatings, 2003. **46**(4): p. 259-265.

92. Steinsmo, U. and E. Bardal, *Use of DC electrochemical methods for evaluation of paint films on steel, aluminum and zinc.* Corrosion, 1992. **48**(11): p. 910-917.

93. Lyon, S., L. Philippe, and E. Tsaousoglou, *Direct measurements of ionic diffusion in protective organic coatings.* Transactions of the Institute of Metal Finishing, 2006. **84**: p. 23-27.

94. Bierwagen, G.P., et al., *Studies of a new accelerated evaluation method for coating corrosion resistance — thermal cycling testing.* Progress in Organic Coatings, 2000. **39**(1): p. 67-78.

95. Posner, R., *Combined Spectroscopic and Electrochemical Studies of Ion Transport and Corrosive de-Adhesion Processes at Polymer/Oxide/Metal Interfaces Dissertation*, in *Faculty of Natural Sciences*. 2009, University of Paderborn: Paderborn. p. 165.

96. Rohwerder, M., *Passivity of Metals and the Kelvin Probe Technique*. 2017.

97. Díez-Pérez, I., F. Sanz, and P. Gorostiza, *Electronic barriers in the iron oxide film govern its passivity and redox behavior: Effect of electrode potential and solution pH.* Electrochemistry Communications, 2006. **8**(10): p. 1595-1602.

98. Sato, N., *An overview on the passivity of metals.* Corrosion Science, 1990. **31**: p. 1-19.

99. Lutton, K. and J.R. Scully, *Kinetics of Oxide Growth of Passive Films on Transition Metals*, in *Encyclopedia of Interfacial Chemistry*, K. Wandelt, Editor. 2018, Elsevier: Oxford. p. 284-290.

100. Wielant, J., et al., *Electronic properties of thermally formed thin iron oxide films.* Electrochimica Acta, 2007. **52**(27): p. 7617-7625.

101. Grundmeier, G. and M. Stratmann, *Influence of oxygen and argon plasma treatments on the chemical structure and redox state of oxide covered iron.* Applied Surface Science, 1999. **141**(1): p. 43-56.

102. Koehler, E.L., *The Oxide Film on Steel and Cathodic Disbondment of a Protective Organic Coating.* J. Electrochem. Soc., 1985. **132**(5): p. 1005-1009.

103. Sørensen, P.A., et al., *Anticorrosive coatings: a review.* JCT Research, 2009. **6**(2): p. 135-176.

104. Knudsen, O.O., U. Steinsmo, and M. Bjordal, *Zinc-rich primers - Test performance and electrochemical properties.* Progress in Organic Coatings, 2005. **54**(3): p. 224-229.

105. Knudsen, O.Ø., et al. *Zinc rich epoxies - Electrochemical properties*. in *CORROSION/2007*. 2007. Nashville, TN, United states: NACE.

106. Knudsen, O.Ø., A. Bjørgum, and L. Teigen, *Long-life, low-maintenance coating systems.* Materials performance, 2012. **51**(6): p. 5 p.

107. Knudsen, O.Ø., A. Bjørgum, and L.T. Døssland. *Low Maintenance Coating Systems for Constructions with Long Lifetime*. in *CORROSION/2012*. 2012. Salt Lake City: NACE.

108. Crespy, D., et al., *Self-Healing for Anticorrosion Based on Encapsulated Healing Agents*, in *Self-healing Materials*, M.D. Hager, S. van der Zwaag, and U.S. Schubert, Editors. 2016, Springer International Publishing: Cham. p. 219-245.

109. Posner, R., M. Santa, and G. Grundmeier, *Wet- and Corrosive De-Adhesion Processes of Water-Borne Epoxy Film Coated Steel: I. Interface Potentials and Characteristics of*

Ion Transport Processes. Journal of The Electrochemical Society, 2011. **158**(3): p. C29-C35.

110.   Montoya, R., et al., *A cathodic delamination study of coatings with and without mechanical defects.* Corrosion Science, 2014. **82**(0): p. 432-436.

111.   Fürbeth, W. and M. Stratmann, *The delamination of polymeric coatings from electrogalvanised steel – a mechanistic approach.: Part 1: delamination from a defect with intact zinc layer.* Corrosion Science, 2001. **43**(2): p. 207-227.

112.   Leng, A., H. Streckel, and M. Stratmann, *The delamination of polymeric coatings from steel. Part 2: First stage of delamination, effect of type and concentration of cations on delamination, chemical analysis of the interface.* Corrosion Science, 1998. **41**(3): p. 579-597.

113.   Fürbeth, W. and M. Stratmann, *The delamination of polymeric coatings from electrogalvanized steel – a mechanistic approach.: Part 3: delamination kinetics and influence of CO2.* Corrosion Science, 2001. **43**(2): p. 243-254.

114.   Kappes, M., G.S. Frankel, and N. Sridhar, *Adhesion and adhesion degradation of a pressure sensitive tape on carbon steel.* Progress in Organic Coatings, 2010. **69**(1): p. 57-62.

115.   Reddy, B. and J.M. Sykes, *Degradation of organic coatings in a corrosive environment: a study by scanning Kelvin probe and scanning acoustic microscope.* Progress in Organic Coatings, 2005. **52**(4): p. 280-287.

116.   Reddy, B., M.J. Doherty, and J.M. Sykes, *Breakdown of organic coatings in corrosive environments examined by scanning kelvin probe and scanning acoustic microscopy.* Electrochimica Acta, 2004. **49**(17–18): p. 2965-2972.

117.   Wapner, K., M. Stratmann, and G. Grundmeier, *In situ infrared spectroscopic and scanning Kelvin probe measurements of water and ion transport at polymer/metal interfaces.* Electrochimica Acta, 2006. **51**(16): p. 3303-3315.

118.   Morsch, S., et al., *Molecularly controlled epoxy network nanostructures.* Polymer, 2017. **108**: p. 146-153.

119.   Nguyen, T., J.B. Hubbard, and J.M. Pommersheim, *Unified model for the degradation of organic coatings on steel in a neutral electrolyte.* JOURNAL OF COATINGS TECHNOLOGY, 1996. **68**(855): p. 45-56.

120.   Legghe, E., et al., *Correlation between water diffusion and adhesion loss: Study of an epoxy primer on steel.* Progress in Organic Coatings, 2009. **66**(3): p. 276-280.

121.   Posner, R., et al., *Transport processes of hydrated ions at polymer/oxide/metal interfaces: Part 1. Transport at interfaces of polymer coated oxide covered iron and zinc substrates.* Electrochimica Acta, 2009. **54**(3): p. 891-899.

122.   Henderson, M.A., *The interaction of water with solid surfaces: fundamental aspects revisited.* Surface science reports, 2002. **46**(1): p. 1-308.

123.   Wielant, J., *Influence of the oxide/coating interface on the adhesion and delamination of organic coatings*, in *Department of Materials & Chemistry*. 2009, Vrije Universiteit Brussel: Brussel. p. 313.

124.   Wielant, J., et al., *Influence of the Iron Oxide Acid–Base Properties on the Chemisorption of Model Epoxy Compounds Studied by XPS.* The Journal of Physical Chemistry C, 2007. **111**(35): p. 13177-13184.

125.   Pletincx, S., et al., *In Situ Characterization of the Initial Effect of Water on Molecular Interactions at the Interface of Organic/Inorganic Hybrid Systems.* Scientific Reports, 2017. **7**: p. 45123.

126. Posner, R., et al., *Transport processes of hydrated ions at polymer/oxide/metal interfaces: Part 2. Transport on oxide covered iron and zinc surfaces.* Electrochimica Acta, 2009. **54**(3): p. 900-908.

127. Iqbal, D., et al., *Study of polymer coating delamination kinetics on zinc modified with zinc oxide of different morphologies.* Materials and Corrosion, 2014. **65**(4): p. 370-375.

128. Iqbal, D., et al., *Synthesis of ultrathin poly (methyl methacrylate) model coatings bound via organosilanes to zinc and investigation of their delamination kinetics.* ACS applied materials & interfaces, 2014. **6**(20): p. 18112-18121.

129. Sykes, J.M. and M. Doherty, *Interpretation of Scanning Kelvin Probe potential maps for coated steel using semi-quantitative current density maps.* Corrosion Science, 2008. **50**(10): p. 2773-2778.

130. Marcus, P. and V. Maurice, *Oxide Passive Films and Corrosion Protection*, in *Oxide Ultrathin Films*, G. Pcchioni and S. Valeri, Editors. 2012. p. 119-144.

131. Holness, R.J., et al., *Polyaniline Inhibition of Corrosion-Driven Organic Coating Cathodic Delamination on Iron.* Journal of The Electrochemical Society, 2005. **152**(2): p. B73-B81.

132. Nagayama, M.i. and M. Cohen, *The Anodic Oxidation of Iron in a Neutral Solution: I . The Nature and Composition of the Passive Film.* Journal of The Electrochemical Society, 1962. **109**(9): p. 781-790.

133. Hoffmann, K. and M. Stratmann, *Delamination of organic coatings from rusty steel substrates.* Corros. Sci., 1993. **34**(10): p. 1625-45.

134. Antony, H., et al., *Study of lepidocrocite γ-FeOOH electrochemical reduction in neutral and slightly alkaline solutions at 25°C.* Electrochimica Acta, 2005. **51**(4): p. 745-753.

135. Haupt, S. and H.H. Strehblow, *Corrosion, layer formation, and oxide reduction of passive iron in alkaline solution: a combined electrochemical and surface analytical study.* Langmuir, 1987. **3**(6): p. 873-885.

136. Knudsen, O. and U. Steinsmo, *Effect of Barrier Pigments on Cathodic Disbonding Part 2: Mechanism of the Effect of Aluminium Pigments.* Journal of Corrosion Science & Engineering, 1999. **2**.

137. Sørensen, P.A., et al., *Reduction of cathodic delamination rates of anticorrosive coatings using free radical scavengers.* Journal of Coatings Technology and Research, 2010. **7**(6): p. 773-786.

138. Wroblowa, H.S., *Intermediate products of atmospheric oxygen reduction and the integrity of metal—organic coating interface.* Journal of Electroanalytical Chemistry, 1992. **339**(1): p. 31-40.

139. Allahar, K.N., M.E. Orazem, and K. Ogle, *Mathematical model for cathodic delamination using a porosity–pH relationship.* Corrosion Science, 2007. **49**(9): p. 3638-3658.

140. Stratmann, M., et al., *On the atmospheric corrosion of metals which are covered with thin electrolyte layers-iii. the measurement of polarisation curves on metal surfaces which are covered by thin electrolyte layers.* Corrosion Science, 1990. **30**(6–7): p. 715-734.

141. Hausbrand, R., M. Stratmann, and M. Rohwerder, *The Physical Meaning of Electrode Potentials at Metal Surfaces and Polymer/Metal Interfaces: Consequences for Delamination.* Journal of The Electrochemical Society, 2008. **155**(7): p. C369-C379.

142. Stratmann, M., et al., *The scanning Kelvin probe; a new technique for the in situ analysis of the delamination of organic coatings.* Progress in Organic Coatings, 1996. **27**(1–4): p. 261-267.

143. J.F.Watts, *Cathodic disbondment*, in *Handbook of Adhesion*, D.E. Packham, Editor. 2005, John Wiley and Sons, Ltd.

144. Harun, M.K., J. Marsh, and S.B. Lyon, *The effect of surface modification on the cathodic disbondment rate of epoxy and alkyd coatings.* Progress in Organic Coatings, 2005. **54**: p. 317-321.

145. Watts, J.F. and J.E. Castle, *The application of X-ray photoelectron spectroscopy to the study of polymer-to-metal adhesion. Part 1 Polybutadiene coated mild steel.* J. Mat. Sci., 1983. **18**: p. 2987-3003.

146. Cambier, S.M., R. Posner, and G.S. Frankel, *Coating and interface degradation of coated steel, Part 1: Field exposure.* Electrochimica Acta, 2014. **133**: p. 30-39.

147. Pourbaix, M., *Atlas of Electrochemical Equilibria in Aqueous Solutions*. 1974, Houston, TX: NACE.

148. Leidheiser, H., W. Wang, and L. Igetoft, *The Mechanism for the Cathodic Delamination of Organic Coatings From a Metal Surface.* Prog. Org. Coat., 1983. **11**(1): p. 19-40.

149. Klimow, G., N. Fink, and G. Grundmeier, *Electrochemical studies of the inhibition of the cathodic delamination of organically coated galvanised steel by thin conversion films.* Electrochimica Acta, 2007. **53**(3): p. 1290-1299.

150. Posner, R., et al., *Transport processes of hydrated ions at polymer/oxide/metal interfaces.* Electrochimica Acta, 2009. **54**(3): p. 891-899.

151. Parks, J. and H. Leidheiser, *Ionic Migration through Organic Coatings and Its Consequences to Corrosion.* Ind. Eng. Chem. Prod. Res. Dev., 1985. **25**(1): p. 1-6.

152. Steinsmo, U.M., *The Cathodic Properties of Painted Steel*. 1986, Norwegian Institute of Technology: Trondheim. p. 160.

153. Steinsmo, U., J.I. Skar, and E. Bardal, *The Effect of the Dry Film Thickness, Temperature, and Electrolyte on the Cathodic Current of Painted Steel.* Journal of The Electrochemical Society, 1989. **136**(12): p. 3583-3588.

154. Skar, J.I., U. Steinsmo, and E. Bardal. *The Effect of Temperature, Dry Film Thickness and Electrolyte on cathodic disbonding and Charge Transport through Organic Coatings*. in *177th Electrochemical Society Meeting*. 1990. The Electrochemical Society.

155. Knudsen, O.Ø. and U. Steinsmo, *Effects of Cathodic Disbonding and Blistering on Current Demand for Cathodic Protection of Coated Steel.* Corrosion, 2000. **56**(3): p. 256-264.

156. Knudsen, O.Ø., *Cathodic disbonding of organic coatings on submerged steel*, in *Department for machine design and materials technology*. 1998, NTNU: Trondheim.

157. Knudsen, O.Ø. and J.I. Skar. *Cathodic Disbonding of Epoxy Coatings - Effect of Test Parameters*. in *CORROSION/08*. 2008. New Orleans: NACE.

158. Stratmann, M., R. Feser, and A. Leng, *Corrosion Protection by Organic Films.* Electrochimica Acta, 1994. **39**(8/9): p. 1207.

159. Williams, G. and H.N. McMurray, *Chromate Inhibition of Corrosion-Driven Organic Coating Delamination Studied Using a Scanning Kelvin Probe Technique.* Journal of The Electrochemical Society, 2001. **148**(10): p. B377-B385.

160. Le Bozec, N., et al., *Influence of stainless steel surface treatment on the oxygen reduction reaction in seawater.* Corrosion Science, 2001. **43**(4): p. 765-786.

161. Sørensen, P.A., et al., *Cathodic delamination of seawater-immersed anticorrosive coatings: Mapping of parameters affecting the rate.* Progress in Organic Coatings, 2010. **68**(4): p. 283-292.

162. Nazarov, A. and D. Thierry, *Application of Scanning Kelvin Probe in the Study of Protective Paints.* Frontiers in Materials, 2019. **6**(192).

163. Steinsmo, U. and J.I. Skar, *FACTORS INFLUENCING THE RATE OF CATHODIC DISBONDING OF COATINGS.* Corrosion, 1994. **50**(12): p. 934-939.

164. Doherty, M. and J.M. Sykes, *A quantitative study of blister growth on lacquered food cans by scanning acoustic microscopy.* Corrosion Science, 2008. **50**(10): p. 2755-2772.

165. Glover, C.F., et al., *Evaluation of multi-layered graphene nano-platelet composite coatings for corrosion control part II – Cathodic delamination kinetics.* Corrosion Science, 2018. **136**: p. 304-310.

166. Fürbeth, W. and M. Stratmann, *The delamination of polymeric coatings from electrogalvanized steel – a mechanistic approach.: Part 2: delamination from a defect down to steel.* Corrosion Science, 2001. **43**(2): p. 229-241.

167. Hsu, L.C., et al., *Effect of Micro- and Nanoscale Topography on the Adhesion of Bacterial Cells to Solid Surfaces.* Applied and Environmental Microbiology, 2013. **79**(8): p. 2703-2712.

168. de Wijn, A.S., *Why surface roughness is similar at different scales.* Nature, 2020. **578**: p. 2.

169. Hutchings, I.M., *Tribology: friction and wear of engineering materials*. 1992: Technology and engineering. 280.

170. Colbeck, S.C., *A review of the friction of snow skis.* J Sports Sci, 1994. **12**(3): p. 285-95.

171. Migita, S., S. Okuyama, and K. Araki, *Sub-micrometer scale surface roughness of titanium reduces fibroblasts function.* J Appl Biomater Funct Mater, 2016. **14**(1): p. e65-9.

172. Pastewka, L. and M.O. Robbins, *Contact between rough surfaces and a criterion for macroscopic adhesion.* Proceedings of the National Academy of Sciences, 2014. **111**(9): p. 3298-3303.

173. Persson, B.N., et al., *On the nature of surface roughness with application to contact mechanics, sealing, rubber friction and adhesion.* J Phys Condens Matter, 2005. **17**(1): p. R1-r62.

174. Evans, A.G., et al., *The fracture energy of bimaterial interfaces.* Metallurgical Transactions A, 1990. **21**(9): p. 2419-2429.

175. ISO 4287, *Geometrical Product Specifications (GPS) - Surface texture: Profile method - Terms, definitions and surface texture parameters.* 2000, International Organization for Standardization: Geneve.

176. ISO 4288, *Geometrical Product Specifications (GPS) - Surface texture : Profile method - Rules and procedures for the assessment of surface texture.* 1996, International Organization for Standardization: Geneve.

177. Harris, A.F. and A. Beevers, *The effects of grit-blasting on surface properties for adhesion.* International Journal of Adhesion and Adhesives, 1999. **19**(6): p. 445-452.

178. Watts, J.F., *Mechanistic aspects of the cathodic delamination of organic coatings.* J. Adhes., 1989. **31**(1): p. 73-85.

179. Watts, J.F., *The application of X-ray photoelectron spectroscopy to the study of polymer-to-metal adhesion. Part 3 The influence of substrate surface chemistry on the*

cathodic disbondment process. Journal of Materials Science, 1984. **19**(10): p. 3459-3465.

180. McBain, J.W. and D.G. Hopkins, *On Adhesives and Adhesive Action.* The Journal of Physical Chemistry, 1925. **29**(2): p. 188-204.

181. Yao, Q. and J. Qu, *Interfacial Versus Cohesive Failure on Polymer-Metal Interfaces in Electronic Packaging—Effects of Interface Roughness.* Journal of Electronic Packaging, 2002. **124**(2): p. 127-134.

182. Longley, J.E., *Surface Modifications in Adhesion and Wetting*, in *Department of Chemical Engineering*. 2013, Lehigh University: Betlehem, Pennsylvania. p. 284.

183. Taylor, R. and L. Scribner, *The Measurement and Correction of Electrolyte Resistance in Electrochemical Tests*. 1990, West Conchohoken: ASTM International.

184. Posner, R., et al., *In situ electrochemical Scanning Kelvin Probe Blister-Test studies of the de-adhesion kinetics at polymer/zinc oxide/zinc interfaces.* Electrochimica Acta, 2009. **54**(21): p. 4837-4843.

185. Ogle, K., S. Morel, and N. Meddahi, *An electrochemical study of the delamination of polymer coatings on galvanized steel.* Corrosion Science, 2005. **47**(8): p. 2034-2052.

186. Nazarov, A., et al., *Scanning Kelvin Probe Investigation of Corrosion Under Thick Marine Paint Systems Applied on Carbon Steel.* Corrosion, 2012. **68**(8): p. 720-729.

187. Nazarov, A., N. Le Bozec, and D. Thierry, *Assessment of steel corrosion and deadhesion of epoxy barrier paint by scanning Kelvin probe.* Progress in Organic Coatings, 2018. **114**: p. 123-134.

188. ISO 12994, *Paints and varnishes - Corrosion protection of steel structures by protective paint systems.* 2007, International Organization for Standardization: Geneve.

189. ISO 15711, *Paints and varnishes - Determination of resistance to cathodic disbonding of coatings exposed to sea water.* 2003, International Organization for Standardization: Geneve.

190. ISO 4624, *Paints and varnishes - Pull-off test for adhesion.* 2003, The International Organization for Standardization: Geneve.

191. ISO 2409, *Paints and varnishes - Cross-cut test*. 1992, The International Organization for Standardization: Geneve.

192. ISO 6272, *Paints and varnishes - Rapid-deformation (impact resistance) tests.*, in *Part 1: Falling-weight test, large-area indenter* 2011, DIN: Germany.

193. Roper, H., E.E.R. Weaver, and J. Brandon, *Peak performance from abrasives.* Journal of Protective Coatings & Linings, 2006(June): p. 24-31.

194. Momber, A.W., *Blast Cleaning Technology*. 1 ed. 2008: Springer-Verlag Berlin Heidelberg.

195. Groover, M., *Principles of modern manufacturing, SI Version*. 5th ed. 2013: Wiley.

196. Ta, V.D., et al., *Laser textured superhydrophobic surfaces and their applications for homogeneous spot deposition.* Applied Surface Science, 2016. **365**: p. 153-159.

197. Pfleging, W., *A review of laser electrode processing for development and manufacturing of lithium-ion batteries.* Nanophotonics, 2018. **7**(3): p. 549.

198. Mottay, E., et al., *Industrial applications of ultrafast laser processing.* MRS Bulletin, 2016. **41**(12): p. 984-992.

199. Pfleging, W. *Technology description at KNMF Laboratory for micro- and nanostructuring. Laser materials processing*. [Web document] 2018 31.08.2018]; Technology description at KNMF Laboratory for micro- and nanostructuring]. Available from: https://www.knmf.kit.edu/LMP.php.

200. Sugioka, K., *Ultrafast Laser Processing of Glass Down to the Nano-Scale*, in *Laser-Surface Interactions for New Materials Production: Tailoring Structure and Properties*, A. Miotello and P.M. Ossi, Editors. 2010, Springer Berlin Heidelberg: Berlin, Heidelberg. p. 279-293.

201. Pfleging, W., M. Przybylski, and H.J. Brückner, *Excimer laser material processing: state-of-the-art and new approaches in microsystem technology*. Lasers and Applications in Science and Engineering. Vol. 6107. 2006: SPIE.

202. Lu, L., et al., *The Influence of Pulse Width and Energy on Temperature Field in Metal Irradiated by Ultrashort-Pulsed Laser.* Physics Procedia, 2012. **32**: p. 39-47.

203. Salem, L., *Epoxies for steel.* Journal of Protective Coatings & Linings, 1996: p. p. 77-98.

204. Nakazawa, M. and G.A. Somorjai, *A study of the adsorption of selected organic molecules to model the adhesion of epoxy resins: thermal desorption of glycidyl and phenoxy compounds from gold, iron oxide and zinc oxide.* Applied Surface Science, 1993. **68**(4): p. 539-555.

205. Nakazawa, M. and G.A. Somorjai, *Coadsorption of water and selected aromatic molecules to model the adhesion of epoxy resins on hydrated surfaces of zinc oxide and iron oxide.* Applied Surface Science, 1995. **84**(3): p. 309-323.

206. El-Din, N.M.S. and M.W. Sabaa, *Thermal degradation of poly(vinyl butyral) laminated safety glass.* Polymer Degradation and Stability, 1995. **47**(2): p. 283-288.

207. Wint, N., et al., *The Kinetics and Mechanism of Atmospheric Corrosion Occurring on Tin and Iron-Tin Intermetallic Coated Steels: I. Cathodic Delamination.* Journal of The Electrochemical Society, 2015. **162**(14): p. C775-C784.

208. Williams, G. and H.N. McMurray, *The mechanism of group (I) chloride initiated filiform corrosion on iron.* Electrochemistry Communications, 2003. **5**(10): p. 871-877.

209. Whyte, E.P. and J.M. Sykes, *Behaviour of a zinc–iron bimetallic couple coated with poly-vinyl butyral lacquer during intermittent exposure to salt solution.* Corrosion Science, 2007. **49**(8): p. 3361-3380.

210. Posner, R., et al., *Simultaneous in situ Kelvin probe and Raman spectroscopy analysis of electrode potentials and molecular structures at polymer covered salt layers on steel.* Electrochimica Acta, 2012. **83**(Supplement C): p. 327-334.

211. de la Fuente, D. and M. Rohwerder, *Fundamental investigation on the stability of the steel/coating interfaces contaminated by submicroscopic salt particles.* Progress in Organic Coatings, 2008. **61**(2): p. 233-239.

212. Fernández-Solis, C. and A. Erbe, *Waterborne chitosan–epoxysilane hybrid pretreatments for corrosion protection of zinc.* Biointerphases, 2016. **11**(2): p. 021001.

213. Cambier, S.M. and G.S. Frankel, *Coating and Interface Degradation of Coated steel, Part 2: Accelerated Laboratory Tests.* Electrochimica Acta, 2014. **136**: p. 442-449.

214. Grundmeier, G., et al., *Corrosion properties of chemically modified metal surfaces.* Electrochimica Acta, 1998. **43**(1): p. 165-174.

215. Terryn, H., et al., *On the importance of the chemical interface between organic coatings and metals*, in *AETOC*. 2017: Billerbeck, Germany.

216. Le Bozec, N., et al., *Influence of climatic factors (UV, salt concentration, wet-dry cycle) in cyclic corrosion tests used for marine paint systems*, in *EUROCORR 2011*. 2011: Stockholm, Sweden.

217. Le Bozec, N., C. Hall, and D. Melot. *Comparison of accelerated ageing tests as per ISO 20340 Annex A and NACE SP0108 standards*. in *CORROSION 2014*. 2014. San Antonio: NACE International.

218. Le Bozec, N., et al., *Performance of marine and offshore paint systems: Correlation of accelerated corrosion tests and field exposure on operating ships.* Materials and corrosion, 2015. **66**(3): p. 215-225.

219. Cambier, S.M., D. Verreault, and G.S. Frankel, *Raman Investigation of Anodic Undermining of Coated Steel During Environmental Exposure.* Corrosion, 2014. **70**(12): p. 1219-1229.

220. ISO 9227, *Corrosion tests in artificial atmospheres - Salt spray tests.* 2017, The International Organization for Standardization: Geneve.

221. ASTM B117, *Standard Practice for Operating Salt Spray (Fog) Apparatus.* 2016: West Conchohoken, PA.

222. ASTM D5894, *Standard Practice for Cyclic Salt Fog/UV Exposure of Painted Metal, (Alternating Exposures in a Fog/Dry Cabinet and a UV/Condensation Cabinet)*. 2016, ASTM International: West Conshohocken, PA.

223. Chang, B., *Critical Review of CD Standards*, in *Technology Exchange Group TEG 349x*. 2007, NACE International: Houston TX.

224. Carlsson, B., *Accelerated corrosion testing for product qualification*, in *CEEES First International Symposium on Environmental Testing Engineering*. 2007: Royal Military Academy, Brussels, Belgium.

225. NORSOK, *Cathodic Protection*. 1994, Standards Norway: Oslo.

226. Le Bozec, N., et al. *Round-robin evaluation of ISO 20340 Annex A test method*. in *CORROSION 2016*. 2016. Houston: NACE International.

227. Posner, R., et al., *Ion transport processes at polymer/oxide/metal interfaces under varying corrosive conditions.* Corrosion Science, 2010. **52**(5): p. 1838-1846.

228. Posner, R., et al., *Influence of interface chemistry and network density on interfacial ion transport kinetics for styrene/acrylate copolymer coated zinc and iron substrates.* Corrosion Science, 2010. **52**(3): p. 754-760.

229. Rohwerder, M., et al., *Application of SKP for in situ monitoring of ion mobility along insulator/insulator interfaces.* Electrochimica Acta, 2009. **54**(25): p. 6058-6062.

230. Rohwerder, M., *The Kelvin Probe Technique as Reference Electrode for Application on Thin and Ultrathin Electrolyte Films*. Handbook of Reference Electrodes., ed. I. G., L. A., and S. F. 2013, Berlin: Springer.

231. Nazarov, A. and D. Thierry, *Studies in the Electrical Double Layer at Metal/Polymer Interfaces by Scanning Capacitive Probe.* Protection of metals 2003. **39**(1): p. 55-62.

232. Nazarov, A. and D. Thierry, *Scanning Kelvin probe study of metal/polymer interfaces.* Electrochimica Acta, 2004. **49**(17–18): p. 2955-2964.

233. Nazarov, A. and D. Thierry, *Hydrolysis of interfacial bonds in a metal/polymer electrical double layer.* Protection of metals 2005. **41**(2): p. 105-116.

234. Fürbeth, W. and M. Stratmann, *Scanning Kelvinprobe investigations on the delamination of polymeric coatings from metallic surfaces.* Progress in Organic Coatings, 2000. **39**(1): p. 23-29.

235. Stratmann, M. and H. Streckel, *On the atmospheric corrosion of metals which are covered with thin electrolyte layers—I. Verification of the experimental technique.* Corrosion Science, 1990. **30**(6): p. 681-696.

236. Stratmann, M. and H. Streckel, *On the atmospheric corrosion of metals which are covered with thin electrolyte layers—II. Experimental results.* Corrosion Science, 1990. **30**(6): p. 697-714.

237. Frankel, G.S., et al., *Potential control under thin aqueous layers using a Kelvin Probe.* Corrosion Science, 2007. **49**(4): p. 2021-2036.

238. Barth, C., et al., *Recent Trends in Surface Characterization and Chemistry with High-Resolution Scanning Force Methods.* Advanced Materials, 2011. **23**(4): p. 477-501.

239. Rohwerder, M. and F. Turcu, *High-resolution Kelvin probe microscopy in corrosion science: Scanning Kelvin probe force microscopy (SKPFM) versus classical scanning Kelvin probe (SKP).* Electrochimica Acta, 2007. **53**(2): p. 290-299.

240. Senöz, C., *High resolution investigation of localized corrosion by in-situ Scanning Kelvin Probe Force Microscopy*, in *Department of Mechanical Engineering*. 2011, Ruhr-Universität Bochum: Bochum. p. 164.

241. Melitz, W., et al., *Kelvin probe force microscopy and its application.* Surface science reports, 2011. **66**: p. 1-27.

242. Larisa-Emilia, C., et al., *Work-function measurement by high-resolution scanning Kelvin nanoprobe.* Measurement Science and Technology, 2007. **18**(3): p. 567.

243. Trasatti, S., *Work function, electronegativity, and electrochemical behaviour of metals: II. Potentials of zero charge and "electrochemical" work functions.* Journal of Electroanalytical Chemistry and Interfacial Electrochemistry, 1971. **33**(2): p. 351-378.

244. Trasatti, S., *The "absolute" electrode potential—the end of the story.* Electrochimica Acta, 1990. **35**(1): p. 269-271.

245. Trasatti, S., *Surface science and electrochemistry: concepts and problems.* Surface Science, 1995. **335**: p. 1-9.

246. Örnek, C., C. Leygraf, and J. Pan, *On the Volta potential measured by SKPFM – fundamental and practical aspects with relevance to corrosion science.* Corrosion Engineering, Science and Technology, 2019. **54**(3): p. 185-198.

247. Bardeen, J., *Theory of the Work Function. II. The Surface Double Layer.* Physical Review, 1936. **49**(9): p. 653-663.

248. Nazarov, A. and D. Thierry, *Application of Volta potential mapping to determine metal surface defects.* Electrochimica Acta, 2007. **52**(27): p. 7689-7696.

249. Nazarov, A., et al., *Effect of Mechanical Stress on the Properties of Steel Surfaces: Scanning Kelvin Probe and Local Electrochemical Impedance Study.* Journal of The Electrochemical Society, 2017. **164**(2): p. C66-C74.

250. Maragliano, C., et al., *Quantifying charge carrier concentration in ZnO thin films by Scanning Kelvin Probe Microscopy.* Scientific Reports, 2014. **4**: p. 4203.

251. Bergveld, P., J. Hendrikse, and W. Olthuis, *Theory and application of the material work function for chemical sensors based on the field effect principle.* Measurement science and technology, 1998. **9**(11): p. 8.

252. Ashcroft, N.W. and N.D. Mermin, *Solid state physics*. 1976: Saunders College.

253. Stimming, U. and J.W. Schultze, *A semiconductor model of the passive layer on iron electrodes and its application to electrochemical reactions.* Electrochimica Acta, 1979. **24**(8): p. 859-869.

254. Davenport, A.J., et al., *The Structure of the Passive Film That Forms on Iron in Aqueous Environments.* Journal of The Electrochemical Society, 2000. **147**(6): p. 2162-2173.

255. Cappadonia, M. and K. Doblhofer, *The electrical state of NAFION coated electrodes emersed from liquid electrolytes.* Electrochimica Acta, 1989. **34**(12): p. 1815-1818.

256. Baikie, I.D., et al., *Noise and the Kelvin method.* Review of Scientific Instruments, 1991. **62**(5): p. 1326-1332.

257.   Baikie, I.D. and P.Z. Estrup, *Low cost PC based scanning Kelvin probe.* Review of Scientific Instruments, 1998. **69**(3902).

258.   Wicinski, M., *Scanning Kelvin Probe with height control - User's manual.* 2017, Wicinski-Wicinski GbR.

259.   Hagen, C.H.M., et al., *Effect of laser structured micro patterns on the polyvinyl butyral/oxide/steel interface stability.* Progress in Organic Coatings, 2020. **147**: p. 105766.

260.   Hagen, C.H.M., et al., *Oxidation of coated steel during exposure to humid air and effects on cathodic disbonding - a qualitative study.* Electrochimica Acta, Submitted 2020.

Appended Papers

Paper I

The effect of surface roughness on corrosion resistance of machined and epoxy coated steel

C.M.H. Hagen[a,*], A. Hognestad[a,1], O.Ø. Knudsen[b], K. Sørby[a]

[a] Department of Mechanical and Industrial Engineering, NTNU, 7491 Trondheim, Norway
[b] SINTEF, Richard Birkelandsvei 2B, 7465 Trondheim, Norway

ARTICLE INFO

ABSTRACT

By incorporating periodic micro-patterns on steel substrates, the effect of surface roughness on corrosion resistance of a two-component polyamine cured epoxy mastic coating has been studied. Machining was employed to pattern the surfaces with periodic peaks of varying peak-to-valley heights, Rz. The focus of the study was to find the surface parameter that contributes most to the stability of an organic coating in corrosive environment, and to evaluate if machining can be comparable to blast cleaning with respect to coating durability. A strong correlation between roughness (Rz) and corrosive delamination of coated surfaces was seen. Increasing Rz from 57 μm to 252 μm on surfaces with triangular peaks, increased the effective contact area by 40% and decreased delamination by 30%. By introducing tilted asperities at Rz = 224 μm while keeping the effective contact area in general unchanged, delamination decreased another 55%. Hence, an increased Rz is found to be only partially beneficial, and the profile shape is more significant than the roughness value per se. The results suggest that mechanical interlocking has a substantial influence on the interfacial stability of protective coatings in corrosive environments. By optimal selection of cutting parameters, machining can give surfaces where protective coatings have long lifetime.

1. Introduction

The most commonly used method for protecting atmospherically exposed steel against corrosion, is the application of protective organic coating systems [1,2]. It is widely recognized that the stability of the coating-substrate interface is related to the interfacial adhesion forces [2–10] and electrochemical properties [1,2,11–16] of this region. The relevance of surface roughness to adhesion has been long recognized [9,17,18]. Already in the classical paper from 1925, "On adhesives and adhesive action", McBain and Hopkins considered the roughness of a surface to contribute to adhesion by mechanical interlocking [19]. Brockman suggested bond durability to be determined by the surface roughness, as mechanical interlocking continues to operate even when chemical bonds fail e.g. due to hydrolysis [6].

Several standards describe the characteristics of surfaces to be painted [20–22]. The performance of protective coatings applied to steel are significantly affected by the state of the steel surface prior to painting. Blast cleaning is recommended as pretreatment for most protective coatings in aggressive environments [23,24]. Nevertheless, for various reasons coatings sometimes must be applied on smooth steel

surfaces. Coatings applied on these surfaces are generally found to degrade early with subsequent corrosion of the steel substrate [25].

Studies show in general decreased cathodic disbonding with increased surface profile height [26–28] or with increased interfacial contact area along the profile (tortuosity) [29]. Cathodic disbonding has been found to advance faster along the direction of the surface texture than perpendicular to the surface texture. [27]. In accelerated corrosion tests, Ward found much higher levels of corrosion creep on shot peened samples compared to samples that were grit blasted [30]. The surfaces had comparable profile heights, but rounded versus sharp topographical features, respectively [30]. The effect was by Ward attributed to mechanical interlocking, but could have been explained by tortuosity as well. Adhesion tests have showed that a certain roughness is needed in order to achieve good adhesion [6,31–33]. A preliminary study to this work showed both weaker adhesion and less corrosion resistance for coatings applied on smooth surfaces compared to grit blasted surfaces [34].

Substantial research has been performed on the effect of various surface parameters on coatings and coating performance, but most of these studies have been performed on surfaces either grit blasted or

---

* Corresponding author.
  E-mail address: catalina.hagen@ntnu.no (C.M.H. Hagen).
  [1] Present affiliation: SINTEF Raufoss Manufacturing, Norway.

abraded with grit papers. The topography on such surfaces is a random distribution of irregular grooves and peaks. Hence, it is difficult to investigate how the morphological changes of the surface may influence the corrosion resistance in such studies.

In practice, grit blasting is sometimes not feasible for roughening of a surface, due to functional requirements, logistical or economic reasons. It is therefore important to understand the effect of surface topography on corrosion resistance, and if it is possible to reproduce this effect by other methods than blast cleaning. Hence, in the present study roughness is created by incorporating periodic micro-patterns on steel substrates. Machining is chosen as the surface structuring method, as it is a manufacturing technology heavily implemented in industry for removal of material. Steel components utilized in structural as well as non-structural applications, often undergo machining before being coated. The focus of the study is to develop a surface texture that improves the stability of an organic coating in corrosive environment. The novelty of the research presented here lies within the use of machining as a method of steel surface preparation, and the combination of machining parameters to create surfaces comparable to grit blasting with respect to coating durability. The goal is to evaluate if machining can be employed to create a surface with equivalent properties to those obtained by grit blasting, with respect to coating stability in corrosive environments.

Through a combination of the machining parameters nose radius, depth of cut, rotational speed and feed, the peak-to-valley height, Rz, of the machined surfaces, was increased. See Table 1 for definition of the roughness parameters used in this study. A periodic pattern of peaks, triangular or rectangular and tilted in profile, was machined into steel surfaces. The surfaces, which were subsequently covered with a commercial two-component polyamine cured epoxy mastic coating, were tested in accelerated corrosion tests and results are correlated with topography (roughness, effective area and morphology). Contact angle measurements were performed to estimate the effect roughness may have on the wetting properties induced by each treatment.

2. Experimental

2.1. Steel and surface preparation

The samples were prepared using 5 mm thick plates of structural steel S355J2G3 often used for shipbuilding applications. The chemical composition was 0.14-0.22% C, 0.36-0.55% Si, 1.23-1.60% Mn, 0.014-0.025% P, 0.029-0.035% S, 0.20 Cr, 0.22 Ni, 0.04 Mo, 0.06% V, 0.27-0.30% Cu, Fe to balance.

Surfaces were machined in CNC machines (computer numerically controlled), by face milling or face turning, see Table 2 for parameters. The parameters were chosen with the intention of creating surfaces with a variation of Rz values, and comparable to the ones found on surfaces after grit blasting. The diameter of the milling cutter was 80 mm. The feed in the milling operation was in the range 0.35–0.73 mm/tooth, and in the range 0.15–0.75 mm/rev in the turning

Table 2
Machining parameters with the resulting roughness, Rz, of the surface. (The values in the parenthesis are standard deviations).

Process	Surface	Nose radius [mm]	Depth of cut [mm]	Feed [mm/tooth]	Feed [mm/rev]	Cutting speed [m/min]	Rz [μm]
Face Milling	M1	0.2	1	0.73	-	25	227 (27)
	M2	0.2	1	0.5	-	25	191 (14)
	M3	0.2	1	0.35	-	25	125 (10)
Face Turning	T1	0.2	0.5	-	0.75	100	675 (9)
	T2	0.2	0.35	-	0.65	100	469 (11)
	T3	0.2	0.3	-	0.5	100	379 (32)
	T4	0.2	0.3	-	0.3	100	62 (2)
	T5	0.2	0.3	-	0.2	100	26 (2)
	T6	0.2	0.3	-	0.1	100	8 (2)
	T7	0.4	0.3	-	0.15	100	11 (3)

operation.

Surfaces blast cleaned with aluminium oxide (Al_2O_3) were used as reference.

The backside of all samples was grit blasted and edges were rounded.

All machined specimens were degreased with an alkaline degreasing agent, thoroughly rinsed with distilled water and ethanol and dried in an oven at 40 °C. Grit blasted samples were washed with ethanol and dried with an air blower. All samples were placed in a desiccator after preparation until painting.

2.2. Surface characterization

For surfaces with Rz < 100, roughness (Rz) and peak density (Pc) were measured with a stylus profilometer according to ISO 4288 [36], while tortuosity (τ) was measured by a non-contact Alicona optical Infinite-Focus Microscope (IFM). In accordance with Watts [26], the ratio of the actual length measured along the surface profile to the geometrical length, will represent the roughness grade of the cross sectional 2D profile.

For surfaces with Rz > 100, roughness (as maximum peak-to-valley distance corresponding to the Rz measured with profilometer), Pc and τ were calculated from cross sections analysed in an Olympus GX51 optical microscope and the IFM. Cross sections were embedded in epoxy, ground with emery papers and polished down to mirror-like surface finish.

Wenzel`s roughness factor (r) was measured with the IFM for all surfaces. The profile parameter was proposed by Wenzel [37], who derived the ratio of the effective contact area divided by the projected geometric area. An increased Wenzel's ratio indicates a higher roughness of the 3D profile and a larger effective contact area at the coating-steel interface.

The morphology of the surfaces was characterized using the 3D-

Table 1
Nomenclature. Roughness parameters according to ISO 4287 [35] and ISO 4288 [36].

Parameter	Description	Mathematical definition	Typical units
A	Actual surface profile area. The effective contact area.		mm^2
A_0	Geometrical area		mm^2
L	Actual surface profile length		mm
L_0	Geometrical length		mm
Pc	Peak density.	The number of peaks higher than a certain pre-defined dead-band, e.g. 10% of Rz	Peaks/cm
r	Wenzel's roughness factor	$r = A/A_0$	
Ra	Arithmetic roughness average	$Ra = \frac{1}{l} \sum_0^l |y|$ l is the measurement length and y the distance from the average line.	μm
Rz	Average maximum peak to valley distance for five sampling lengths within the measurement length l	$Rz = \frac{1}{5} \sum_{i=1}^5 (Rp + Rv)_i$ Rp is the largest profile peak height and Rv the maximum profile valley depth within one of the five sampling lengths of the measurement length l.	μm
τ	Tortuosity	$\tau = L/L_0$	

imaging capability of the IFM. Rz values measured by profilometer were confirmed by IFM 3D-imaging measurements.

To analyze the roughness and topography data, the Spearman's correlation coefficient (ρ) was calculated using data analysis software. This coefficient is less sensitive to outliers and shows a low variability [38–40]. The coefficient does not measure the causal relationship between variables, but is used for analyzing correlations. It was assumed that parameters were correlated when the absolute value of the correlation coefficient was greater than 0.7.

As surface roughness/topography affects the wetting properties of surfaces - "the extent to which, at equilibrium, a liquid adhesive will come into contact with a solid surface" [9] - contact angle measurements were conducted to analyze if the corrosion resistance found was influenced by this effect. Static contact angle was measured with a computerized contact angle analyzer (CAM 200, KSV, Finland). A water droplet (MQ-water) was delivered onto the sample surface with a Hamilton syringe mounted on the sample stage. A camera was used to capture side view images of the droplet profile. The contact angle was next calculated by fitting the Young-Laplace equation [41] to the droplet profile. Contact angles were measured in at least two positions for every sample.

2.3. Coating

A commercial two-component polyamine cured epoxy mastic coating was applied on all samples. The coating is specially designed for areas where optimum surface preparation is not possible or desired, and can be used as primer, mid coat or finish coat in atmospheric and immersed environments. The volume fraction of solids was 82%. In this study, the corrosion resistance was studied on samples having at least two layers with total dry film thickness (TDFT) measured to 350-400 μm. On milled surfaces, the coating was applied by an adjustable film applicator, while turned surfaces were spray coated. Each coat was allowed to cure for one day before application of next coat. The coatings were finally baked for two days at 40 °C. The backside and the edges of the samples were sealed with the same epoxy mastic coating.

2.4. Accelerated corrosion test

An accelerated corrosion test was performed according to ISO 12944-9, except that the samples were only exposed in 6-8 test cycles instead of 25 [42]. This is a cyclic wet/dry corrosion test, widely used for testing the performance of marine and offshore coatings and found to have a certain correlation to field performance [43,44], see Table 3.

A 50 mm long and 2 mm wide scribe was machined down to the steel substrate prior to testing, to initiate corrosion perpendicular to the surface texture. The test evaluates the resistance against corrosion creep. Cathodic disbonding was found in front of the corrosion creep on many of the machined surfaces. Corrosion creep and cathodic disbonding was measured at 9 different positions along the 50 mm scribe, according to ISO 15711[45]. At least three replicate panels for each surface treatment were tested.

3. Results and discussion

3.1. Surface characterization

In machining operations, the surface roughness increases rapidly with the increase in feed rate [46,47]. By face turning and milling at variable feed rates, two types of periodic surface profiles were produced: 1) surfaces with a periodic distribution of peaks triangular in profile and 2) surfaces with a periodic distribution of rectangular, tilted peaks. Fig. 1 shows images of cross-sections and surface area representing the two profiles, along with a grit blasted surface.

The roughness Rz on surfaces patterned with periodic triangular peaks was measured to be in the range 7–252 μm. Surfaces patterned with periodic rectangular, tilted peaks was in the range 224–683 μm. The inclination of the peaks was measured to be in the range 50-180 μm. The inclination was measured as the longest distance between the peak and the normal to the peak, as illustrated by the arrow in the middle image of Fig. 1.

Grit blasting generated surfaces with a random distribution of irregular cavities and coarse morphologies with undercuts. Surfaces with Rz between 27 to 48 μm were obtained and used as reference.

There are several available standards with recommendations regarding the pre-treatment of steel surfaces to be coated. Selection of protective coatings for offshore installations and associated facilities can follow NORSOK M-501 [24] or ISO 12944 [23]. Both recommend blast cleaning that complies with ISO 8501-1 Sa 2½, which is a cleanliness recommendation. The roughness is stated to be in accordance with the requirements for the coating system chosen and correspond to a roughness Rz 50-115 μm. Considering these recommendations, the roughness grades of the machined surfaces were well beyond the requirements, while blast cleaned surfaces had lower roughness. The surfaces were however fitted for the epoxy employed.

Wenzel's roughness factor increased linearly with Rz. The relationship was confirmed with a high significance for the periodic (r = 0.96, p < 0.01) and grit blasted surfaces (r = 0.922, p < 0.01), indicating a strong positive correlation between the effective contact area at the coating-substrate interface and the peak-to-valley height. The increase in effective contact area can potentially provide a larger interface for bonding of the applicable organic coating [9,48].

Grit blasted surfaces had Wenzel's roughness factors from 1.2 to 1.3. Sørensen found the ratio of actual length to geometrical length to be 1.15 and 1.18 on grit blasted steel with surface roughness values, Rz = 52 μm and Rz = 41.6 μm respectively[29], hence measurements correlate well with earlier findings. See Fig. 2 for information about the relationship between the roughness Rz and the effective contact area defined by Wenzel's roughness factor. Surfaces with periodic triangular peaks had Wenzel's roughness factors from 1.1 to 1.9. Surfaces with periodic rectangular tilted peaks had Wenzel's roughness factor from 2 to 4.3.

Fig. 2 shows that machined surfaces with triangular peaks at Rz < 100 μm and grit blasted surfaces had similar Wenzel's roughness factor at comparable Rz roughness values.

It was wished to estimate the effect roughness may have on the wetting properties induced by each treatment. In Fig. 3 average values for apparent contact angles are reported for the surfaces in this study. On non-ideal surfaces, e.g. rough, non-porous or heterogenous surfaces, contact angle measurements are quite challenging and frequently produce unreliable results [49,50]. On such surfaces, the only measurable value is the apparent contact angle.

On rough surfaces the apparent contact angle will however be affected by the droplet volume and may also change from point to point along the contact line between the water droplet and the substrate. Measuring and calculating an average value of the apparent contact angle over several droplets is advised in order to overcome the latter problem [51]. For surfaces with triangular peaks, apparent contact angles were between 71° and 98°. For rectangular peaks these were between 0° and 118°, while for grit blasted surfaces these were found to be between 97° and 116°.

Apparent contact angles correlated well with previous findings. On mild steel treated to have different types of oxides, it has been measured water contact angles between 20° and 75° [52]. On mild steel surfaces prepared with a range of techniques like water-jetting and
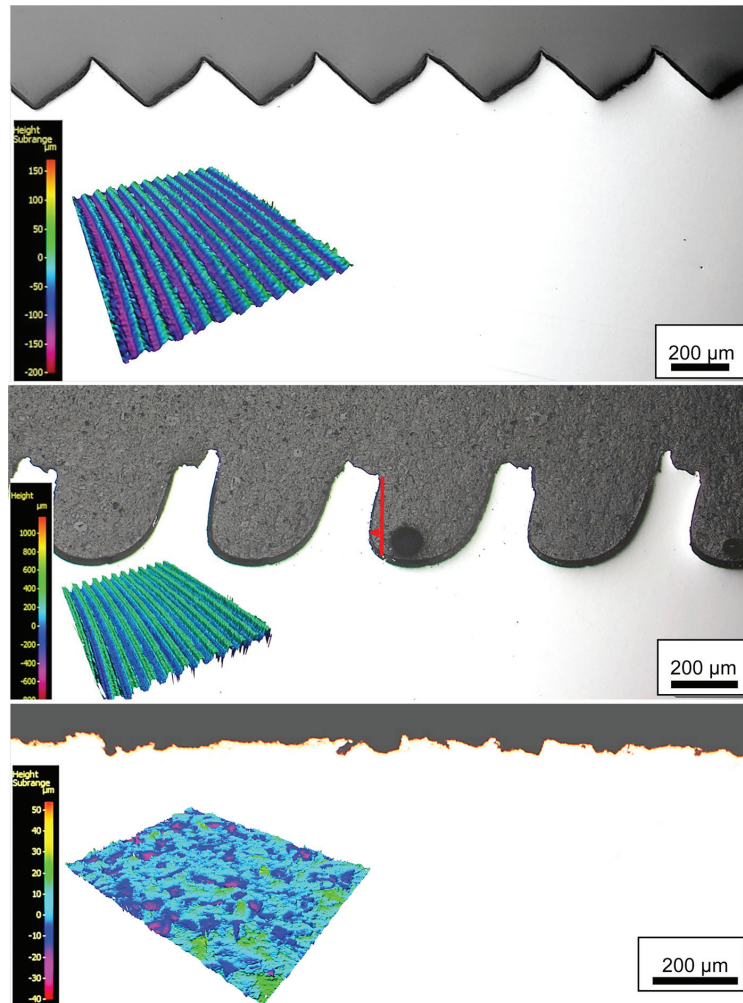
Table 3
Description of ISO 12944-9 test cycle.

Day 1	Day 2	Day 3	Day 4	Day 5	Day 6	Day 7
4 h UVA 60 °C / 4 h Condensation 50 °C			Salt spray NaCl 5% 35 °C			− 20 °C

Fig. 1. Optical microscope images, in black and white, of cross sections of surfaces machined with triangular peaks (upper), rectangular and tilted peaks (center), and grit blasted surfaces (lower). 3D images of surface area scanned by focus-variation with IFM, seen in colors indicating the level of roughness. Red arrow in the middle image indicates how the inclination was measured.
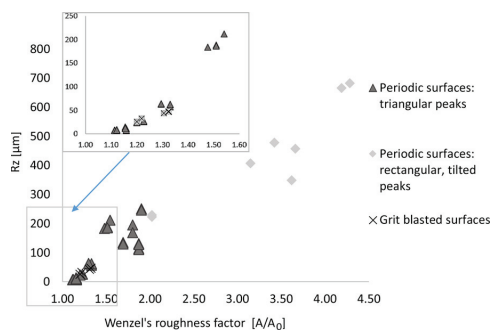

Fig. 2. The relationship between roughness Rz, and Wenzel's roughness factor (effective contact area).
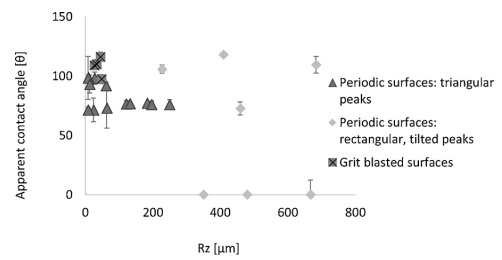

Fig. 3. The relationship between contact angle values - on surfaces patterned with periodic triangular peaks and rectangular and tilted peaks - and roughness Rz. Grit blasted surfaces for comparison.
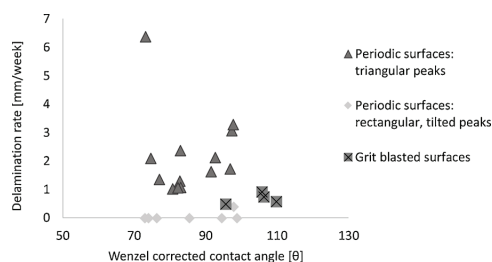
Fig. 4. The effect of roughness on wettability and delamination rate. Delamination rate as a function of Wenzel corrected contact angles, hence angles corrected for the effect of roughness, for the surfaces employed in this study.

abrasive blasting, the measured contact angle was between 62.8° and 114.2° [33]. Contact angles were seen to increase with the effective contact area. To examine the wettability of the surfaces, it is necessary to correct for the effect of the surface profile on the measured apparent contact angles. The Wenzel's roughness factor was derived for this purpose, who stated that adding roughness to a surface would amplify the wetting properties of a given surface, by influencing the intrinsic contact angle according to the equation Eq. (1)

$$\cos\theta_{apparent} = r \times \cos\theta_{intrinsic} \tag{1}$$

There was no indication of differences in wetting properties for the different surfaces, as no relationship was found between delamination rates and Wenzel corrected contact angles measured on bare surfaces, see Fig. 4.

It is worth to highlight that one main implication of Wenzel's equation, is that roughness makes hydrophilic surfaces ($\theta_{intrinsic} < 90°$) more hydrophilic and hydrophobic surfaces ($\theta_{intrinsic} > 90°$) more hydrophobic. This is in general not in accordance with the results presented here, which indicate increased hydrophobicity on surfaces with rectangular peaks or irregular profile (grit blasted surfaces). Several workers have also observed that roughening a substrate usually causes its wettability to decrease [31,33,53], and a number of hypotheses have been proposed to explain the wetting properties of smooth and rough surfaces. The authors explained the findings as most likely caused by the topography, and Herminghaus has shown that by creating overhanging intendations on initially hydrophilic surfaces, these will behave hydrophobically [54]. This liquid-repellent property will not be an equilibrium property. His findings resemble our own experience, as the droplet of liquid placed on surfaces grit blasted or patterned with rectangular, tilted peaks, spread out after 9-20 seconds and resulted in complete wetting of the surface.

3.2. Delamination

In general, two different delamination behaviors were seen in this study: corrosion creep following a cathodic disbonding front, and corrosion creep alone (at much lower rates).

On surfaces machined with triangular peaks, delamination was found to happen as a combination of corrosion creep and cathodic disbonding, see Fig. 5. The cathodic disbonding was identified as a non-corroded area ahead of the corrosion creep with delaminated coating. The pH at this location was measured with pH indicator strips to be above 10. This is representative for cathodic disbonding, caused by reduction of oxygen beneath the paint.

Delamination rates were calculated as the sum of the corrosion creep and cathodic disbonding and divided by the time the test lasted [55]. Delamination rates were seen to decrease with increased Rz, see Fig. 6. Results from delamination tests have not been averaged but are presented for all 76 tests (15 grit blasted and 61 machined surfaces).
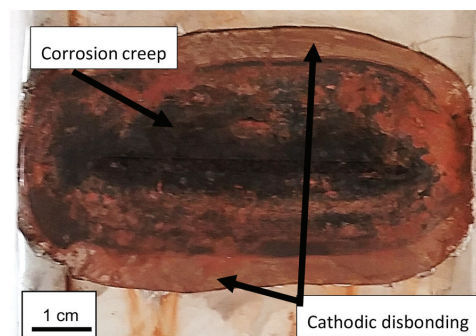

Fig. 5. The delaminated area, containing a zone covered with corrosion products, identified as corrosion creep and an area area ahead of the corrosion creep, with delaminated coating but no corrosion products present on the surface, identified as cathodic disbonding.
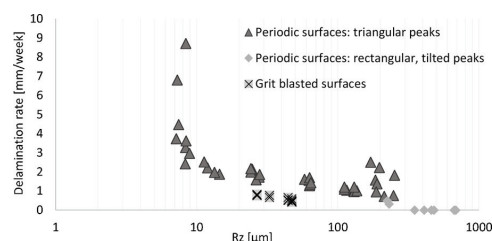

Fig. 6. Semi-log plot of delamination rate as function of surface roughness, Rz. The scale on the x-axis is logarithmic.

It was found that at comparable roughness and effective contact area, delamination was two-three times higher for surfaces machined with triangular peaks than for grit blasted surfaces. A six-seven times increase in Rz was needed for machined surfaces with periodic triangular peaks to give similar delamination rate values as found for grit blasted surfaces at comparable roughness and effective contact area. For example, grit blasted surfaces with Rz = 33 μm, were found to have a delamination rate of 0.74 mm/week. The triangular peaks had comparable delamination rates at Rz > 212 μm.

No delamination was found on surfaces with rectangular, tilted peaks with Rz > 350 μm after 8 test cycles. For these surfaces, the cyclic testing was therefore prolonged to a total of 30 cycles. The delamination rates seen in Fig. 6 for these samples, are hence calculated from the delamination found after the 30 test cycles.

The contrast in corrosion resistance between the surfaces with triangular peaks and surfaces with rectangular and tilted peaks is noteworthy to highlight: The delamination – sum of corrosion creep and cathodic disbonding – after 8 weeks of testing, was found to be 8.84 mm on the average on surfaces with triangular peaks having Rz values between 212 μm and 252 μm. On the surfaces with rectangular, tilted peaks at Rz = 224-230 μm, the delamination – measured solely as corrosion creep – was measured to be 3.2 mm on the average after 8 weeks of testing. After 30 weeks of testing, the delamination – measured solely as corrosion creep – was measured to 1.71 mm on the average on surfaces with rectangular tilted peaks with Rz = 350 μm. No grit blasted surfaces at such high Rz values were tested, but the delamination – measured solely as corrosion creep – on grit blasted surfaces with Rz = 47 μm, was measured to 3.9 mm after 8 weeks of testing. Hence at the same level as found on surfaces with rectangular, tilted peaks at Rz = 224-230 μm. As the effective contact area was found to increase with increase Rz, as seen in Fig. 2, the effective contact area was comparable at comparable Rz values on the surfaces with

triangular peaks and grit blasted surfaces. Similarly, for surfaces with triangular peaks and rectangular tilted peaks the effective contact area was comparable at comparable roughness Rz.

The humid environment is probably the main determinant on the durability of the coating-metal bond. During exposure to a corrosive environment, several factors contribute to degradation of the coating-steel interface: i) the saturation of the coatings by water lowers coating adhesion [6,8], ii) the cyclic wet/dry exposure increases the internal stresses in the polymer and lead to microcracking at the coating surface [27], iii) corrosion products at defects exert stresses on the coating-substrate interface [56,57], iv) the cathodic reaction underneath the coating will increase the local pH and break the coating-substrate bonds. In humid environments, electrochemical de-adhesion is found to initiate at damage or weaknesses in the coating [2,58–60] and to propagate by anodic undermining [2,12,15], cathodic disbonding [59–64] or oxide wedging [56], depending on the coating system, exposure environment and substrate.

Increasing Rz from 57 μm to 252 μm on surfaces with triangular peaks, increased the effective contact area by 40% and decreased delamination by 30%. By introducing tilted asperities at Rz = 224 μm while keeping the effective contact area unchanged, delamination decreased another 55%. Hence, an increased Rz is found to be only partially beneficial, verifying that the surface profile is more significant than the roughness value per se, as previously reported by Ward [30]. Machined surfaces with triangular peaks have poor wet adhesion properties, at least at low roughness values, when compared to grit blasted surfaces [34]. It is assumed that although wet-adhesion properties may improve with increased roughness, a coating/metal interface weakened by exposure to humidity will greatly facilitate corrosive delamination when the surface does not allow for mechanical interlocking [48].

The tilted peaks introduce cavities at the surface, resembling the irregular topography with undercuts found on grit blasted surfaces. The coating adhering within these pockets may result in the improved delamination resistance seen not only on the surfaces with tilted peaks, but also explaining the higher corrosion resistance of coatings on grit blasted surfaces.

The increase in effective contact area is however also important. Interfacial adhesion is known to originate from several contributions: a) physical interactions, b) chemical bonds, c) mechanical interlocking and d) heat dissipation [65,66]. Both the physical and the chemical interactions are related to the unit area of interface and will be affected by an increase in the effective contact area. The increase will however not only lead to a change in the contribution to interfacial adhesion with respect to a) and b), but also to mechanical interlocking c), where this is possible.

Based on the results presented, it is believed that machining can be employed as pre-treatment to fabricate surfaces that may present similar properties as grit blasted surfaces when it comes to corrosion resistance of a two-component polyamine cured epoxy mastic coating. Roughness values must however be well above 200 μm to show a delamination behaviour comparable to grit blasted surfaces at fine-medium roughness grade, Rz = 30-40. It is believed that a certain inclination must be added to the peaks, for surfaces to have the same properties or better as grit blasted have in means of corrosion resistance of a two-component polyamine cured epoxy mastic coating.

4. Conclusions

Face turning and milling of steel at different feeds and depth of cuts resulted in surfaces patterned with peaks of varying size and morphology - triangular and tilted rectangular peaks. The rectangular peaks were however only possible to fabricate at roughness values Rz > 224 μm.

Accelerated corrosion tests showed that the corrosive delamination of a two-component polyamine cured epoxy mastic coating from

machined surfaces is partially explained by the lower roughness found on these surfaces. Increasing the roughness by means of increased peak-to-valley height, resulted in decreased delamination rate on all surfaces. A linear correlation between the roughness and the effective contact area was found for both grit blasted and machined surfaces. The effective contact area affects the physical and chemical interactions, as these are related to the unit area they are acting over. Hence, the decreased delamination rates found with increased roughness may be related to an increase in effective contact area. However, the lack of cavities on surfaces with triangular peaks eliminates their ability for mechanical interlocking. As long as the surface's ability for mechanical interlocking remains low, the interfacial stability of protective coatings in corrosive environments will need roughness values at least six times higher than needed for grit blasted surfaces. High roughness may hence be a partial substitution for mechanical interlocking.

Data availability

The raw/processed data required to reproduce these findings cannot be shared at this time as the data also forms part of an ongoing study.

References

[1] M. Stratmann, R. Feser, A. Leng, Corrosion protection by organic films, Electrochim. Acta 39 (8–9) (1994) 1207–1214.

[2] G. Grundmeier, W. Schmidt, M. Stratmann, Corrosion protection by organic coatings: electrochemical mechanism and novel methods of investigation, Electrochim. Acta 45 (15–16) (2000) 2515–2533.

[3] J. Wielant, et al., Influence of the iron oxide acid − base properties on the chemisorption of model epoxy compounds studied by XPS, J. Phys. Chem. C 111 (35) (2007) 13177–13184.

[4] J. Wielant, et al., SKP as a tool to study the physicochemical interaction at buried metal–coating interfaces, Surf. Interface Anal. 42 (6–7) (2010) 1005–1009.

[5] W. Funke, Toward a unified view of the mechanism responsible for paint defects by metallic corrosion, Ind. Eng. Chem. Prod. Res. Dev. 24 (3) (1985) 343–347.

[6] W. Brockmann, Durability of adhesion between metals and polymers, J. Adhes. 29 (1-4) (1989) 53–61.

[7] K.L. Mittal, Adhesion measurement: Recent progress, unsolved problems, and prospects, in: K.L. Mittal (Ed.), Adhesion Measurement Of Thin Films, Thick Films, And Bulk Coatings, ASTM, Philadelphia, PA, 1978.

[8] H. Leidheiser, W. Funke, Water disbondment and wet adhesion of organic coatings on metals: a review and interpretation, J. Oil Colour Chem. Assoc. 70 (5) (1987) 121–132.

[9] D.E. Packham, Surface roughness and adhesion, in: M. Chaudhury, A.V. Pocius (Eds.), Adhesion Science and Engineering, Elsevier Science B.V., Amsterdam, 2002, pp. 317–349.

[10] A. Nazarov, D. Thierry, Hydrolysis of interfacial bonds in a metal/polymer electrical double layer, Protection Metals 41 (2) (2005) 105–116.

[11] R. Hausbrand, M. Stratmann, M. Rohwerder, The physical meaning of electrode potentials at metal surfaces and polymer/metal interfaces: consequences for delamination, J. Electrochem. Soc. 155 (7) (2008) C369–C379.

[12] R. Posner, O. Ozcan, G. Grundmeier, Water and ions at polymer/metal interfaces, in: M.L.F. Silva, C. Sato (Eds.), Design of Adhesive Joints Under Humid Conditions, Springer Berlin Heidelberg, Berlin, Heidelberg, 2013, pp. 21–52.

[13] A. Nazarov, D. Thierry, Studies in the electrical double layer at metal/polymer interfaces by scanning capacitive probe, Protection Metals 39 (1) (2003) 55–62.

[14] A. Nazarov, D. Thierry, Mechanism of the corrosion exfoliation of a polymer coating from carbon steel, Protection Metals 45 (6) (2009) 735–745.

[15] A. Nazarov, D. Thierry, Influence of electrochemical conditions in a defect on the mode of paint corrosion delamination from a steel surface, CORROSION 2010, (2010).

[16] M. Stratmann, 2005 W.R. Whitney Award Lecture: corrosion stability of polymer-coated metals - new consepts based on fundamental understanding, Corrosion 61 (12) (2005) 1115–1126.

[17] D.E. Packham, The mechanical theory of adhesion - a seventy year perspective and its current status, in: W.J.v. Ooij, H.R. Andersen (Eds.), First International Congress On Adhesion Science And Technology, VSP: Utrecht, Netherlands, 1998p. 28.

[18] D.E. Packham, Surface energy, surface topography and adhesion, Int. J. Adhes. Adhes. 23 (6) (2003) 437–448.

[19] J.W. McBain, D.G. Hopkins, On Adhesives and Adhesive Action, The Journal of

Physical Chemistry 29 (2) (1925) 188–204.

[20] Standardization, I.O.f, Preparation of Steel Substrates before Application of Paints And Related Products – Visual Assessment Of Surface Cleanliness – Part 1: Rust Grades And Preparation Grades Of Uncoated Steel Substrates And Of Steel Substrates After Overall Removal Of Previous Coatings, International Organization for Standardization, Switzerland, 2007.

[21] Standardization, I.O.f, Surface Roughness Characteristics Of Blast-Cleaned Steel Substrates – Part 4: Method For The Calibration Of Iso Surface Profile Comparators And For The Determination Of Surface Profile – Stylus Instrument Procedure, International Organization for Standardization, Switzerland, 2012.

[22] Standardization, I.O.f, Preparation Of Steel Substrates Before Application Of Paints And Related Products – Surface Roughness Characteristics Of Blast-Cleaned Steel Substrates – Part 2: Method For The Grading Of Surface Profile Of Abrasive Blast-Cleaned Steel – Comparator Method, International Organization for Standardization, Switzerland, 2012.

[23] Standardization, I.O.f, Paints And Varnishes – Corrosion Protection Of Steel Structures By Protective Paint Systems, International Organization for Standardization, Switzerland, 2007.

[24] S. Norway, Surface Preparation And Protective Coating, Standards Norway, Oslo, 2012.

[25] O. Knudsen, Review of Coating Failure Incidents on the Norwegian Continental Shelf since the Introduction of NORSOK M-501, CORROSION 2013, NACE, 2013 NACE, Editor.

[26] J.F. Watts, J.E. Castle, The application of X-ray photoelectron spectroscopy to the study of polymer-to-metal adhesion. Part 2 The cathodic disbondment of epoxy coated mild steel, J. Mater. Sci. 19 (1984) 2259–2272.

[27] N.W. Khun, G.S. Frankel, Effects of surface roughness, texture and polymer degradation on cathodic delamination of epoxy coated steel samples, Corros. Sci. 67 (2013) 152–160.

[28] M. Ghaffari, et al., Demonstration of epoxy/carbon steel interfacial delamination behavior: Electrochemical impedance and X-ray spectroscopic analyses, Corros. Sci. 102 (Supplement C) (2016) 326–337.

[29] P.A. Sørensen, et al., Influence of substrate topography on cathodic delamination of anticorrosive coatings, Prog. Org. Coat. 64 (2–3) (2009) 142–149.

[30] D. Ward, An investigation into the effect of surface profile on the performance of coatings in accelerated corrosion tests, CORROSION 2007, NACE, Houston, TX, 2007, p. 16.

[31] A.F. Harris, A. Beevers, The effects of grit-blasting on surface properties for adhesion, Int. J. Adhes. Adhes. 19 (6) (1999) 445–452.

[32] M.S. Islam, L. Tong, P.J. Falzon, Influence of metal surface preparation on its surface profile, contact angle, surface energy and adhesion with glass fibre prepreg, Int. J. Adhes. Adhes. 51 (0) (2014) 32–41.

[33] S.S. Jamali, D.J. Mills, Steel surface preparation prior to painting and its impact on protective performance of organic coating, Prog. Org. Coat. 77 (12, Part B) (2014) 2091–2099.

[34] C.H.M. Hagen, A. Kristoffersen, O.Ø. Knudsen, The effect of surface profile on coating adhesion and corrosion resistance, CORROSION 2016, NACE, Vancouver, 2016, p. 15 NACE, Editor.

[35] Standardization, I.O.f, Geometrical Product Specifications (GPS) - Surface Texture: Profile method -Terms, Definitions And Surface Texture Parameters, International Organization for Standardization, Switzerland, 2000.

[36] Standardization, I.O.f, Geometrical Product Specifications (GPS) - Surface Texture: Profile Method – Rules And Procedures For The Assessment Of Surface Texture, International Organization for Standardization, Switzerland, 1996.

[37] R.N. Wenzel, Resistance of solid surfaces to wetting by water, Ind. Eng. Chem. 28 (8) (1936) 988–994.

[38] J. Hauke, T. Kossowski, Comparison of values of Pearson's and Spearman's correlation coefficients on the same sets of data, Quaestiones Geographicae 30 (2) (2011) 87–93.

[39] O. Hryniewicz, J. Karpinski, Prediction of reliability – the pitfalls of using Pearson's correlation, Mainten. Reliab. 16 (3) (2014) 472–483.

[40] Y. Kim, T.-H. Kim, T. Ergün, The instability of the Pearson correlation coefficient in the presence of coincidental outliers, Finance Res. Lett. 13 (2015) 243–257.

[41] P.C. Hiemenz, R. Rajagopalan, Principles of Colloid And Surface Chemistry, 3rd ed, CRC Press, New York - Basel, 1997, p. 672.

[42] Standardization, I.O.f, Paints and Varnishes – Corrosion Protection Of Steel Structures By Protective Paint Systems – Part 9: Protective Paint Systems And Laboratory Performance Test Methods For Offshore And Related Structures, International Organization for Standardization, Switzerland, 2018.

[43] N. Le Bozec, et al., Performance of marine and offshore paint systems: Correlation of accelerated corrosion tests and field exposure on operating ships, Mater. Corros. 66 (3) (2015) 215–225.

[44] N. Le Bozec, C. Hall, D. Melot, Comparison of accelerated ageing tests as per ISO 20340 Annex A and NACE SP0108 standards, CORROSION 2014, NACE International, San Antonio, 2014.

[45] Standardization, I.O.f, Paints and Varnishes – Determination of Resistance to Cathodic Disbonding of Coatings Exposed To Sea Water, International Organization for Standardization, Switzerland, 2003.

[46] P.G. Benardos, G.C. Vosniakos, Predicting surface roughness in machining: a review, Int. J. Mach. Tools Manuf. 43 (8) (2003) 833–844.

[47] D. Karayel, Prediction and control of surface roughness in CNC lathe using artificial neural network, J. Mater. Process. Technol. 209 (7) (2009) 3125–3137.

[48] J.D. Venables, Adhesion and durability of metal-polymer bonds, J. Mater. Sci. 19 (8) (1984) 2431–2453.

[49] T.S. Meiron, A. Marmur, I.S. Saguy, Contact angle measurement on rough surfaces, J. Colloid Interface Sci. 274 (2) (2004) 637–644.

[50] T.T. Chau, A review of techniques for measurement of contact angles and their applicability on mineral surfaces, Miner. Eng. 22 (3) (2009) 213–219.

[51] G. Wolansky, A. Marmur, Apparent contact angles on rough surfaces: the Wenzel equation revisited, Colloids Surf. A: Physicochem. Eng. Asp. 156 (1) (1999) 381–388.

[52] J. Wielant, et al., Cathodic delamination of polyurethane films on oxide covered steel – Combined adhesion and interface electrochemical studies, Corros. Sci. 51 (8) (2009) 1664–1670.

[53] F. Rupp, et al., Roughness induced dynamic changes of wettability of acid etched titanium implant modifications, Biomaterials 25 (7) (2004) 1429–1438.

[54] S. Herminghaus, Roughness-induced non-wetting, Europhys. Lett. 52 (2) (2000) 165–170.

[55] S.B. Axelsen, O. Knudsen, The effect of water-soluble salt contamination on coating performance, CORROSION 2011, NACE, 2011.

[56] M. Kappes, G.S. Frankel, N. Sridhar, Adhesion and adhesion degradation of a pressure sensitive tape on carbon steel, Prog. Org. Coat. 69 (1) (2010) 57–62.

[57] M.L. Tayler, et al., Scribe creep and underpaint corrosion on ultra-high molecular weight epoxy resin coated 1018 Steel Part 2: scribe creep model as a function of environmental severity factors, Corrosion 71 (3) (2015) 326–342.

[58] R. Montoya, et al., A cathodic delamination study of coatings with and without mechanical defects, Corros. Sci. 82 (0) (2014) 432–436.

[59] W. Fürbeth, M. Stratmann, The delamination of polymeric coatings from electrogalvanised steel – a mechanistic approach.: Part 1: delamination from a defect with intact zinc layer, Corros. Sci. 43 (2) (2001) 207–227.

[60] W. Fürbeth, M. Stratmann, The delamination of polymeric coatings from electrogalvanized steel – a mechanistic approach.: Part 2: delamination from a defect down to steel, Corros. Sci. 43 (2) (2001) 229–241.

[61] A. Leng, H. Streckel, M. Stratmann, The delamination of polymeric coatings from steel. Part 2: First stage of delamination, effect of type and concentration of cations on delamination, chemical analysis of the interface, Corros. Sci. 41 (3) (1998) 579–597.

[62] A. Leng, H. Streckel, M. Stratmann, The delamination of polymeric coatings from steel. Part 1: Calibration of the Kelvinprobe and basic delamination mechanism, Corros. Sci. 41 (3) (1998) 547–578.

[63] A. Leng, et al., The delamination of polymeric coatings from steel. Part 3: Effect of the oxygen partial pressure on the delamination reaction and current distribution at the metal-polymer interface, Corros. Sci. 41 (3) (1999) 599–620.

[64] W. Fürbeth, M. Stratmann, The delamination of polymeric coatings from electrogalvanized steel – a mechanistic approach.: Part 3: delamination kinetics and influence of CO₂, Corros. Sci. 43 (2) (2001) 243–254.

[65] O. Hölck, et al., Comparative characterization of chip to epoxy interfaces by molecular modeling and contact angle determination, Microelectron. Reliab. 52 (7) (2012) 1285–1290.

[66] O.v.d. Sluis, S.P.M. Noijen, P.H.M. Timmermans, On the effect of microscopic roughness on macroscopic polymer-metal adhesion, in: W.D.v. Driel, X.J. Fan (Eds.), Solid state lighting reliability: components to systems, Springer, 2013.

Paper II

Effect of laser structured micro patterns on the polyvinyl butyral/oxide/steel interface stability

C.H.M. Hagen[a,*], O.Ø. Knudsen[b], A.H. Zavieh[c], W. Pfleging[d,e]

[a] *Department of Mechanical and Industrial Engineering, NTNU, 7491 Trondheim, Norway*
[b] *SINTEF, Richard Birkelandsvei 2B, 7465 Trondheim, Norway*
[c] *NTNU Nanolab, Sem Sælands vei 14, 7491 Trondheim, Norway*
[d] *Karlsruhe Institute of Technology, IAM-AWP, P.O. Box 3640, 76021 Karlsruhe, Germany*
[e] *Karlsruhe Nano Micro Facility, Hermann-von-Helmholtz-Platz 1, 76344 Eggenstein-Leopoldshafen, Germany*

ABSTRACT

This work investigated the effect of steel substrate topography and roughness on cathodic disbonding resistance and wet adhesion of the polyvinyl butyral/oxide/steel interface. Laser structuring was employed to pattern steel surfaces with controlled, periodic peaks of different peak-to-valley height, Rz, and geometry. Grinded smooth samples were used for reference. The in-situ scanning Kelvin probe technique was used to follow the cathodic disbonding in humid air and wet adhesion loss in inert atmosphere (3 ppm O_2). Both cathodic disbonding and wet adhesion loss depended on the ability of the surface for mechanical adhesion, even when compensating for the increased effective contact area. X-ray photoelectron spectroscopy excluded the possibility for oxide chemistry effects on the delamination rate. Surfaces with features that enabled mechanical interlocking forces, had the best cathodic disbonding resistance and wet adhesion properties.

1. Introduction

Conventional wisdom in the heavy-duty coating industry says that blast cleaning improves coating performance by enabling mechanical interlocking between coating and substrate, i.e. mechanical adhesion forces. The scientific community, on the other hand, has focused mostly on chemical bonds and intermolecular forces [1]. However, results from a recent study indicated that mechanical interlocking is vital for the performance of heavy duty protective coatings [2].

It is widely accepted that the resistance of an organic coating against propagation of electrochemical degradation is determined more by the steel/coating interface than its barrier properties [3]. The amount of oxygen and water present in organic coatings is normally sufficient to sustain a considerable corrosion rate [4,5]. Hence, the properties of the interface are critical, but still not fully understood. The standard explanation for the protective action of coatings, has been that coatings provide a high resistance between anodes and cathodes [6]. This work aims to study the effect of steel substrate topography and roughness on the stability of the coating/steel interface, measured as its wet adhesion property and resistance to cathodic disbonding (CD).

Various studies have addressed the role of roughness on the corrosion resistance of the coating/steel interface. However, all of them have

been performed on samples with non-uniform, heterogeneous topographies having a stochastic distribution of peak heights [7–13]. Most of the studies argue that the increased corrosion resistance is due to an increased effective contact area, as this will either offer more available area for bonds at the interface [14], or by increasing the interfacial path length and hence decrease the kinetics of failure [7,13]. Several studies have shown that coating/steel interfaces without mechanical interlocking, fail early when exposed to corrosive conditions [2,11,12]. Another study, although only covering a relative small range of roughness values (Ra of $0-1$ μm), argued that mechanical interlocking increased the stability of the coating/steel interface [10].

In this work, surfaces with periodic peaks of different peak-to-valley height and geometry were prepared by ultrafast laser structuring. Smooth samples prepared by grinding were used for reference. The composition of the bare steel surface oxide was characterized with X-ray photoelectron spectroscopy (XPS). Samples were coated with a model polyvinyl butyral-*co*-vinylalcohol-*co*-vinylacetate (PVB) coating [15–20], and 0.5 M NaCl electrolyte was added at a penetrative artificial defect in the coating. The potential of the coated surfaces was measured with the scanning Kelvin probe (SKP) technique as a function of exposure time in air and N_2 atmosphere.

The SKP technique has been established as an unique and powerful

---

method for non-destructive studies of the buried coating/metal interface [21–23]. It has mostly been employed for CD studies, but also for studies of wet adhesion properties of coatings by applying the technique in inert atmospheres [24]. The technique is able to map surface potentials through insulating layers of coatings as thick as 300 μm [25] with a typical lateral resolution of 100–150 μm [26].

CD proceeds from damages in organic coatings exposing the metal substrate and is believed to be the main de-adhesion mechanism on steels in humid and corrosive environments. The production of hydroxyls by the oxygen reduction reaction taking place underneath coatings, is balanced by migration of cations from the coating damage. The ingress of hydrated cations couples the intact steel-coating interface to external anodic sites, resulting in CD. The disbonding in air is driven by an electrochemical cell that comprises two separated galvanic half cells with anodic dissolution at the defect, coupled with the cathodic reduction of oxygen at the intact coating/oxide/steel interface. The progress follows parabolic kinetics, reflecting interfacial transport of ions as a rate determining step. The transport of hydrated ions at the coating/steel interface is a premise for the corrosion-induced degradation of organic coating-steel interfaces [22,27–31]. In inert atmosphere, the ingress of electrolyte from an artificial defect will not be controlled by an advancing corrosion cell but governed by the wet adhesion capability of the coating.

2. Experimental

2.1. Materials and samples preparation

The substrates were cold-rolled steel plates, EN 10130, with a chemical composition (in weight percent) of 0.04% C, 0.008% Si, 0.284% Mn, 0.0071% P, 0.0184% S, 0.033% Al, Fe to balance. The plates, with dimensions 30 mm × 60 mm and 4 mm in thickness, were grinded with SiC papers. Some were kept solely grinded, while the rest had 10 mm × 10 mm of the surface laser structured with ultrafast pulsed laser. See Table 2 for information about the surface structuring methods. The intention with the laser structuring was to create steel surfaces patterned with controlled 2D roughness profiles, representing different topographies with various roughness Rz. Ultrafast laser structuring enables high efficient material ablation without melt formation or heat impact to the surrounding material and offers the possibility of contactless rapid manufacturing of functional designs with high flexibility and process reliability [34,35]. It also allows for production of a uniform and homogenous surface texture. Before coating, all samples were thoroughly rinsed in ultrasonic bath with acetone and isopropanol and dried with an air blower. Samples were then stored in desiccators until the coating was applied. All grinded samples were exposed to ambient laboratory conditions (50–60% RH and 20–22 °C) for 2 days after grinding, before storage in desiccators. Studies performed by the authors and submitted for publishing, have shown that ongoing oxidation of the steel surface underneath the coating affects the coatings stability and cathodic disbonding resistance [36].

A polyvinyl butyral-*co*-vinylalcohol-*co*-vinylacetate (PVB) solution was prepared in isopropanol at 15.5% w/w PVB, by overnight stirring. Phenolphthalein was added at 6% w/w concentration for pH indication. Samples were coated using a draw-down bar. The PVB coating is a model coating often used for in-situ studies of the coating/steel interface stability [15–20]. The PVB coating cured for 6 days at ambient temperature inside a desiccator followed by 1 h in oven at 60 °C. The dry film thickness was 30 ± 5 μm above the peaks, measured with a magnetic coating thickness gauge.

Artificial defects were created by peeling the coating off the substrate to create a bare steel area of 10 mm × 10 mm metal in front of the laser structured area. The coating and defect preparation method was based on that of Stratmann et al. [4,37,38] and also used in other studies [15,18]. A sketch of the sample can be seen in Fig. 1.
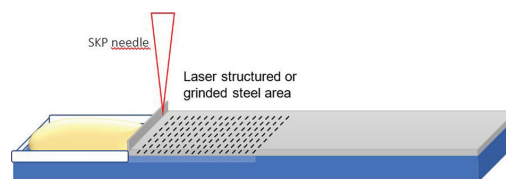
All chemicals were obtained from Sigma-Aldrich and VWR.

Fig. 1. Sketch of the sample employed for evaluation of cathodic disbonding. A reservoir was created next to the area of interest, here indicated by the dashed lines. This was an area either uniformly micro patterned by laser, or grinded. The dimensions of the laser structured area were 10 × 10 mm. Electrolyte was added to the defect created according to Stratmann et al. [4,37,38], here seen at the left.

2.2. Laser structuring

Ultrafast laser-structuring was carried out on a micromachining workstation (PS450-TO, Optec, Belgium) equipped with a tunable fiber laser (Tangerine, Amplitude Systèmes, France).The maximum average power was 35 W and the maximum pulse energy was specified to 175 μJ at 1030 nm (TEM00 with $M^2 < 1.2$). The pulse repetition rate could be varied from single pulse to 2 MHz and the laser pulse duration from 380 fs to 10 ps, respectively. The laser beam was scanned over the sample surface for all experiments using a Rhothor™ Laser Deflection Systems scan head (Newson Engineering BV). All laser structuring processes were carried out under ambient air and the ablated material was removed by an exhaust. For details about the laser parameters, see Table 2.

2.3. Topography characterization

On the A surfaces, a non-contact Alicona optical Infinite-Focus Microscope (IFM) and a stylus profilometer was used to assess the ratio of effective contact area to geometrical area and the roughness Rz [33], respectively. Rz was measured by the profilometer according to the ISO 4287 definition.

On the laser structured surfaces, measurement of Rz and effective contact area were performed on cross-sections of minimum 2 samples, analysed with an Olympus GX51 optical microscope. The cross-sections were embedded in an acrylic resin, grinded with SiC papers (ANSI grade 80-320-500-1000-2400) and polished to mirror-like surface finish (water-based diamond suspensions with 3 μm followed by 1 μm particle size).

The regularity of the laser pattern was examined by scanning electron microscopy (SEM, Zeiss Ultra 55).

2.4. Chemical characterization of surfaces by XPS

X-ray photoelectron spectroscopy (XPS) was performed with an Ultra DLD Kratos system to study the composition of the various surfaces investigated in this work. Samples were analyzed immediately before the coating was applied, at two different positions, each of 0.7 × 0.3 mm, to ensure that the results represented the surface and not inclusions or certain defects at the surface. The pressure in the analysis chamber was kept below 5×10^{-10} Torr. Al Kα monochromatic source was used with emission current of 10 mA and 10 kV. The information depth was in the range of 3 nm. Spectra were calibrated using the carbon peak at 284.5 eV. The wide elemental scan was acquired for the wide energy range (0–1200 eV) with a pass energy of 160 eV and a step size of 1 eV. The high-resolution spectra were acquired with a pass energy of 20 eV and step size of 0.1 eV for precise energy position and peak shape determination.

CasaXPS was used for curve fitting, evaluation and quantification of the data. Shirley background subtraction was applied for peak deconvolution and fitting [39]. Full width half maximum (FWHM) was kept

constant for oxide components of each element and Gaussian/Lorentzian asymmetry was used for curve fitting using the parameters of standard peaks. Fe 2p 3/2 was used to investigate relative surface concentration of Fe_3O_4, FeO, Fe^{3+} (Fe_2O_3 and FeOOH) and metallic Fe. The splitting and peak position of metallic iron at 706.9 ± 0.2 eV and shifts in the oxides were in good agreement with reference peaks [40].

2.5. Scanning Kelvin probe measurements

In-situ SKP measurements were performed to investigate the effect of the steel substrate topography and roughness on the stability of the interface, measured as resistance to CD in air and ionic mobility in N_2 atmosphere. The SKP chamber was for the latter case flushed with nitrogen at RH 95% till 3 ppm oxygen concentration was measured. The stream of humid nitrogen through the $20 \times 20 \times 20$ cm^3 chamber was kept at 10 L/h.

All experiments were carried out at 25 °C and 95% RH, using 0.5 M non-deaerated aqueous NaCl in the defect reservoir. The NaCl employed in the experiments was from the same batch, i.e. the electrolyte was expected to contain the same oxygen concentration in all tests.

The SKP measurements were performed in a steel chamber, which both enabled accurate climatic control and acted as a Faraday cage. The instrument was a Height-regulated SKP custom-made by Wicinski-Wicinski GbR. The theory behind the instrument has been covered by other works [4,21,37,38,41,42]. The probe was a 150 μm diameter NiCr needle, vibrating at 957 Hz with 5 μm amplitude above the sample surface accurately controlled by a double coil and permanent magnet displacement device. The working distance was approximately 60 μm. The resolution of the measurement depends on the needle diameter and the working distance, and was approximately 113 μm for this study [26]. The potential of the probe was calibrated in air against a Cu/CuSO$_4$ electrode ($+0.320$ V$_{SHE}$). All potentials are given relative to SHE. The SKP probe was scanned in steps of 40 μm over the coated surface along an 8 mm line normal to the defect-coating boundary and the profile lines, starting at this boundary. Minimum 2 parallel samples were tested for each condition. Several parallels were investigated simultaneously. The potentials of the bare steel surfaces employed in this study, were also measured with the SKP technique.

3. Results and discussion

3.1. Topography characterization

The laser patterning resulted in a series of equidistant and uniform linear peaks and grooves. Fig. 2 shows an example of a laser structured surface in plan-view, in this case the B2 surface. The profiles of all the surfaces are shown in Fig. 3. On the B, C and D surfaces the profiles differed in shape and height.

Tortuosity was calculated as the ratio of effective contact length to geometrical length across the surface profile according to Watts and Castle [7,13]. The ratios of effective contact area to geometrical area (Wenzel's roughness factor) were the same, since the profiles are straight in one dimension. Roughness and tortuosity are given in Table 2

3.2. Oxide characterization

The atomic concentration of the various iron oxidation states is shown in Fig. 4. The A surface had the highest concentration of metallic iron at the surface and the lowest concentration of Fe_2O_3/FeOOH. The oxides on the micro patterned samples were formed during the laser structuring. Within a surface layer of a few nm, a temperature rise in the order of 1000 K might be expected [43]. Together with the presence of oxygen, the process resulted in thermal oxidation of the steel surface. C surfaces had the highest concentration of Fe_3O_4 and Fe_2O_3/FeOOH at the surface.

Table 2 shows the Fe^{3+}/Fe^{2+} ratios for the surfaces. The C surfaces contained more trivalent iron than divalent. The increased presence of trivalent iron is not favorable to the oxygen reduction reaction due to reduced conductivity. However, a significant effect of the ratio on the electron transfer rate is seen first at a 10-fold increase in the ratio and higher [44,45]. The highest Fe^{3+}/Fe^{2+} ratio measured in this study was 1.26 on C surfaces, and the lowest was 0.80 on A surfaces. Hence, both the ratio and the variation between the surfaces were too small to affect the oxygen reduction reaction and the cathodic disbonding behavior. A difference of 60 mV was measured between the surface with the highest and lowest potential, which confirms that the electrochemical properties of the surfaces were quite similar. It has been shown before though that the surface composition affects not only the electron transfer rates during cathodic disbonding processes, and hence the CD rate, but may also affect adhesion forces [27,46]. A relationship between surface oxide chemistry and adhesion strength was demonstrated. The meaning of this is that it cannot be completely excluded that oxide chemistry may have contributed to the polyvinyl butyral/oxide/steel properties.

3.3. Coating/oxide/steel interface behavior in air and nitrogen atmosphere

The influence of steel topography and roughness on CD resistance and ionic mobility in inert atmosphere, the latter representing wet adhesion properties of the interface, were studied by SKP.

The CD results are shown in Fig. 5. CD in air proceeded with the typical sigmoid potential profiles as previously reported [15–20], characterized by two potential levels. The high potential plateau, corresponding to an intact coating/substrate interface, varied for the

Fig. 2. SEM micrograph showing example top view of the equidistant lines produced by laser structuring steel surfaces with a periodic pattern of peaks. Sample B2 is shown here.
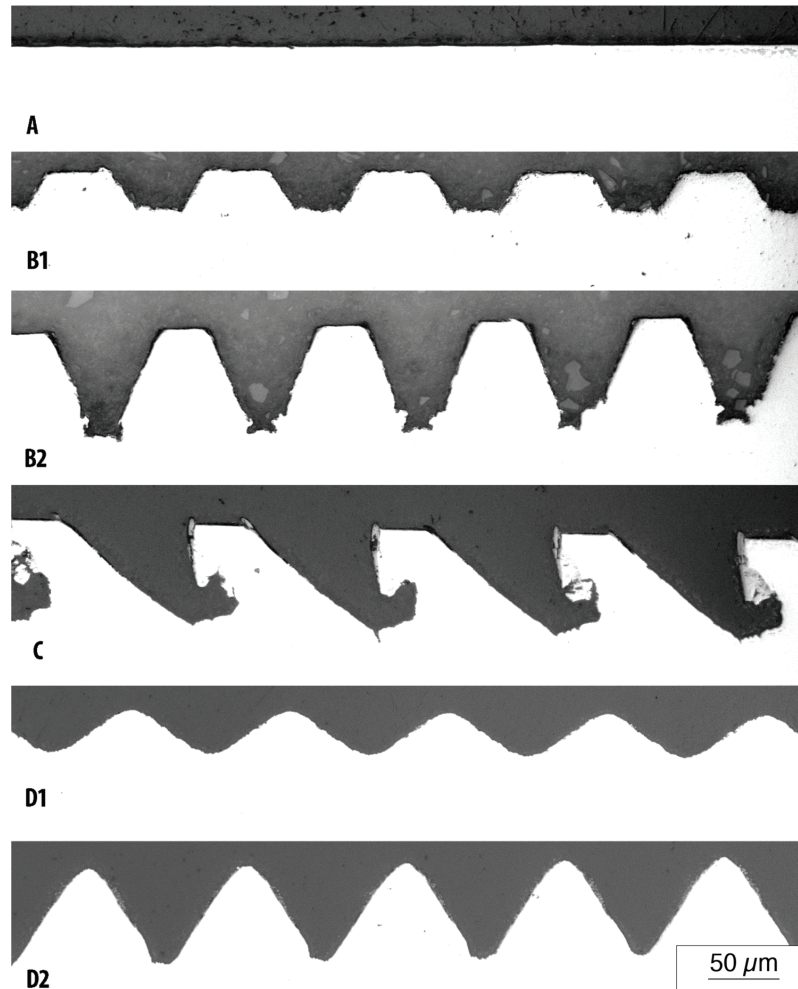
Fig. 3. Optical microscope images of cross-sections of the surfaces a) A, b) B1, c) B2, d) C, e) D1 and f) D2.

substrates in this study between 0.48 and 0.52 V_{SHE}. The potential of the intact interface is known to depend on the oxide composition [44], the applied coating [47], oxide/coating interactions [27,48] and the ingress of humidity and gasses [49]. Since the oxide composition was rather similar for all the surface profiles tested (see Fig. 4), and the test conditions were the same, the small variations in this potential between the various surfaces was expected.

The low potential area close to the defect is attributed to the area with disbonded coating. Potentials of -0.1 to $-0.2\,V_{SHE}$ were measured close to the defect, which correlates well with previous studies [50].

The CD front, or the "electrolyte front position" [41], has been defined as the position of largest potential change between these two areas [4,37,38]. The NaCl electrolyte at the defect feeds the interface with hydrated cations. Once an electrolytic contact is established with the intact interface, the potential at the respective position is cathodically shifted towards the anodic defect potential. The potential of corroding steel in 0.5 M NaCl is typically -0.3 to $-0.4\,V_{SHE}$ [42]. The electrolytic contact of the intact interface with the coating defect,

allows the oxygen reduction reaction to occur underneath the coating without the kinetical inhibition that an intact interface represents [51]. The disbonding front position is hence located at the transition from areas where the oxygen reduction reaction is kinetically free to happen, to areas where it is hindered. The location of this front is seen at the inflection point in the sigmoid potential profile, and its lateral shift is commonly used as a sign for the propagation of the CD process.

The potentials close to the defect on B2 and D2 surfaces decreased to $-0.1\,V_{SHE}$ during the first $3-4\,h$ of the test, before increasing to about 0 V_{SHE} towards the end of the test. On C surfaces, the potential close to the defect never decreased beyond 0 V_{SHE}, and during the test the potential increased to about 0.2 V_{SHE}. In all cases the potential profiles were sigmoid shaped, typical for the CD process. Considering all the six types of surfaces, the final potential at the defect correlates to some degree with the CD distance. Samples with little disbonding had higher final potential near the defect. A potential increase on bare steel can be caused by passivation. Wielant et al. [27] explained deceleration of CD propagation with passivation of the defect. The driving force for the CD is then decreased as the defect potential is increased [38,51].
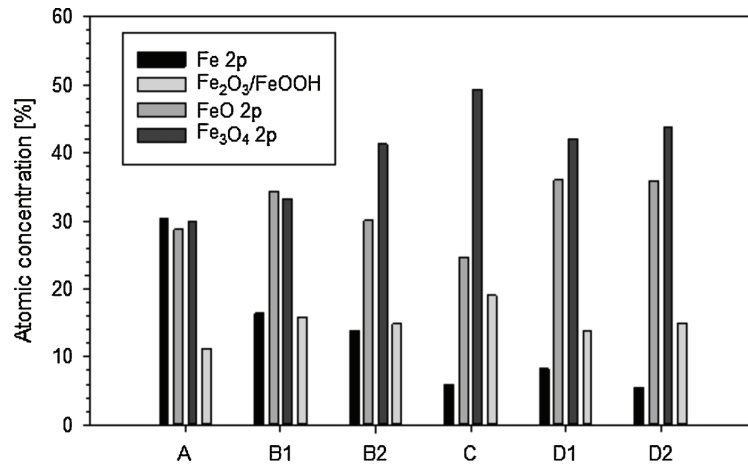
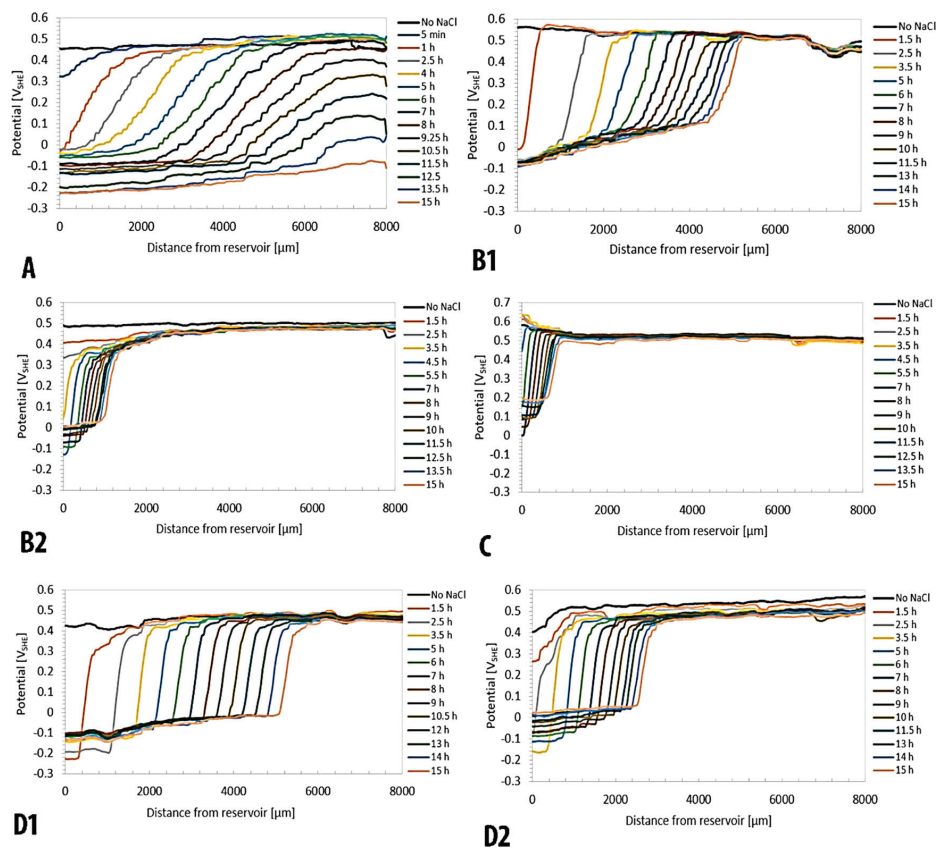**Fig. 4.** The amount of iron species measured by XPS on the surfaces.

Fig. 5. Potential profile recorded on PVB coated steel in air atmosphere at 95% RH and 25 °C, during 15 h with 0.5 M NaCl electrolyte in the coating defect. The potential profiles were recorded on a) A surfaces, b) B1 surfaces, c) B2 surfaces, d) C surfaces, e) D1 surfaces and f) D2 surfaces.

The CD resistance on B2, C and D2 was indeed higher than on the other samples. However, an increasing defect potential is not explaining the large effect of surface roughness on CD. The effect has also been found with cathodically polarized samples, where the defect potential was constant [11].

The phenolphthalein indicator in the PVB coating showed that an alkaline environment developed under the coating, initially close to the defect and propagating with time. The violet phenolphthalein chromophore is at its strongest at pH 10, hence the color that developed implied that the local pH underneath the disbonded coating was at 10 [52]. The color front followed in all cases the disbonding front identified from potential profiles. The color change propagation during the test was not accurately measured, but after the test the color front was found to be identical to the location of the potential increase.

On A surfaces, the potential above *the intact* coating/oxide/steel interface was seen to decrease after about 8 h. Potential decreases above intact coating/steel interfaces, are usually related to a weakening of bonds [49] and activation of the metal surface. Hence, the coating also failed by a second degradation mechanism, probably a general adhesion loss due to hydrolysis of adhesive bonds caused by water absorbed in the film. On A surfaces the PVB coating had disbonded completely, allowing the electrolyte to leak through the coating.

After the test, the disbonded PVB coating was removed on all samples. After 15 h, the trend for the measured disbonded length was A > D1 > B1 > D2 > B2 > C.

Despite the cathodic disbonding process identified in the potential profile scans, and the phenolphthalein pH indicator color shift in the coating close to the defect, the coating still adhered strongly to the B2 and C surfaces in the areas with CD. On the D2 surfaces, post-test adhesion in the disbonded area varied between parallels. These observations are probably explained by mechanical interlocking with the surface profile of the substrate.

The wet adhesion loss observed on the A surfaces was further studied on all the surfaces in an oxygen deficient atmosphere. Wapner et al. found that the ingression of electrolyte along the interface from a defect measured in inert gas, may result in wet de-adhesion [24]. If the potential in the vicinity of the defect does not return to values corresponding to the pristine coating/steel interface (see Fig. 5), when changing from inert air to oxygen atmosphere, a de-adhesion of the coating happened with the incorporation of hydrated ions along the interface in inert atmosphere.

The oxygen concentration was kept at 3 ppm with the exception for $3 - 5$ min when the chamber door was opened and oxygen containing air was entered, first when the samples were introduced, and later when the NaCl electrolyte was added in the defect. The oxygen content temporarily increased, but after 5 min the 3 ppm oxygen concentration was reached upon new nitrogen purging. Surfaces were kept in the humid nitrogen atmosphere for up to 45.5 h, see Fig. 6.

The A surfaces without the ability for mechanical interactions experienced decreased adhesion even in the absence of oxygen, and the coating could be peeled-off at the end of the test. The samples seem to have suffered from a hydrolytic induced destabilization of adhesive bonds. Previously it has been suggested that water reaching the interface may more readily result in bond breaking [53] on such surfaces. Beside breaking of secondary bonds by hydrolysis, a mechanical breaking of bonds has also been proposed [54]. When in addition structural changes take place at the interface due to swelling of the coating, adhesive bonds may be broken [27].

The potential profiles confirm otherwise results from previous studies, showing that ionic mobility in oxygen deficient atmosphere mirrors the ionic mobility in air but happens at lower rates [28,29]. The length over which ions were found to have entered, was smaller compared to the length measured in air, but in general the same trend as seen from potentials scans in air were found. B2 and C, followed by D2 surfaces again display an interface that most efficiently resists the ingress of ions. The ingress of sodium ions at the interface is believed to be migration driven by the hydroxyl production either from the hydrogen reduction reaction [55] or from the reduction of small amounts oxygen trapped at the oxide surface [28,29], or to be a pure diffusive process [24].

3.4. The effect of topography on CD rate

It is found that CD is inversely proportional to tortuosity, see Fig. 7. The relationship presented here on surfaces patterned with a uniform and homogeneous surface texture, confirms thereby results from a previous study on heterogeneous surfaces with different blast cleaning profiles [7]. It was then concluded that roughness affects the cathodic disbonding resistance by the increased interfacial path length for ionic transport, although the study covered a relatively small population of interfacial area (tortuosity measured at 1–1.12). The number of bonds broken by CD should therefore scale with increased contact length at
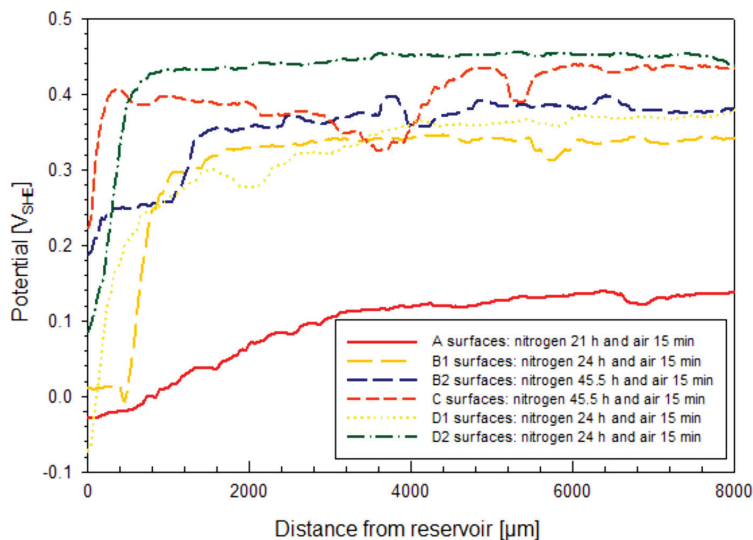

Fig. 6. SKP potential scanning of the ionic mobility in oxygen deficient atmosphere (O$_2$ = 3 ppm) at 95% RH and 25 °C, with 0.5 M NaCl as defect electrolyte. The potential profiles on A, B1, D1 and D2 were scanned after 21–24 h of nitrogen and 15 min with air. B2 and C surfaces were taken after 45.5 h of nitrogen and 15 min with air.
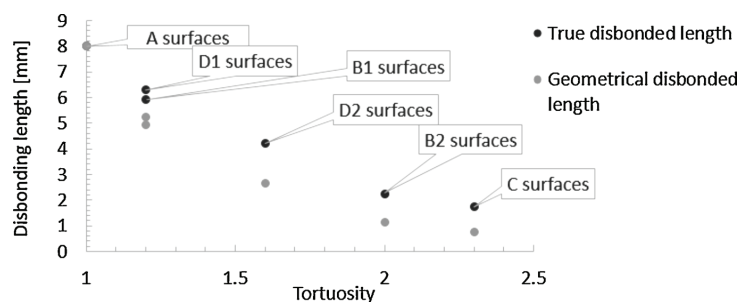
Fig. 7. The disbonded length, as it was measured and as it was calculated as a function of tortuosity, i.e. the ratio between effective interfacial length and geometrical length.

Table 1

Nomenclature. Roughness parameters according to ISO 4287 [32] and ISO 4288 [33].

Parameter	Description	Mathematical definition
A	Actual surface profile area. The effective contact area.	
A_0	Geometrical area	
L	Actual surface profile length. The effective contact length.	
L_0	Geometrical length	
Rz	Average maximum peak to valley distance for five sampling lengths within the measurement length l	$Rz = \frac{1}{5}\sum_{i=1}^{5}(Rp + Rv)_i$ Rp is the largest profile peak height and Rv the maximum profile valley depth within one of the five sampling lengths of the measurement length l.
Tortuosity	Ratio between actual surface profile length to geometrical length	$T = L/L_0$
Wenzel's roughness factor	Ratio between actual surface profile area to geometrical area	$W = A/A_0$

Table 2

Surface conditions, structuring method and roughness of the steel samples used in the study. The Fe^{3+}/Fe^{2+} ratio calculated from the amount of iron species measured by XPS on the surfaces and the potentials [V_{SHE}] measured on uncoated surfaces at 95% RH and 25 °C measured by the SKP.

Surface	Structuring method	Roughness Rz [μm]	Tortuosity	Surface potential [V_{SHE}]	Fe^{3+}/Fe^{2+} ratio
A	Abrasive grinding 80-320-500-1000 grit (ANSI) SiC papers	0.40 ± 0.01	1.01 ± 0.10	0.47 ± 0.01	0.80
B1	Wavelength: 1030 nm Power: 4.05 W Repetition rate: 400 kHz Scan speed: 400 mm/s	25.0 ± 0.10	1.21 ± 0.01	0.50 ± 0.00	0.84
B2	Hatch distance: 10 μm Laser pulse length: 380 fs Number of repetitions: 20 (B1), 50 (B2)	64.1 ± 0.10	1.99 ± 0.05	0.50 ± 0.00	0.97
C	Tilt angle (Sample – working stage): 30° Wavelength: 1030 nm Average laser power: 2 W Laser repetition rate: 400 kHz Scanning speed: 2 m/s Hatch distance: 5μm Pulse duration: 380 fs Number of repetitions: 120	58.4 ± 3.80	2.31 ± 0.1	0.52 ± 0.02	1.26
D1	Wavelength: 1030 nm Average laser power: 1.22 W Laser repetition rate: 400 kHz Scanning speed: 2 m/s	28.0 ± 0.70	1.17 ± 0.04	0.48 ± 0.02	0.84
D2	Hatch distance: 5μm Laser pulse length: 380 fs Number of repetitions: 8 ablation lines with varying rep. numbers	60.7 ± 0.20	1.61 ± 0.01	0.53 ± 0.03	0.87

the interface, such that same disbonded length would be measured on rough surfaces as on smooth surfaces, after a given time. Disbonded length multiplied with tortuosity should be constant for the various profiles tested. However, in this study we found a decay.

Fig. 7 shows the disbonded length as it was measured geometrically after 15 h, and the true disbonded length when geometrical length is multiplied with the tortuosity (see Tables 1 and 2), and plotted against tortuosity. The plot shows a decay. Using least-squares regression,

different trendlines can be fitted to the data set. An exponential inverse relationship was found with an $R^2 > 0.99$ for both series. The relative standard deviation for the disbonding lengths measured after 15 hours, was calculated for two parallel samples treated and tested according to the same scheme, and found to be 18% for B2, 13% for C and < 4% for the other surfaces.

In the mechanistic studies of CD on iron and steel, the disbonding has often been found to be proportional to the square root of time,
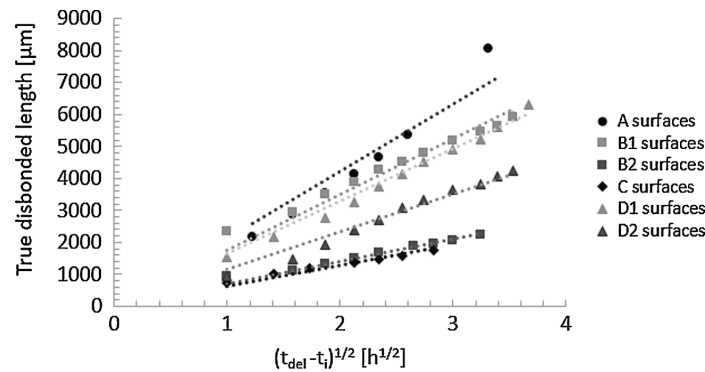
Fig. 8. Plots of true CD distance measured in air atmosphere as a function of $(t_{del} - t_i)^{1/2}$ at 25 °C for a 30 μm PVB coating on steel with different peak patterns and roughness Rz. The electrolyte at the defect is 0.5 M NaCl (aq).

indicating that the transport of hydrated ions at the coating/substrate interface determines the CD rate [3]. This has been reported both for PVB [56] and epoxy coatings [57–59]. The disbonded distance is then related to the time of electrolytic contact (t_{del}) and an initiation time, (t_i), by Eq. (1) [56]

$$X_{del} = k_{del}\sqrt{(t_{del} - t_i)} \qquad (1)$$

k_{del} is the disbonding rate constant. In Fig. 8, the term X_{del} in Eq. (1) has been corrected to the true interfacial disbonded length and plotted as a function of $(t_{del} - t_i)^{1/2}$. The initiation time for CD is understood as the time needed for diffusion of water and oxygen into the coating and establishment of the galvanic cell [60,61]. The initiation time was found to be similar on A, B1, D1 and D2, while it was twice as high on B2 and three times as high on C, with 4.5 h and 7 h respectively. The curves are straight lines, consistent with a rate control by cation migration. The slopes of the lines, corresponding to the k_{del} term in Eq. (1), confirms the trend for CD seen in potential profile plots in Fig. 5. On smooth A surfaces, the CD advances much faster than on C surfaces patterned with tilted and curved peaks, even when compensating for the increased effective contact area. Increased effective contact area therefore cannot explain the increased CD resistance alone. Mechanical interlocking is probably the explanation.

In theory, mechanical adhesion will decrease lifting of the disbonded coating, narrowing the gap between the disbonded coating and the substrate. Hence, the cross-sectional area for cation migration between the coating defect and the CD front will decrease, increasing the ohmic resistance. The potential drop in this area, is explained to be an ohmic potential drop according to Eq. (2) where i_{galv} is the interfacial current density approximated by i_c, the interfacial cation current density. And R is the ohmic resistance in the electrolyte against interfacial cation transport

$$\Delta U_\Omega = i_{galv} \times R_\Omega(x) \qquad (2)$$

A narrower gap at the interface, would increase the potential drop between the defect and the CD front, i.e. an increased potential profile underneath the disbonded coating. The potential profiles for D1 and D2 surfaces in Fig. 5, however, do not seem to differ. In fact, except for B1, all the surfaces have rather flat potential profiles between the coating damage and the CD front.

The quantification of the interfacial cation current density and the electrolytic resistance is difficult. A reduced potential drop will however result from an increased resistance accompanied by a decreased galvanic current. This implies a decreased cationic mobility rate at the interface. Obvious reasons for such a decrease may be explained with increased interfacial transport path for the ions. The surface asperities increased the effective contact area on the surfaces studied here. In

addition, the asperities develop friction forces at the interface, i.e. between the coating and the substrate. The friction forces depend on the specific structure and height of the asperities. See Fig. 9.

The balance of friction forces acting at the interface will determine the resulting mean mechanical interlocking force, also called the anchoring force or simply the mechanical adhesion force [62]. The effective contact area is in either case a key property, as it scales the contribution of friction forces to the resulting anchoring force, according to the relationship in Eq. (3)

$$F_{mechanical} = F_{anchor} = \bar{\mu}\bar{P}R \qquad (3)$$

where $\bar{\mu}$ is the mean friction coefficient between the coating and the substrate and hence depending on the specific topography, $\bar{P}$ is the mean theoretical pressure needed to keep the coating from sliding off the substrate at a given inclination and R is Wenzel's roughness factor [63].

The relationship between mechanical interlocking force $F_{mechanical}$ and R in Eq. (3) is not new information. In general, the simplest theory of promotion of stability at the coating/steel interface due to roughening of the surface, is explained to be the increase in the surface area available for the formation of primary and secondary bonds, provided that the coating can completely wet the substrate. But the number of bonds formed by mechanical interlocking will also increase, as the equation also states [64,65]. Particularly, it is well established that mechanical interlocking is the primary bonding mechanism for thermally sprayed coatings. Its validity for the stability of organic coatings has however been overlooked and even dismissed for years by the scientific community.

The results presented here show the significant effect mechanical interlocking has on the cathodic disbonding resistance of the polyvinyl butyral/oxide/steel interface. When compensating for the increased effective contact area, the CD resistance was higher on surfaces with features that enabled mechanical interlocking forces. Hence, CD resistance was improved by both increasing effective contact area and mechanical interlocking. Also, water induced adhesion loss improved with mechanical interlocking, as was shown in Fig. 6. The results indicate that CD and wet adhesion depend on the ability of the surface for mechanical interlocking.

Mechanical interlocking will affect the interfacial stability in several ways. It is believed to suppress water accumulation at the interface [66] and total rupture of bonds when accumulation has happened [53] thus increasing the hydrolytic stability of the coating at the interface. A high interfacial stability under humid exposure is suggested to result in higher resistance to lateral ingress of ions from the electrolyte covered defect [51]. This is necessary for a slower CD rate, but also for hydrolytic stability as hydrated cations may contribute to wet de-adhesion
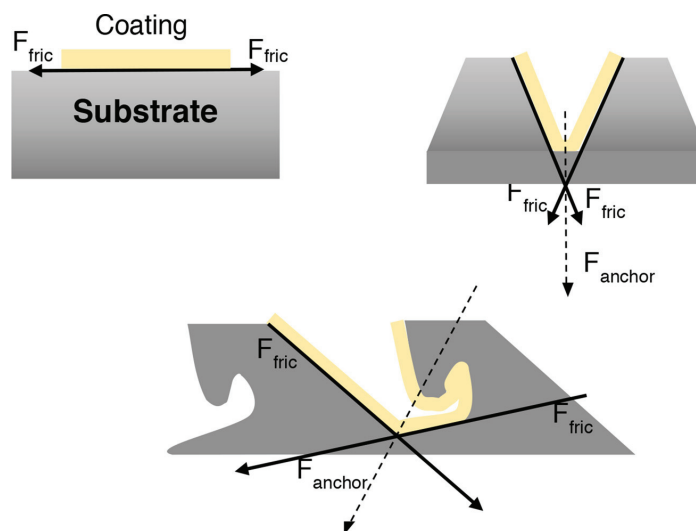
Fig. 9. Sketch of the anchoring force F_{anchor} of a coating as function of the topography of the substrate. Adapted from [62] to explain the anchoring forces in this study.

[67]. The CD progress is believed to proceed by the formation of an area where the coating/substrate interface is affected by the alkaline environment and undergoes structural changes before bonds ultimately fail [38]. Mechanical interactions may stabilize the coating such that coating/substrate bonds are not necessarily broken [42].

Contributions from mechanical interactions have been claimed to make up most of the total adhesion forces at the interface for an organic coating, as mechanical adhesion is expected to be much larger than the adhesion relying on secondary bonding forces that vary with surface oxide chemistry [65,68,69]. Therefore, variations in surface oxide chemistry are not assumed to be responsible for the CD resistance and wet adhesion properties measured. The XPS analysis and surface potentials measured by SKP on bare substrates contribute to this recognition.

Since the mechanical adhesion force scales up with increased effective contact area and interlocking forces the ranking of the surfaces with respect to their ability for mechanical adhesion is: C > B2 > D2 > D1/B1 > A. This ranking mirrors their measured CD resistance.

4. Conclusions

All but the flat A surface allowed for mechanical interlocking. These surfaces had the highest CD rate and highest interfacial ionic mobility. In addition, they suffered from hydrolytic destabilization.

Increasing substrate roughness increased the effective contact area between coating and substrate, and partly explained the improved CD resistance. Features enabling mechanical interlocking forces increased CD resistance even further.

Surface B1 and D1 had similar effective contact area but differed in topography, with more interlocking presumed to be offered by the rectangular peaks on B1. The CD rate was similar on these surfaces. D2 surfaces gave almost twice as much CD as B2 surfaces, even though the tortuosity was only 20% lower. The structures at the bottom of the grooves on B2, probably added to the interlocking of the PVB coating though, which may have increased the CD resistance.

The C surfaces have the highest effective interfacial length, but also the surface with highest ability for mechanical interlocking due to the tilted and curved peaks that can entrap the coating. Little CD and ionic mobility were found on these surfaces.

Data availability

The raw/processed data required to reproduce these findings cannot be shared at this time as the data also forms part of an ongoing study.

CRediT authorship contribution statement

C.H.M. Hagen: Conceptualization, Methodology, Investigation, Data curation, Writing - original draft. **O.Ø. Knudsen:** Supervision, Writing - review & editing. **A.H. Zavieh:** Writing - review & editing. **W. Pfleging:** Writing - review & editing.

Declaration of Competing Interest

The authors declare that they have no known competing financial interests or personal relationships that could have appeared to influence the work reported in this paper.

Acknowledgements

Appendix A. Supplementary data

Supplementary material related to this article can be found, in the online version, at doi:https://doi.org/10.1016/j.porgcoat.2020.105766.

References

[1] L.H. Lee, The chemistry and physics of solid adhesion, in: Lee L.H (Ed.), Fundamentals of Adhesion, Plenum Press, London, 1991, pp. 1–86.

[2] C.M.H. Hagen, et al., The effect of surface roughness on corrosion resistance of machined and epoxy coated steel, Prog. Org. Coat. 130 (2019) 17–23.

[3] S.B. Lyon, R. Bingham, D.J. Mills, Advances in corrosion protection by organic coatings: what we know and what we would like to know, Prog. Org. Coat. 102 (2017) 2–7.

[4] A. Leng, H. Streckel, M. Stratmann, The delamination of polymeric coatings from steel. Part 1: calibration of the Kelvin probe and basic delamination mechanism, Corros. Sci. 41 (3) (1998) 547–578.

[5] M. Stratmann, 2005 W.R. Whitney award lecture: corrosion stability of polymer-coated metals - new concepts based on fundamental understanding, Corrosion 61 (12) (2005) 1115–1126.

[6] J.E.O. Mayne, The mechanism of protection by organic coatings, Met. Finish. 12 (143) (1966) 437–441.

[7] P.A. Sørensen, et al., Influence of substrate topography on cathodic delamination of anticorrosive coatings, Prog. Org. Coat. 64 (2–3) (2009) 142–149.

[8] B.C. Rincon Troconis, G.S. Frankel, Effect of roughness and surface topography on adhesion of PVB to AA2024-T3 using the blister test, Surf. Coat. Technol. 236 (0) (2013) 531–539.

[9] D. Ward, An Investigation Into The Effect Of Surface Profile On The Performance Of Coatings In Accelerated Corrosion Tests, Corrosion 2007, NACE, Houston, TX, 2007, p. 16.

[10] J.P.B. van Dam, et al., Effect of surface roughness and chemistry on the adhesion and durability of a steel-epoxy adhesive interface, Int. J. Adhes. Adhes. 96 (2020) 102450.

[11] C.H.M. Hagen, A. Kristoffersen, O.Ø. Knudsen, The effect of surface profile on coating adhesion and corrosion resistance, in: NACE (Ed.), Corrosion 2016, NACE Vancouver, 2016, p. 15.

[12] H.M.C. Hagen, O.Ø. Knudsen, T. Hemmingsen (Ed.), Corrosion Protection of Smooth Surfaces - Coating Adhesion, in Nordic Corrosion Congress, Stavanger, 2015, p. 12.

[13] J.F. Watts, J.E. Castle, The application of X-ray photoelectron spectroscopy to the study of polymer-to-metal adhesion. Part 2 the cathodic disbondment of epoxy coated mild steel, J. Mater. Sci. 19 (1984) 2259–2272.

[14] S.S. Jamali, D.J. Mills, Steel surface preparation prior to painting and its impact on protective performance of organic coating, Prog. Org. Coat. 77 (12, Part B) (2014) 2091–2099.

[15] R.J. Holness, et al., Polyaniline inhibition of corrosion-driven organic coating cathodic delamination on iron, J. Electrochem. Soc. 152 (2) (2005) B73–B81.

[16] N. Wint, et al., The kinetics and mechanism of atmospheric corrosion occurring on tin and iron-tin intermetallic coated steels: I. Cathodic delamination, J. Electrochem. Soc. 162 (14) (2015) C775–C784.

[17] D. Iqbal, et al., Synthesis of ultrathin poly (methyl methacrylate) model coatings bound via organosilanes to zinc and investigation of their delamination kinetics, ACS Appl. Mater. Interfaces 6 (20) (2014) 18112–18121.

[18] G. Williams, H.N. McMurray, Chromate inhibition of corrosion-driven organic coating delamination studied using a scanning Kelvin probe technique, J. Electrochem. Soc. 148 (10) (2001) B377–B385.

[19] G. Williams, H.N. McMurray, Inhibition of corrosion driven delamination on iron by smart-release bentonite cation-exchange pigments studied using a scanning Kelvin probe technique, Prog. Org. Coat. 102 (2017) 18–28.

[20] G. Williams, H.N. McMurray, The mechanism of group (I) chloride initiated filiform corrosion on iron, Electrochem. Commun. 5 (10) (2003) 871–877.

[21] M. Rohwerder, et al., Application of Scanning Kelvin Probe in Corrosion Science, (2005), pp. 605–648.

[22] M. Rohwerder, et al., Application of SKP for in situ monitoring of ion mobility along insulator/insulator interfaces, Electrochim. Acta 54 (25) (2009) 6058–6062.

[23] M. Rohwerder, The Kelvin probe technique as reference electrode for application on thin and ultrathin electrolyte films, in: I. G, L. A, S. F (Eds.), Handbook of Reference Electrodes. Springer, Berlin, 2013.

[24] K. Wapner, M. Stratmann, G. Grundmeier, In situ infrared spectroscopic and scanning Kelvin probe measurements of water and ion transport at polymer/metal interfaces, Electrochim. Acta 51 (16) (2006) 3303–3315.

[25] A. Nazarov, N. Le Bozec, D. Thierry, Assessment of steel corrosion and deadhesion of epoxy barrier paint by scanning Kelvin probe, Prog. Org. Coat. 114 (2018) 123–134.

[26] M. Wicinski, W. Burgstaller, A.W. Hassel, Lateral resolution in scanning Kelvin probe microscopy, Corros. Sci. 104 (2015).

[27] J. Wielant, et al., Cathodic delamination of polyurethane films on oxide covered steel – combined adhesion and interface electrochemical studies, Corros. Sci. 51 (8) (2009) 1664–1670.

[28] R. Posner, et al., Transport processes of hydrated ions at polymer/oxide/metal interfaces: part 1. Transport at interfaces of polymer coated oxide covered iron and zinc substrates, Electrochim. Acta 54 (3) (2009) 891–899.

[29] R. Posner, et al., Transport processes of hydrated ions at polymer/oxide/metal interfaces: part 2. Transport on oxide covered iron and zinc surfaces, Electrochim. Acta 54 (3) (2009) 900–908.

[30] R. Posner, et al., Transport processes of hydrated ions at polymer/oxide/metal interfaces, Electrochim. Acta 54 (3) (2009) 891–899.

[31] B. Salgin, R.F. Hamou, M. Rohwerder, Monitoring surface ion mobility on aluminum oxide: effect of chemical pretreatments, Electrochim. Acta 110 (Supplement C) (2013) 526–533.

[32] ISO 4287, Geometrical Product Specifications (GPS) - Surface Texture: Profile Method -Terms, Definitions and Surface Texture Parameters, International Organization for Standardization, Switzerland, 2000.

[33] ISO 4288, Geometrical Product Specifications (GPS) - Surface Texture : Profile Method – Rules and Procedures for the Assessment of Surface Texture, International Organization for Standardization, Switzerland, 1996.

[34] E. Mottay, et al., Industrial applications of ultrafast laser processing, MRS Bull. 41 (12) (2016) 984–992.

[35] W. Pfleging, A review of laser electrode processing for development and manufacturing of lithium-ion batteries, Nanophotonics 7 (3) (2018) 549.

[36] C.H.M. Hagen, et al., Oxidation of coated steel during exposure to humid air and effects on cathodic disbonding, Electrochimica Acta (2020) submitted for publication.

[37] A. Leng, H. Streckel, M. Stratmann, The delamination of polymeric coatings from steel. Part 2: first stage of delamination, effect of type and concentration of cations on delamination, chemical analysis of the interface, Corros. Sci. 41 (3) (1998) 579–597.

[38] A. Leng, et al., The delamination of polymeric coatings from steel. Part 3: effect of the oxygen partial pressure on the delamination reaction and current distribution at the metal-polymer interface, Corros. Sci. 41 (3) (1999) 599–620.

[39] D.A. Shirley, High-resolution X-Ray photoemission Spectrum of the valence bands of gold, Phys. Rev. B 5 (12) (1972) 4709–4714.

[40] J.F. Moulder, et al., Handbook of X-Ray Photoelectron Spectroscopy, Perkin-Elmer Corp, Physical Electronics Division, Eden Prairie, Minnesota, 1995.

[41] G. Grundmeier, M. Stratmann, Adhesion and de-adhesion mechanisms at polymer/metal interfaces: mechanistic understanding based on in situ studies of buried interfaces, Annu. Rev. Mater. Res. 35 (2005) 571–615.

[42] M. Stratmann, et al., The scanning Kelvin probe; a new technique for the in situ analysis of the delamination of organic coatings, Prog. Org. Coat. 27 (1–4) (1996) 261–267.

[43] L. Lu, et al., The influence of pulse width and energy on temperature field in metal irradiated by ultrashort-pulsed laser, Phys. Procedia 32 (2012) 39–47.

[44] G. Grundmeier, M. Stratmann, Influence of oxygen and argon plasma treatments on the chemical structure and redox state of oxide covered iron, Appl. Surf. Sci. 141 (1) (1999) 43–56.

[45] N. Le Bozec, et al., Influence of stainless steel surface treatment on the oxygen reduction reaction in seawater, Corros. Sci. 43 (4) (2001) 765–786.

[46] J. Wielant, et al., SKP as a tool to study the physicochemical interaction at buried metal–coating interfaces, Surf. Interface Anal. 42 (6-7) (2010) 1005–1009.

[47] A. Nazarov, D. Thierry, Studies in the electrical double layer at Metal/Polymer interfaces by scanning capacitive probe, Prot. Met. 39 (1) (2003) 55–62.

[48] J. Wielant, et al., Influence of the Iron oxide acid – Base properties on the chemisorption of model epoxy compounds studied by XPS, J. Phys. Chem. C 111 (35) (2007) 13177–13184.

[49] A. Nazarov, D. Thierry, Hydrolysis of interfacial bonds in a metal/polymer electrical double layer, Prot. Met. 41 (2) (2005) 105–116.

[50] S.M. Cambier, R. Posner, G.S. Frankel, Coating and interface degradation of coated steel, Part 1: field exposure, Electrochim. Acta 133 (2014) 30–39.

[51] R. Posner, O. Ozcan, G. Grundmeier, Water and ions at Polymer/Metal interfaces, in: M.L.F. Silva, C. Sato (Eds.), Design of Adhesive Joints Under Humid Conditions, Springer Berlin Heidelberg, Berlin, Heidelberg, 2013, pp. 21–52.

[52] W. Fürbeth, M. Stratmann, Scanning Kelvin probe investigations on the delamination of polymeric coatings from metallic surfaces, Prog. Org. Coat. 39 (1) (2000) 23–29.

[53] W. Brockmann, Durability of adhesion between metals and polymers, J. Adhes. 29 (1-4) (1989) 53–61.

[54] H. Leidheiser, W. Funke, Water disbondment and wet adhesion of organic coatings on metals: a review and interpretation, J. Oil Colour Chem. Assoc. 70 (5) (1987) 121–132.

[55] M. Doherty, J.M. Sykes, Micro-cells beneath organic lacquers: a study using scanning Kelvin probe and scanning acoustic microscopy, Corros. Sci. 46 (5) (2004) 1265–1289.

[56] G. Williams, et al., Dopant effects in polyaniline inhibition of corrosion-driven organic coating cathodic delamination on Iron, J. Electrochem. Soc. 153 (10) (2006) B425–B433.

[57] O.Ø. Knudsen, J.I. Skar, Cathodic disbonding of epoxy coatings - effect of test parameters, Corrosion/08, NACE, New Orleans, 2008.

[58] J.I. Skar, U. Steinsmo, Cathodic disbonding of paint films: transport of charge, Corros. Sci. 5 (8) (1993) 1385–1389.

[59] U. Steinsmo, J.I. Skar, Factors influencing the rate of cathodic disbonding of coatings, Corrosion 50 (12) (1994) 934–939.

[60] H. Bi, J. Sykes, An investigation of cathodic oxygen reduction beneath an intact organic coating on mild steel and its relevance to cathodic disbonding, Prog. Org. Coat. 87 (2015) 83–87.

[61] C.F. Glover, et al., Evaluation of multi-layered graphene nano-platelet composite coatings for corrosion control part II – cathodic delamination kinetics, Corros. Sci. 136 (2018) 304–310.

[62] R. Kromer, et al., Laser patterning pretreatment before thermal spraying: a technique to adapt and control the surface topography to thermomechanical loading and materials, J. Therm. Spray Technol. 25 (3) (2016) 401–410.

[63] R. Kromer, et al., Laser surface patterning to enhance adhesion of plasma sprayed coatings, Surf. Coat. Technol. 278 (2015) 171–182.

[64] S.P.M. Noijen, et al., Numerical prediction of failure paths at a roughened metal/polymer interface, Microelectron. Reliab. 49 (9) (2009) 1315–1318.

[65] Ovd. Sluis, S.P.M. Noijen, P.H.M. Timmermans, On the effect of microscopic roughness on macroscopic polymer-metal adhesion, in: W.Dv. Driel, X.J. Fan (Eds.),

Solid State Lighting Reliability: Components to Systems, Springer, 2013.

[66] J.D. Venables, Adhesion and durability of metal-polymer bonds, J. Mater. Sci. 19 (8) (1984) 2431–2453.

[67] M. Kendig, D.J. Mills, An historical perspective on the corrosion protection by paints, Prog. Org. Coat. 102 (2017) 53–59.

[68] A.G. Evans, et al., The fracture energy of bimaterial interfaces, Metall. Trans. A 21 (9) (1990) 2419–2429.

[69] S.P.M. Noijen, et al., A semi-analytic method for crack kinking analysis at isotropic bi-material interfaces, Eng. Fract. Mech. 83 (2012) 8–25.

Paper III

Oxidation of coated steel during exposure to humid air and effects on cathodic disbonding - a qualitative study

C.H.M.Hagen (a), O.Ø.Knudsen (a,b), R.Johnsen (a), A.H. Zavieh (c), W.Pfleging (d,e)

a Department of Mechanical and Industrial Engineering, NTNU, 7491 Trondheim, Norway

b SINTEF, Richard Birkelandsvei 2B, 7465 Trondheim, Norway

c NTNU Nanolab, Sem Sælands vei 14, 7491 Trondheim

d Karlsruhe Institute of Technology, IAM-AWP, P.O. Box 3640, 76021 Karlsruhe, Germany

e Karlsruhe Nano Micro Facility, Hermann-von-Helmholtz-Platz 1, 76344 Eggenstein-Leopoldshafen, Germany

Corresponding author: Hagen. E-mail: catalina.hagen@ntnu.no

Abstract

This work investigated the oxidation of steel under a poly-vinyl butyral coating during exposure to humid air, and the effects on cathodic disbonding. Laser structuring and grinding was employed to pattern steel surfaces with periodic peaks of different peak-to-valley height, Rz, and geometry. Using a combination of the in-situ scanning Kelvin probe technique and X-ray photoelectron spectroscopy, it has been demonstrated that the steel surface oxidises underneath adhering coating, depending on oxide condition from the start. The amount of oxidised iron species increased significantly with exposure, and the relative amount of the various oxidation states shifted towards trivalent iron. The changes in surface oxide under the coating were found to be independent of the topography or roughness of the steel substrate. On smooth surfaces however, the oxidation resulted in loss of adhesion. The cathodic disbonding rate depended on iron oxide condition and oxidation level. Mechanical interlocking and increased surface roughness increased the stability of the interface and the cathodic disbonding resistance.

Highlights

- The steel surface oxidised under coating in humid air
- Surface topography did not affect the oxidation
- On smooth surfaces, oxidation of the steel caused the PVB coating to lose adhesion
- The cathodic disbonding rate depended on iron oxide condition and oxidation
- Topography affected the stability of the coating/steel interface

Keywords

Scanning Kelvin probe, cathodic disbonding, organic coatings, topography, effective contact area, mechanical interlocking

1 Introduction

Both oxygen and water are penetrating protective organic coatings at a sufficient rate to sustain corrosion reactions, but in spite of this they protect against corrosion [1]. A vital property of the organic coating is therefore believed to be its ability to protect passivating surface oxides on the substrate, i.e. that the oxide actually provides the corrosion protection [2].

The passivating oxide film on iron is formed by the oxidation of iron to iron cations at the metal/oxide interface, while dissolved oxygen in the water is ionised at the oxide/electrolyte interface to oxygen anions. The growth proceeds by oxygen ions migrating inwards from the electrolyte-oxide interface to react with metal ions to form the inner part of the oxide, and iron ions that migrate outwards from the iron-oxide interface towards the oxide/electrolyte interface to react with the oxygen ions [3]. At the same time, electrons from the anodic reaction under the oxide are transported to the cathodic reaction on the electrolyte oxide interface. The oxide is considered to have a bipolar character, consisting of an Fe^{2+} rich anion-selective inner layer and an Fe^{3+} rich cation-selective outer layer [4]. As the oxide thickens, the resistance against transport of ions in the oxide increases and the steel passivates [3].

However, at the oxide surface, redox transitions from $Fe^{2+} \rightarrow Fe^{3+}$ can take place, providing the oxygen reduction on the oxide surface with a supply of electrons [4]. Since the cathodic oxygen reduction causing cathodic disbonding takes place on top of the steel surface oxide, electrons from the external anodic reaction will have to be transported through the surface oxide. The effect of oxide semiconducting properties on cathodic disbonding (CD) has been investigated [5]. Transport of hydrated cations from a defect in the coating e.g. Na^+, to the organic coating/oxide interface, will connect the oxide with external anodic reactions and thus accelerate the cathodic oxygen reduction on top of the oxide, resulting in cathodic disbonding [6].

It is acknowledged that adding roughness to a surface, increases the effective contact area at the interface. Chemical and physical interactions at the coating/substrate interface will increase with roughness due to increased contact area [7, 8]. In addition, roughness may promote mechanical adhesion at the coating/steel interface [9]. Mechanical adhesion will increase the total amount of adhesive forces at the interface [10] and may contribute substantially to the interface's stability especially during exposure to humidity [11, 12]. Mechanical interlocking may therefore improve the protective properties and durability of the coating. Both field experience and lab testing have shown that coating/steel interfaces without mechanical interlocking, fail early when exposed to corrosive conditions [11, 13]. In addition, for electrochemical disbonding mechanisms relying on transport of ions along the coating/steel interface, it has been shown that changes in the surface profile will alter the interfacial path length and hence the kinetics of failure [14-17]. On surfaces abraded with SiC paper in one

direction, producing parallel abrasion lines, cathodic disbonding was found to progress faster parallel to the lines than perpendicular to the lines [18].

Although water and oxygen are known to diffuse into organic coatings, their effects on the coating/steel interface are still much debated. Since the 1980s, the scanning Kelvin probe (SKP) technique has emerged as a powerful method for studies of buried interfaces [19, 20]. It is a non-destructive method that allows to map surface potentials through insulating layers of coatings as thick as 300 μm [21] with a typical lateral resolution of 100-150 μm [22].

In this paper a qualitative investigation of the effect of humid air on the coating/steel interface and the stabilising effects of surface roughness is presented. The investigation aims to document: i) the changes in the surface oxide under the coating with time when exposed to various levels of humid air, ii) the resistance to CD as a function of the preceding exposure to humid air, and iii) the stabilising effects of surface roughness on coating adhesion. The effect of roughness was included by controlled laser micro-patterning with various topographies and roughness, Rz. The surface oxides on the steel samples were electrochemically reduced prior to coating. The coated samples were therefore susceptible to oxidation when exposed to humid air during testing. X-ray photoelectron spectroscopy (XPS) was employed to evaluate the changes in surface oxide under the coating. See Figure 1 for information about the structure of the study.
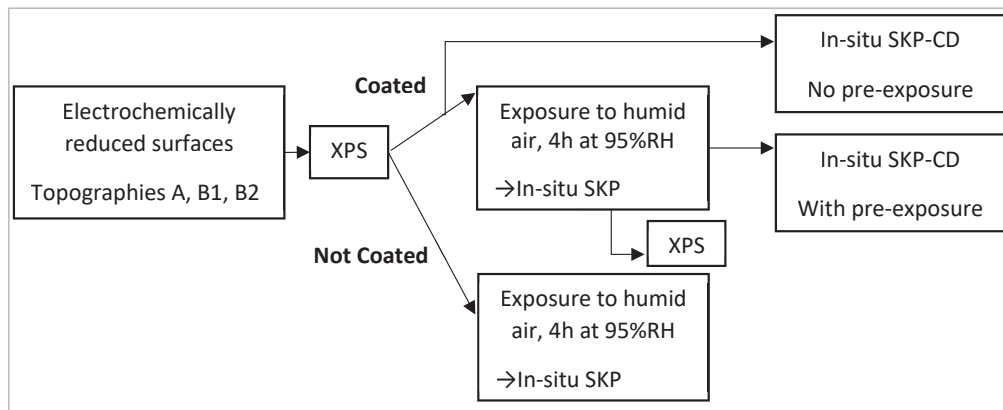

Figure 1. Schematic illustration of the experimental steps in the study.

See Table 1 for definition of the roughness parameters used in this study.

Table 1. Nomenclature. Roughness parameters according to ISO 4287 [23] and ISO 4288 [24].

Parameter	Description	Mathematical definition
A	Actual surface profile area.	
A_0	The effective contact area. Geometrical area	

Rz	Average maximum peak to valley distance for five sampling lengths within the measurement length l	$Rz = \frac{1}{5}\sum_{i=1}^{5}(Rp+Rv)_i$	Rp is the largest profile peak height and Rv the maximum profile valley depth within one of the five sampling lengths of the measurement length l.

2 Experimental

2.1 Materials and sample preparation

The samples were prepared using 3 mm thick cold-rolled steel plates, EN 10130. The chemical composition (in % by weight) was 0.04% C, 0.008% Si, 0.284% Mn, 0.0071% P, 0.0184% S, 0.033% Al, Fe to balance.

Surfaces with and without the ability for mechanical interactions at the coating/steel interface were produced. Grinding was used to produce a smooth surface, while laser structuring was used to make a periodic pattern of peaks and grooves. The surfaces are described in Table 2. Surfaces labelled A were grinded with SiC papers, while surfaces labelled B1 and B2 were ultrafast laser structured.

Table 2. Surface conditions, structuring method and roughness of the steel samples used in the study.

Surface	Structuring method	Roughness Rz [μm]
A	Abrasive grinding using 80-320-500-1000 grit (ANSI) SiC papers	0.4
B1	Femtosecond laser structuring Wavelength: 1030 nm Power: 4.05 Watt	25
B2	Laser repetition rate: 400 kHz Scanning speed: 400 mm/s Hatch distance: 10 μm Pulse duration: 380 fs Number of repetitions: 20 (B1), 50 (B2)	64

The dimensions of the laser structured areas were 10 mm x 10 mm. All samples were thoroughly rinsed in ultrasonic bath with acetone and isopropanol and dried with an air blower. Samples were then stored in a desiccator.

Substrates were electrochemically treated to have their as-prepared surface oxide removed. A reduction was performed by cathodic polarisation for 60 min at -0.76 V_{SHE} in a 0.075 M $Na_2B_4O_7 \cdot 10H_2O$ + 0.3 M H_3BO_3 solution (pH = 8.2). Samples with as-prepared oxides were reference. The coating was applied immediately after reduction of the oxides, ultrasonic cleaning in dehydrated isopropanol (max 0.005% H_2O) and hot air drying, in that order. The uncoated parts of the samples were covered by insulating tape. All samples were stored in desiccators, until the measurements were performed.

A polyvinylbutyral-*co*-vinylalcohol-*co*-vinylacetate (PVB) solution was prepared in isopropanol at 15.5% w/w PVB, by stirring overnight. Phenolphthalein was added as pH-indicator at 6% w/w concentration in the solution. The coating was applied using a

draw-down bar. This is a model coating often used for in-situ studies of the coating/steel interface stability [25-30].

The dry film thickness was 35 ± 6 μm above the peaks, measured with a magnetic coating thickness gauge and confirmed by cross-sections. Samples with 50 ± 7 μm PVB thickness were also prepared to study the effect of film thickness. The PVB coating cured for 6 days at ambient temperature inside a desiccator followed by 1 hour in oven at 60 °C. The coating was then partially peeled back to create a defect of 10 mm x 10 mm bare metal in front of the laser structured area. The coating defect preparation method was based on that of Stratmann et al. [31-33] and also used in other studies [25, 28].

All chemicals were obtained from Sigma-Aldrich[1] and VWR[2].

2.2   Laser structuring

Ultrafast laser structuring is related to laser pulse lengths smaller than the electron-phonon interaction time, which is typically in the range of a few ps (10^{-12} s). Therefore, this type of laser ablation enables the formation of micro-patterns at steel surfaces, without significant heat impact to the surrounding material [34]. For femtoseconds lasers the thermal diffusion length can be almost ignored (<nm), although the heat accumulation can be very high locally. Furthermore, it offers the possibility of contactless rapid manufacturing of functional designs with high flexibility and process reliability [34, 35]. It also allows for production of a uniform and homogenous surface texture, in contrast to the heterogenous and random surface texture created by e.g. blast cleaning.

Ultrafast laser-structuring of surfaces B1 and B2 was carried out on a micromachining workstation (PS450-TO, Optec, Belgium) equipped with a tunable fiber laser (Tangerine, Amplitude Systèmes, France). See Table 2 for parameters. The maximum average power was 35 W and the maximum pulse energy was specified to 175 μJ at 1030 nm (TEM00 with a beam quality factor, M^2 < 1.2). The pulse repetition rate could be varied from single pulse to 2 MHz and the laser pulse duration from 380 fs (10^{-15} s) to 10 ps, respectively. The laser beam was scanned over the sample surface for all experiments using a Rhothor™ Laser Deflection Systems scan head (Newson Engineering BV). All laser structuring processes were carried out under ambient air and the ablated material was removed by an exhaust.

2.3   Topography characterisation

On the A surfaces, a non-contact Alicona [3] optical Infinite-Focus Microscope (IFM) and a stylus profilometer was used to assess the ratio of effective contact area to geometrical area and the roughness Rz [24], respectively. Rz was measured by the profilometer according to the ISO 4287 definition.

On laser structured B1 and B2 surfaces, all measurements were made on cross-sections analysed with an Olympus GX51 optical microscope. The cross-sections were embedded in an acrylic resin, grinded with SiC papers (ANSI grade 80-320-500-1000-

---

[1] *www.sigmaaldrich.com*
[2] *www.vwr.com*
[3] *www.alicona.com*

2400) and polished to mirror-like surface finish (water-based diamond suspensions with 3 μm followed by 1 μm particle size).

The regularity of the laser pattern was examined by a non-contact Alicona optical Infinite-Focus Microscope (IFM).

2.4 Characterisation of surface oxides by XPS

X-ray photoelectron spectroscopy (XPS) was performed with an Ultra DLD Kratos system to study the composition of the various surfaces investigated in this work. The pressure in the analysis chamber was kept below 5×10^{-10} Torr. Al Kα monochromatic source was used with emission current of 10 mA and 10 kV. An area of 0.7 x 0.3 mm was analysed to ensure that the results represent the surface and not inclusions or certain defects at the surface. The information depth was in the range of 3 nm. Spectrums were calibrated using the carbon peak at 284.5 eV. The wide elemental scan was acquired for the wide energy range (0 – 1200 eV) with a pass energy of 160 eV and a step size of 1 eV. The high-resolution spectra were acquired with a pass energy of 20 eV and step size of 0.1 eV for precise energy position and peak shape determination.

CasaXPS was used for curve fitting, evaluation and quantification of the data. Shirley background subtraction was applied for peak deconvolution and fitting [36]. Full width half maximum (FWHM) was kept constant for oxide components of each element and Gaussian/Lorentzian asymmetry was used for curve fitting using the parameters of standard peaks. Fe 2p 3/2 was used to investigated surface compositions and it consists of Fe_3O_4, FeO, Fe^{3+} (Fe_2O_3 and $FeOOH$) and metallic Fe. The splitting and peak position of metallic iron at 706.9 ±0.2 eV, and shifts in the oxides are in good agreement with reference peaks [37].

The time between the surface treatment or tests and to the introduction in the chamber was within an hour, and samples were kept in a desiccator during this time.

2.5 Scanning Kelvin probe measurements

In-situ SKP potential profile measurements were performed in air, in a steel chamber which in addition to function as a Faraday cage, allows for accurate climatic control. The instrument was a height-regulated SKP custom-made by Wicinski-Wicinski GbR. The probe was a 150 μm diameter NiCr needle, vibrating at 957 Hz with 5 μm amplitude above the sample surface accurately controlled by a double coil and permanent magnet displacement device. The working distance was approximately 60 μm. The SKP needle was scanned above the surface by a combination of the double magnetic coils and the motorised stepping positioner on which the SKP head assembly is mounted. The resolution of the measurement depends on the needle diameter and the working distance and was approximately 113 μm for this study [22]. The potential of the probe was calibrated against a $Cu/CuSO_4$ electrode (+0.320 V_{SHE}). The theory behind the instrument has been covered by several workers [6, 31-33, 38, 39]. All potentials are given relative to SHE.

Two types of measurements were performed:

i)   Potential measurements on bare or coated samples exposed to dry air, (35% RH) or humid air (60 or 95% RH), at 25 °C.

ii)   Potential measurements performed on samples on which the cathodic disbonding mechanism was initiated by the application of 0.5 M aqueous NaCl in the coating defect, at 25 °C and 95% RH.

A sketch of the coated sample can be seen in Figure 2. Artificial defects were created by peeling the coating off the substrate to create a bare steel area of 10 mm x 10 mm metal in front of the laser structured area.

Several parallels were investigated simultaneously. Line scans were performed in steps of 40 µm across an 8 mm surface length, on minimum 2 duplicates. The speed of the motors in the XY-plane was 0.4 mm/s, but the scanning happened at a velocity of ca. 1.5 mm/min due to topography tracking and SKP signal calculation.
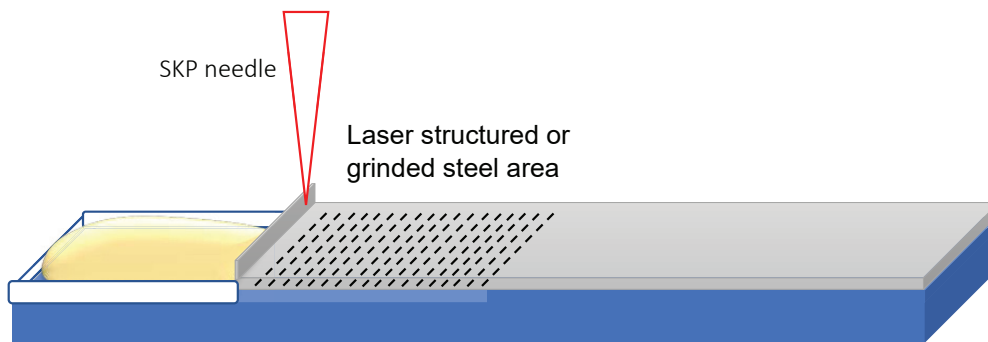

Figure 2. Sketch of the sample employed for evaluation of cathodic disbonding. A reservoir was created next to the area of interest, here indicated by the dashed lines. This was an area either uniformly micro patterned by laser, or grinded. The dimensions of the laser structured area were 10 x 10 mm. Electrolyte was added to the defect created according to Stratmann et al. [31-33], here seen at the left.

3   Results

3.1   Topography characterisation

The profile of the A, B1 and B2 surfaces are shown in Figure 3.The roughness, Rz, was 0.40 ± 0.01 µm, 25.0 ± 0.10 µm and 64.1± 0.10 µm, respectively (see Table 2). B1 and B2 surfaces can be described as alternating rectangular grooves and peaks uniformly distributed over the surface, as can be seen in the 3D scanning (IFM) images in Figure 2. The effective contact area to geometrical area ratio was found to be 1.01 ± 0.10, 1.21 ± 0.01 and 1.99 ± 0.05 for A, B1, and B2, respectively.
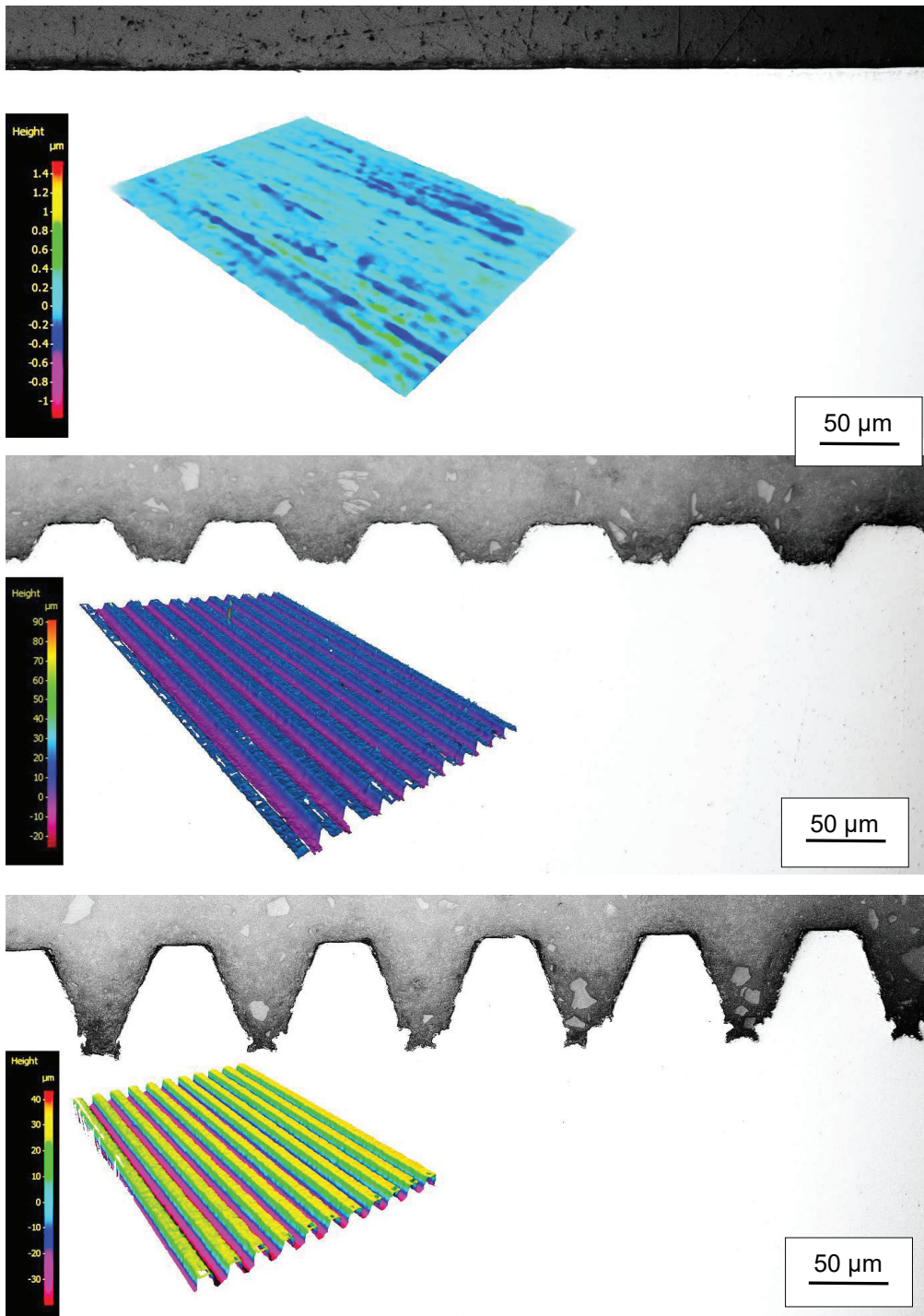
Figure 3. Optical microscope cross-sections and 3D images of surface area scanned by focus-variation with IFM. Colours are indicating the level of roughness. From the top, surface A, B1 and B2 respectively.

8

3.2 Oxidation of PVB coated steel in humid air

Potentials were acquired by SKP on reduced surfaces with and without PVB coating, when exposed to air with various humidities. Line scans were used instead of point measurements to have more representative measurements of the surface potential. Values in Table 3, are hence calculated and averaged based on 200 individual potential measurements on minimum 2 duplicates. Reduced samples with and without coating were introduced in the SKP chamber and kept at 25-30% RH while preparing for the scans. Then the humidity was stabilised at 35% RH, and the first scan (t=0) was performed around 40 minutes after the introduction of the samples into the SKP chamber. At lower humidity, a stable control of the humidity was difficult, and the $Cu/CuSO_4$ electrode needed for calibration of the SKP dried out. After the scan, the humidity was increased to 95% RH, and scans were performed after 1, 2, 3 and 4 hours. Table 3 shows the average line scan potentials for bare and PVB coated surfaces at 35% RH and after 4 hours at 95% RH. See also Figure 5.

The potential of the *uncoated surfaces* increased with 0.4 V on the average, during the exposure to 95% RH air. The *coated surfaces* had a higher initial potential, but the final potential was similar to the uncoated samples. On average, the potential of the coated surfaces increased with 0.25 V during the exposure to 95% RH air. The changes in electrochemical potential of the surfaces were found to be independent of the topography or roughness of the steel substrate.

Table 3. Potential [V_{SHE}] measured on bare and PVB coated A, B1 and B2 surfaces by SKP in air at 35% and 95% RH. The potentials given for 95% RH were measured after 4 hours exposure.

	Uncoated		Coated with 35 μm PVB	
	35% RH	95% RH	35% RH	95% RH
A	-0.27	0.14	-0.07	0.18
B1	-0.27	0.17	-0.12	0.16
B2	-0.22	0.15	-0.06	0.16

To exclude that the chemistry of the PVB film or that changes in this chemistry with exposure to humid air could have affected the potential measurements, a series of additional experiments were designed. The potential on uncoated B1 surfaces with as-prepared surface oxide, formed during the laser profiling, was 0.47 V_{SHE} at 35% RH and did not change in time. When coating the sample with 35 μm PVB, the same potential was measured as on un-coated surfaces, and again the potential did not change during 4 hours of exposure to 95% RH, see Figure 5. Increasing the thickness of the PVB film did not affect the potential measurements either. On a B1 surface with as-prepared oxide now coated with 50 μm PVB, similar potentials were measured as for the samples coated with 35 μm PVB. The similar observation was done with reduced B2 samples with 35 and 50 μm PVB, as the potential on these increased identically as function of exposure time in humid air. Hence, the PVB film did not have any effect on the measured potentials, or on the oxidation process at the steel surface during the 4 hours of exposure, at the film thickness here employed.

B1 and B2 samples with electrochemically reduced oxides were analysed by XPS immediately after the electrochemical reduction step, and after application of coating and the exposure to humid air at 95% RH for 4 hours. Figure 4 shows the atomic concentration of the various iron oxidation states on B1 and B2 surfaces with reduced oxide, and after reduction, coating and exposure to humid air. The figure also shows the various iron oxidation states on reduced A surfaces. The comparison of oxidation state before and after exposure to humid air was not possible, as the coating was found to delaminate with exposure, see next chapter.

An as-prepared B1 surface was analysed for reference. The oxides on as-received samples were formed during the laser structuring. Within a surface layer of a few nm, a temperature rise in the order of 1000 K might be expected [40]. Together with the presence of oxygen, the process resulted in thermal oxidation in a 3 nm thick layer of the outer steel surface. This surface had the lowest signal from metallic iron and the strongest signal from trivalent iron oxides.
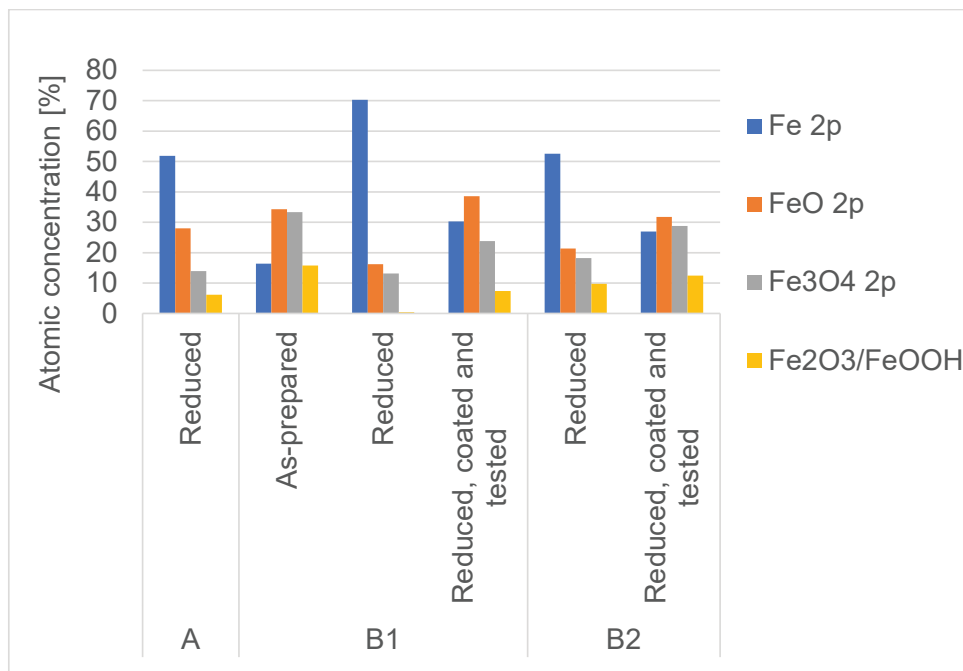

Figure 4. The amount of iron species measured by XPS on A, B1 and B2 surfaces.

Metallic iron gave the strongest signal on the reduced surfaces. After exposure to humid air, the amount of oxidised iron species had increased significantly. The signal from metallic iron was weaker and the signal from the various oxides were stronger. The exposure to humid air evidently resulted in oxidation.

3.3 Effect of humid air on adhesion

The PVB coating on the A surfaces – which were grinded to 0.40 ± 0.01 µm before being electrochemically reduced - disbonded from the steel surface during exposure to humid air. The coating lifted completely off from the surfaces underneath and slid off the surface upon evaluation, while the coating on B1 and B2 surfaces maintained its strong adhesion to the substrate. No electrolyte was employed in this test, hence the samples were only exposed to humid air as all the others.

The phenolphthalein indicator in the coating on these A samples remained colourless during the test. Phenolphthalein is colourless below pH 8.2 and turns violet between pH 8.2 and 10. The violet phenolphthalein chromophore is at its strongest at pH 10 [41]. Hence, the adhesion loss was not caused by the CD mechanism. Average potentials under the coating measured during the 4 hours test are given in Figure 5, showing that the potential increased during exposure due to oxidation of the steel surface.
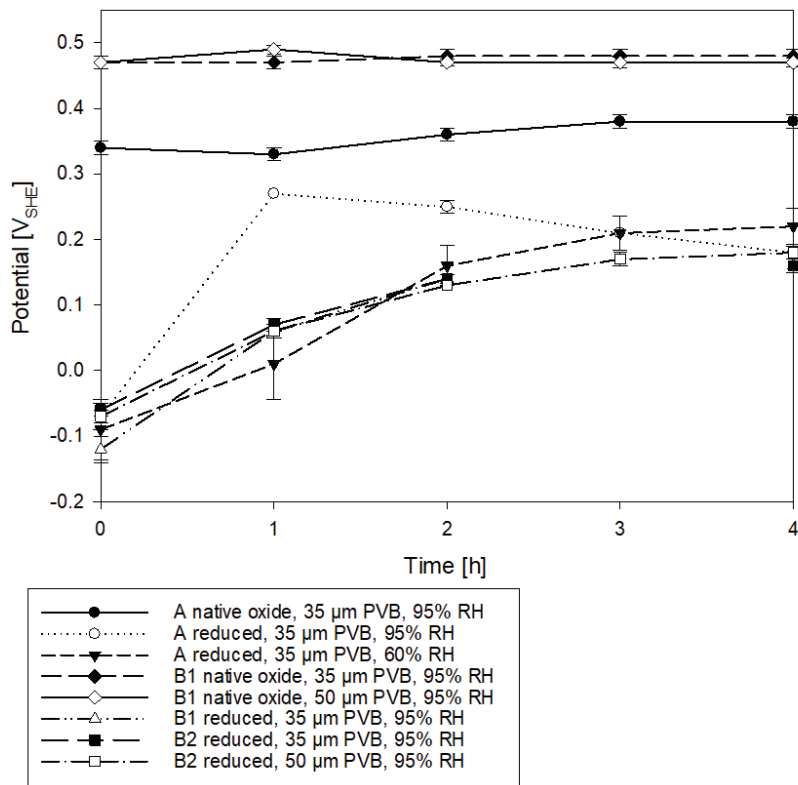

Figure 5. The potential change measured across 8 mm surface length on two duplicate samples of A, B1 and B2 surfaces, during 4 hours of exposure at 95% RH and 60% RH, and 25 °C. Standard deviations calculated for the duplicate samples are shown by error bars.

An additional test performed on reduced and coated A surfaces at 60% RH, gave a similar result to the 95% RH test, both with respect to potential increase and disbonded coating. The potential measurements at 60% RH as function of exposure time are also shown in Figure 5, see line with filled triangular markers. The potential increased somewhat slower at 60% RH than at 95% RH, but after 4 hours the potentials were approximately the same.

Two A samples were exposed to ambient laboratory conditions (about 50% RH and 20-22 °C) for 6 weeks after the grinding, before application of the PVB coating. During 4 hours of exposure at 95% RH in the SKP, the potential stabilised around 0.36 V_{SHE}. See line with filled circular markers in Figure 5. The PVB coating did not lose adhesion during this test. Evidently, the adhesion loss on the reduced surfaces was related to the oxidation of the steel.

3.4 Effect of oxide condition on CD

CD was initiated on the PVB coated surfaces by applying 0.5 M aqueous NaCl in the reservoir at the artificial coating defect. To evaluate the effect of oxide condition and oxidation on the CD rate, reduced samples were tested both with and without a 4 hours pre-exposure to 95% RH humid air. In addition, samples with as-prepared oxides were tested with and without pre-exposure.

On the samples that should not be exposed to humid air before the initiation of CD, the "No NaCl" scan is taken after 40 minutes of exposure at 25-30% RH and 5 minutes at 35% RH, before NaCl was added to the reservoir. When NaCl was added to the reservoir, the humidity was increased to 95% RH and potential scans were performed with regular intervals for 8 hours.

The samples that were exposed to 95% RH before the initiation of CD, were kept in the SKP chamber at this humidity. The electrolyte was then added to the reservoir after 4 hours. These samples were scanned immediately (minutes) before addition of the electrolyte, and then with regular intervals during 8 to 15.5 hours.

For B1 samples with as-prepared oxide and coated with 35 μm of PVB, the CD behaviour was similar for samples pre-exposed to humid air as for those not pre-exposed before CD was initiated. In Figure 6, the plot for the pre-exposed sample can be seen. Potentials of around -0.1 to -0.15 V_{SHE} were measured close to the defect for both, after addition of the NaCl electrolyte. The potential ahead of the CD front was stable at about 0.45 V_{SHE} and remained constant and high throughout the experiment. CD progressed with typical sigmoid potential profile as previously reported [25-30]. The potential increased between the defect and the CD front with a slope of 60 mV/mm and 50 mV/mm on the plot for the 8.5 and 15.5 hours scan, respectively. Then an abrupt potential increase marked the electrolyte front position.

The alkaline violet colour change of the phenolphthalein pH-indicator followed the CD front. The curves indicate that CD initiated approximately 2 hours after addition of the NaCl to the defect reservoir, and the violet colour was also seen to appear close to the reservoir by this time. At the end of the test, the violet coating was easily removed, verifying that the adhesion loss was due to CD.
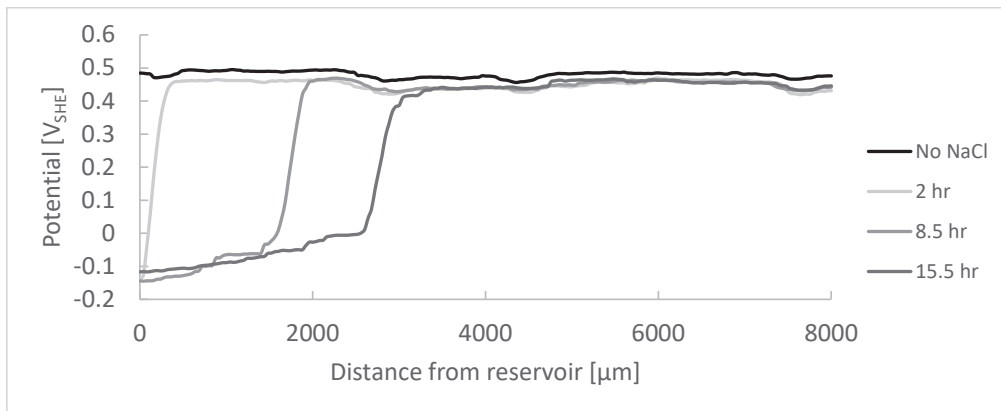
Figure 6. CD at 95% RH and 25 °C during 15.5 hours on B1 surfaces covered with as-prepared oxides and coated with 35 µm PVB coating, after an initial exposure to 95% RH humid air of 4 hours. The scan "No NaCl" is taken after 4 hours of exposure, and just minutes before NaCl was added to the reservoir.

On the reduced B1 surfaces without pre-exposure to humid air, a 50 mV potential increase was measured 15 minutes after the humidity was increased to 95% RH. At the same time NaCl electrolyte had been added to the reservoir, see Figure 7. A strong violet band started by this time to develop and spread from the reservoir, indicating an ongoing CD process underneath the coating. After 3 hours, the potential 8 mm from the reservoir had increased to about 0.1 V_{SHE} due to oxidation of the steel under the coating. A CD front could not be identified from the potential profiles, as the potential was more or less linearly distributed between the -0.24 V_{SHE} close to the reservoir and the 0.1 V_{SHE} at the far end of the reservoir. After 8 hours, the potential at the far end of the reservoir had dropped to 0.05 V_{SHE}. The entire surface was violet, and the coating was easily removed.
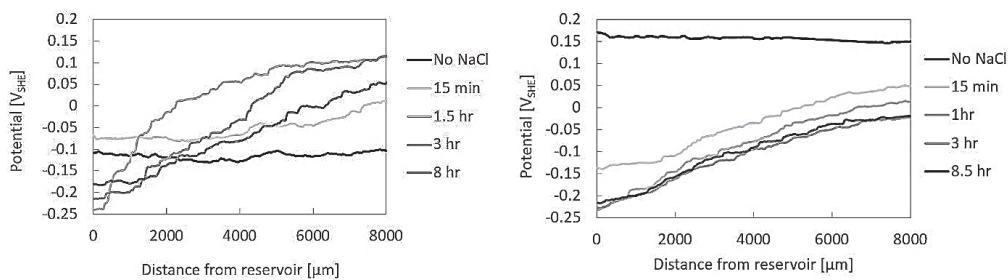

Figure 7. CD at 95% RH and 25 °C during 8.5 hours on reduced B1 surfaces coated with 35 µm PVB coating. To the left, without pre-exposure to humid air. The scan "No NaCl" is taken after 40 minutes of exposure at 25-30% RH and 5 minutes at 35% RH, before NaCl was added to the reservoir. To the right, with pre-exposure. The scan "No NaCl" is taken after 4 hours of exposure, and just minutes before NaCl was added to the reservoir.

13

The reduced B1 surfaces that had been exposed to humid air, had a potential of about 0.15 V_{SHE} before addition of the NaCl electrolyte. Fifteen minutes after NaCl was added to the defect, the potential dropped to about 0.05 V_{SHE} in the area with a supposedly intact coating/steel interface at the far end of the reservoir, see Figure 7. Close to the reservoir the potential was about -0.14 V_{SHE} but again, no CD front could be identified from the potential profiles. After 1 hour of testing a violet colour change had developed to cover the 2 mm closest to the coating defect. After 8.5 hours, the violet colour had spread across the test area, and the coating was easily removed. Previously reported potentials under cathodically disbonded PVB are typically -0.1 V_{SHE} to -0.2 V_{SHE} [42], which is similar to potentials measured close to the reservoir for B1, while higher potentials were measured in this test for B2.

On the reduced B2 sample without pre-exposure to humid air, the potential under the coating had increased after the humidity was increased to 95% RH and NaCl electrolyte was added, as for the B1 surface. After 1.5 hours, the potential had increased uniformly to about 0.1 V_{SHE}, see Figure 8. At the end of the test, the potential near the defect was about 0.01 V_{SHE} and the CD front was difficult to identify from the potential profiles. However, the 2.5 mm of coating close to the reservoir had a strong violet colour while the rest of the surface had a weak violet colour change. Only the 2.5 mm coating with full violet colour change – close to the reservoir – could be removed.
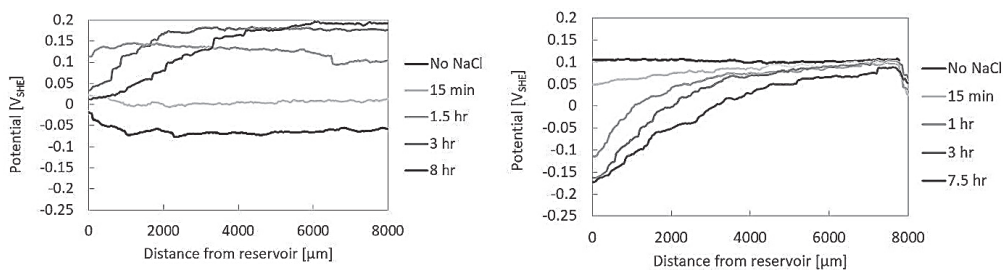

Figure 8. CD at 95% RH and 25 °C during 8.5 hours on reduced B2 surfaces coated with 35 μm PVB coating. To the left, without pre-exposure to humid air. The scan "No NaCl" is taken after 40 minutes of exposure at 25-30% RH and 5 minutes at 35% RH, before NaCl was added to the reservoir.   To the right, with pre-exposure. The scan "No NaCl" is taken after 4 hours of exposure, and just minutes before NaCl was added to the reservoir.

Pre-exposure of B2 samples to humid air resulted in a uniform potential of about 0.1 V_{SHE} under the coating before addition of the NaCl electrolyte. One hour after the addition of electrolyte, the potential close to the reservoir dropped to -0.11 V_{SHE}, see Figure 8. A weak violet colour covered the entire coating surface at the end of the test, and the coating adhered strongly.

The CD test could not be performed on reduced A surfaces, as the NaCl electrolyte was found to leak underneath the coating shortly after it was added to the reservoir. As described above, the coating on A surfaces lost adhesion when exposed to humid air, which explains this behaviour.

14

4 Discussion

4.1 Oxidation under the coating

Exposure to air at 95% RH resulted in positive potential shifts on reduced surfaces, both bare and coated with PVB. Initial potentials were in the order of -0.22 to -0.27 V_{SHE} for all *reduced uncoated surfaces*, and -0.06 to -0.12 V_{SHE} for *surfaces coated* with PVB. During the exposure to humid air, the potential increased to 0.14 - 0.18 V_{SHE} on all surfaces, both uncoated and coated. The positive potential shift must have been caused by oxidation of the steel. On the coated surfaces the oxidation has happened under the adhering coating, as documented by the XPS results.

The potentials measured with the SKP on coated steel has previously been found to depend on the redox reactions on the surface, and hence the oxidation state of the surface [43, 44]. However, the applied coating [45], the interactions between the steel surface and the coating [46], and the processes occurring at the interface during exposure to humid air [47], have also been seen to affect the potentials on coated steel. The latter has previously been explained by a change in the electrical double layer at the coating/metal interface, with the absorption of water [47].

The coating employed in this study was found not to affect the measured potentials or the potential changes. Varying the thickness of the coating did not affect the measured potentials either. Both these observations prove that the PVB did not have any effect on the measured potentials. It has previously been documented that coatings which do not result in a potential change on the substrate they are applied to, do not rely on chemical interactions with the substrate, and hence are weakly adsorbed on the metal and oxide surfaces by van der Waals interactions [46]. As the surfaces B1 and B2 in this study have a significant micro-roughness, contributions from mechanical interactions at the interface, are expected to dominate the bond strength for these.

The higher initial potential of the coated samples compared to the much lower potential measured on uncoated samples was hence due to oxidation of the steel during application and curing of the PVB coating, and not related to a coating effect. The increase in potential seen on reduced surfaces, uncoated and coated, is therefore only explained by the oxidation of the steel surface.

On reduced surfaces – either laser structured or grinded – the density of Fe^0 and Fe^{2+} states at the surface is very high, which results in potentials of roughly -0.25 V_{SHE} in air. With exposure to humid air oxides grow, first following an equilibrium between the oxidation of Fe^0 to Fe^{2+} at the iron/oxide interface and the reduction of Fe^{3+} to Fe^{2+} within the oxide, increasing the conductivity and finally leading to the onset of the oxygen reduction reaction as the prominent counter reaction to the anodic oxidation [44]. The oxygen reduction reaction leads to increased oxidation of Fe^{2+} states at the surface, pulling the potential under an adhering coating to more anodic potentials [6, 48]. This continues until further charge transfer through the surface oxide is slowed down and eventually inhibited [44]. On PVB coated surfaces with as-prepared oxides, a potential of 0.47 V_{SHE} was measured. Such a noble anodic potential is related to thicker oxide film and enrichment of the film by Fe^{3+} [39], which was confirmed by the XPS analysis shown in Figure 4. The oxidation process is driven by the oxygen

15

reduction and can hence take place also in dry air. However, in wet air, the increase in Fe^{3+} concentration at the surface is accelerated, leading to a faster passivation rate [49, 50].

A variety of reactions have been proposed to contribute to the oxide growth mechanism, but here we intend to consider only the reactions below. The possible electrochemical reactions on steel at the conditions encountered here, is the cathodic oxygen reduction reaction (Eq. 1), coupled with the oxidation of metallic iron and divalent iron (Eq. 2):

$$\frac{1}{2}O_2 + H_2O + 2e^- \rightarrow 2OH^-$$
(Eq. 1)

$$Fe \rightarrow Fe^{2+} + 2e^-$$
(Eq. 2)
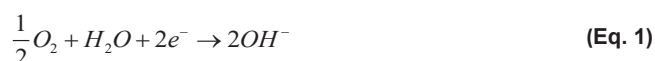
The Fe^{2+} produced through Eq.2 exists transiently before being oxidised further to a Fe^{3+} hydrous layer of (hydr)oxide [25, 51, 52] of $FeOOH/Fe_2O_3$.

The PVB coating applied on reduced A surfaces lost adhesion when exposed to humid air at both 95 and 60 % RH, while the potential increased from -0.1 V_{SHE} to 0.2 V_{SHE}. However, if the samples were exposed to ambient laboratory conditions before application of the coating, the exposure to humid air did not cause adhesion loss, and the samples showed stable potentials of 0.36 V_{SHE}. This indicates that the adhesion loss was caused by the steel surface oxidation process, and not simply by the ingress of water. In either case, the ingress of water may result in a swelling of the PVB and the accumulation of water at the interface. On smooth surfaces, or on surfaces with poor ability for mechanical interlocking, water accumulation at the interface may happen more readily, due to the low strength of the interface to mechanically resist water from spreading [53]. However, it is observed that the interfacial stability fails first when the steel surface undergoes oxidation. The oxidation of the steel surface results in structural and morphological changes at the oxide surface [48, 54], and partially weakened bonds by humidity may ultimately fail [33]. The absence of phenolphthalein colour change proves that the pH was close to neutral. Assuming that the interfacial chemistry - and hence the electrochemical properties of the surfaces - is the same for both the A, B1 and B2 surfaces when reduced, as indicated by the XPS analysis and the potentials measured on reduced bare steel surfaces, the different behaviour of A from B1 and B2 must be attributed to the missing ability of the surface for mechanical interlocking.

Mechanical interlocking will affect the interfacial stability in several ways. It is believed to suppress water accumulation at the interface [12] and total rupture of bonds when accumulation has happened [11], thus increasing the hydrolytic stability of the coating at the interface.

4.2 Cathodic disbonding behaviour
The qualitative investigation documented that the steel surface oxidation affects the CD behaviour. Only on the B1 surface with as-prepared oxide, the measured potential profiles showed the frequently reported sigmoid shape, where a low potential area close to the defect is attributed to disbonded coating, while an area of more positive

potentials ahead is attributed to intact coating/steel interface. The CD front is located at the position of largest potential change between these two areas [31-33]. This position is assigned to the "electrolyte front position" [6], as hydrated cations are fed from the electrolyte-filled defect into the interface. This allows the oxygen reduction reaction to occur underneath the coating without the kinetic barrier that an intact interface represents. A steep potential increase marks the transition from areas where the oxygen reduction reaction is kinetically free to happen, to areas where it is hindered underneath intact coating, i.e. the CD front.

On electrochemically reduced surfaces this steep CD front potential transition was not found. The potential profiles measured on reduced B1 samples resembles the potential gradient between reservoir and CD front on B1 with as-prepared oxides. The potential gradient between reservoir and CD front has earlier been attributed to ohmic resistance [31]. The potential profiles measured for the reduced B1 surfaces therefore indicate that the reservoir was in electrolytic contact with the entire interface. On B2, the potential profiles were slightly less linear, and the potential of the intact interface, did not decrease in time similar to what was observed for B1. The coating was also still adhering after the test, although the coating had a weak violet colour. This can probably be attributed to mechanical interlocking due to the higher roughness compared to B1.

Linear potential profiles between defect and intact interface have been found earlier and assigned to wet de-adhesion processes masking the position of largest potential change [55]. On PVB-coated steel surfaces exposed for 1 month in outdoor conditions before performing CD tests, similar linear potential profiles were measured and attributed to a "damaged interface" [42]. The negative potential shifts measured after the addition of NaCl are due to polarisation of the coated area by the reservoir. The exposure to humid air is, as pointed out earlier, assumed to result in a swelling of the PVB, the accumulation of water at the interface, and to cause the oxidation of the reduced surfaces. The interfacial bonds are weakened and may ultimately fail. Reduced adhesion during exposure to humid air enables higher rates of ionic ingress and electrolytic contact between the reservoir and the steel/coating interface.

With the addition of the NaCl electrolyte to the defect, the migration of sodium ions to the location of oxygen reduction exerts an (electro)osmotic pressure that tends to force off partially disbonded PVB [17, 28]. The PVB molecule has both hydrophilic groups (hydroxyl, butyral and acetate) and a hydrophobic vinyl chain. The hydrophilic groups can interact with the oxide/hydroxide on the steel surface. The electro-osmotic factor on the CD mechanism, has been proposed to be effective for all kinds of coatings [56]. Hence, the CD mechanism of the model coating is comparable to that of other organic coatings [57].

A low roughness and hence smooth steel surface topography affects negatively the CD resistance, as the ingress of water and the steel surface oxidation process on such surfaces has critical consequences with respect to destabilisation of the interface. The CD behaviour observed here, is however also strongly affected by the surface oxide itself and not only by the processes mentioned. On surfaces with as-prepared oxides, the potential in the region of intact interface was stable and high. Also, the CD rate was lower than for the reduced surfaces. This is in line with previous work, emphasising the

importance of the surface composition on CD [58]. Oxide layers rich in Fe^{3+} will inhibit the electron transfer processes, and hence the oxygen reduction rate and CD [43]. The CD proceeded significantly faster on the reduced surfaces having lower concentration of Fe^{3+}.

5   Conclusions

Positive potential shifts of 0.25 V on the average were measured on reduced and coated surfaces during exposure to humid air. XPS analysis of surfaces after the exposure, confirmed oxidation of the steel surface underneath the adhering PVB coating. At the steel surface, the oxidation of Fe^0 to Fe^{2+} - the latter existing transiently before being oxidised further to Fe^{3+} - is balanced by the oxygen reduction reaction. The process leads to increased oxidation of Fe^{2+} states, and hence the enrichment of Fe^{3+} in the oxide, pulling the potential under an adhering coating to more anodic potentials.

The CD behaviour was affected negatively by the decrease in bond strength with exposure to humidity and the oxidation of the steel surface by oxygen. Potential profiles indicating a weakened interface, were measured during the CD tests. Sigmoid shaped profiles were only found on surfaces with as-prepared oxides at the interface. On all others, the potential profiles were more or less linear, resembling the potential gradients usually indicative of ohmic resistance between reservoir and disbonding front during the CD process. Hence it seems plausible that as a consequence of the exposure to humid air, the intact interface was weakened. The hydrolytic destabilisation of the bonds was accompanied of an ongoing oxidation process at the steel surface believed to destabilise the coating/steel interface and ultimately lead to the failure of bonds. When electrolyte is added at the defect, the migration of sodium ions at the interface exerts an (electro)osmotic pressure that also acts negatively on coating/steel bonds partially weakened with exposure to humid air. An electrolytic contact between the reservoir and the entire surface could be established quickly by the lateral ingress of hydrated ions.

On smooth surfaces with no ability for mechanical interlocking, the coating disbonded already during the oxidation process with exposure to humid air.

On surfaces patterned with periodic peaks of Rz=25 µm the coating disbonded only after 8-9 hours of CD testing with NaCl electrolyte added at the defect.

On surfaces with periodic peaks of Rz=64 µm the coating was still adhering after this time, although both SKP-measured potential profiles and the phenolphthalein indicated electrolytic contact between the NaCl filled defect and intact interface.

Roughness is suggested to add stability at the interface during the exposure to humid air. Hence, roughness affects the CD process, when electrolyte covers the defect.

6   Acknowledgements

7 Data availability

The raw/processed data required to reproduce these findings cannot be shared at this time as the data also forms part of an ongoing study.

REFERENCES

1. Mayne, J.E.O., *The Mechanism of the Inhibition of the Corrosion of Iron and Steel by Means of Paint.* Official Digest, 1952. **24**: p. 127.
2. Grundmeier, G., W. Schmidt, and M. Stratmann, *Corrosion protection by organic coatings: electrochemical mechanism and novel methods of investigation.* Electrochimica Acta, 2000. **45**(15–16): p. 2515-2533.
3. Sato, N., *An overview on the passivity of metals.* Corrosion Science, 1990. **31**: p. 1-19.
4. Díez-Pérez, I., F. Sanz, and P. Gorostiza, *Electronic barriers in the iron oxide film govern its passivity and redox behavior: Effect of electrode potential and solution pH.* Electrochemistry Communications, 2006. **8**(10): p. 1595-1602.
5. Wielant, J., et al., *Electronic properties of thermally formed thin iron oxide films.* Electrochimica Acta, 2007. **52**(27): p. 7617-7625.
6. Grundmeier, G. and M.Stratmann, *Adhesion and de-adhesion mechanisms at polymer/metal interfaces: Mechanistic understanding based on in situ studies of buried interfaces.* Annual Review of Materials Research, 2005. **35**: p. 571-615.
7. Noijen, S.P.M., et al., *Numerical prediction of failure paths at a roughened metal/polymer interface.* Microelectronics Reliability, 2009. **49**(9): p. 1315-1318.
8. Sluis, O.v.d., S.P.M. Noijen, and P.H.M. Timmermans, *On the effect of microscopic roughness on macroscopic polymer-metal adhesion*, in *Solid state lighting reliability: components to systems*, W.D.v. Driel and X.J.Fan, Editors. 2013, Springer.
9. van der Leeden, M.C. and G. Frens, *Surface Properties of Plastic Materials in Relation to Their Adhering Performance.* Advanced Engineering Materials, 2002. **4**(5): p. 280-289.
10. Evans, A.G., et al., *The fracture energy of bimaterial interfaces.* Metallurgical Transactions A, 1990. **21**(9): p. 2419-2429.
11. Brockmann, W., *Durability of Adhesion Between Metals and Polymers.* The Journal of Adhesion, 1989. **29**(1-4): p. 53-61.
12. Venables, J.D., *Adhesion and durability of metal-polymer bonds.* Journal of Materials Science, 1984. **19**(8): p. 2431-2453.
13. Nazarov, A., et al., *An SKP and EIS investigation of amine adsorption on zinc oxide surfaces.* Surface and Interface Analysis, 2011. **43**(10): p. 1286-1298.
14. Sørensen, P.A., et al., *Influence of substrate topography on cathodic delamination of anticorrosive coatings.* Progress in Organic Coatings, 2009. **64**(2–3): p. 142-149.

15. Watts, J.F. and J.E. Castle, *The application of X-ray photoelectron spectroscopy to the study of polymer-to-metal adhesion. Part 2 The cathodic disbondment of epoxy coated mild steel.* Journal of Materials Science, 1984. **19**: p. 2259-72.

16. Kendig, M., et al., *Environmental Integrity of Coating/Metal Interface.* 1990. 60.

17. Williams, G., H.N. McMurray, and D.A. Worsley *Cerium(III) Inhibition of Corrosion-Driven Organic Coating Delamination Studied Using a Scanning Kelvin Probe Technique.* Journal of The Electrochemical Society, 2002. **149**(4): p. B154-B162.

18. Khun, N.W. and G.S. Frankel, *Effects of surface roughness, texture and polymer degradation on cathodic delamination of epoxy coated steel samples.* Corrosion Science, 2013. **67**: p. 152-160.

19. Nazarov, A. and D. Thierry, *Application of Scanning Kelvin Probe in the Study of Protective Paints.* Frontiers in Materials, 2019. **6**(192).

20. Stratmann, M., *2005 W.R. Whitney Award Lecture: Corrosion stability of Polymer-Coated Metals - New Consepts Based on Fundamental Understanding.* Corrosion, 2005. **61**(12): p. 1115-1126.

21. Nazarov, A., N. Le Bozec, and D. Thierry, *Assessment of steel corrosion and deadhesion of epoxy barrier paint by scanning Kelvin probe.* Progress in Organic Coatings, 2018. **114**: p. 123-134.

22. Wicinski, M., W. Burgstaller, and A.W. Hassel, *Lateral resolution in scanning Kelvin probe microscopy.* Corrosion Science, 2015. **104**.

23. *ISO 4287, Geometrical Product Specifications (GPS) - Surface texture: Profile method -Terms, definitions and surface texture parameters*. 2000, International Organization for Standardization: Switzerland.

24. *ISO 4288, Geometrical Product Specifications (GPS) - Surface texture : Profile method -- Rules and procedures for the assessment of surface texture*. 1996, International Organization for Standardization: Switzerland.

25. Holness, R.J., et al., *Polyaniline Inhibition of Corrosion-Driven Organic Coating Cathodic Delamination on Iron.* Journal of The Electrochemical Society, 2005. **152**(2): p. B73-B81.

26. Wint, N., et al., *The Kinetics and Mechanism of Atmospheric Corrosion Occurring on Tin and Iron-Tin Intermetallic Coated Steels: I. Cathodic Delamination.* Journal of The Electrochemical Society, 2015. **162**(14): p. C775-C784.

27. Iqbal, D., et al., *Synthesis of ultrathin poly (methyl methacrylate) model coatings bound via organosilanes to zinc and investigation of their delamination kinetics.* ACS applied materials & interfaces, 2014. **6**(20): p. 18112-18121.

28. Williams, G. and H.N. McMurray, *Chromate Inhibition of Corrosion-Driven Organic Coating Delamination Studied Using a Scanning Kelvin Probe Technique.* Journal of The Electrochemical Society, 2001. **148**(10): p. B377-B385.

29. Williams, G. and H.N. McMurray, *Inhibition of corrosion driven delamination on iron by smart-release bentonite cation-exchange pigments studied using a scanning Kelvin probe technique.* Progress in Organic Coatings, 2017. **102**: p. 18-28.

30. Williams, G. and H.N. McMurray, *The mechanism of group (I) chloride initiated filiform corrosion on iron.* Electrochemistry Communications, 2003. **5**(10): p. 871-877.

31. Leng, A., H. Streckel, and M. Stratmann, *The delamination of polymeric coatings from steel. Part 2: First stage of delamination, effect of type and concentration of cations on delamination, chemical analysis of the interface.* Corrosion Science, 1998. **41**(3): p. 579-597.

32. Leng, A., H. Streckel, and M. Stratmann, *The delamination of polymeric coatings from steel. Part 1: Calibration of the Kelvinprobe and basic delamination mechanism.* Corrosion Science, 1998. **41**(3): p. 547-578.

33. Leng, A., et al., *The delamination of polymeric coatings from steel. Part 3: Effect of the oxygen partial pressure on the delamination reaction and current distribution at the metal-polymer interface.* Corrosion Science, 1999. **41**(3): p. 599-620.

34. Pfleging, W., *A review of laser electrode processing for development and manufacturing of lithium-ion batteries.* Nanophotonics, 2018. **7**(3): p. 549.

35. Mottay, E., et al., *Industrial applications of ultrafast laser processing.* MRS Bulletin, 2016. **41**(12): p. 984-992.

36. Shirley, D.A., *High-Resolution X-Ray Photoemission Spectrum of the Valence Bands of Gold.* Physical Review B, 1972. **5**(12): p. 4709-4714.

37. Moulder, J.F., et al., *Handbook of X-Ray Photoelectron Spectroscopy*. 1995, Eden Prairie, Minnesota: Perkin-Elmer Corp, Physical Electronics Division.

38. Rohwerder, M., et al., *Application of Scanning Kelvin Probe in Corrosion Science*. 2005. p. 605-648.

39. Stratmann, M., et al., *The scanning Kelvin probe; a new technique for the in situ analysis of the delamination of organic coatings.* Progress in Organic Coatings, 1996. **27**(1–4): p. 261-267.

40. Lu, L., et al., *The Influence of Pulse Width and Energy on Temperature Field in Metal Irradiated by Ultrashort-Pulsed Laser.* Physics Procedia, 2012. **32**: p. 39-47.

41. Fürbeth, W. and M. Stratmann, *Scanning Kelvinprobe investigations on the delamination of polymeric coatings from metallic surfaces.* Progress in Organic Coatings, 2000. **39**(1): p. 23-29.

42. Cambier, S.M., R. Posner, and G.S. Frankel, *Coating and interface degradation of coated steel, Part 1: Field exposure.* Electrochimica Acta, 2014. **133**: p. 30-39.

43. Grundmeier, G. and M. Stratmann, *Influence of oxygen and argon plasma treatments on the chemical structure and redox state of oxide covered iron.* Applied Surface Science, 1999. **141**(1): p. 43-56.

44. Rohwerder, M., *Passivity of Metals and the Kelvin Probe Technique*. 2017.

45. Nazarov, A. and D. Thierry, *Studies in the Electrical Double Layer at Metal/Polymer Interfaces by Scanning Capacitive Probe.* Protection of metals 2003. **39**(1): p. 55-62.

46. Wielant, J., et al., *SKP as a tool to study the physicochemical interaction at buried metal–coating interfaces.* Surface and Interface Analysis, 2010. **42**(6-7): p. 1005-1009.

47. Nazarov, A. and D. Thierry, *Hydrolysis of interfacial bonds in a metal/polymer electrical double layer.* Protection of metals 2005. **41**(2): p. 105-116.

48. Posner, R., O. Ozcan, and G. Grundmeier, *Water and Ions at Polymer/Metal Interfaces*, in *Design of Adhesive Joints Under Humid Conditions*, M.L.F. Silva and C. Sato, Editors. 2013, Springer Berlin Heidelberg: Berlin, Heidelberg. p. 21-52.

49. Grosvenor, A.P., B.A. Kobe, and N.S. McIntyre, *Studies of the oxidation of iron by air after being exposed to water vapour using angle-resolved x-ray photoelectron spectroscopy and QUASES™*. Surface and Interface Analysis, 2004. **36**(13): p. 1637-1641.

50. Ohtsuka, T., K. Kubo, and N. Sato, *Raman Spectroscopy of Thin Corrosion Films on Iron at 100 to 150 C in Air.* CORROSION, 1986. **42**(8): p. 476-481.

51. Williams, G., et al., *Dopant Effects in Polyaniline Inhibition of Corrosion-Driven Organic Coating Cathodic Delamination on Iron.* Journal of The Electrochemical Society, 2006. **153**(10): p. B425-B433.

52. Nagayama, M.i. and M. Cohen, *The Anodic Oxidation of Iron in a Neutral Solution: I . The Nature and Composition of the Passive Film.* Journal of The Electrochemical Society, 1962. **109**(9): p. 781-790.

53. Leidheiser, H. and W. Funke, *Water Disbondment and Wet Adhesion of Organic Coatings on Metals: a Review and Interpretation.* J. Oil Colour Chem. Assoc., 1987. **70**(5): p. 121-132.

54. Hoffmann, K. and M. Stratmann, *Delamination of organic coatings from rusty steel substrates.* Corros. Sci., 1993. **34**(10): p. 1625-45.

55. Posner, R., M. Santa, and G. Grundmeier, *Wet- and Corrosive De-Adhesion Processes of Water-Borne Epoxy Film Coated Steel: I. Interface Potentials and Characteristics of Ion Transport Processes.* Journal of The Electrochemical Society, 2011. **158**(3): p. C29-C35.

56. Kendig, M. and D.J. Mills, *An historical perspective on the corrosion protection by paints.* Progress in Organic Coatings, 2017. **102**: p. 53-59.

57. Grundmeier, G., et al., *Corrosion properties of chemically modified metal surfaces.* Electrochimica Acta, 1998. **43**(1): p. 165-174.

58. Wielant, J., et al., *Cathodic delamination of polyurethane films on oxide covered steel – Combined adhesion and interface electrochemical studies.* Corrosion Science, 2009. **51**(8): p. 1664-1670.

Paper IV

Corrosion protection of smooth surfaces – coating adhesion

Catalina H.Musinoi Hagen, Alexander Kristoffersen
Norwegian University of Science and Technology, 7491 Trondheim, Norway
Ole Øystein Knudsen
SINTEF Materials and Chemistry, 7465 Trondheim, Norway

Abstract

Coatings on machined surfaces are generally found to degrade early, and this has been attributed to poor adhesion. Good adhesion normally requires blasting, but not all surfaces can be blast cleaned due to other functional requirements, such as seal (flange surface) or assembly (tightness of nuts). Our findings show that machined surfaces had poor resistance to cathodic disbonding and corrosion creep. Impact toughness was found on the average to be four times lower on machined surfaces than on blasted surfaces. Dry adhesion tests gave no discernable difference between machined and blasted surfaces. Wet adhesion testing, however, indicated that adhesion was strongly weakened on machined surfaces by permeation of water into the coating.

1. Introduction

In the Norwegian waters, protective coating systems for offshore installations and associated facilities are selected according to the standard NORSOK M-501 [1]. ISO 12944 is used in other industries [2]. Both standards relate the performance of coatings applied on steel to the state of the surface immediately prior to coating, and in most cases recommend blasting of the surface to increase coating adhesion. The purpose with the blasting is removal of unwanted surface layers and contaminants and the increase of surface roughness to increase adhesion. The blast cleaning method is however not suited for all surfaces. Surfaces that are machined for functional requirements, such as seal (flange surface) or assembly (tightness of nuts), cannot be blast cleaned before being coated. Smooth machined surfaces are therefore found on many components on ships and offshore installations, and are generally found to degrade early with subsequent corrosion of the steel substrate. The loss of adhesion to the steel surface is regarded as the main failure mechanism of protective coatings [3] as it results in the exposure of the steel to the corrosive environment.

It has been stated that corrosion is not possible as long as coating adhesion persists [13]. The loss of adhesion to the steel surface is regarded as the main failure mechanism of protective coatings [3] as it results in the exposure of the steel to the corrosive environment. Corrosion is found to initiate at damages in the coating. It is believed that in order to achieve a good adhesion the surface roughness must be increased to a sufficient level [3, 6-9], although

evidence is also found for the opposite [10-12]. The increase of adhesion strength with surface roughness has been linked to an increase in surface area and specific surface energy [11].

The corrosion induced coating degradation is initiated by processes that lead to the formation of a water phase on the surface of the metal, e.g. mechanical damage, osmotic blistering (salts present on the surface during coating), low film thickness or cracking of the coating. Corrosion may then propagate under the coating by three recognized mechanisms [4, 14, 15, 5]

1) Cathodic disbonding (cathodic front alkalizes the water phase and disbonds the coating)
2) Anodic undermining (bonding sites on the substrate disappear due to corrosion)
3) Tearing of the coating by corrosion products with increased volume

This spreading of corrosion is commonly known by the names "corrosion creep", "underfilm corrosion" or "scribe creep". It is seldom seen to be initiated on undamaged surfaces.

Previous studies have reported about the effect of surface roughness on the initiation of a corrosion on painted steel [3-15]. Although there is some agreement about the importance of an increased interfacial area between the coating and steel in order to diminish the rate of delamination, the exact mechanism for the adhesion loss or what parameters that may determine the delamination rate are not agreed upon. The roughness necessary to provide sufficient disbonding resistance in corrosive environments is also disputed.

The recent work of Sørensen *et al.*[7] suggests that the commonly used surface roughness parameters Ra, Ry or Rz do not describe the surface topography precisely. Substrates blasted with finer grit showed lower rates of cathodic disbonding than substrates blasted with larger grit particles, even for substrates with comparable profile height and peak densities. The experimental study indicated that the tortuosity of the surface is a parameter of greater importance compared to the traditional surface roughness parameters, as it describes the actual interfacial area more precisely than the profile height and peak density. Tortuosity is defined as the actual length of the steel-coating interface along a cross section, divided by the length of a straight line between the two end points.

However, wet adhesion is key to understanding corrosion resistance of coatings, as few coatings are able to resist hydrolysis over time [16]. The presence of water in the coating affects adhesion negatively, weakening it to a partially reversible value known as wet adhesion. Adhesion in wet conditions is hence lower than in dry, but it is stated that due to residual adhesive forces not all adhesion is lost. Wet adhesion is not seen as a failure mechanism but as a coating property [17].

This paper presents results for corrosion resistance and adhesion of organic coatings on machined surfaces with varying surface roughness. Four different machining processes have been evaluated with respect to surface topography and tested with respect to coating adhesion (ISO 4624, ISO 16276-2), impact toughness (ISO 6272-1) and corrosion creep resistance

(ISO 20340). Blast cleaned and zinc metallized (TSZ) samples were used as reference surfaces in all tests.

The preliminary conclusion from the study is that the poor coating performance on machined surfaces is due to low wet adhesion strength, which caused little resistance against corrosion creep. Cathodic disbonding seems to be the mechanism by which adhesion loss spreads over the surface. Corrosion then follows behind.

The long term objective with this study is to improve coating lifetime in terms of a durable corrosion protection on machined surfaces by finding the right combination of coating and machining process. The objective with the work reported here was to investigate the properties of coatings applied on machined surfaces and to propose one or more hypotheses to why they degrade so rapidly.

2. Experimental

2.1 Materials

Samples representing four different machining processes – end milled, rolled milled, angle grinded and turned – have been tested for dry and wet adhesion, creep corrosion and impact toughness properties. Blast cleaned and zinc metallized (TSZ) samples were used as reference surfaces in all tests.

Information about the samples is given in Table 1. Test panels, 75x150 mm large and 4 - 5 mm thick, were prepared from various species of steel and cast iron. The samples were delivered by two different suppliers: supplier 1 delivered samples which had been end milled, rolled milled or turned, see systems A and B in Table 1. They applied an epoxy based antifouling coating system used for submerged parts on ships. Samples from supplier 2 had been angle grinded or end milled to a defined surface roughness R_a=1,6 µm and R_a=12 µm, see system C and D in Table 1. They applied a coating system used for equipment on boat decks.

Table 1. Materials, surface preparation and coatings.

	Material	Machining	Coating system	
			Generic type	Thickness [µm]
A1		End milled		
A2		Rolled milled		
A3	Mild steel S355 EN10025	Turned		
A4		Blast cleaned	Epoxy primer	50
B1		End milled	Epoxy	150
B2		Rolled milled	Epoxy vinyl tiecoat	150
B3	Cast iron SG400-12	Turned	Antifouling coat	150
B4				
		Blast cleaned		

C1		End milled R_a=1.6 µm		
C2	S355 J2G3	End milled R_a=12µm	Epoxy primer	40
C3		Angle grinded	Polysiloxane	125
C4		Zinc metallized	Polysiloxane	75
D1		End milled R_a=1.6 µm		
D2	S690QL	End milled R_a=12µm		
D3		Angle grinded		
D4		Zinc metallized		

2.2 Adhesion

It is difficult to investigate adhesion phenomena with the test methods available today. Several parameters have been found to influence the reliability of results [18, 19], as skills of the test operator, the coating thickness, curing time of the coating and adhesive. For the cut tests, both the tape used and the angle the knife cuts the coating is found to impact the results. For tensile tests the type of dollies used affects the result [20]. In the present study we performed a pull-off test according to ISO 4624 [21] and a cross-cut test according to ISO 2409 [22]. Pull-off tests are usually not measuring adhesive fracture since the coating typically fails cohesively, therefore a cross-cut test was included. The latter also gives more reliable wet adhesion results. The tests were performed both in dry and in wet conditions. For wet adhesion testing, samples had been immersed in tap water at 10 °C to room temperature for one week for saturation of the coating prior to testing.

For pull-off tests, three test dollies were glued to each coated surface and pulled off after one day of curing. The dry adhesion test measures the minimum tensile stress necessary to detach the coating in the perpendicular direction to the substrate. Results are reported in MPa. A right-angle lattice pattern was cut into the coating for the cross-cut test and the cut-area was examined and classified from 0 (good adhesion) to 5 (bad adhesion) by a visual comparison with the illustrations in the standard. The test does not assess the adhesion quantitatively but gives a qualitative indication on the adhesion of the coating to either the preceding coat or the substrate.

2.3 Impact toughness

To evaluate the resistance of the dry film of paint to cracking or peeling, an impact toughness test was performed according to ISO 6272-1 [23]. A 20-mm-diameter spherical indenter was dropped on the samples under standard conditions and about 50% relative humidity. The mass of the falling weight used was 2 kg, and the drop height was increased until deformations were produced. The test measures the minimum drop height which will cause cracking or peeling when coating is subjected to a falling weight, and results are reported in Joules (energy absorbed).

2.4 Accelerated weathering laboratory test

To evaluate the resistance to underfilm corrosion creep and cathodic disbonding, an accelerated weathering test was performed according to ISO 20340 [24]. Samples were scribed with a 2 mm milling cutter down to the steel substrate in order to initiate corrosion. The length of the scribe was 50 mm. Three parallels of each machining process and coating system were exposed to cyclic tests intended to have a duration of 25 weeks. However, due to rapid degradation the samples were collected after 7-8 weeks, photographed and degraded coating scraped away for measurement of corrosion creep under the coating from the scribe. The amount of cathodic disbonding of the coating in front of the corrosion was also evaluated.

2.5 Surface characterization

The surface roughness was measured with a profilometer on unpainted machined samples. The profilometer is a contact method where the stylus tip moves on the surface in order to measure traditional surface parameters as Ra, Rq and Rz. Scanning Electron Microscopy (SEM) of cross sections was used to examine the surface morphology of the different machined substrates studied.

3. Results

3.1 Adhesion

The results from dry adhesion tests showed contrary to expectation that adhesion was just as good for the machined surfaces as it was on the blast cleaned surfaces. Both pull-off adhesion tests and cross-cut tests revealed only minor differences.

Pull-off testing gave fracture strengths between 16 and 21 MPa for all samples. The coatings generally failed cohesively, so the test did not actually measure adhesion. The metallized reference samples gave cohesive fracture in the zinc layer. There was no difference between machined samples and blast cleaned samples. Pull-off strength of wet coatings was also in this range. The pull-off test was performed on samples with glued dollies cured for 24 hours. The wet pull-off test is recommended to be conducted within 24 hours of removal from water as coating adhesion is found to recover most of its initial value as the water evaporates from the film [20]. Apparently samples regained adhesive strength.

The cross-cut test on the other hand differentiated better between the surface preparation methods. The wet adhesion was much lower on machined surfaces with the epoxy/polysiloxane coating than on the blast cleaned and metallized surfaces, see results in Table 2. For the antifouling coating the wet adhesion was comparable to the dry adhesion.

Table 2. Cross-cut adhesion measurements in wet and dry conditions.

	Material	Machining	Cross-cut [score]	
			Dry	Wet
A1		End milled	2	3
A2	Mild steel S355 EN10025	Rolled milled		
A3		Turned	2	0-1
A5		Blast cleaned		
B1		End milled	2	0-1
B2	Cast iron SG400-12	Rolled milled	2	0-1
B3		Turned	2	0-1
B4		Blast cleaned		
C1		End milled R_a=1.6 µm	1-2	3
C2	S355 J2G3	End milled R_a=12µm	1-2	4-5
C3		Angle grinded	1-2	5
C4		Zinc metallized	1-2	1-2
D1		End milled R_a=1.6 µm	1-2	4
D2	S690QL	End milled R_a=12µm	1-2	5
D3		Angle grinded	1-2	4
D4		Zinc metallized	1-2	1-2

3.2 Impact toughness

Results from impact toughness tests can explain some of the experienced problems with organic coating on machined surfaces. The impact resistance testing showed only small differences among the different machining methods. However, impact resistance was found to be about four times higher on blast cleaned surfaces, see Table 3.

It is to be noted the considerable difference between the two reference samples C4 and D4. The substrates are of different materials, and D4 was prepared of a harder material which probably explains the large difference between C4 and D4.

Table 3. Impact toughness measurements.

	Material	Machining	Impact toughness [J]
A1		End milled	5
A2	Mild steel S355 EN10025	Rolled milled	7.5
A3		Turned	5
A4		Blast cleaned	18
B1		End milled	7.5
B2	Cast iron SG400-12	Rolled milled	5
B3		Turned	7
B4		Blast cleaned	18
C1		End milled R_a=1.6 µm	3
C2	S355 J2G3	End milled R_a=12µm	4
C3		Angle grinded	3
C4		Zinc metallized	19
D1		End milled R_a=1.6 µm	3
D2	S690QL	End milled R_a=12µm	3
D3		Angle grinded	3
D4		Zinc metallized	3.5

3.3 Corrosion

Very poor corrosion creep resistance was found on all machined samples already after 7-8 weeks in the ISO 20340 test, with some minor differences between the various machining methods. On all the machined samples several mm cathodic disbonding was found in front of the corrosion creep. No corrosion creep was found on the zinc metallized reference samples. Table 4 shows information about the measured corrosion creep on all samples. Values are obtained by averaging over 9 measurements on three parallels according to the test standard.

While the measured corrosion creep was 7 mm on the angle grinded samples C3 and D3, it was found to be twice as high on the other machined samples. Cathodic disbonding was believed to be the precursor of the corrosion process on all samples, but on angle grinded also some blistering was identified.

A close visual inspection of samples after removal of disbonded coating layers, see Figure 1, shows that red rust has formed uniformly at the defect spreading under the coating. Also black rust having formed in circular shapes can be seen in the close vicinity of the defect. However, no corrosion products can be seen in the areas nearest the disbonding front.

Table 4. Corrosion creep measured on samples.

|	Material	Machining	Corrosion creep [mm]	Cathodic disbonding [mm]
A1		End milled	11	3
A2		Rolled milled	13	6
A3	Mild steel S355 EN10025	Turned	14	5
A4		Blast cleaned		
B1		End milled		
B2		Rolled milled		
B3	Cast iron SG400-12	Turned		
B4		Blast cleaned		
C1		End milled R_a=1.6 µm	12	2
C2		End milled R_a=12µm	13	2
C3	S355 J2G3	Angle grinded	7	0
C4		Zinc metallized	0	0
D1		End milled R_a=1.6 µm	13	1
D2	S690QL	End milled R_a=12µm	13	1
D3		Angle grinded	6	0
D4		Zinc metallized	0	0
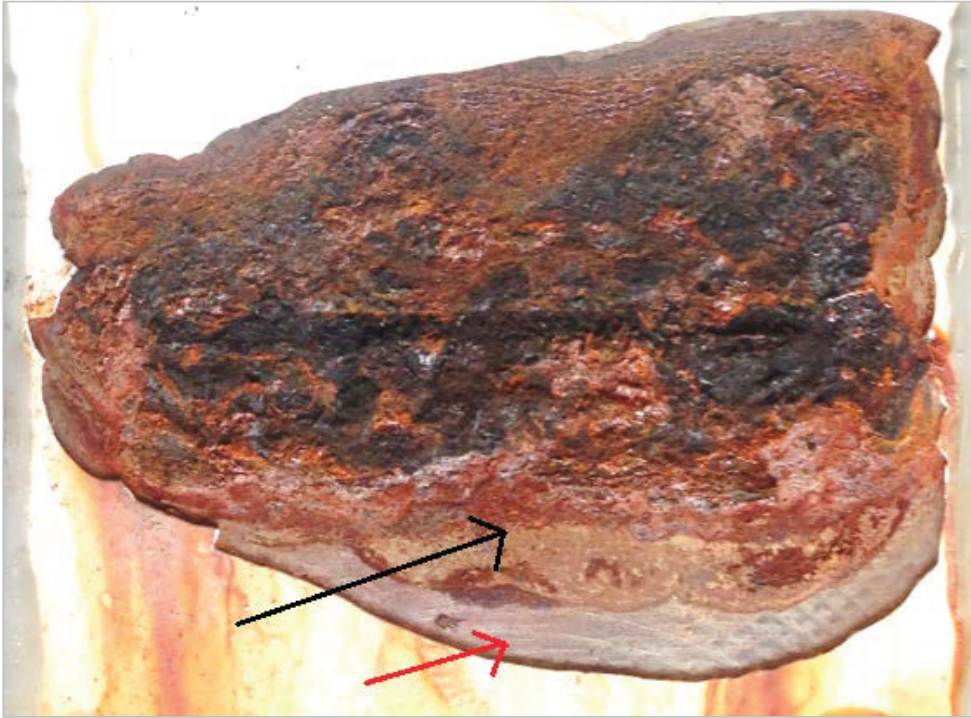
Figure 1. Corrosion creep identified on milled sample C1. Red arrow indicates cathodic disbonding while the black arrow points out the area with corrosion products.

3.4 Surface characterization

Only small differences in surface roughness were found among the machining methods, all measuring Ra between 0.6-2.6 µm. Images taken by SEM confirmed this, see Figure 2.
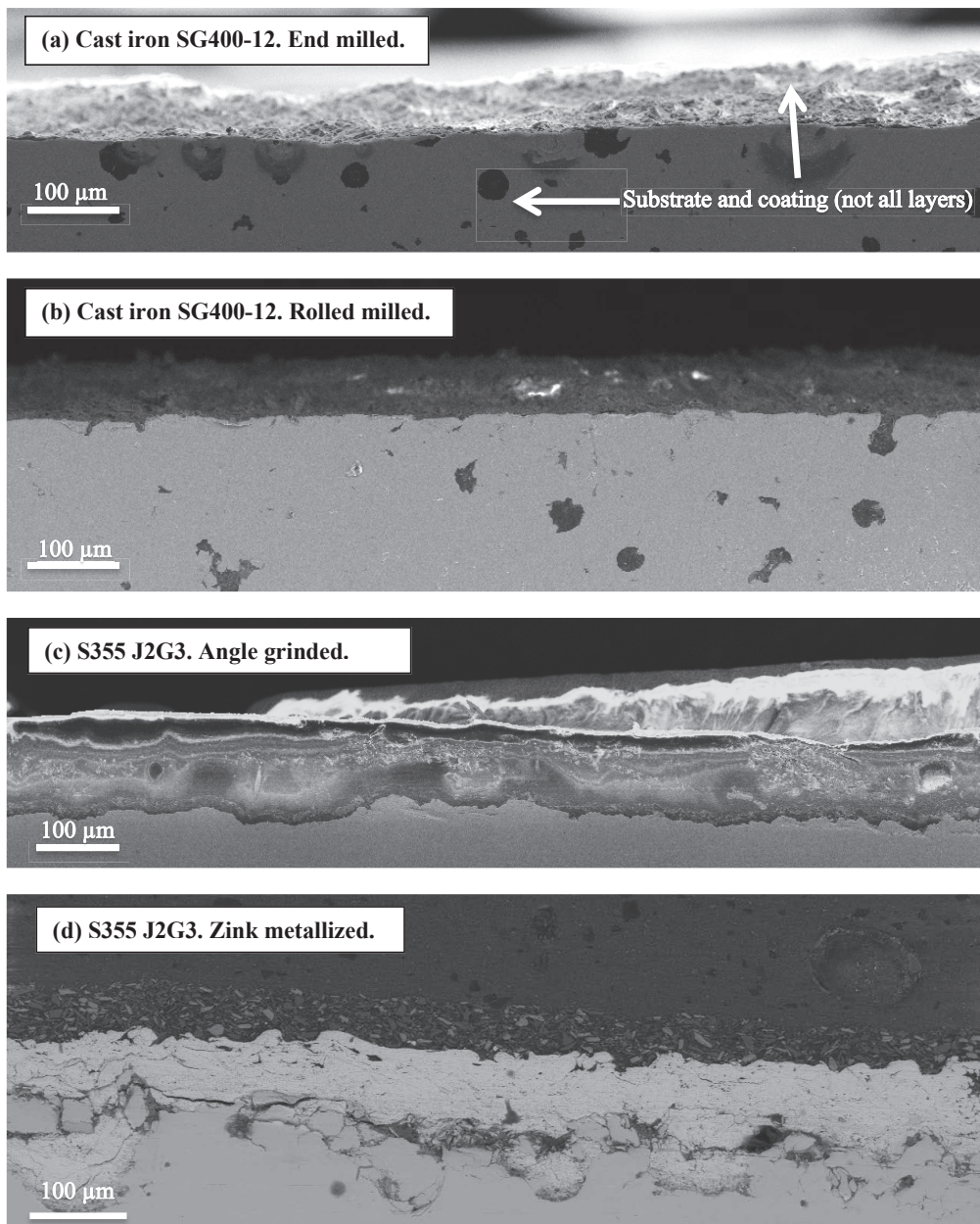
(a) Cast iron SG400-12. End milled.

100 µm

Substrate and coating (not all layers)

(b) Cast iron SG400-12. Rolled milled.

100 µm

(c) S355 J2G3. Angle grinded.

100 µm

(d) S355 J2G3. Zink metallized.

100 µm

Figure 2. SEM images of machined surfaces (a-c) and the metallized surface (d). Some corrosion may be seen on substrate due to preparation for microscopy. White spots are areas with charging of electrons, possibly due to organic materia (coating) being smeared out during polishing.

4. Discussion

It is stated that corrosion cannot happen as long as adhesion persists [16, 25, 26]. It is therefore believed that a combination of weak wet adhesion and poor impact toughness is of

importance for the observed coating failures on machined surfaces in the field. From impact toughness tests we see that coatings on machined surfaces are more prone to damage caused by impacts, as impact toughness was on the average four times higher on blasted compared with the machined surfaces. We believe that a substrate profile with low surface roughness on machined surfaces will not be able to absorb lateral forces. This probably partly explains the poor performance of coatings on machined surfaces.

Wet cross-cut tests showed that coatings on machined surfaces loose much of their adhesion strength when saturated with water. Cross-cut tests on machined surfaces gave quite different results, as the score on three of the wet samples was actually very good. Wet pull-off tests measured high pull-off strength even when testing happened within 24 hours of exposure. All dry adhesion tests gave good results and therefore little information about the different corrosion behavior of machined surfaces compared to blasted. It is to be noted that both the pull-off and the cross-cut test are characterized by several disadvantages: They may overestimate adhesion as a result of energy loss in deformation of the coating. When performed in wet conditions, dollies have to be glued with the same glue used for dry conditions, but the glue may be affected by the water in the film. Water may also evaporate during curing of the glue. Pull-off usually results in cohesive fracture. The main disadvantage with the cross-cut test is that it is a qualitative test. Besides, the state of the coating (wet/dry, degree of curing etc) may significantly affect how the forces from the knife are transmitted to the substrate/coating interface.

These results, and results from other studies [27], have shown that moisture in the coating reduce adhesion strength. However, it is not clear why this has such dramatic effect on machined surfaces and not on blast cleaned ones. It is hard to see how the physical forces and chemical bonds between the coating and the steel substrate can differ between machined and blasted surfaces.

On all machined surfaces significant cathodic disbonding was found in front of the corrosion creep. Hence, it seems that cathodic reactions first cause the coating to detach from the steel, and corrosion comes after. The observed red rust Fe_2O_3 (hematite) usually forms due to high oxygen and water exposure, while black Fe_3O_4 (magnetite) usually forms when oxygen diffusion to the steel surface is limited. Alkalis generated at cathodic sites inhibit corrosion but destroy adhesion, hence eventually leading to more and more exposed steel. Oxygen is during this process depleted by the cathodic reaction, while the value at the defect is higher. Concentration differences in oxygen will form aeration cells, resulting in a polarity switch: the initial cathodic site will become anodic. It has been shown in several studies [28-30] that for unpolarized samples, cathodic disbonding propagates by a series of electrochemical cycles where initially cathodic sites under the coating get depleted of oxygen and switch polarity and become anodic. The previously anodic areas – covered by red rust - will now deliver cathodic currents to the electrochemical circuit. Possible cathodic reactions will foremost be the oxygen reduction, and the reduction of hematite Fe_2O_3 to magnetite Fe_3O_4. Cathodic reactions might also happen at other sites close to the anodic, hence resulting in an advancing disbonding front.

The transport of cations to cathodic sites will be greatly enhanced by adhesion loss, as rate determining step (RDS) for the cathodic disbonding has been found to be the transport of cations along the metal-coating interphase and not the path through the coating [7, 31]. According to Sørensen (2009) the findings could mean that the abrasive blasting, to some extent, can be used for minimizing the rate of cathodic delamination. It seems likely that the degree of wet adhesion, related to the surface roughness of the substrate is of major influence on cathodic disbonding and corrosion creep rate.

5. Conclusions

Cathodic disbonding seems to be a precursor to corrosion creep, so increasing the resistance against cathodic disbonding in some way may improve coating durability.

From the above results it is possible to suggest four hypotheses for coating degradation on machined surfaces.

1. The low surface roughness affects impact toughness resistance: defects are easily created.
2. The wet adhesion properties of the coating are low
3. Cathodic disbonding spreads easily on machined surfaces.
4. Machining activates the surface, and cathodic and anodic local spots will more readily be formed on the surface.

Acknowledgements

References

[1]   "Surface preparation and protective coating " vol. NORSOK M-501, ed, 2012.
[2]   "ISO 12944 Paints and varnishes -- Corrosion protection of steel structures by protective paint systems," ed, 2007.
[3]   B. C. Rincon Troconis and G. S. Frankel, "Effect of Roughness and Surface Topography on Adhesion of PVB to AA2024-T3 using the Blister Test," *Surface and Coatings Technology,* vol. 236, pp. 531-539, 2013.
[4]   A. T. A. Jenkins and R. D. Armstrong, "The breakdown in the barrier properties of organic coatings due to filiform corrosion," *Corrosion Science,* vol. 38, pp. 1147-1157, 1996.
[5]   N. W. Khun and G. S. Frankel, "Effects of surface roughness, texture and polymer degradation on cathodic delamination of epoxy coated steel samples," *Corrosion Science,* vol. 67, pp. 152-160, 2013.
[6]   R. Montoya, F. R. García-Galván, A. Jiménez-Morales, and J. C. Galván, "A cathodic delamination study of coatings with and without mechanical defects," *Corrosion Science,* vol. 82, pp. 432-436, 2014.

[7]   P. A. Sørensen, S. Kiil, K. Dam-Johansen, and C. E. Weinell, "Influence of substrate topography on cathodic delamination of anticorrosive coatings," *Progress in Organic Coatings,* vol. 64, pp. 142-149, 2009.

[8]   J. Votava, "The influence of roughness of machined surface on adhesion of anticorrosion system," *Acta universitatis agriculturae et silviculturae mendelianae Brunensis,* vol. LXI, 2013.

[9]   A. Collazo, M. Izquierdo, X. R. Nóvoa, and C. Pérez, "Surface treatment of carbon steel substrates to prevent cathodic delamination," *Electrochimica Acta,* vol. 52, pp. 7513-7518, 2007.

[10]   A. F. Harris and A. Beevers, "The effects of grit-blasting on surface properties for adhesion," *International Journal of Adhesion and Adhesives,* vol. 19, pp. 445-452, 1999.

[11]   O. Ø. Knudsen, "Cathodic disbonding of epoxy coatings - effect of test parameters," presented at the NACE International Corrosion Conferance, 2008.

[12]   D. de la Fuente, J. Simancas, and M. Morcillo, "Effect of variable amounts of rust at the steel/paint interface on the behaviour of anticorrosive paint systems," *Progress in Organic Coatings,* vol. 46, pp. 241-249, 2003.

[13]   M. Morcillo, J. M. Bastidas, J. Simancas, and J. C. Galvan, "The effect of the abrasive work mix on paint performance over blasted steel," *Anti-Corrosion Methods and Materials,* vol. 36, pp. 4-8, 1989.

[14]   X. Jin, K. Tsay, A. Elbasir, and J. Scantlebury, "The Adhesion and Disbonding of Chlorinated Rubber on Mild Steel," in *X. H. Jin, K. C. Tsay, A. Elbasir, and J. D. Scantlebury, In: Proc. Symp. on Corrosion Protection by Organic Coatings, M. W. Kendig*, 1987, pp. 37-47.

[15]   S. S. Jamali and D. J. Mills, "Steel surface preparation prior to painting and its impact on protective performance of organic coating," *Progress in Organic Coatings,* vol. 77, pp. 2091-2099, 2014.

[16]   P. A. Sørensen, S. Kiil, K. Dam-Johansen, and C. E. Weinell, "Anticorrosive coatings: a review," *JCT Research,* vol. 6, pp. 135-176, 2009.

[17]   A. Forsgren, *Corrosion Control Through Organic Coatings*: CRC Press, 2006.

[18]   C. A. Bishop, "9 - Adhesion and Adhesion Tests," in *Vacuum Deposition onto Webs, Films and Foils (Second Edition)*, C. A. Bishop, Ed., ed Oxford: William Andrew Publishing, 2011, pp. 177-185.

[19]   T. Cunningham and J. Steele, "Measuring Adhesion of Coatings to Concrete and Steel."

[20]   Y. H. C. Baek, K.M.; Son, M.S.; Song, E.H.; Shin, C.S; Baek, K.K., "Reliability on Coating Pull-Off Adhesion Strength Test," presented at the NACE Corrosion Conferance & Expo 2009, 2009.

[21]   "ISO 4624 Paints and varnishes -- Pull-off test for adhesion," ed: DIN, 2002.

[22]   "ISO 2409 Paints and varnishes -- Cross-cut test," ed: DIN, 2007.

[23]   "ISO 6272 Paints and varnishes -- Rapid-deformation (impact resistance) tests," in *Part 1: Falling-weight test, large-area indenter* ed: DIN, 2011.

[24]   "ISO 20340 Paints and varnishes -- Performance requirements for protective paint systems for offshore and related structures ", ed: DIN, 2009.

[25]   P. A. Sørensen, K. Dam-Johansen, C. E. Weinell, and S. Kiil, "Cathodic delamination of seawater-immersed anticorrosive coatings: Mapping of parameters affecting the rate," *Progress in Organic Coatings,* vol. 68, pp. 283-292, 2010.

[26]   M. Stratman, "W.R. Whitney award lecture: Corrosion stability of Polymer- Coated Metals - New Concepts Based on Fundamental Understanding. ," *Corrosion,* vol. 61, pp. 1115-1126, 2005.

[27]   H. Leidheiser, "Polymeric Materials for Corrosion Control," in *ACS Symposium Series* R. A. Dickie and F. L. Floyd, Eds., ed. Washington: American Chemical Society, 1986.

[28]   M. Doherty and J. M. Sykes, "Micro-cells beneath organic lacquers: a study using scanning Kelvin probe and scanning acoustic microscopy," *Corrosion Science,* vol. 46, pp. 1265-1289, 2004.

[29]   B. Reddy and J. M. Sykes, "Degradation of organic coatings in a corrosive environment: a study by scanning Kelvin probe and scanning acoustic microscope," *Progress in Organic Coatings,* vol. 52, pp. 280-287, 2005.

[30]   B. Reddy, M. J. Doherty, and J. M. Sykes, "Breakdown of organic coatings in corrosive environments examined by scanning kelvin probe and scanning acoustic microscopy," *Electrochimica Acta,* vol. 49, pp. 2965-2972, 2004.

[31]   P. A. Sørensen, K. Dam-Johansen, C. E. Weinell, and S. Kiil, "Cathodic delamination: Quantification of ionic transport rates along coating–steel interfaces," *Progress in Organic Coatings,* vol. 68, pp. 70-78, 2010.

Paper V

NACE INTERNATIONAL® CORROSION 2016 CONFERENCE & EXPO

The effect of surface profile on coating adhesion and corrosion resistance

Catalina H.Musinoi Hagen
Norwegian University of Science and Technology
Richard Birkelands vei 2B
7034 Trondheim
Norway

Alexander Kristoffersen
Norwegian University of Science and
Technology
Richard Birkelands vei 2B
7034 Trondheim
Norway

Ole Øystein Knudsen
SINTEF
Richard Birkelands vei 2B
7034 Trondheim
Norway

ABSTRACT

Coatings on machined surfaces are generally found to degrade early and this has been attributed to poor adhesion. Good adhesion normally requires blasting, but surfaces machined for functional requirements, such as seal (flange surface) or assembly (tightness of nuts) are not blasted before being coated. The effect of surface roughness, peak density and contact area on coating adhesion and protective performance has been studied. Machined and grit blasted samples have been tested for corrosion creep, cathodic disbonding and adhesion. The results showed that machined surfaces have lower contact area than blasted samples. The contact area increased with decreasing peak density for both blasted and machined samples. Adhesion loss was however positively related to the contact area on machined surfaces and inversely related on blasted surfaces. High peak density seems to be key factor for increasing coating adhesion on machined surfaces, while a high peak density seemed to decrease adhesion on profiles with sharp features and high surface roughness.

Key words: Underfilm corrosion, corrosion creep, cathodic disbonding, adhesion, roughness, grit blasting, machining.

INTRODUCTION

Blast cleaning is widely recommended before coating steel. The purpose with the blasting is to remove unwanted surface layers and contaminants, and to increase surface roughness and adhesion. It has been stated that corrosion is not possible as long as adhesion persists.[1] The blast cleaning method is however not suited for all surfaces. Surfaces that are machined for functional requirements, such as seal (flange surface) or assembly (tightness of bolts), are not blast cleaned before being coated. Blasting of machined surfaces is also sometimes omitted for economical and production rate

considerations. Smooth machined surfaces are therefore found on many constructions, vessels and installations. Coatings applied on these surfaces are generally found to degrade early with subsequent corrosion of the steel substrate.

Several studies have evaluated the effect of surface roughness on coating performance. Jin et al. studied the effect of surface roughness on cathodic disbonding and found a linear decrease with roughness.[2] However, they concluded that the actual disbonded area was equal for low and high roughness values, and that the geometrical disbonded area would hence vary (actual and geometrical area are defined in Table 1). The coating studied was a 20 µm chlorinated rubber lacquer and the roughness varied around R_a=1µm. The effect of directional and random abrasion with SiC paper from grit # 60 up to #1200 on cathodic disbonding, was studied by Kuhn and Frankel using epoxy coatings.[3] The roughness was not higher than R_q=0.3 µm. They concluded that cathodic disbonding decreased with increased roughness up to R_q=0.07 µm.

In recent years the influence of peak density on coating performance has also been studied. The effect of peak density on corrosion creep was evaluated in studies by Ward[4] and Roper[5,6] analyzing epoxy and polyurethane coatings on shot and grit blasted steel. Ward observed that the shape of the irregularities affected the coating performance. Corrosion creep decreased with increased surface roughness and was least on grit blasted surfaces, while the peak density did not have any significant influence on the results. Roper concluded the opposite regarding the peak density. Testing samples at the same R_{max} (63 µm) but with different peak densities, he stated that the peak density should be chosen as high as possible as long as the coatings are still able to wet the surface. See Table 1 for nomenclature.

Sørensen et al. suggested that neither the commonly used surface roughness parameters nor the peak density describe the surface topography precisely.[7] Substrates blasted with finer grit showed less cathodic disbonding than substrates blasted with larger grit particles, even for substrates with comparable profile height and peak densities. He found that the ratio of the actual length of surface profilometry trace to the apparent length along the surface, correlated well with cathodic disbonding, and suggested that the ratio described the actual interfacial area more precisely than the profile height and peak density. The epoxy coated samples showed less cathodic disbonding with increased ratio.

Watts and Castle found already in 1984 that it was a correlation between the abovementioned ratio, which they called tortuosity, and the disbonding rate.[8] Cathodic disbonding was found to increase with a decrease in tortuosity, and they suggested that the effect was due to a decrease in the diffusion path under the coating from the scribe to the disbonding front. A similar profile parameter was proposed by Wenzel who derived the ratio of the contact area divided by the projected geometric area, known as Wenzel's roughness factor, r.[9]

This paper presents results for corrosion resistance and adhesion of organic coatings on surfaces with varying surface topography and roughness. Samples were machined by three different machining processes and blasted with four different grit sizes. Surface roughness parameters, peak density and Wenzel's roughness factor were measured. Coating performance was evaluated as corrosion creep resistance and cathodic disbonding. Adhesion was measured by pull-off and cross-cut. Profile data and corrosion test results were statistically correlated in an attempt to identify which parameter/s is/are mainly responsible for promoting adhesion and corrosion resistance.

The long term objective with this study is to improve coating lifetime on machined surfaces by finding the right combination of coating and machining process. The objective with the work reported here was to investigate the properties of coatings applied on machined surfaces and to propose one or more hypotheses to why they degrade so rapidly.

NOMENCLATURE

Table 1
Nomenclature. Roughness parameters according to ISO[(1)] 4287 [10]

Parameter	Definition
A	Actual surface profile area. [mm²]
A_0	Geometrical area. [mm²]
N	Number of measurements along the profilometry trace.
P_c	Peak density. The number of peaks higher than a certain pre-defined dead-band, e.g. 10% of Rz. [Peaks/cm]
r	Wenzel's roughness factor. [A/ A$_0$]
R_a	Arithmetic roughness average: $R_a = \frac{1}{l}\sum_1^l |y|$ Where l is the measured length and y the distance from the average line. [μm]
R_t	The maximum peak to valley distance within the measured length: $R_t = R_p + Rv$ [μm]
R_{max}	The maximum peak to valley distance within a sampling length: $R_t = R_p + Rv$ [μm]
R_z	Average maximum peak to valley distance for five sampling lengths: $R_z = \frac{1}{5}\sum_1^1 (Rp + Rv)$ Where R$_p$ is the highest peak and R$_v$ is the lowest valley within one sampling length. [μm]

EXPERIMENTAL PROCEDURE

Three replicate panels for each coating/pre-treatment system were tested for corrosion creep. For all other tests two replicate panels were used.

Steels and surface treatments

The samples were prepared from UNS[(2)] G10150 carbon steel. Two types of commonly used abrasive media were employed: chilled iron grit and aluminum oxide. The grit was of various sizes to investigate the effect of grain size on the surface roughness and topography. Three different machining processes were used to investigate the effect of machining on the surface roughness and topography. The machining methods in this study represent the most commonly used processes in industry for machining parts to specific shape and size. See Table 2 for information about materials, surface preparations and coatings.

Surface characterization

Surface roughness and peak density was measured with a profilometer according to ISO 4287.

Wenzel's roughness factor was measured with an infinite focus microscope (IFM). The IFM was also used to analyze the topography.

To analyze the roughness and topography data, the Spearman's correlation coefficient (ρ) was calculated using data analysis software. This coefficient is less sensitive to outliers and shows a low

---

variability.[11-13] The coefficient does not measure the causal relationship between variables, but is used for analyzing correlations. It was assumed that parameters were strongly correlated when the absolute value of the correlation coefficient was greater than 0.7.

Coatings
Five different coating systems were used in this study. Primers both with and without aluminum (Al) flake pigments were used. Prior to coating, the specimens were degreased with an alkaline degreasing agent, thoroughly rinsed with water and ethanol and dried in an oven at 40 °C. The first layer of coating was applied within one hour after drying to avoid rust formation.

Table 2
Materials, surface preparation and coatings

Sample	Surface treatment	Surface roughness		Pc [Peaks/cm]	Wenzel's roughness factor [A/A$_0$]	Process conditions	Coat system
		Ra [μm]	Rz [μm]				
A1	Roll milled 1	1.54	9.01	89.70	1.04	Unknown Metal working fluid A	i) EP/ EP-Al TDFT = 282
A2	Face turned 1	2.07	11.28	82.53	1.04	Unknown Metal working fluid A	ii) EP-Al / EP-Al TDFT= 289
A3	End milled 1	1.32	7.18	74.70	1.06	Unknown Metal working fluid A	
A4	Metallized	14.39	79.99	24.74	-	0.5 -1 mm iron grit Thermal spray zinc	iii) EP / Polysiloxane/ Polysiloxane TDFT=240
A5	End milled 2	16.53	54.59	7.75	-	Unknown Metal working fluid B	
B1	End milled 3	16.88	74.57	14.2	1.11	Cutter diameter= 80 mm. Cutting speed=280 RPM. Feeding speed=350 mm/min. Tooth radius=0.8 mm No metal working fluid	iv) EP-Al / EP TDFT=261
B2	Blasted 1	3.49	26.66	92.40	1.11	0.2-0.3 mm Al$_2$O$_3$	v) EP / EP TDFT=265
B3	Blasted 2	4.38	32.64	76.80	1.22	0.3-0.4 mm Al$_2$O$_3$	
B4	Blasted 3	6.95	44.29	54.77	1.31	0.4-0.5 mm Al$_2$O$_3$	
B5	Blasted 4	16.68	113.3	28.67	1.46	0.5-1 mm iron grit	
C1	End milled 3	16.88	74.57	14.2	1.11	See above	i) ii) iv) v)

Note: TDFT= Total dry film thickness

The coatings used are all commercial protective coatings for marine environment. The coatings were applied by an adjustable film applicator, except for the A4-A5 samples that were sprayed. The applicator blade was adjusted with a micrometer head. The coatings were allowed to cure for one day between each applied layer. After application of the final coat, all samples for corrosion tests were cured for two days in an oven at 40 °C. Samples for adhesion tests were cured for various time periods: Samples A4 and A5 were cured 2 weeks for dry tests and 25 weeks for wet tests under ambient laboratory conditions, while C1 samples were cured either 3 weeks at ambient conditions and 5 days in

the oven at 40 °C, or 4 weeks at ambient conditions and 2 days in the oven at 40 °C. The backside and the edges of the samples were sealed with epoxy containing Al-pigments.

Accelerated corrosion tests

An accelerated weathering test was performed according to ISO 20340 Annex A, except that the test only lasted for 8 weeks instead of 25.[14] Samples were scribed with a 2 mm milling cutter down to the steel substrate in order to initiate corrosion. The length of the scribe was 50 mm. The amount of cathodic disbonding of the coating in front of the corrosion was also measured.

Cathodic disbonding was tested with the same conditions as in ISO 15711.[15] Instead of drilling a circular holiday, the scribe was used as the intentional holiday. Samples were electronically coupled to sacrificial anodes of zinc in artificial seawater at room temperature (RT). After twelve days of exposure the samples were retrieved. The cathodic disbonding was measured at 9 different positions along the 50 mm scribe.

Adhesion tests

It is difficult to investigate adhesion phenomena with the test methods available today for a number of reasons. Several parameters have been found to influence the reliability of results, as skills of the test operator, the coating thickness, curing time of the coating and adhesive.[16] Pull-off tests are usually not measuring adhesive fracture since the coating typically fails cohesively, therefore a cross-cut test was included. Pull-off was measured according to ISO 4624.[17] Cross-cut adhesion was measured according to ISO 2409.[18] A right-angle lattice pattern was cut into the coating for the cross-cut test and the cut-area was examined and classified from 0 (good adhesion) to 5 (bad adhesion) by a visual comparison with the illustrations in the standard. The tests were performed both in dry and in wet conditions. For wet adhesion testing, samples had been immersed in tap water at room temperature for one week.

RESULTS

Characterization of surface roughness

Blasted samples were found to have a perfect inverse relationship between roughness R_z and the peak density. Blasting with increasing grit size increased the surface roughness but decreased the peak density, (r=-1, p<0.01). For machined surfaces there was no significant relationship between the surface roughness R_z and the peak density.

The highest surface roughness corresponded to the lowest peak density for both machined and blasted, while the highest peak density corresponded to the lowest surface roughness only on blasted samples. Profile traces for the surfaces are shown in Figure 1.
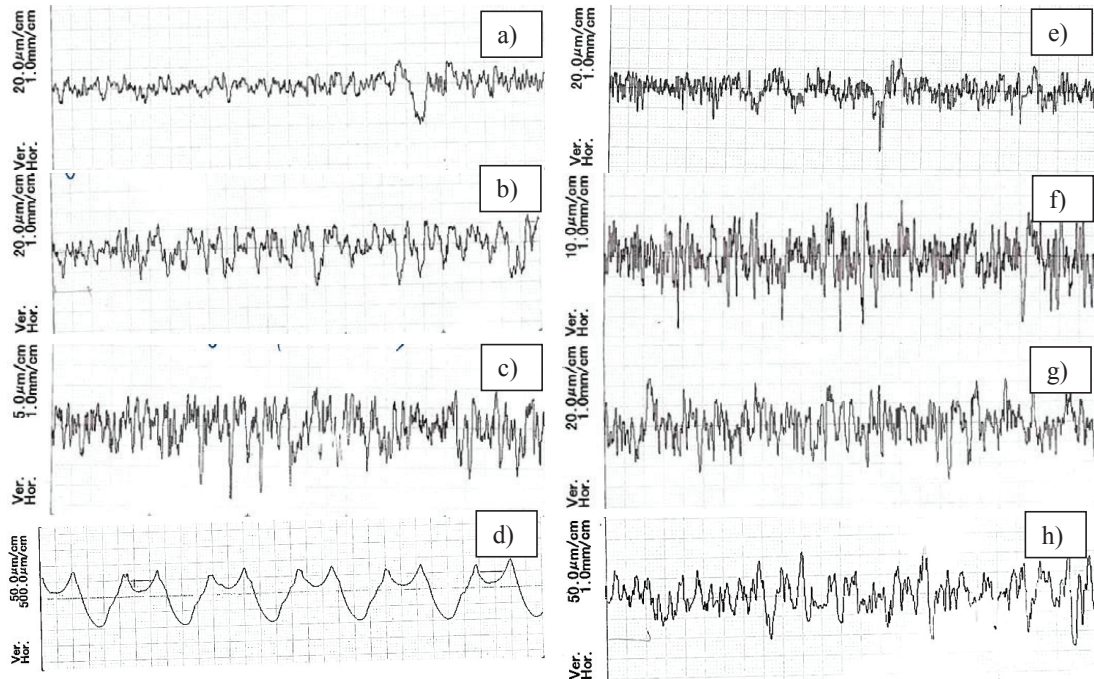
Figure 1: Surface profile traces captured by the profilometer for machined samples : a) A1, b) A2, c) A3, d) B1 and blasted samples: e) B2, f) B3, g) B4 and h) B5.

The topography of the surfaces was analyzed using the 3D surface imaging technique by IFM. The profiles of the surfaces having the highest roughness or peak density are seen for both blasted and machined surface in Figure 2-Figure 5. R_z values measured with profilometer were found to correspond with R_z values observed from IFM imaging.

For both machined and blasted surfaces, peak density decreased as the contact area increased. The inverse relationship was confirmed with a high significance ($r=-1$, $p<0.01$). For blasted surfaces, the contact area was found to increase with increased roughness ($r=1$, $p<0.01$), while no correlation between roughness and contact area was found for machined.
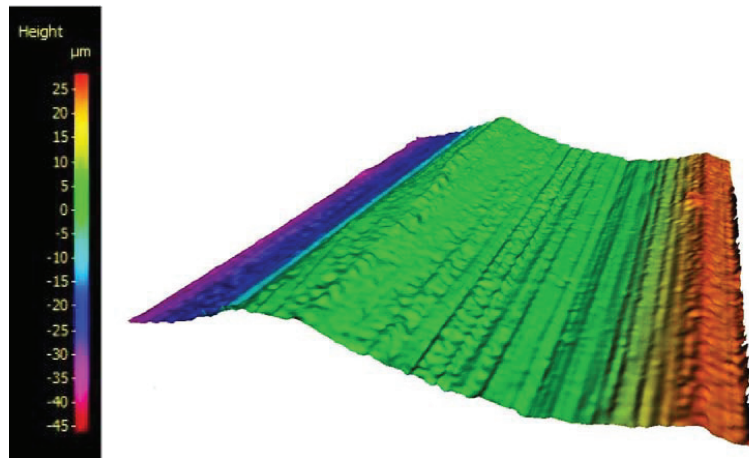
Figure 2: End milled sample B1, having the highest roughness corresponding to the lowest peak density.
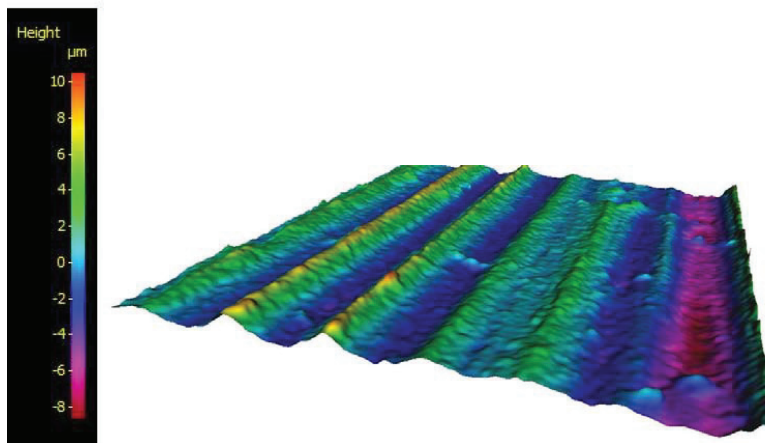
Figure 3: Rolled milled sample A1, having the highest peak density corresponding to the next lowest roughness
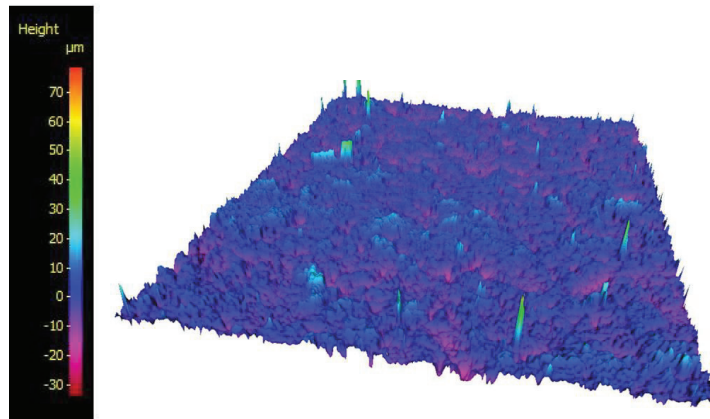
Figure 4: Blasted sample B2, having the lowest roughness corresponding to the highest peak density.
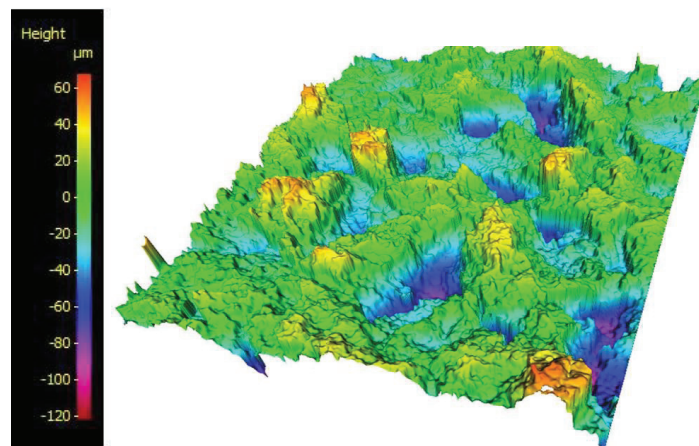
Figure 5: Blasted sample B5, having the highest roughness corresponding to the lowest peak density

Effect of surface roughness and topography on corrosion resistance

The corrosion creep test resulted in both corrosion creep and some cathodic disbonding (CD) between the coating and the substrate. Figure 6 shows the total adhesion loss for both machined and blasted samples, defined as the sum of cathodic disbonding and corrosion creep, as a function of surface roughness R_z. The contact area between the coating and the substrate, represented by Wenzel's roughness factor, is also shown as a function of R_z. It was found that surface roughness had a large effect on the total adhesion loss. Increasing R_z on machined surfaces from 10 µm to 75 µm increased the adhesion loss from 9 mm to 17 mm. At the same time Wenzel's roughness factor increased from 1.04 to 1.11. Increasing R_z on blasted surfaces from 27 µm to 113 µm decreased the adhesion loss from 8 mm to 2 mm. At the same time Wenzel's roughness factor increased from 1.11 to 1.46.

Machined surfaces gave on average twice as high adhesion loss compared to blasted surfaces. On machined surfaces 1.6-3.8 mm of cathodic disbonding was found in front of the corrosion creep, while 0-0.33 mm was found on blasted surfaces. To understand the role of cathodic disbonding on the total adhesion loss, samples primed with epoxy mastic containing Al pigments were also tested. The variant with Al pigments is known to have better resistance against CD.[19] Cathodic disbonding was then evaluated both in ISO 20340 tests (corrosion creep test) and in ISO 15711 tests (CD test).

Blasted surfaces experienced little to no CD in both CD tests and corrosion creep tests, independent of the coating. On machined surfaces the average disbonding from CD tests was 11.2 mm for epoxy mastic without Al-pigments, see Figure 7. With Al-pigments the CD was 5.2 mm. Hence, the Al-pigments decreased cathodic disbonding significantly on machined surfaces. The effect on CD was lower in the corrosion creep test, but still significant, reducing CD by 35 percent. However, although the Al-pigments decreased cathodic disbonding in the corrosion creep test, an increase in the overall adhesion loss was found due to an increase in corrosion creep, see Figure 8. The beneficial role of Al on blasted surfaces was insignificant, as both cathodic disbonding and the total adhesion loss was more or less unaffected. The adhesion loss was hence found to be mostly due to corrosion creep on machined and blasted surfaces.
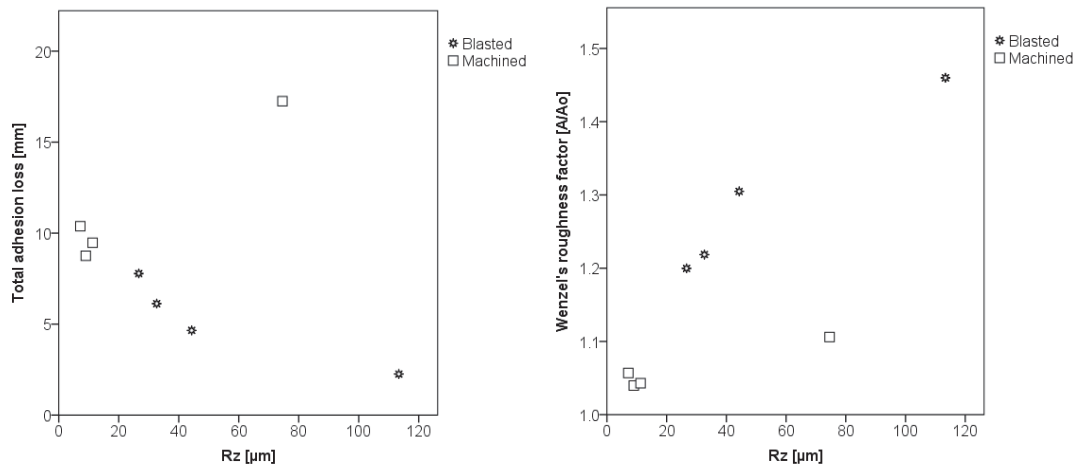

Figure 6: Total adhesion loss as a function of surface roughness and the available bonding area represented by Wenzel's roughness factor.
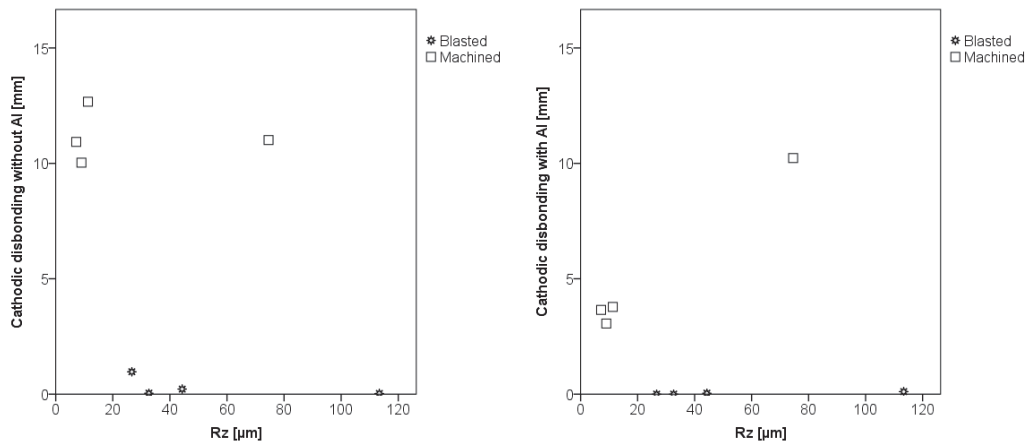
Figure 7: Cathodic disbonding, for blasted and machined samples, as a function of surface roughness R_z measured from CD tests. Samples without Al-pigmented primer to the left and with Al-pigmented primer to the right.
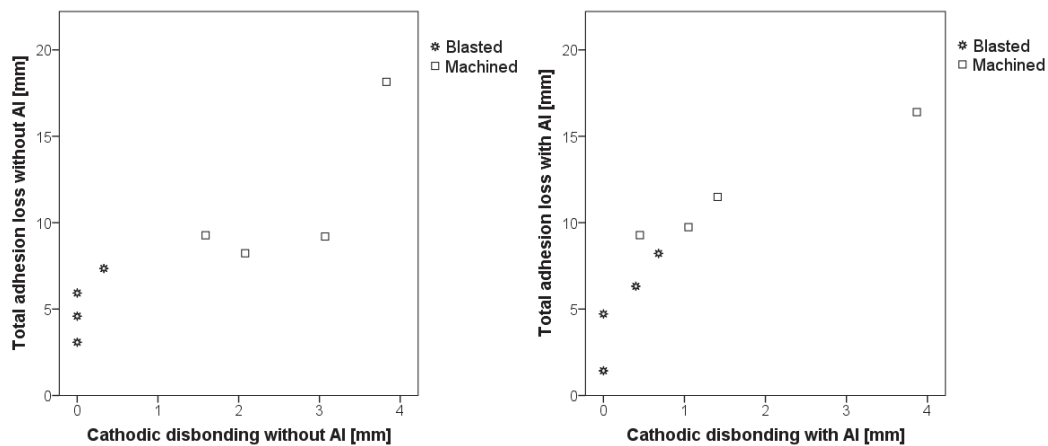

Figure 8: Total adhesion loss as a function of cathodic disbonding, for blasted and machined samples measured from corrosion creep tests: Samples without Al-pigmented primer to the left and with Al-pigmented primer to the right.

A correlation analysis of blasted and machined surfaces treated as one population, showed that surface roughness R_z and contact area (Wenzel's roughness factor) are strongly positively associated (r= 0.786, p<0.05), as Figure 6 shows. The total adhesion loss measured after corrosion creep tests decreased with increased contact area (r= -0.762, p<0.05). No significant relationship was found between the total adhesion loss and the surface roughness or the peak density.

A closer analysis of the relationship between surface parameters and total adhesion loss (Figure 9 and Figure 10) showed that the machined and blasted surfaces have to be treated as two subgroups. On machined surfaces total adhesion loss increased with the contact area (r= 1, p<0.05), while on blasted surfaces the effect was opposite (r= -1, p<0.05), which can be seen from the plot in Figure 9. The coating performance was found to decrease with increased peak density on blasted, while machined experienced an improved performance with increased peak density, see Figure 10.

When studying the population as one, correlation analysis showed that both cathodic disbonding and corrosion creep were related to the total adhesion loss. Treated as two individual groups, correlation calculations showed that on blasted surfaces the total adhesion loss both with and without Al-pigmented primer was associated to corrosion creep (r=1, p<0.01). The corrosion creep was found to be perfectly increasing with increased peak density, corresponding to a decreased contact area. On machined surfaces, the total adhesion loss with Al-pigmented primer was on the contrary associated to cathodic disbonding (r=1, p<0.05), and inversely related to peak density (r=-1, p<0.05). Without Al-primer, the total adhesion loss was neither explained by corrosion creep nor by cathodic disbonding.
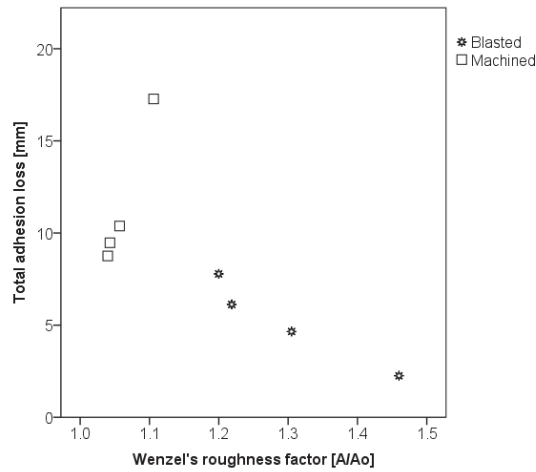
Figure 9: Total adhesion loss as a function of the contact area, represented by Wenzel's roughness factor
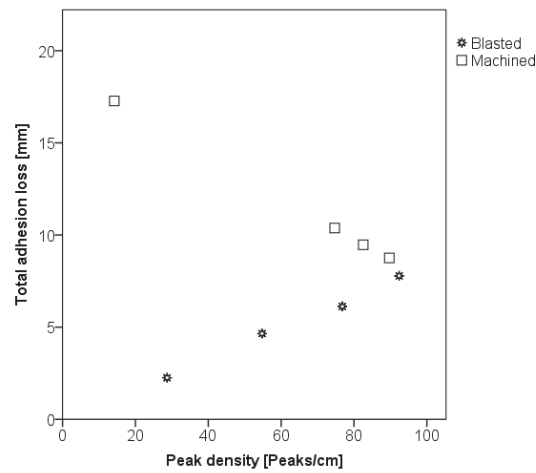

Figure 10: Total adhesion loss as a function of peak density, for all samples, with Al-pigmented primer on the left axis and without Al-pigmented primer, on the right.

The effect of surface roughness and topography on adhesion and impact strength
Pull-off tests showed fracture strengths between 7 and 21 MPa for all samples in both wet and dry tests. No difference was seen between metallized and machined surfaces. Results varied with curing time for the coatings. Longer curing times gave higher pull-off values. The coatings generally failed cohesively in and between the different layers of coat, but also some adhesive fracture was seen between the substrate and the primer.

Dry cross-cut test results showed no difference between machined and metallized surfaces as it was measured a score of 1-2 on all samples. In wet conditions a score of 1-2 was found for metallized samples, while machined resulted in a score of 4-5.

DISCUSSION

Surface roughness, peak density and contact area
This study started with the assumption that the contact area between the coating and the substrate would be proportional with both surface roughness and the peak density. However, it was found that the contact area was proportional only with surface roughness, while it was inversely proportional with peak density.

The latter was surprising. For blasted surfaces the invers proportionality may be explained by the size of the blasting grit: when grit size increases and the velocity of the particles is maintained, the peak density will decrease as stated by several workers.[5,6] The larger grit will make wider impacts in the surface. A decrease in velocity would have decreased the penetration depth and hence the distance between the peaks produced, increasing peak density. However, a decrease in penetration depth would also decrease surface roughness. The surface roughness on blasted surfaces was indeed found to be inversely related with peak density with a high significance ($r=-1$, $p<0.01$). Findings were however contradicting Sørensen's who found the finer grit to give an increased tortuosity. [7]

For machined surfaces there was however not found any significant relationship between the surface roughness R_Z and the peak density, indicating that parameters are less mutually related than for the blasting process. Several machining parameters have to be manipulated to obtain a specific combination of profile height and peak density. [20,21]

Effect of surface roughness and topography on corrosion resistance
Several studies have established that coating adhesion is affected by the contact area between the coating and the substrate, which should be high.[22,23] The plot of total adhesion loss as a function of contact area (Figure 9) showed that an increased contact area resulted in less cathodic disbonding and corrosion creep. Hence, the result is consistent with earlier work. However, machined surfaces may not benefit from an increased area as blasted surfaces were found to do.

Measuring peak density is a relative new concept in the coating industry and only a few have reported this parameter.[4-7] Contact area or length (tortuosity) is also rarely reported. Based on empirical evidence, it has been stated that a combination of ca. 63 μm R_{max} surface roughness and a peak density between 40-60 peaks/cm would results in a complete wetting of the surface and an optimum performance for industrial coatings.[5,6] Both plots and correlation calculations of the results in this study showed however a different trend. Blasted surfaces were in this study found to give the best coating performance at the lowest peak densities (29 peaks/cm), corresponding to the highest contact areas. Surfaces blasted with grit have sharp features as can be seen from Figure 4 - Figure 5, and increasing the density of the features may lead to a lower degree of wetting, which overrides the beneficial effect of a high peak number. On the other hand, machined surfaces were found to experience lower adhesion loss with increased peak density, corresponding to a decreased contact area (and surface roughness).

It may be that the number of anchoring sites is the key factor [24] on smooth surfaces with relatively low surface roughness, and more important than contact area or roughness.[25] Since the machined surfaces in this study had roughness values R_z of 10 μm - 74 μm an increase in peak density seems to offer an increased adhesion and coating performance. Ward analyzed the relationship between surfaces that had been either shot or grit blasted.[4] Although shot blasting gave high surface roughness and comparable to the grit blasted, the shot blasted surfaces gave much higher levels of corrosion creep in ISO 20340 testing. Shot blasted surfaces had a more rounded profile than grit blasted, and had in addition low peak densities (between 20-40 peaks/cm).

ISO 20340 is an accelerated cyclic corrosion test inducing an ageing of the coating. Both increased micro-cracking and pore-formation have been seen after cyclic exposure on coating surfaces.[3] Although the objective is to measure the resistance to underfilm corrosion creep from an artificial scribe, also cathodic disbonding may take place, as it was found also in this study.[26] The hypothesis early in the study was that cathodic reactions may first cause the coating to detach from the steel, and corrosion creep follows from behind. It has been shown in several studies that for unpolarized samples, cathodic disbonding propagates by a series of electrochemical cycles where initially cathodic sites under the coating get depleted of oxygen and switch polarity and become anodic.[27-29] Corrosion follows then from behind.

Cathodic disbonding was seen to be halved with Al-pigments on machined surfaces in CD tests. The effect was lower in corrosion creep tests, as corrosion creep was found to increase with decreased cathodic disbonding. CD on blasted surfaces was insignificant and not found with the Al-pigmented epoxy. The results indicate firstly that primers with Al-pigments are less beneficial in atmospheric environment than under cathodic protection. Secondly, corrosion creep seems to be the mechanism by which adhesion loss happens on blasted surfaces, while it is not possible to conclude for machined surfaces.

Effect of surface roughness and topography on adhesion

The results from dry adhesion tests showed contrary to expectation that adhesion was just as good for the machined surfaces as it was on the blasted and metallized surfaces. All dry adhesion tests gave therefore little information about the coating adhesion on machined surfaces compared to blasted surfaces. However, wet adhesion tests indicated that coatings on machined surfaces loose much of their adhesion strength when saturated with water. Wet cross-cut tests discriminated between the machined and the metallized samples, while pull-off results indicated that samples apparently regained adhesive strength. When performing pull-off tests in wet conditions, dollies have to be glued with the same glue used for dry conditions, but the glue may be affected by the water in the film. The wet pull-off test is recommended to be conducted within 24 hours of removal from water as coating adhesion is found to recover most of its initial value as the water evaporates from the film.[30] Water may hence evaporate during curing of the glue.
.

CONCLUSIONS

These results, and results from other studies, have shown that moisture in the coating reduces adhesion strength. Internal stresses will likely increase during cyclic exposure resulting in lateral forces in the coating. Rougher surfaces with more anchoring will increase the ability of the coating to resist these forces. We can therefore assume that smooth surfaces with low peak densities give lower adhesion strength compared to blasted upon cyclic exposure to a corrosive environment. The investigation has indeed shown that the total adhesion loss is perfectly correlated to peak density: on machined a decrease in peak density resulted in increased adhesion loss. On blasted surfaces the opposite was found. The trend seen on blasted is probably related to a decrease in roughness. Other studies have shown that increasing grit size without changing the velocity of the particles gives similar trends.

Adhesion loss may happen by cathodic disbonding, and corrosion creep will follow from behind. On blasted surfaces little to no cathodic disbonding was found, as expected. Hence adhesion loss on blasted will mostly happen due to corrosion creep.

This study has identified increased adhesion loss on machined surfaces with decreased peak densities. Corrosion creep is identified as the predominant mechanism on blasted, while both cathodic disbonding and corrosion creep are found to give adhesion loss on machined. Adhesion loss was found to increase on blasted with increased peak densities. The results implicate that machined and blasted surfaces cannot be directly compared. Increasing contact area will not necessarily be beneficial for coating adhesion on smooth surfaces.

- Total adhesion loss decreased with increased contact area for blasted surfaces, while the opposite was found for machined surfaces.
- Pull-off adhesion testing did not reveal any differences between machined and blasted surfaces.
- Cross-cut adhesion testing was better at revealing weak adhesion in wet exposure conditions.

ACKNOWLEDGEMENTS

REFERENCES

1   M. Stratmann, "2005 W.R. Whitney Award Lecture: Corrosion stability of Polymer-Coated Metals - New Consepts Based on Fundamental Understanding", Corrosion 61, 12 (2005): pp. 1115-1126

2   X. Jin, K. Tsay, A. Elbasir, J. Scantlebury, "The Adhesion and Disbonding of Chlorinated Rubber on Mild Steel". X. H. Jin, K. C. Tsay, A. Elbasir, and J. D. Scantlebury, In: Proc. Symp. on Corrosion Protection by Organic Coatings, M. W. Kendig, 1987)

3   N.W. Khun, G.S. Frankel, "Effects of surface roughness, texture and polymer degradation on cathodic delamination of epoxy coated steel samples", Corrosion Science 67, (2013): pp. 152-160

4   D. Ward, "An Investigation Into The Effect Of Surface Profile On The Performance Of Coatings In Accelerated Corrosion Tests", CORROSION 2007, paper no. 07001 (Houston, Tx: NACE, 2007)

5   H. Roper, E.E.F. Weaver, J. Brandon, "The effect of peak count of sourghess roughness on coating performance", The Journal of Protective Coatings and Linings (June 2005): pp. 52-65

6   H. Roper, E.E.R. Weaver, J. Brandon, "Peak performance from abrasives", Journal of Protective Coatings & Linings (June 2006): pp. 24-31

7   P.A. Sørensen, S. Kiil, K. Dam-Johansen, C.E. Weinell, "Influence of substrate topography on cathodic delamination of anticorrosive coatings", Progress in Organic Coatings 64, 2–3 (2009): pp. 142-149

8   J.F. Watts, J.E. Castle, "The application of X-ray photoelectron spectroscopy to the study of polymer-to-metal adhesion. Part 2 The cathodic disbondment of epoxy coated mild steel", Journal of Materials Science 19, (1984): pp. 2259-2272

9   R.N. Wenzel, "Resistance of solid surfaces to wetting by water", Industrial & Engineering Chemistry 28, 8 (1936): pp. 988-994

10   ISO 4287, Geometrical Product Specifications (GPS) - Surface texture: Profile method -Terms, definitions and surface texture parameters (1997)

11   J. Hauke, T. Kossowski, "Comparison of values of Pearson's and Spearman's correlation coefficients on the same sets of data", Quaestiones Geographicae 30, 2 (2011): pp. 87-93

12   O. Hryniewicz, J. Karpinski, "Prediction of reliability – the pitfalls of using Pearson's correlation", Maintenance and Reliability 16, 3 (2014): pp. 472-483

13   Y. Kim, T.-H. Kim, T. Ergün, "The instability of the Pearson correlation coefficient in the presence of coincidental outliers", Finance Research Letters 13, (2015): pp. 243-257

14   ISO 20340, Paints and varnishes — Performance requirements for protective paint systems for offshore and related structures (2009)

15   ISO 15711, Paints and varnishes - Determination of resistance to cathodic disbonding of coatings exposed to sea water (2003)

16   O.Ø. Knudsen STF24 F99256, Methods for quantitative measurement of adhesion (1999)

17   ISO 4624, Paints and varnishes - Pull-off test for adhesion (1978)

18   ISO 2409, Paints and varnishes - Cross-cut test (1992)

19   O. Knudsen, U. Steinsmo, "Effect of Barrier Pigments on Cathodic Disbonding Part 2: Mechanism of the Effect of Aluminium Pigments", Journal of Corrosion Science & Engineering 2, (1999)

20   P.G. Benardos, G.C. Vosniakos, "Predicting surface roughness in machining: a review", International Journal of Machine Tools and Manufacture 43, 8 (2003): pp. 833-844

21   Y. Quinsat, S. Lavernhe, C. Lartigue, "Characterization of 3D surface topography in 5-axis milling", Wear 271, 3–4 (2011): pp. 590-595

22   A.F. Harris, A. Beevers, "The effects of grit-blasting on surface properties for adhesion", International Journal of Adhesion and Adhesives 19, 6 (1999): pp. 445-452

23   D.E. Packham, Chapter 7 - Surface roughness and adhesion, in Adhesion Science and Engineering, ed. M.C.V. Pocius (Amsterdam: Elsevier Science B.V., 2002)

24   H. Leidheiser, "Inhibition in the context of coating delamination". CORROSION 1989, paper no. 142 (Houston, Tx: NACE, 1989)

25   O. Knudsen, "Review of Coating Failure Incidents on the Norwegian Continental Shelf since the Introduction of NORSOK M-501", CORROSION 2013, paper no. 2500 (Houston, TX: NACE 2013)

26   C. Reed, "Underfilm Corrosion Creep and Cathodic Delamination: Under the Microscope", CORROSION 2014, paper no. 4271 (Houston, Tx: NACE, 2014)

27   M. Doherty, J.M. Sykes, "Micro-cells beneath organic lacquers: a study using scanning Kelvin probe and scanning acoustic microscopy", Corrosion Science 46, 5 (2004): pp. 1265-1289

28   B. Reddy, J.M. Sykes, "Degradation of organic coatings in a corrosive environment: a study by scanning Kelvin probe and scanning acoustic microscope", Progress in Organic Coatings 52, 4 (2005): pp. 280-287

29   B. Reddy, M.J. Doherty, J.M. Sykes, "Breakdown of organic coatings in corrosive environments examined by scanning kelvin probe and scanning acoustic microscopy", Electrochimica Acta 49, 17–18 (2004): pp. 2965-2972

30   Y.H.C. Baek, K.M.; Son, M.S.; Song, E.H.; Shin, C.S; Baek, K.K., "Reliability on Coating Pull-Off Adhesion Strength Test", CORROSION 2009, paper no. 09007 (Houston, Tx: NACE, 2009)